DEPARTMENT OF THE INTERIOR

U.S. GEOLOGICAL SURVEY

Preliminary Report

of

Investigations of the Central Chile Earthquake of March 3, 1985

Edited by

S. T. Algermissen[1]

Open-File Report 85-542

This report is preliminary and has not been edited or reviewed for conformity with U.S. Geological Survey publication standards and stratigraphic nomenclature. The views and conclusions contained in this document are those of the authors and should not be interpreted as necessarily representing the official policies, either expressed or implied, of the United States Government. Any use of trade names and trademarks in this publication is for descriptive purposes only and does not constitute endorsement by the U.S. Geological Survey.

[1]U. S. Geological Survey
Denver, Colorado

1985

CONTENTS

	Page
Introduction S. T. Algermissen	1
The Earthquakes of March 3, 1985, and the Seismicity of Central Chile S. T. Algermissen and E. Kausel	3
Geologic Reconnaissance of the March 3, 1985, Chile Earthquake George Plafker	13
Site Selection and Field Experiments S. T. Algermissen, E. Kausel, E. Sembera, and P. C. Thenhaus	21
The Recording System J. Sena, C. Dietel, E. Sembera, G. Maxwell, G. Jensen, J. Gibbs, R. Borcherdt, and J. VanSchaack	29
Data Processing and Computation of Seismograms J. Watson, C. Mueller, and D. Carver	33
Site Spectra and Spectral Ratios B. Askew, C. Mueller, A. Converse, J. Watson S. T. Algermissen, R. Borcherdt, and A. Tarr	74
Preliminary Analysis of Ground Response and Observed Intensity S. T. Algermissen, E. Kausel, C. Mueller, R. Borcherdt, P. C. Thenhaus, and B. Askew	117
Preliminary Evaluation of Performance of Structures M. Celebi, in collaboration with E. Sembera	125
Acknowledgements S. T. Algermissen	180

INTRODUCTION

by

S. T. Algermissen
U.S. Geological Survey
Denver, CO 80225

The March 3, 1985, earthquake is the largest earthquake to strike central Chile since 1906. Preliminary reports of the wide distribution of the damage soon made it apparent that the earthquake was very significant as a geophysical event and that the scientific and engineering study of this major shock would be of great value in improving our understanding of plate margin earthquakes, the distribution of strong ground motion, resulting building damage and geologic effects such as soil liquefaction and landsliding. Accordingly, the decision was made to send a U.S. Geological Survey team and instrumentation to Chile with the following objectives: 1) to aid Chilean seismologists in locating the many aftershocks following the main shocks by providing portable seismographs to supplement the Chilean seismograph network; 2) to provide some additional strong motion seismographs; 3) to conduct a study of ground response, and its relation to geological factors and observed Modified Mercalli intensity; and 4) to investigate the geological and engineering (damage) consequences of the earthquake.

The field investigation began on March 21 and ended on April 8, 1985. Participants from the U.S. Geological Survey in the field investigation were S. T. Algermissen, Mehmet Celebi, George Plafker, Eugene Sembera and Paul Thenhaus. The seismic equipment taken to Chile consisted of two strong motion accelerographs, two portable, smoked paper recording seismographs (for location of aftershocks) and 8 GEOS (General Earthquake Observation System) digital seismograph systems (for ground response investigations). In all of the field investigations, close cooperation with scientists and engineers at the Universidad de Chile (Santiago), the Universidad Frederico Santa Maria (Valparaiso) and the Universidad Catolica (Santiago). During the time the seismic equipment was in Chile, the two smoked paper recording seismographs and two accelerographs were operated by the Universidad de Chile and a team from the Universidad Nacional Autónoma de México (UNAM). Immediately after the March 3 earthquake the UNAM team, in cooperation with the Universidad de Chile, fielded a number of portable seismographs to supplement the Chilean seismograph network (Ponce and others, 1985).

The U.S. Geological Survey team made a reconnaissance investigation of the damage, occupied 12 sites with the GEOS digital seismographs, and conducted damage and intensity surveys. Over 55 earthquakes were recorded at two or more sites during the study; 12 were recorded at four or more sites and six were recorded at six sites. Preliminary results of the field studies are outlined in this report to show the general nature of the engineering and geological effects of the earthquake and the scope of the site response investigations.

REFERENCE

Ponce, L., Singh, S. K., Suarez, G., and Vargas, J., 1985, El terremoto de la Zona Central de Chile del 3 de Marzo de 1985: Centro Regional de Sismologia para América del Sur (CERESIS) and the United Nations Educational, Scientific and Cultural Organization (UNESCO), Lima, Peru, 18 p.

THE EARTHQUAKES OF MARCH 3, 1985, AND THE SEISMICITY OF CENTRAL CHILE

by

S. T. Algermissen, U.S. Geological Survey, Denver, CO 80225;
and E. Kausel, University of Chile, Santiago, Chile

The Earthquakes of March 3, 1985

The main shock was actually at least two shocks. The initial motion began at 22:46:56.4 followed by a larger event at 22:47:069 (Greenwich Mean Time). Hypocenter parameters for the two shocks computed by the National Earthquake Information Service (NEIS) and the Department of Geophysics, University of Chile, are shown in table 1. The magnitude (m_b) of the first event was 5.2. The magnitude (m_b) of the second event was 6.9. The composite motion produced a magnitude (M_s) of 7.8 (U.S. Geological Survey, 1985). It is probable that more research will result in the resolution of additional, discrete events within the second, larger shock. The main shocks were preceded by an interesting foreshock sequence. Some characteristics of the sequence of earthquakes preceding the main shock are shown in figure 1, based on earthquakes located by the U.S. Geological Survey National Earthquake Information Service (NEIS). Note the period of quiescence from January 26 through February 20 and the greatly increased activity from February 21 through February 27 followed by no significant energy release prior to the main shocks of March 3. Figure 1 also shows approximate relative strain release based on the assumption that earthquakes in central Chile located by NEIS, but not assigned magnitudes, had an average magnitude of about m_b=4.2. For this assumption, the equivalent numbers of m_b=4.2 earthquakes were computed using $\log_{10}E = 5.8 + 2.4m_b$ (Richter, 1958). For shocks larger than m_b=5.5 the equivalent M_s magnitude and relationship $\log_{10}E = 11.8 + 1.5M_s$ was used to compute energy release. The same procedure was used in figure 2 which shows some characteristics of the aftershock sequence through June 17, 1985. The proportion of energy released as aftershocks through June 17 is about 36 percent of the energy released in the main shock. This relatively high ratio of energy released in aftershocks compared with the main shocks, is, to some extent, a result of the M_s=7.2 aftershock of April 9, 1985. A focal mechanism for the earthquake has not yet been computed from instrumental data. However, Plafker (this report) believes that the mechanism was a relative seaward thrusting along the plate boundary dipping from the Peru-Chile Trench beneath the continental margin. Figure 3 shows the magnitude distribution of foreshocks and aftershocks and figure 4 shows the locations of aftershocks located by NEIS through June 17, 1985. The aftershock zone is about 200 km in length north-south and is at least 100 km wide in an east-west direction along the dip of the subducted Nazca plate.

TABLE 1.--Hypocenter parameters of the principal shocks of March 3, 1985

Origin time	Latitude	Longitude	Depth km	m_b	M_s	Source
22:46:56.4	33.118° S.	71.822° W.	33 N.	5.2	___	NEIS (PDE No. 9-85, March 21, 1985).
22:47:06.9	33.155° S.	71.980° W.	33 N.	6.9	7.8	Do.
22:46:56.9	33.24° S.	71.86° W.	16			Univ. of Chile, Dept. of Geophysics (E. Kausel, oral commun., 1985) (only initial shock located).

SEISMICITY OF CENTRAL CHILE

The purpose of the following discussion is only to give some general information about the seismicity of central Chile and to provide a frame of reference for the location of the March 3 earthquake. Earthquakes $M_s \geq 6.0$ in central Chile and western Argentina from 1570 to 1981 are shown in figure 5. The earthquake hypocenter data shown in figure 5 and subsequent figures are taken from a new catalog of hypocenter and intensity data for earthquakes in South America to be published this year (Askew and Algermissen, eds., 1985).

Large earthquakes (M_s about 8 or larger) have occurred in central Chile in 1570, 1647, 1657, 1730, 1751, 1822, 1835, 1906, 1922, and 1928. Many other shocks in the magnitude 7-8 range have also caused extensive damage in Chile. An example is the Chillán earthquake of 1939 that resulted in about 30,000 deaths and essentially destroyed Chillán. The 1647 earthquake heavily damaged Santiago and life loss was estimated at about 1,000 or 20 percent of the inhabitants (Lomnitz, 1970). Santiago also experienced significant damage in 1730, 1822 and 1906 as a result of offshore earthquakes that heavily damaged Valparaiso. Many other areas, and especially the cities of Concepción and Copiapó have been repeatedly, heavily damaged in historic times. Nishenko (1985) has pointed out that in the coastal zone between lat 32° and 35° S. all of the large shocks since 1906, with the exception of the 1928 Talca earthquake, are located in the vicinity of the Juan Fernandez Rise-Chile-margin intersection at lat 33° S.

Figure 6 is an east-west profile through the main shock (A-A' in fig. 5) showing earthquakes $M_s=6.0$ and larger from 1570 to 1981 together with the March 3, 1985 main shock and the large aftershock of April 9, 1985. Earthquakes that have occurred 100 km to the north and south of the profile have been projected on to the profile. Note that earthquake depths based on instrumental data are not available for many of the important shocks and for these shocks the depths have been estimated from other data. A better idea of the depth range of

earthquakes along the same profile may be obtained by plotting all of the earthquakes regardless of magnitude. This data set (shown in fig. 7) contains a much higher percentage of recent, small earthquakes for which focal depths have been computed from instrumental data.

REFERENCES

Askew, B., and Algermissen, S. T., eds., 1985, A catalog of earthquake hypocenter and intensity data for South America: Centro Regional de Sismología para América del Sur (CERESIS), Lima, Peru (in press).

Lomnitz, C., 1970, Major Earthquakes and tsunamies in Chile during the period 1535-1955: Geol. Rundschau, v. 59, p. 938-960.

Nishenko, S., 1985, Seismic Potential for Large and Great Intraplate Earthquakes Along the Chilean and Southern Peruvian Margins of South America: A Quantitative Reappraisal: Journal of Geophysical Research, v. 30, p. 3589-3615.

Plafker, G. 1985, Geologic reconnaissance of the 3 March 1985 Chile earthquake: U.S. Geological Survey Open-File Report (this report).

Richter, C. F., 1958, Elementary seismology: San Francisco, W. H. Freeman and Company, 768 p.

U.S. Geological Survey, 1984, Preliminary determination of epicenters: Golden, Colo., National Earthquake Information Service, nos. 49-84 to 52-84.

_____1985, Preliminary determination of epicenters: Golden, Colo., National Earthquake Information Service, nos. 1-85 to 22-86

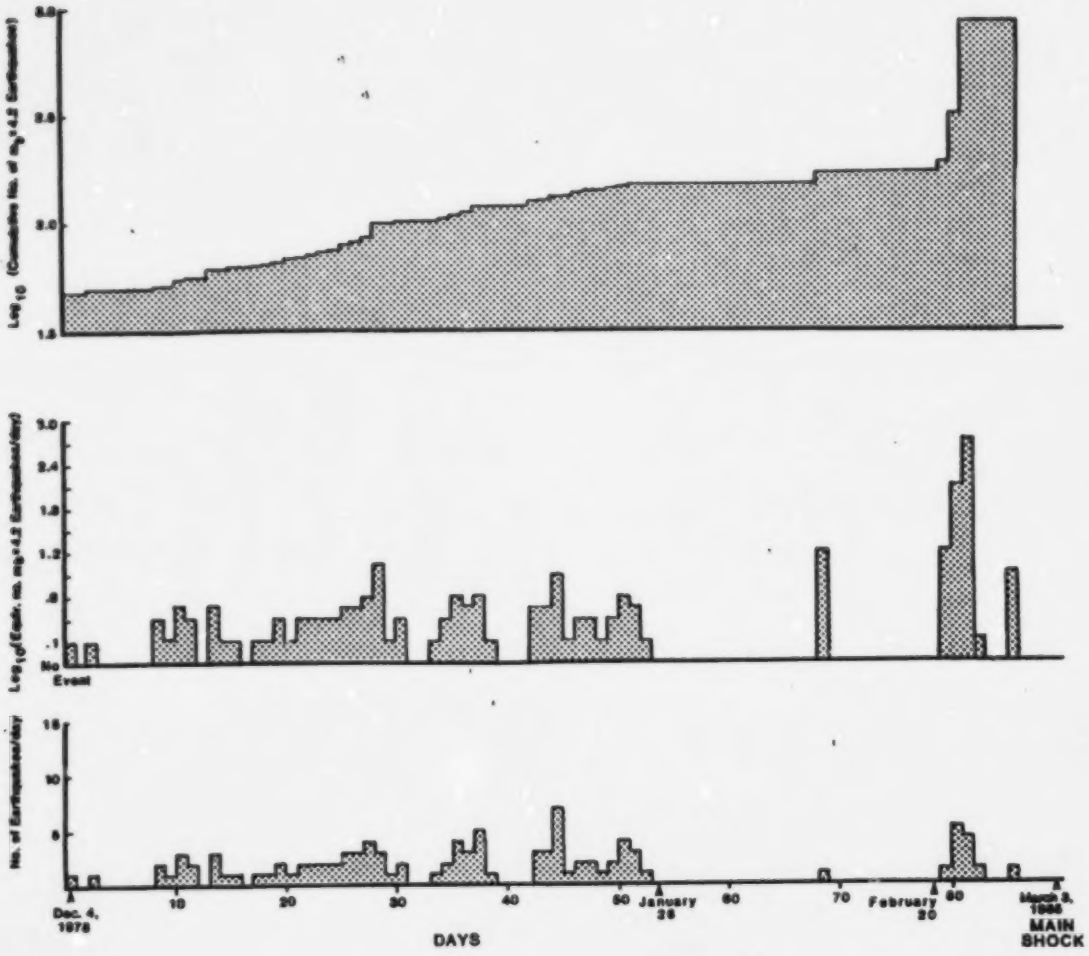

Figure 1.--Temporal distribution of preshock activity and energy release from December, 4, 1984, to March 3, 1985, in the area bounded by 32 -35 S. lat. and 70.5 -73.5 W. long., roughly the aftershock area of the March 3 earthquake. Note the lack of activity from January 26 - February 20 (day 53 to day 78), 1985, in the zone.

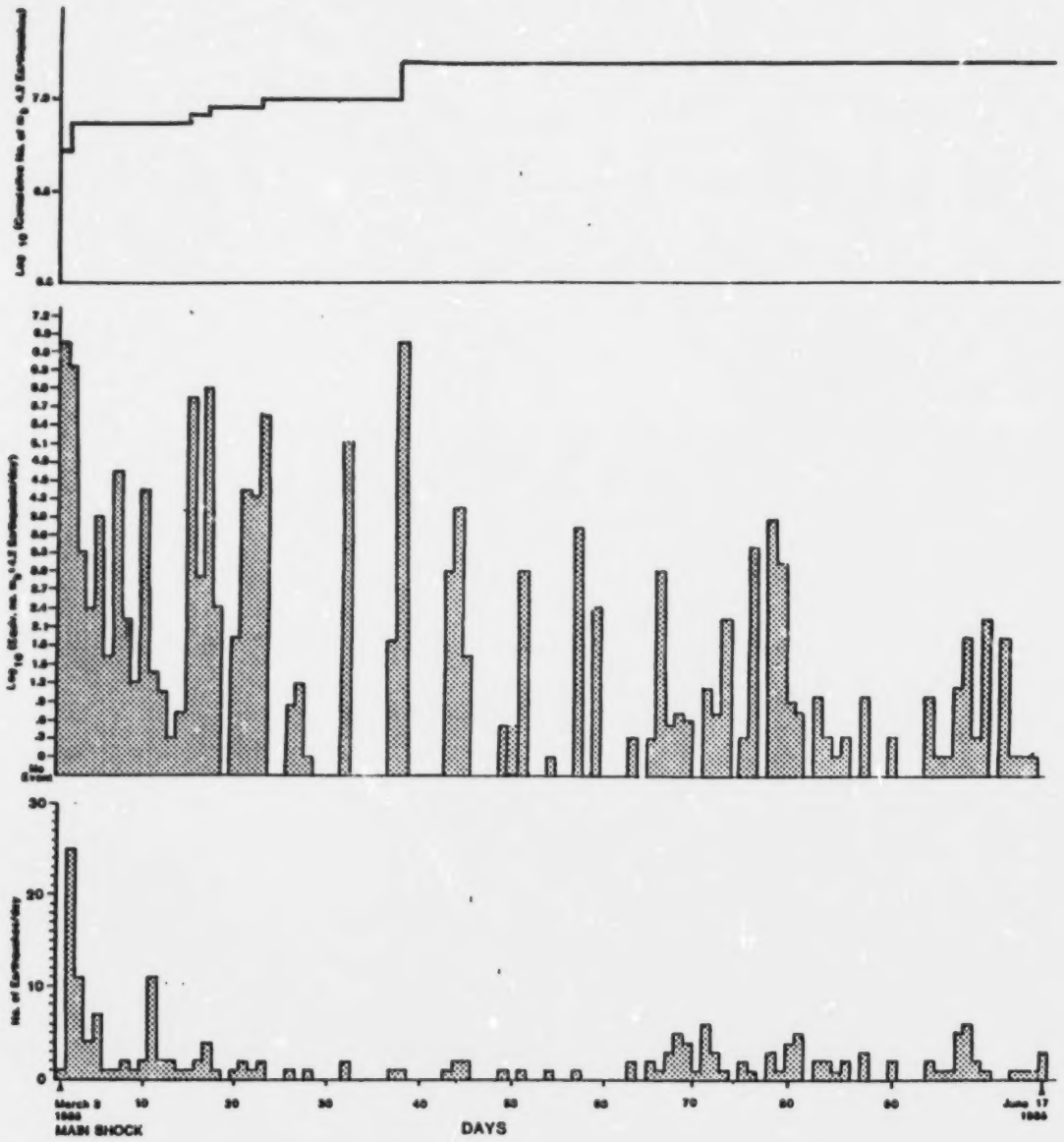

Figure 2.--Temporal distribution and energy release from March 3, 1985, through June 17, 1985 (not including the two main shocks) in the area bounded by 32°-35° S. lat. and 70.5°-73.5° W. long.

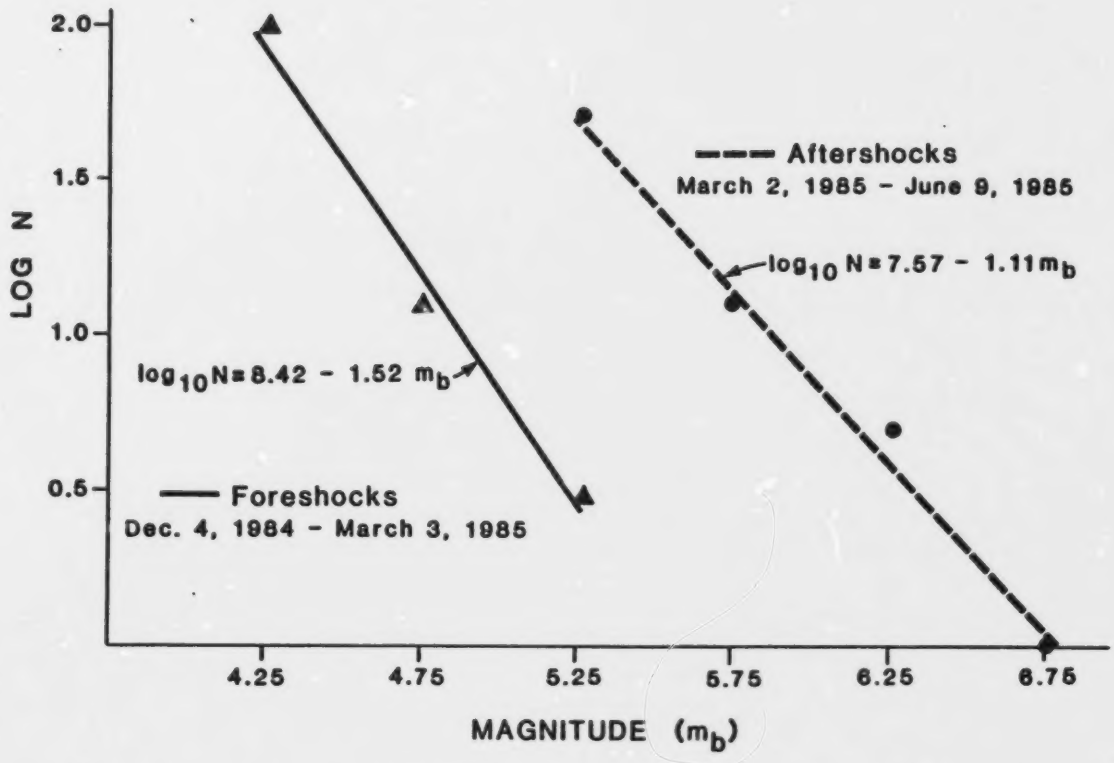

Figure 3.--Magnitude distribution of foreshocks (Dec. 4, 1984 - March 3, 1985) and aftershocks (March 3, 1985 - June 17, 1985) that occurred in the area 32°-35° S. lat. and 70.5°-73.5° W. long. N is the cumulative number of earthquakes greater than or equal to the specified m_b. The values on the magnitude axis represent a range $\pm 1/4$ magnitude unit from the labeled value.

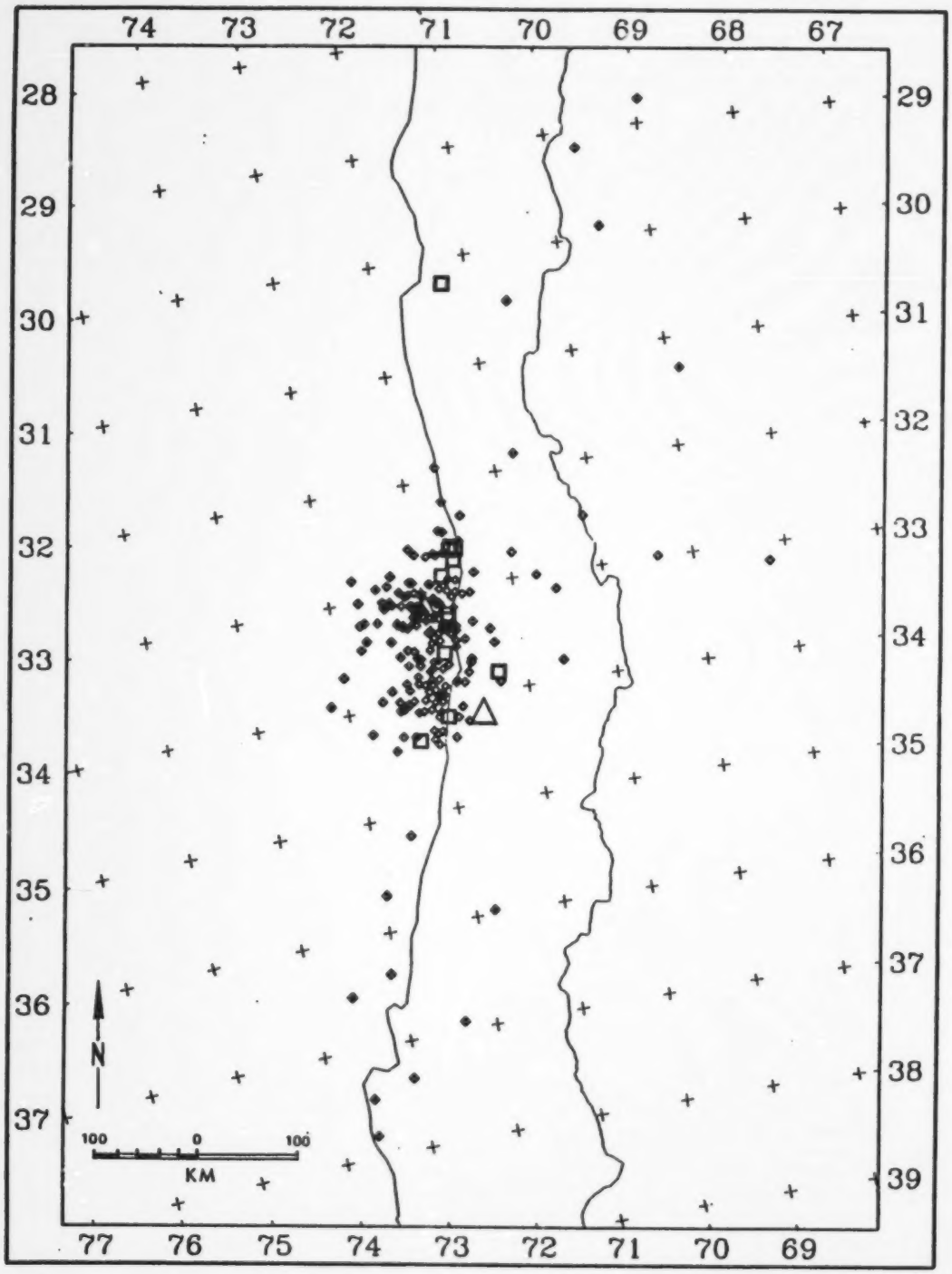

Figure 4.—Earthquakes in central Chile, March 3, 1985 - June 17, 1985. The diamonds represent earthquakes $m_b < 6.0$; The squares represent earthquakes $6.0 \leq m_b < 7.0$ and the triangle is the M_s=7.2 aftershock of April 9, 1985.

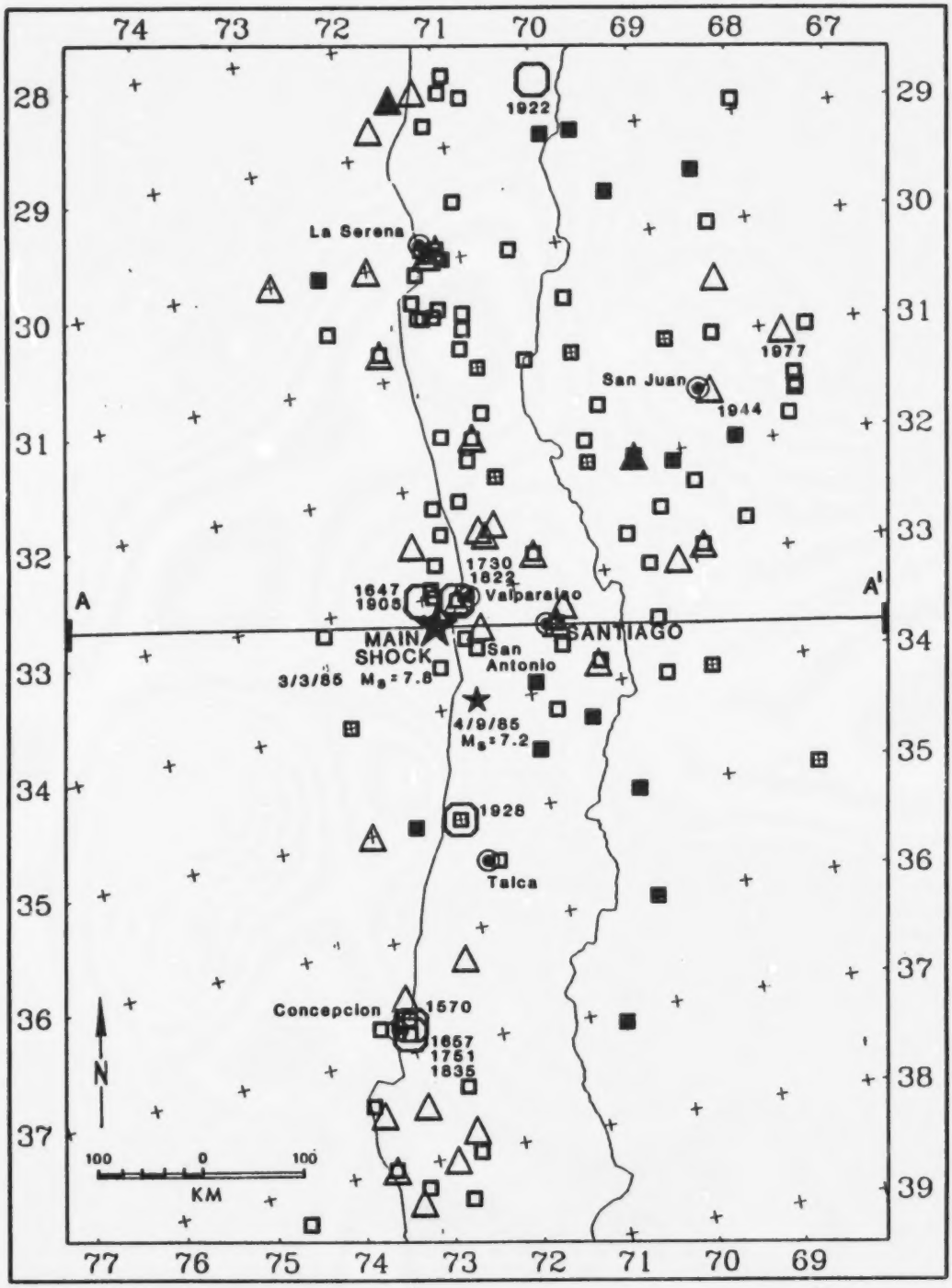

Figure 5.--Earthquakes in central Chile and western Argentina, 1570-1981. The main shock of March 3, 1985, and the large aftershock of April 9, 1985, are also shown. The large octagons represent earthquakes $M_s \geq 8.0$; The triangles $7.0 \leq M_s < 8.0$; the squares $6.0 \leq M_s < 7.0$. Open symbols represent earthquakes < 70 km in depth; solid symbols ≥ 70 km in depth. Stars represent cities. Hypocenters prior to this century are based on non-instrumental data.

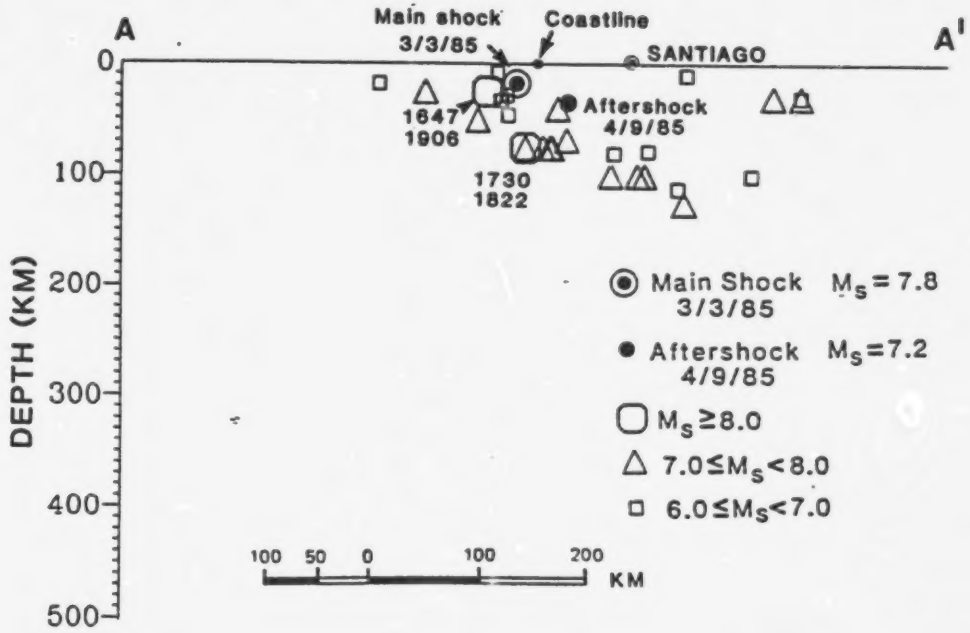

Figure 6.--East-west section, through the main shock showing the large earthquakes in Central Chile, 1570-1981, together with the March 3 main shock and the large April 9 aftershock. Earthquakes 100 km north to 100 km south of the section have been projected into the section. Hypocenters prior to this century are based on non-instrumental data.

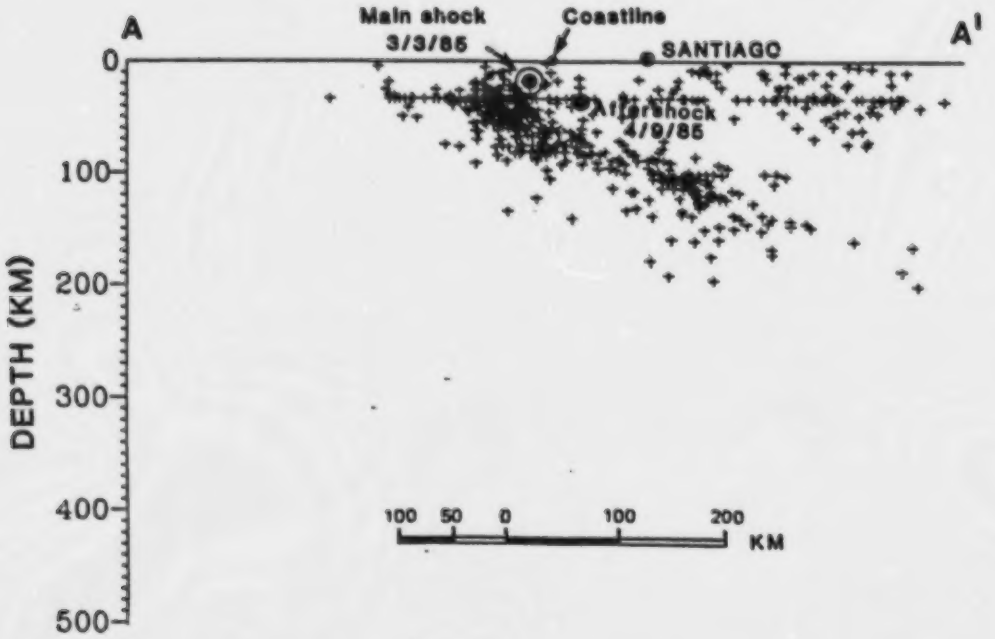

Figure 7.--Same east-west section as figure 6 showing all of the known earthquakes 1570-1981 together with the March 3, 1985, main shock and the large April 9, 1985, aftershock. Hypocenters prior to this century are based on non-instrumental data.

GEOLOGIC RECONNAISSANCE OF THE MARCH 3, 1985, CHILE EARTHQUAKE

by

George Plafker, U.S. Geological Survey,
Menlo Park, CA 94025

with contributions from

Anibal Gajardo C., Irma Gonzalez M., and Eduardo Valenzuela,
University of Chile, Santiago Chile; and J. C. Savage,
U.S. Geological Survey, Menlo Park, CA 940025

A field reconnaissance of the geologic aspects of the March 3, 1985, Chile earthquake and its associated tsunami was made by the writer from March 27 through April 1 as part of a U.S. Geological Survey four-person team effort funded by the Office of Foreign Disaster Assistance. The other U.S. Geological Survey personnel, Ted Algermissen, Paul Thenhaus, and Eugene Sembera, are geophysicists who were engaged in seismic regionalization studies of the earthquake sequence. The field work was greatly expedited by voluntary participation of Anibal Gajardo C., Eduardo Valenzuela, and Irma Gonzales from the Department of Geology, University of Chile, during the period March 27-29 and by the assistance of Gajardo in expediting logistic arrangements and obtaining data from Chilean agencies involved in post-quake emergency studies.

Primary goals of the geologic study were to determine whether the earthquake sequence was accompanied by surface faulting on land and (or) permanent vertical tectonic displacement along the coast. This type of information, together with the seismologic data, can be used to construct models for the causative faults that generated the earthquake sequence and the associated seismic sea waves as well as for interpreting the relationship of surface damage to faulting. Secondary goals of the field study were to determine the nature and distribution of surficial geologic effects of the seismic shaking, most notably compaction and liquefaction of unconsolidated deposits, and landslides. Information on these phenomena is essential for evaluating the roles of seismic shaking and foundation failure in structural damage and the potential behavior of different geologic deposits for seismic zonation.

Vertical tectonic displacements and the tsunami: The March 3, 1985, earthquake occurred beneath the continental shelf within the Peru-Chile arc which represents a zone of active convergence between the oceanic Nazca plate and the South American continental plate. Such earthquakes may be accompanied by regional vertical and horizontal tectonic displacements in and near the focal region and by tsunamis resulting from earthquake-related vertical displacement of the sea floor. Just such effects accompanied the great 1960 earthquake which affected a segment of the Chile coast extending 1,000 km south from Concepcion. Both vertical displacements and tsunamis occurred in that same region during earthquakes in 1835 and 1837.

Vertical and horizontal displacements on land can be measured by geodetic techniques where suitable pre-quake surveys are available. However, a rapid and effective method of approximating vertical displacements along the coast is through observations of the upper growth limits of sessile intertidal

organisms relative to tide levels and from observations made by local residents of tide levels relative to known reference markers along the shore. In addition, data on the nature and distribution of offshore vertical displacements may be inferred indirectly from analysis of the tsunami waves they generate.

Both the observations of intertidal organisms and observations of local fishermen or shellfish gatherers indicate that there is no detectable permanent vertical displacement of the shoreline in the area studied, which extends from Matanzas on the south to Papudo on the north. However, the occurrence of a tsunami along the entire coast near the focal region suggests that regional vertical tectonic displacement of the sea floor did occur during the earthquake. At all localities the tsunami was described as very fast-changing tides with periods of a few minutes to tens of minutes that reached to about extreme high tide levels. The amount of deformation is not determinable, but was large enough to generate water waves with half-wave amplitudes of 1.2 to 1.8 m between Valparaiso and Cartagena, and possibly as large as 3 m at Matanzas (fig. 1). Furthermore, reports that the tsunami sea level changes were noted at these coastal localities within 10 min after it started, and in some cases "immediately" after the earthquake, suggest that the eastern limit of the generative region was at or very close to the coast in most places.

There are consistent reports by local residents in the coastal area from Matanzas to several kilometers north of Algarrobo of unusually low tides for a period of 3 to 5 days following the earthquake after which the tides apparently returned to normal (fig. 1). Near Algarrobo, an estimate of the change reflects roughly 20 cm uplift. This suggests the intriguing possibility that there was a small amount of earthquake-related uplift along parts of the coast and that it was recovered in 3 to 5 days after the earthquake.

Such an effect could result from a propagating thrust mechanism for the earthquake in which the initial rupture was at the down-dip end of the Benioff zone and subsequently propagated progressively up-dip towards the Chile Trench following the earthquake as illustrated diagrammatically in figure 2. Aftershock data suggest an initial rupture zone about 100 km long and roughly 40 km wide with the eastern limit extending from just beneath the coast to 10 km inland and a depth at the coast on the order of 40 km (Mario Pardo and Lautaro Ponce, oral commun., 1985). The plate convergence rate along this segment of the Peru Trench is 9.2 cm/yr so that since the last major earthquake in 1906, the maximum elastic strain accumulation and slip along the plate boundary during the March 3, 1985 event could be on the order of 7.2 m. Figure 2 is a dislocation model prepared by J. C. Savage of the U.S. Geological Survey showing the vertical surface displacements resulting from 7.2 m slip on a propagating fault with dip of 21° and widths of 40 km (fig. 2,A), 90 km (fig. 2,B), and 120 km (fig. 2,C). The model for the initial conditions (A) causes sudden offshore uplift with maximum amplitude 2.1 m and E-W width of about 55 km and this uplift of the continental shelf in turn generated the tsunami.

The dislocation model is compatible with the available near-field data on the maximum wave heights and the short time between the earthquake and onset of the tsunami. It could also account for the reports of anomalously low tides at some coastal localities, where uplift could be as much as 50 cm, depending upon the position of the shoreline relative to the eastern edge of the focal region. Subsequent up-dip migration of the dislocation would shift the null point between uplift and subsidence as much as 12 km westward thereby

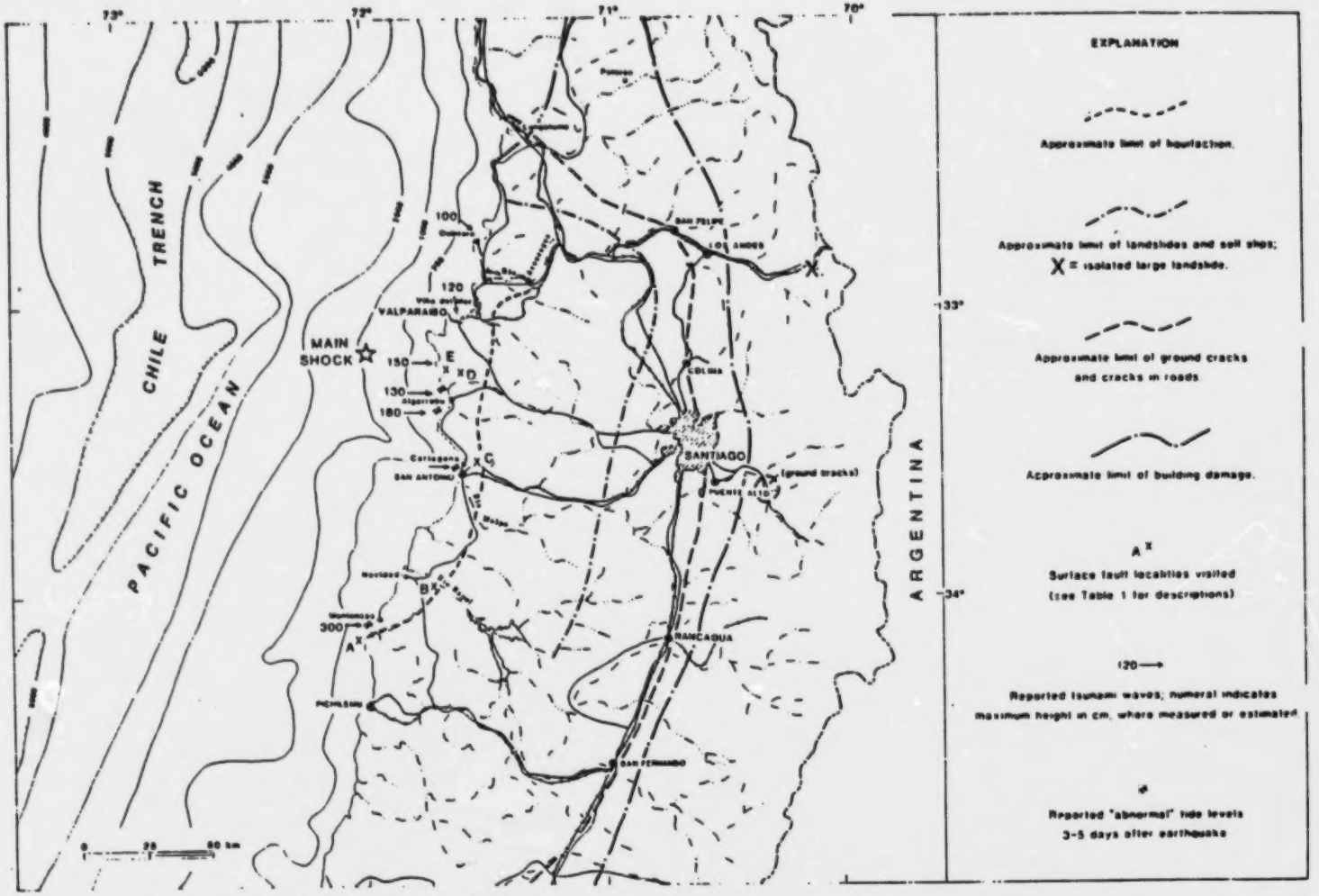

Figure 1. Area affected by the 3 March 1985 earthquake and tsunami.

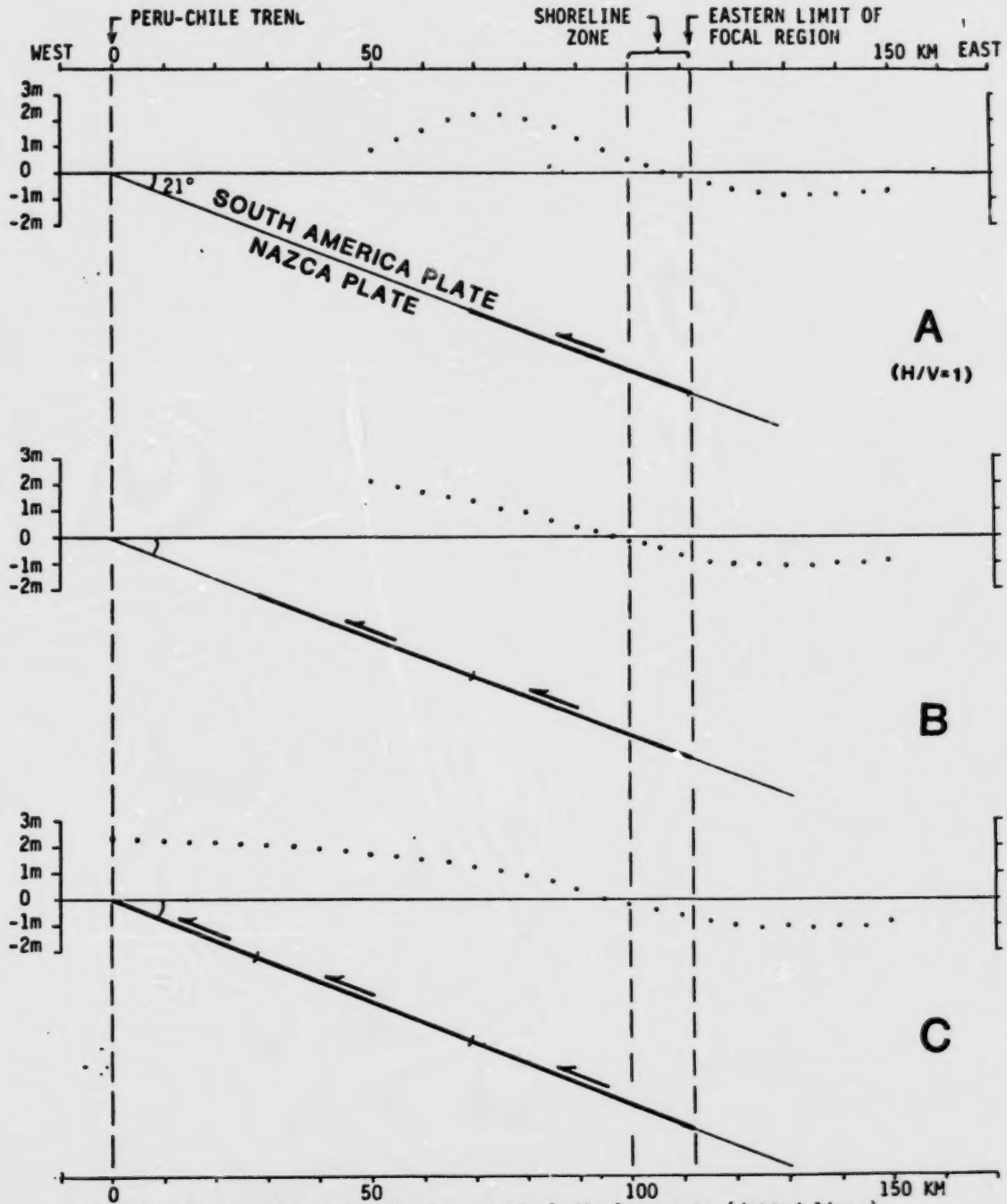

Figure 2. Dislocation model showing vertical displacements (dotted lines) resulting from a propagating thrust offset of 7.2 m along the plate boundary beneath the Peru-Chile arc. Rupture lengths shown are: A = 40 km, B = 90 km, C = 120 km.

bringing shorelines that were initially uplifted back to normal or possible even into the zone of subsidence. The model predicts that small amounts of tectonic subsidence on the order of a few tens of centimeters is possible for the more easterly segments of the coast. Although no evidence for such changes was found during my reconnaissance, small amounts of coastal submergence are inherently more difficult to detect than small amounts of emergence. The effect of subsidence may not become apparent to coastal residents until after they experience tidal cycles that include maximum annual highs and lows, which provide the best reference datums along the coast.

The dislocation model implies large permanent subsidence of as much as 120 cm at about 20-30 km east of the coast (fig. 2,C). Such displacements should be readily detectable by releveling of first-order lines that extend inland from the coast. Although the data for horizontal strains are not shown on figure 2, they are large enough to give angular changes of as much as 5 seconds of arc for favorably oriented triangulation configurations near the coast and should be easily measured by retriangulation of the first-order net in that region. Thus, suitable geodetic surveys in the coastal region adjacent to the focal region could provide crucial quantitative data on regional tectonic deformation associated with the earthquake.

A check on the reasonableness of the dislocation model chosen for the initial rupture can be obtained by comparing its theoretical seismic moment with the moment to be expected for a 7.8 M_s earthquake. Seismic moment (Mo) is given by:

$$Mo = \mu \bar{S} D$$

where μ is the shear modulus (4×10^{11} dyne/cm^2), $\bar{S}$ is average slip (7.2 m), and D is area of the fault plane (100 km x 40 km). Thus, the calculated moment of 1.1×10^{28} dyne-cm is within a factor of 2 of the moment of 5×10^{27} dyne-cm appropriate for a 7.8 M_s earthquake.

Surface faults: No evidence, either direct or indirect, was found to indicate that surface faults were activated in the focal region of the March 3, 1985, earthquake. Numerous faults that have had late Cenozoic vertical displacement, some as young as Quaternary, occur in the focal region (geologic map of the Valparaiso-San Antonio sheet, 1:250,000, Jose Corvalan D. and Andres Davila D., 1963-1964; Eduardo Valenzuela, unpub. data). The majority of these faults trend generally NW-SE, a few trend NE-SW, and at least one is essentially N-S. During this study five faults in the focal region were examined for indications of displacement possibly related to the earthquake of March 3. No evidence of renewed displacement was found. In a few localities, open extension cracks occur in steep bedrock outcrops in or near the faults that apparently result from shaking-induced gravitational settling of fracture-bounded blocks. Furthermore, although some of these faults intersect the coast, no indication of differential vertical displacement of tide-controlled shoreline features could be detected as would be expected for earthquake-related vertical offsets along these faults. Cenozoic faults checked in the field are listed below.

Table 1.--Surface faults examined
[See fig. 1 for locations.]

No.	Locality	Trend	Displacement	Age
A.	Pta. Extremo (1 km SW Matanzas)	NNE	E side down	Late Cenozoic
B.	Rio Rapel (1 km SE Rapel)	NE	SE side down 20 m+	Post-Miocene or ?Pliocene
C.	Highway 78 (2 km NE San Antonio)	WNW	NE side down	Post-early Pleistocene
D.	Loma de la Cruz	NW	SW side down	Post-Miocene
E.	Loma della Cruz	NNE	E side down	Post-Miocene

Landslides, rockfalls, and debris falls: The earthquake shaking triggered a modest number of landslides and falls or slides of rock and debris on natural slopes along the coast and in the mountains as well as in man-made cuts for highways, railroads, and structures (fig. 1). Occurrence of the earthquake towards the end of the dry season at a time of minimum ground saturation undoubtedly significantly minimized the effect of downslope mass wasting effects.

Larger rotational slides are surprisingly rare despite the moderately rugged terrain of the Coastal Mountain belt. Only one such slide, located near Navidad, occurs on a natural slope (fig. 1); all others seen were in areas of oversteepened slopes in man-made cuts for transportation facilities and structures. Rockfalls and debris falls are especially numerous along the more rugged coastal sea cliffs and in steep cuts in the late Cenozoic marine strata and old dune deposits in the coastal areas. Foundation failure due to landslides or incipient landslides caused significant damage to structures, roads, and utilities in Valparaiso, Viña del Mar, in suburbs along the coast north of Viña del Mar, and in San Antonio. Except for one large rockfall that temporarily closed a highway in the Andes Mountains northeast of Santiago (fig. 1), landsliding in these high mountains generally appears to have been minor. This contrasts markedly with the 1970 Peru earthquake, which was comparable in magnitude, location and mechanism, but which was accompanied by extensive and destructive landslides in a large area of the Peruvian Andes as much as 200 km inland from the coast.

Liquefaction and compaction of unconsolidated sediments: In a number of localities along the coast and the flood plains of rivers, water-laid saturated sediments and man-made fills responded to the earthquake shaking by cracking and settling induced by compaction and (or) lateral spreading through liquefaction. In many places, engineered fills and structures on such materials were damaged by differential settling or by extension cracking. Damage to highways and bridges or approaches, mainly from differential compaction, occurred in river flood plains throughout much of the Coastal

Mountains and in the Central Valley, but liquefaction effects were observed only along the coast and along the larger rivers at or near the coast (fig. 1). Liquefaction, with attendant lateral spreading and subsidence, has resulted in costly damage to waterfront facilities in the port cities of Valparaiso and San Antonio, has destroyed part of a major bridge near the mouth of the Rio Maipo (Lo Gallardo), and has caused damage to one span of the bridge across Rio Rapel.

In Valparaiso, lateral spreading of unconsolidated deposits along the shore has caused local cracking and misalignment of pavements, roads, and railroad lines at numerous localities. Major damage to the largest wharf facility in the port (Muelle Prat) resulted from lateral spreading of the fill placed within the perimeter bulkheads. As a consequence, there was about 58 cm extension (as determined from open cracks) across the wharf, which was originally 100 m wide, with attendant differential settling of the surface and misalignment of the railroad tracks for wharf cranes.

At San Antonio, extension and surface subsidence caused extensive damage to the breakwater and wharf facilities and to the road and railroad lines along the waterfront. Differential subsidence of as much as 90 cm of the fill relative to the breakwaters on the west wharf resulted in tilting and toppling of the wharf cranes.

The Lo Gallardo bridge across Rio Maipo is a reinforced concrete bridge 840 m long with 28 spans 30 m long on reinforced concrete piers and piling driven to 14 m beneath the piers. Liquefaction of the unconsolidated fill in the river, which is more than 30 m thick, resulted in differential settling of the northern approaches, and in lateral flow of the liquefied sediment towards the river channel in a zone roughly 100 m wide on either side of the channel. The bottoms of piers on both sides of the channel were tilted inwards towards the channel and settled vertically to the extent that one pier collapsed dropping two of the bridge spans into the river. Incipient liquefaction of sediments beneath two of the central piers of the Rio Rapel bridge, a reinforced concrete structure about 250 m long, is suggested by a shift of the span they supported as much as 38 cm in a downstream direction with up to 14.5 cm relative subsidence on the downstream side.

At the San Antonio pier and along the Rio Viña in Viña del Mar, liquefaction was accompanied by extrusion of water and sand (sand boils). Although such extrusions undoubtedly also occurred elsewhere, evidence for them was largely obliterated by the time of my reconnaissance almost 4 weeks after the earthquake.

Summary and conclusions:

A) The earthquake and tsunami were generated by relative seaward thrusting along the plate boundary that dips from the Peru-Chile Trench beneath the continental margin. The main shock rupture may have involved a 40-km-wide section of the eastern down-dip part of the plate boundary with its eastern limit about 40 km deep and within 10 km of the coast. Dislocation modeling predicts small amounts of tectonic subsidence (<50 cm) in suitably located coastal areas increasing gradually to a maximum of 120 cm subsidence 20-30 km east of the coast.

B) There were no active faults on land, in accord with aftershock data indicating consistent focal depths of 40 km or more beneath the coast.

C) Landslides and related mass gravitational movements occurred primarily in the coastal mountains in a belt about 50 km wide. However, damage resulting from downslope gravitational movements was largely limited to extensive areas of dune sands and, to a lesser extent, poorly consolidated late Cenozoic deposits that overlie crystalline bedrock in the coastal cliffs in the San Antonio, Valparaiso, and Viña del Mar areas. Considering the earthquake magnitude, landslide effects are relatively minor. This may be in part because the earthquake occurred at the end of the dry season at a time of minimum ground saturation and because much of the coastal mountain belt is underlain at shallow depth by crystalline bedrock. The importance of other factors, such as the mechanism of slip and velocity structure of the upper plate, is not known and merits further investigation.

D) Liquefaction and compaction of unconsolidated materials was largely limited to sediments and fills along the coast and on some river flood plains. Saturated fine dune and beach sand, whether in man-made or natural deposits, appears to be especially susceptible to liquefaction. The general scarcity of liquefaction effects in most major river flood plains may be attributable to the coarseness of the river deposits, which commonly are in the boulder to cobble size range near the surface.

SITE SELECTION AND FIELD EXPERIMENTS

by

S. T. Algermissen, U.S. Geological Survey, Denver, CO 80225;
E. Kausel, University of Chile, Santiago, Chile;
E. Sembera, U.S. Geological Survey, Menlo Park, CA 94025;
and P. C. Thenhaus, U.S. Geological Survey, Denver, CO 80225

The principal objective of the field experiment was to make use of the aftershock sequence to obtain digital recordings of ground motions at a number of sites having the following characteristics: (1) variable epicentral distances from the aftershocks; (2) different geological and geotechnical properties; (3) when possible, strong ground motion records of the main shock; (4) different degrees of Modified Mercalli intensity (MMI) observed at different sites as a result of the main shock.

Twelve sites were occupied during a 3-week period of time. A general overview of the geographic distribution of the stations is shown in figure 1. Figures 2, 3 and 4 show the locations of each site in more detail. Table 1 contains the site number (used to identify the sites in figs. 2, 3 and 4) a preliminary description of the material beneath the site, a preliminary estimate of the Modified Mercalli intensity (MMI) observed as a result of the main shock and information about accelerations recorded at sites during the main shock.

REFERENCES

Corvalán, D., José and Munizaga, S., Fernando, 1972, Edades, radiométricas de rocas intrusivas y metamórficas de la Hoja Valparaíso-San Antonio: Inst. Invest. Geológicas, Chile, Boletin no. 28, 40 p.

Grimme, K., and Alvarez Sch., L., 1964, El suelo de fundación de Valparaiso y Viña del Mar: Inst. Invest. Geológicas, Chile, Boletin no. 16, 60 p.

University of Chile, 1985, Informe preliminar de los resultados de la red nacional de acelerografos para el terremoto del 3 de Marzo de 1985: Dept. de Ingenieria Civil, 1 p.

Valenzuela, B. Gloria, 1978, Suelo de Fundacion del Gran Santiago: Inst. Invest. Geológicas, Chile, Boletin no. 33, 45 p.

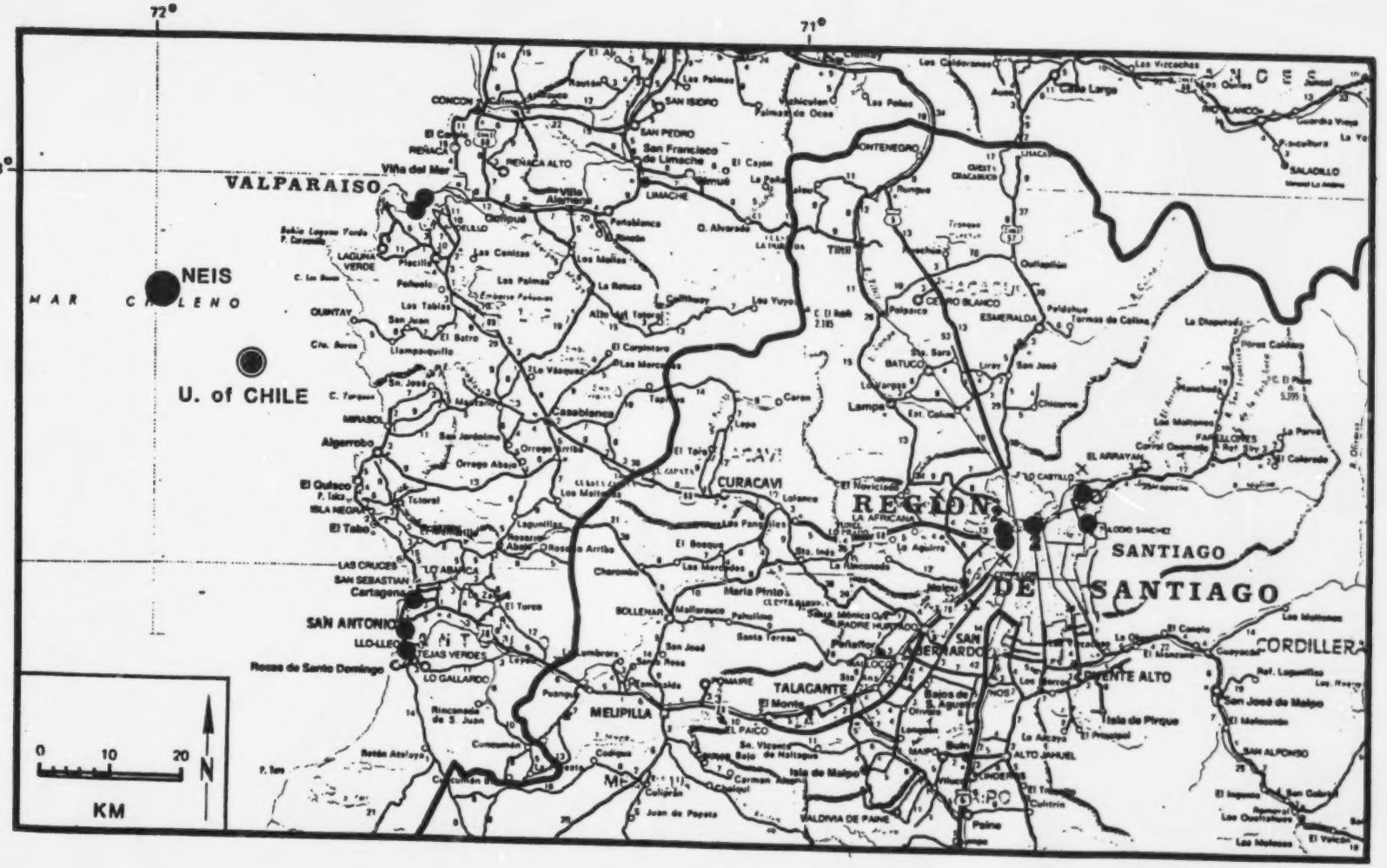

Figure 1.--Location map showing the geographic relationship of the 12 recording sites (solid circles) and the epicentral locations of the main shock of March 3, 1985 as determined by the National Earthquake Information Service, U.S. Geological Survey and the Department of Geophysics, University of Chile. The number "2" beside two of the solid circles means that two sites are in the vicinity of the circle.

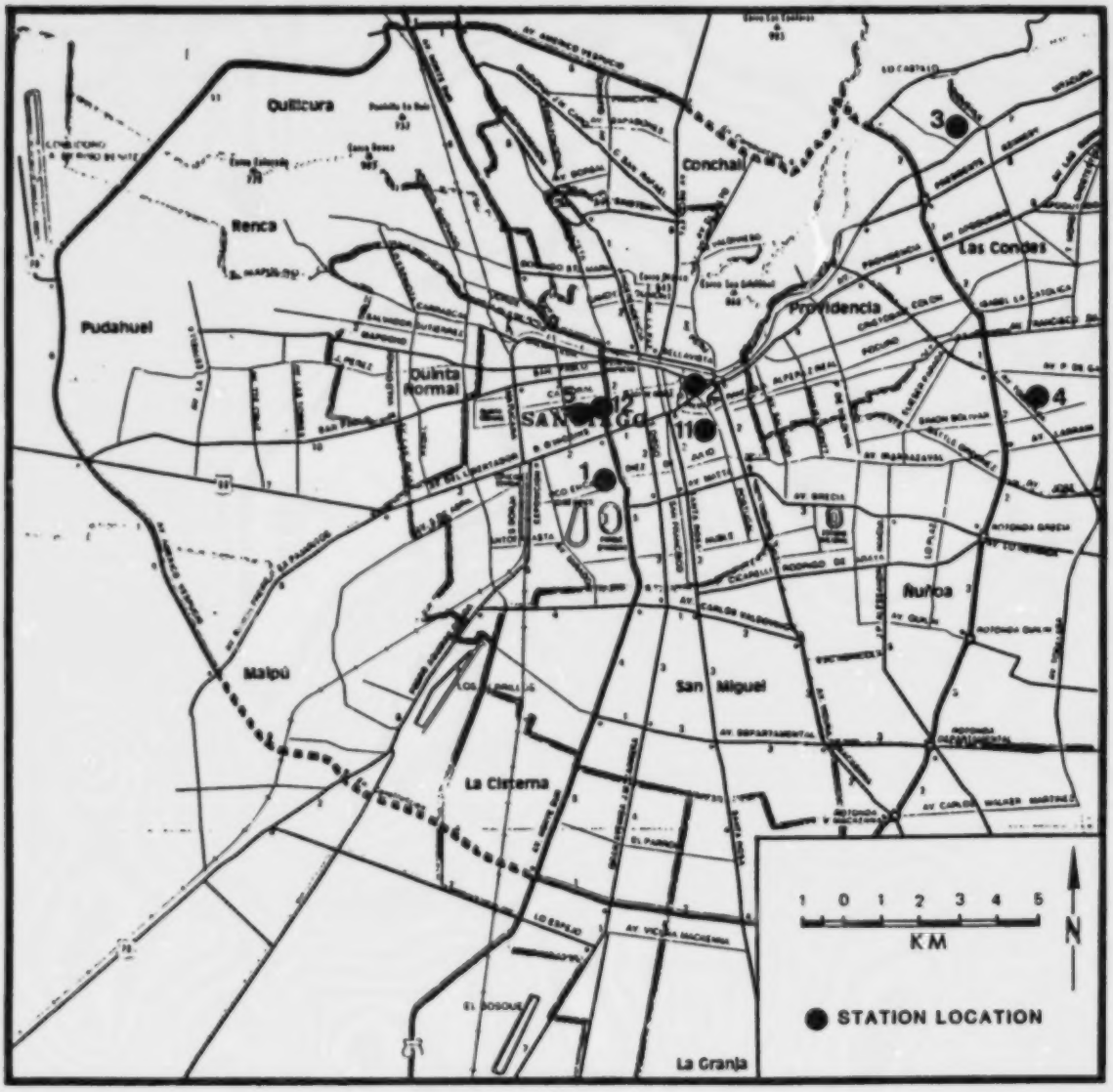

Figure 2.--Recording sites in Santiago (solid circles). The numbers identify the sites listed in table 1.

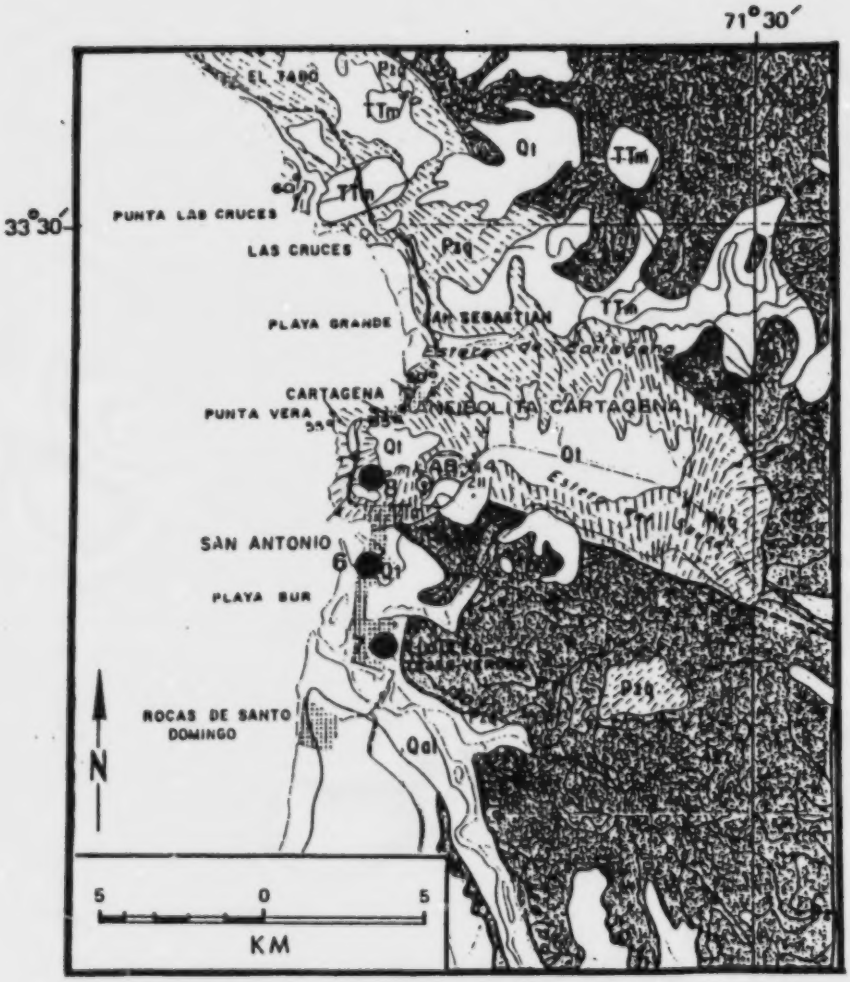

Figure 3.--Recording sites (solid circles) in Llolleo, Barranca (San Antonio) and Cartagena (the map is adapted from Corvalán and Munizaga, 1972). The numbers identify the sites listed in table 1. Qal = Quaternary alluvial deposits and dunes; Qt = Quaternary terrace deposits; TTm = Upper Tertiary marine sedimentary rocks including the Navidad formation (Miocene) and Pliocene strata; Pzq = Quintay formation (lower Paleozoic and older) amphibolites and gneisses.

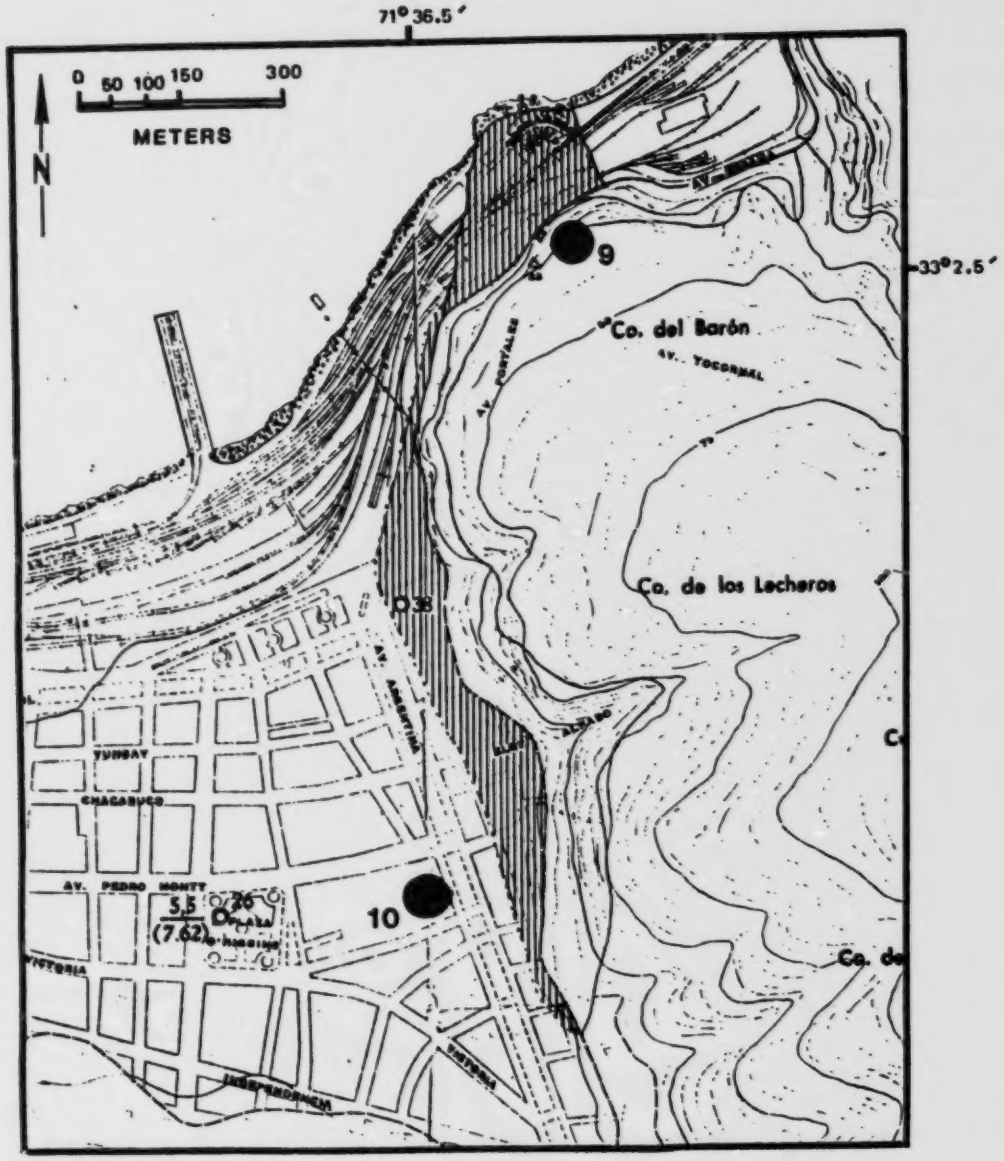

Figure 4.--Recording sites (solid circles) in Valparaiso (the map is adapted from Grimme and Alvarez, 1964). The large numbers (9, 10) identify the sites listed in table 1. Station 10 is located on artificial fill and Station 9 on a granite and amphibolite gneiss.

TABLE 1.—Location and Characteristics of Recording Site

Site no.*	Location	Site geology**	Observed MM intensity (main shock)	Comments
1 (SAA)	Dept. of Geophysics, Univ. of Chile Blanco Encalada 2085 Santiago (fig. 2)	Mapacho River outwash material, boulders up to 80 cm in diameter, sandy, limey and clayey gravels, sandy limestones, muds and clays, thickness at the site is greater than 100 m.	VII	
2 (SAB)	Vault of seismograph station "Santa Lucia" (no longer in operation) north slope of Cerro Santa Lucia, Santiago (fig. 2)	Andesite plug	VI	Accelerograph operated at this site for a number of years but not currently in operation.
3 (SAC)	Residence, Avenida Buenaventura 1696 Santiago (fig. 2)	Same as site 1	VI	
4 (SAD)	Residence, Avenida Echenique 6504 Santiago (fig. 2)	Debris cone material grading downslope from blocks of limey sand predominating at the the apex of the cone. Downslope the deposits show some stratification.	VII	
5 (SAE)	Collegio Pedro de Valdivia (fig. 2)	Same as site 1	VII	
6 (SAN)	Provincial Administrative Bldg., Barranca (1.5 km south of the center of San Antonio) (fig. 3)	Remnants of terrace deposits, very sandy.	VII	

TABLE 1.—Location and Characteristics of Recording Site—Continued

Site no.*	Location	Site geology**	Observed MM intensity (main shock)	Comments
7 (SCH)	School at Llolleo (fig. 3)	Same as site 6	1X	This school was extensively damaged and was partly torn down after the earthquake. During the mainshock, a maximum horizontal acceleration of 0.67 g were recorded on Univ. of Chile accelerograph (Univ. of Chile, 1985).
8 (CAR)	Municipal Bldg. Cartagena (fig. 3)	Amphibolite and granite gneisses	VI	
9 (VAL)	Univ. Frederico Santa María, Valparaiso (fig. 4)	Amphibolite and granite gneisses	VI	
10 (VC4)	Church, Valparaiso (fig. 4)	Artificial fill	VIII	
11 (END)	ENDESA Bldg., Santiago	Same as site 1	VI	The only accelerograph record of the main shock recorded in Santiago was at this site. Maximum horizontal acceleration .11 g. (Univ. of Chile, 1985).

TABLE 1.—Location and Characteristics of Recording Site—Continued

Site no.*	Location	Site geology**	Observed MM intensity (main shock)	Comments
12 (AGU)	Basilica Salvador	Same as site 1	VIII	

*The alphabetic code for each site is used in the computer printouts throughout this report. The numbers are used here to simplify the identification of sites on various illustrations.

**For sites 1, 2, 3, 4, 5, 11 and 12, site geology taken from Valenzuela (1978). For sites 6, 7 and 8, from Corvalán and Munizaga (1972). For sites 9 and 10, from Grimme and Alvarez (1964).

THE RECORDING SYSTEM

by

J. Sena, C. Dietel, E. Sembera, G. Maxwell,
G. Jensen, J. Gibbs, R. Borcherdt, and
J. VanSchaack, Menlo Park, CA 94025

The recording system used in this study is the "General Earthquake Observation System" (GEOS) (fig. 1) designed for use in a wide range of seismic studies. The system is designed around a central-processing-unit (microcomputer) for control of modular software and hardware components. The six channel system was equipped with a three-component forced-balanced accelerometer (Kinemetrics) and a three-component velocity transducer (L-22, Mark Products).

The digital seismic signals were recorded on a cartridge style (data quality) magnetic tape at a throughput rate of 1200 samples per second. The system was operated in the self-trigger mode. Trigger ratios of 4:1 and 2:1 were used (STA/LTA, fig. 1) depending upon cultural noise levels. Butterworth filters selected at 50 Hz were used throughout the recording period (fig. 2). Two seconds of pre-event memory for recording onset of seismic events were used in the self-trigger mode. Timing signals were provided by an internal clock which was set to a master clock or synchronized automatically to WWVB. The response of the system with a three-component velocity transducer and accelerometer is shown in figure 3. The response shown in figure 3 is that of the system using a L-4 geophone with a natural frequency of 1 Hz. The L-22 geophones used in this study have a natural frequency of 2 Hz; this would have the effect of shifting the corners of the response curve 1 Hz to the right. A manuscript detailing the developmental motivation, systems functions, and adaptability has been submitted for publication by Borcherdt and others (1985) in the Seismological Society of America Bulletin.

REFERENCES

Aki, K., and Richards, P. G., 1980, Quantitative seismology theory and methods: San Francisco, Calif., W.H. Freeman and Co., v. 1, 557 p.

Borcherdt, R. D., Fletcher, J. B., Jensen, E. G., Maxwell, G. L., VanSchaack, J. R., Warrick, R. E., Cranswick, E., Johnston, M. J. S., and McClearn, R., 1985, A general earthquake observation system (GEOS): Submitted to Seismological Society of America Bulletin.

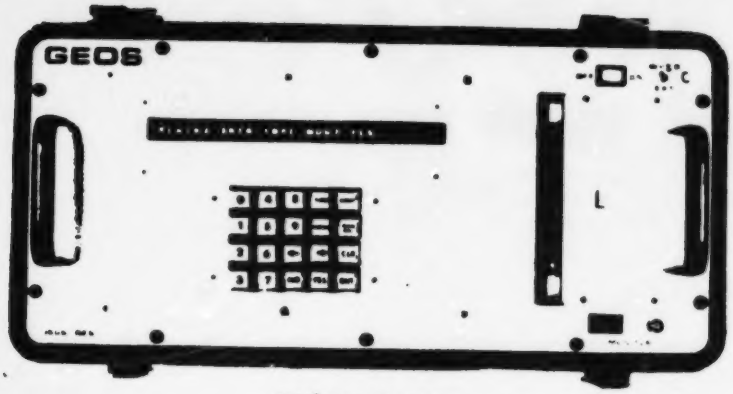

GEOS* Specifications

Microcomputer and Communications

Internal CPU: CMOS, 12 Bit.
External CPU: optional.
Data transfer:
  Internal: Direct Memory Access
  I/O Port: RS-232 compatible baud rate programmable to standard rates.
  Telecommunications: UART, Modems optional.
  Analog playback via A/D.

Program Memory

Executable Memory: 8K 12 Bit word CMOS RAM.
Program Storage: 16K 12 Bit word CMOS PROM.
Alternate Program Storage: Programs may be stored on magnetic tape for loading directly into program RAM.

Sensor Inputs and Signal Conditioning

Input Channels: 6 balanced differential inputs, program selectable.
Preamplifier Dynamic Range: greater than 100 dB at 0 dB gain, programmable in 6 dB steps 60 to 0 dB.
Filters: low pass Butterworth, 42 dB per octave; program selectable, 17 Hz, 33 Hz, 50 Hz, and 100 Hz; high pass .1 Hz 6 dB per octave.
Calibration: Internal, automatic with or without sensors.
Transient Protection: ± 15 V

Analog to Digital Conversion

Resolution: 16 bits (1 part in 65,536).
Stability and Linearity: ± 1 count-no missing codes over full temperature range of -20°C to + 60°C.
Conversion Rate (Total samples per second for all active channels): 1200 samples per second maximum, .29 samples per second minimum; programmable as 1,200/N where N is 1 through 4,096.

Pre-Event Data Memory

Size: 4,096 words, 16 bits per word.
Pre-trigger memory: Five, 512 word blocks minimum at 1,200 samples per second (2.14 seconds), six 512 work blocks at 300 samples per second (10.24 seconds), program selectable.

Mass Data Storage/Retrieval

Cartridge: Read/Write 3M type, 1600 bpi.
Tape capacity: 3,680 512 word blocks (1.88 million samples) typical for 450 ft. tape, 26 minutes continuous record time at the maximum sample rate.
Tape Speed: 30 ips write or read.
Slave Recorders: 2 optional, separate housing.

Time Control

External:
  WWVB Receiver: Automatic synchronization of internal clock to WWVB under program command.
  Master Clock: Synchronization of internal clock with external pulse and corresponding time corrections derivable at selectable times under program command.
  Manual: Time entered through keyboard and synchronized manually.
Internal:
  Frequency: 3 MHz.
  Temperature Stability: ± 1 x 10^{-6}; - 20°C to + 70° C.
  Aging Rate: less than 5 x 10^{-7} per year.

Operator Interface

Operation Environment: English language commands under software control.
Display: 32 character, alphanumeric display, 18 segment, character height .15 in. LED with optical filters.
Keyboard: Mechanical switch with dust cover and water seal, 20 button keyboard with numeric and function entry.
Status Checks: Time, battery voltage, no. of events, % of tape used, elapsed time since power on.
Debug: single and subroutine stepping.

Operating Modes

Self triggering:
  Near field: Selectable short term average (STA), long term average (LTA), ratio.
  Teleseismic: Comparative ratios for two selectable frequency bands.
Pre-set time: record at selectable times and intervals.
Both: operate in both pre-set time and self triggering modes.
Manual: record under keyboard control for start-stop functions.

Power Requirements

Voltage, current: + 24 VDC nominal ± 15%, 40 mA nominal in operating mode with display off, 300 mA nominal with display on, 600 mA with display on and recording.
Internal batteries: ± 24 V, 5 AH Gates type, will operate about 3 days on internal batteries, connector provided for internal battery charging or external battery operation.

Physical and Environmental Requirements

Case Type: Waterproof aluminum case, 20 1/2" long, 9 7/8" wide 13 3/4" high.
Weight: 47 lbs. with internal batteries.
Operating Temperature Range: - 20°C to + 60°C, 15% to 95% rel. humidity.

---

* Patent pending.

Figure 1.--Specifications for GEOS recording system.

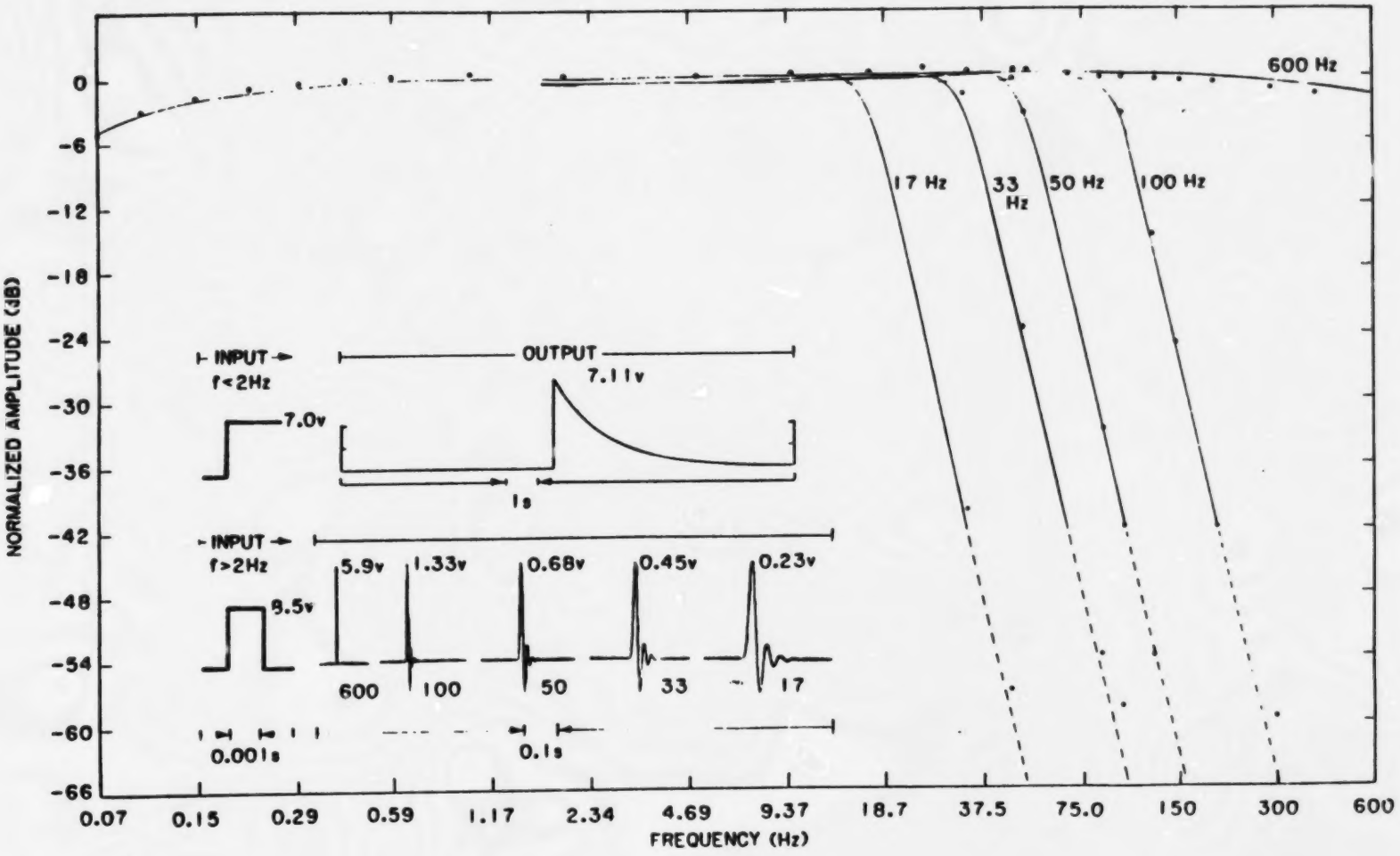

Figure 2. Normalized amplitude response of the GEOS to steady-state (symbols) and transient input signals (curves) with software-selectable antialiasing filters of 17, 33, 50, 100 Hz, and a single 600 Hz high-cut Butterworth filter.

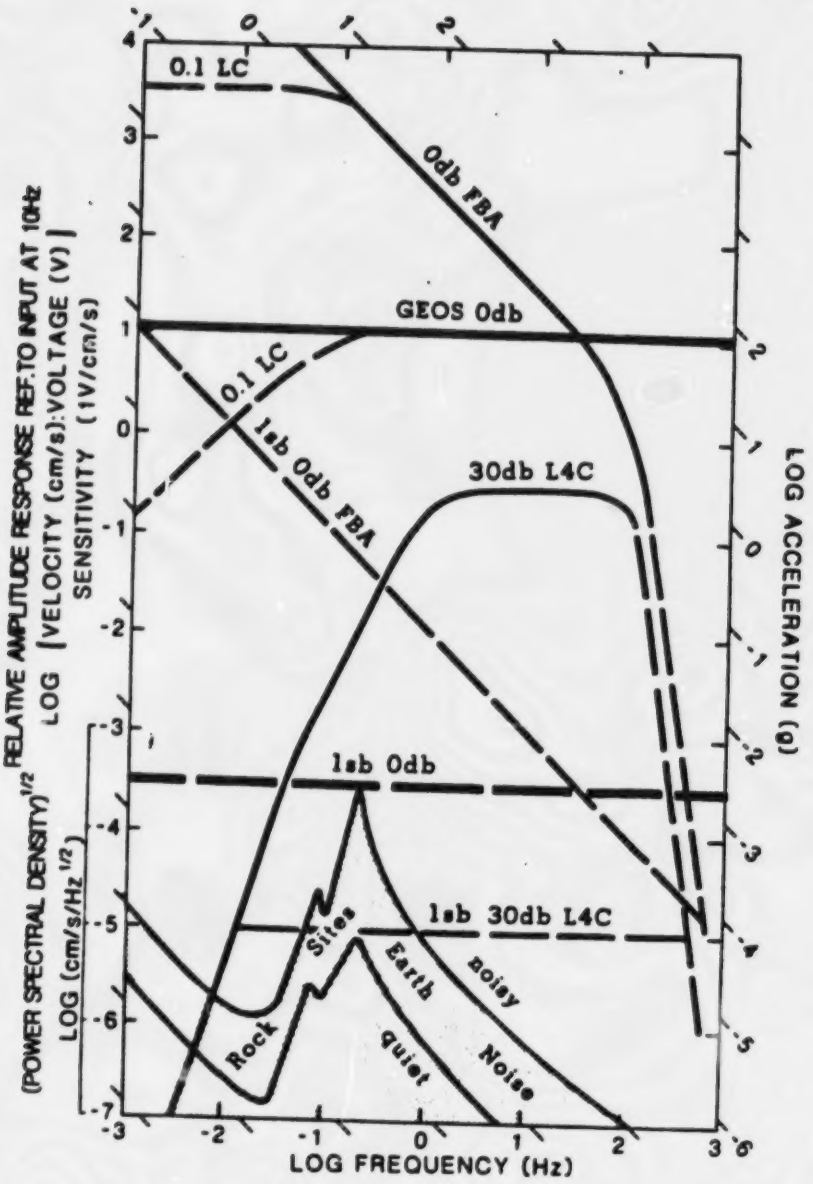

Figure 3.--Relative amplitude response of the GEOS recorder, GEOS with L4-C velocity transducer and forced balanced accelerometer (FBA), and square root of power spectral density for Earth noise (Aki and Richards, 1980). Amplitude responses were determined for recorder with constant input voltage of 10V, for recorder with L4-C constant input velocity of 10 cm/sec of 10 V at sensitivity of 1 V/cm/sec at 10 Hz, and for recorder with FBA with constant input acceleration of 2 g. Two sets of sensors operating simultaneously and linear dynamic range of 96 dB allow system to record 10 Hz signals with amplitudes ranging from 2 cm in displacement to 2 g in acceleration on scale without operator intervention.

DATA PROCESSING AND COMPUTATION OF SEISMOGRAMS

by

J. Watson and C. Mueller, U.S. Geological Survey, Menlo Park, CA 94025;
and D. Carver, U.S. Geological Survey, Denver, CO 80225

Aftershocks following the May 3, 1985, Chile earthquake (M_s=7.8) yielded an extensive set of digital strong motion recordings. The aftershock data set consists of forty-five DC300XL data cartridges from twelve stations recorded on wide-dynamic-range GEOS instruments (Borcherdt and others,1985). Each GEOS operated in trigger mode, simultaneously recording six channels of ground motion at 200 samples-per-second-per-channel: three-component ground acceleration (Kinemetrics FBA-13 force-balance accelerometer) and three-component ground velocity (Mark Products L-22 geophone). FBAs were recorded at relatively low gain in order to obtain unclipped recordings of large ground motions while geophones were recorded at higher gain in order to obtain high-signal-to-noise recordings of smaller ground motions. This scheme provided high quality recordings over a wide range of ground motion amplitude. No clipped records were observed. Each GEOS clock was set once at installation using a portable master clock; thereafter clock-drift errors were not measured and clocks were allowed to drift without adjustment. For this reason event times can be used only to correlate trigger times for the purpose of event identification. Other instrument parameters are described elsewhere in this report.

Data cartridges were returned to Menlo Park for processing. During playback, the computer directory structure (and the subsequent magtape archival structure) were organized by increasing trigger time. Data cartridges were played back with a Tandberg TDC3000 digital cartridge recorder onto a PDP11/70 minicomputer. The software interface is the FORTRAN program RDGEOS written by Gary Maxwell of the USGS, Menlo Park. The data were demultiplexed and stored, one trace per file, in blocked binary format. Each file name consists of 13 characters following the Branch of Engineering Seismology and Geology file name convention:

```
char 1-3 --- Julian day
char 4-5 --- hour
char 6-7 --- min
char 8 --- seconds ('A'=0-3, 'B'=3-6, ..., 'T'=57-60)
char 9 --- component ('1-3'=acceleration, '4-6'=velocity)
char 10 --- '.'
char 11-13 --- station-instrument identifier
```

Each file consists of two header blocks which contain relevant field and playback parameters followed by data blocks. Figure 1 is a plot of trigger times, per station, (for all events) versus Julian day.

With the files on disk two archival tapes were made and all seismograms were plotted for preliminary seismic interpretation. The data set was then winnowed using DSD map (Cranswick and Dietel, 1985) so that single-station triggers were excluded. Considering the overall network configuration

(station-to-epicenter distances ranged up to 100 kilometers), a twenty-second sliding window was chosen in order to select common-event triggers. The winnowed data set was then copied to the VAX-11/750 minicomputer for more detailed seismic analysis. Table 1 lists aftershocks that were recorded at two or more stations. Magnitudes were calculated by the University of Chile from the durations of seismograms recorded by their local network and are preliminary (E. Sembera, written commun., 1985). The three letter station-instrument codes appear in the first row and the origin times of events appear in the first column. If a station recorded an event, character 8 of the file name (the triggertime 'seconds' character, a useful file identifier) appears in the table. Of 1082 triggers from all twelve stations, 55 events were recorded at two or more stations, 12 events at four or more stations, and six events at six stations.

Figures 2 through 35 are scaled-amplitude plots of recorded velocity for all events occuring at four or more stations plus several events of engineering interest recorded at fewer stations. Velocity is shown in these plots because, for the smaller ground motions, velocity traces are higher quality than acceleration for the reasons given above. In each plot vertical-component traces are plotted at the top (positive amplitude corresponds to upward ground motion) followed by first-horizontal-component traces (positive amplitude corresponds to northward ground motion) second-horizontal-component traces (positive amplitude corresponds to eastward ground motion). Hypocentral P-arrival times are aligned at one second to facilitate waveform comparison. The peak amplitude is annotated on each trace. Figures 36 and 37 show all six components for events 0840515A at SAC (magnitude=5.5) and 0931306J at VAL (magnitude=5.3), respectively. These plots show the quality of the data for two relatively large events and allow a direct comparison between acceleration and velocity.

REFERENCES

Borcherdt, R. B., Fletcher, J. B., Jensen, E. G., Maxwell, G. L., Cranswick, E., VanSchaak, J. R., and Warrick, R. E., 1985, A general earthquake observation system (GEOS): Submitted to Seismological Society of America Bulletin.

Cranswick, E., and Dietel, C. N., 1985, DSDMAP: Digital seismic data management/analysis package: U.S. Geological Survey Open-File Report (in preparation).

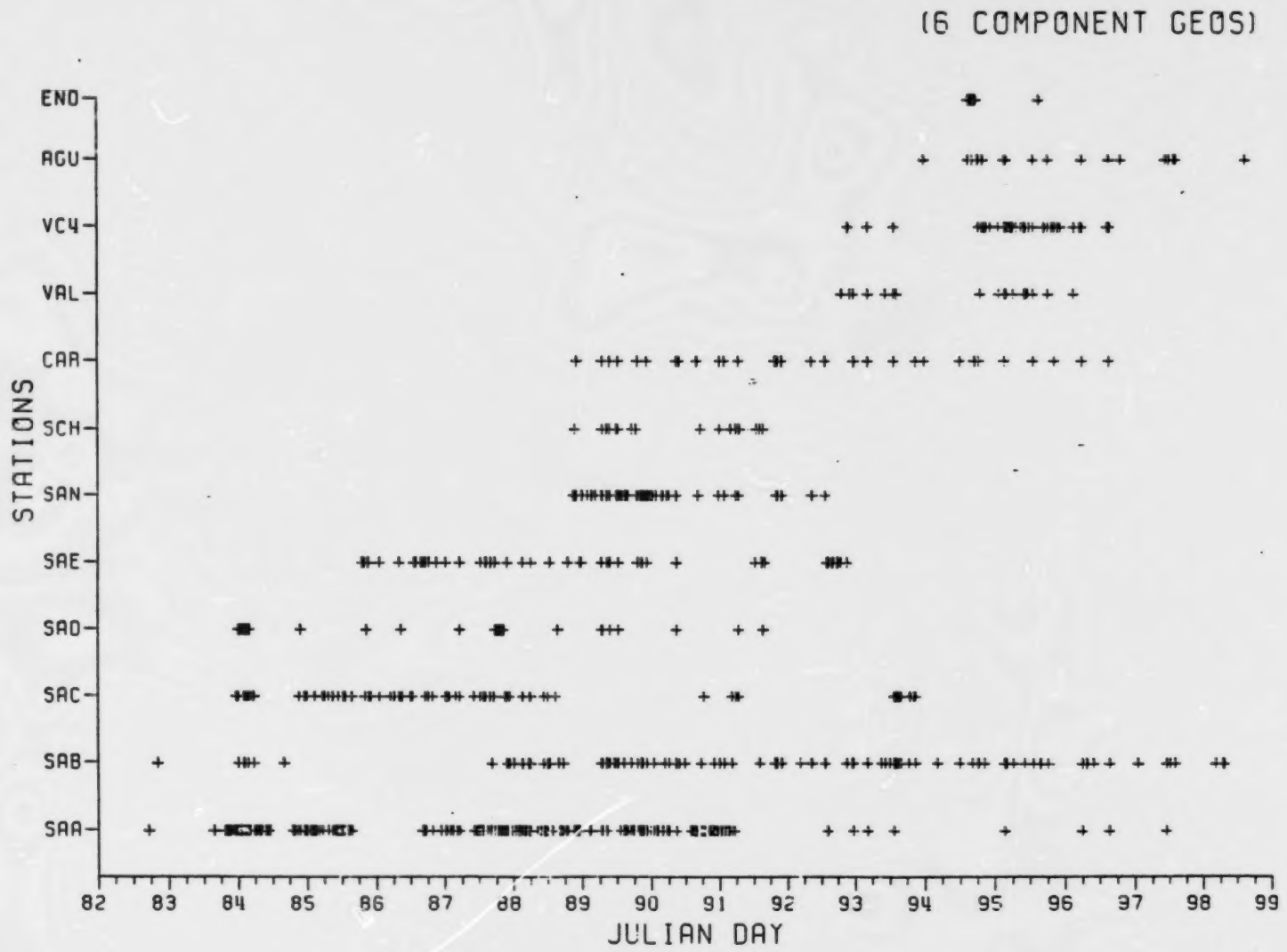

Figure 1.--Plot of trigger times versus Julian day for all stations. Recorded ground-motion durations typically range from 20 to 100 seconds.

Table 1.--Events recorded by two or more GEOS instruments. (Times correspond to ES&G Branch filename convention (see text). Preliminary duration magnitudes are from the University of Chile local network.)

WHERE CUT=[illegible], TRACK= 5.0, TAHEAD= 20.0. 2 RECORDS TO DECLARE AN EVENT.

	MEI	SAA	SAE	SAC	SAD	SAE	SAN	SCH	CAF	VAL	VC4	AGU	END
08323126		F		F									
08323466	4.2	F	E	F	D								
08400018		1			E								
08400256		E			E								
08401268		E			E								
08401296	4.4	K	K	K	K								
08401556	4.6	M	M	K	K								
08402096		K		L									
08402416		D		E									
08402576		F			I								
08403046	3.9	C	C	C	C								
08403206		I			D								
08403466		E		F									
08405146	5.5	I	A	A									
08407236		I											
08422416	4.8	G		F									
08422496		G		F									
08423316	0.0	J		K									
08501576		J											
08502146		F		F									
08507036	4.5	J		K									
08510216	4.4	L		K									
08511596	0.0	L		M									
08512376	0.0	M		I									
08520466	4.4			E		E							
08600386	4.4			K		K							
08607326	4.5			C		I							
08608106				E	F								
08615506		H				M							
08616526		D		D		D							
08617546	4.3			D		M							
08623536	4.4	P		G		F							
08700216		C											
08704436	4.6	I		S	I	I							
08709496	4.2	E		I									
08711596		F		G									
08717076					S								
08721236		A	G	A		A							
08722096			G	A									
08802516		S	I	A		I							
08804596		L	L										
08805136	4.3	J	J	K									
08805466		E	E	D		E							
08810136		F	F										
08810206			F	F									
08811426			S										
08817096		D	E										
08906186	4.3	G	G		I	G	C						
08906336	4.3	G	G		C		N	K	K				
08907586			B				R	R					
08908146	4.3	A	A			A	R	R					
08909056	4.4		K		L	L	H	H	H				
08911296	4.1						E	E					
08912106	4.7		F		S	F	N	N	N				
08916486	4.7	S	S			S	O		A				
08920056	0.0	C	C			C							

Table 1.--Events recorded by two or more GEOS instruments--Continued

	NET	SAA	SAE	SAC	SAD	SAE	SAN	SCH	CAR	VAL	VC4	AGU	END
08920206R		S	S			S	R						
08921521F		F					H						
08922091T	4.5	T	T			T	B		A				
08923311K		K					M						
09005440			S				O						
09008141			D				T						
09008250	4.6	H	H		H	H	D		D				
09009220			M						J				
09021350		A	I										
09023420			J					J	H				
09101120			E				A		A				
09103560		F	F	F									
09105170				I			F	F					
09106190	4.4			D	D		T	T	C				
09119070			G						M				
09120090			H				H		H				
09121260			N				L		L				
09121390			N				K		K				
09208010			I				G		Q				
09208230			J				K						
09213020	4.4		S				N		C				
09220410			L			F							
09222590			E						L	I			
09223030	4.7	P	E							L			
09303570	4.7	S	S						O	N	N		
09310150	4.3		L							H			
09313060	5.3	N	N	N					L	J	J		
09313210			J	I									
09313380			C	N									
09314080			I	I						S			
09314420			G	E									
09315430			G	G									
09320410	4.7		P	P					S				
09411410			C						M				
09417540			C									O	
09418060	4.3		J									R	
09418140			J						K		F	K	
09420050			K								H		
09502530		L	L						K	K	N	L	
09503120			E							E	E		
09503340			G							H	H	G	
09505510			M							I	K		
09509460										C	B		
09510200										F	P		
09512400	4.2		T						T	D	D	T	
09517440			H								A	H	
09519570									P		F		
09605250		K	J						H		P	K	
09614420	4.3	A	T						S			A	
09710290		H										H	
09711350			C									C	
09713290			N									O	

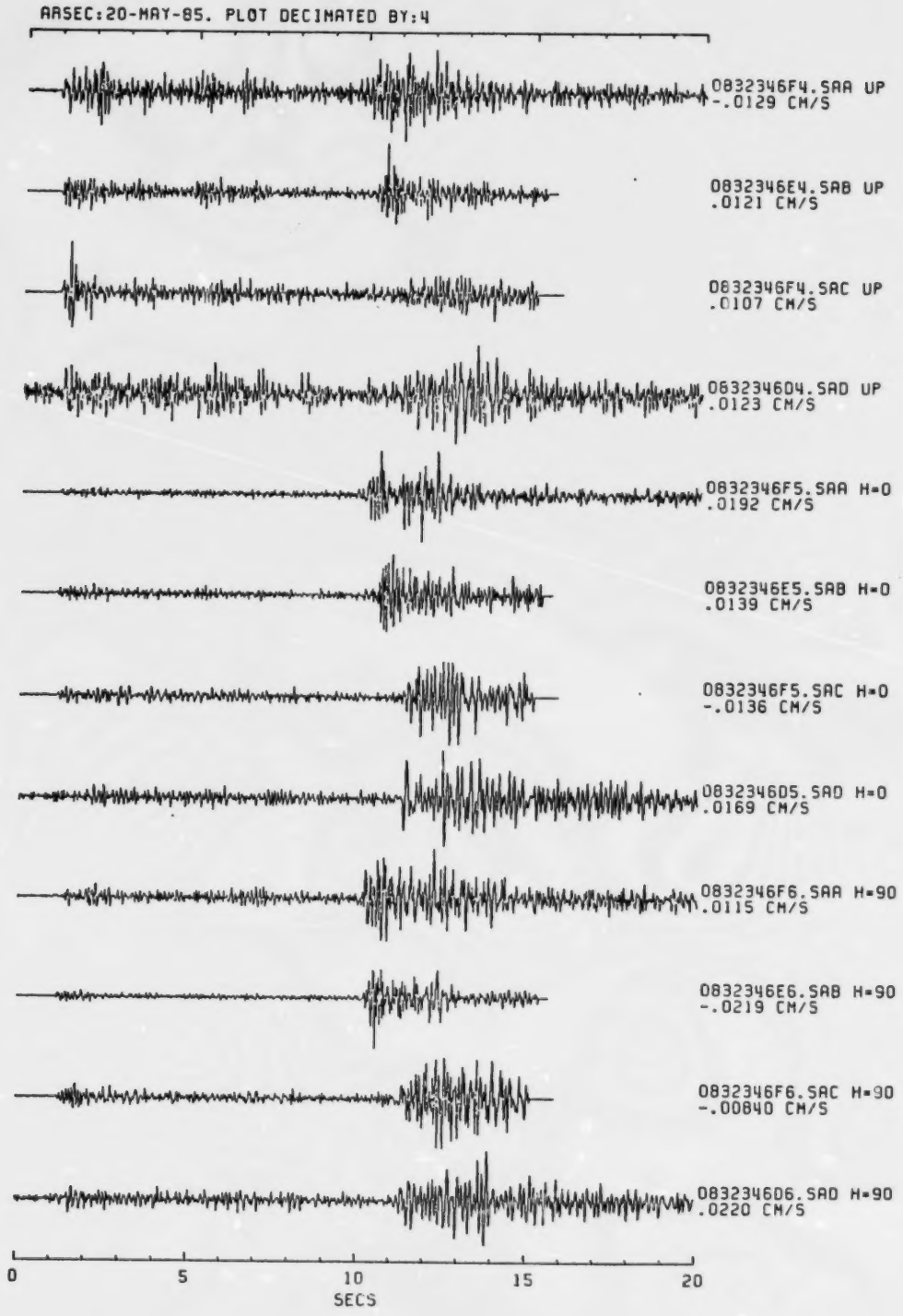

Figure 2.--Scaled amplitude plots for event 0832346. Hypocentral P-wave arrivals are aligned at 1 second. If the recorder triggered on S, the trace is arbitrarily shifted. Peak velocity is annotated.

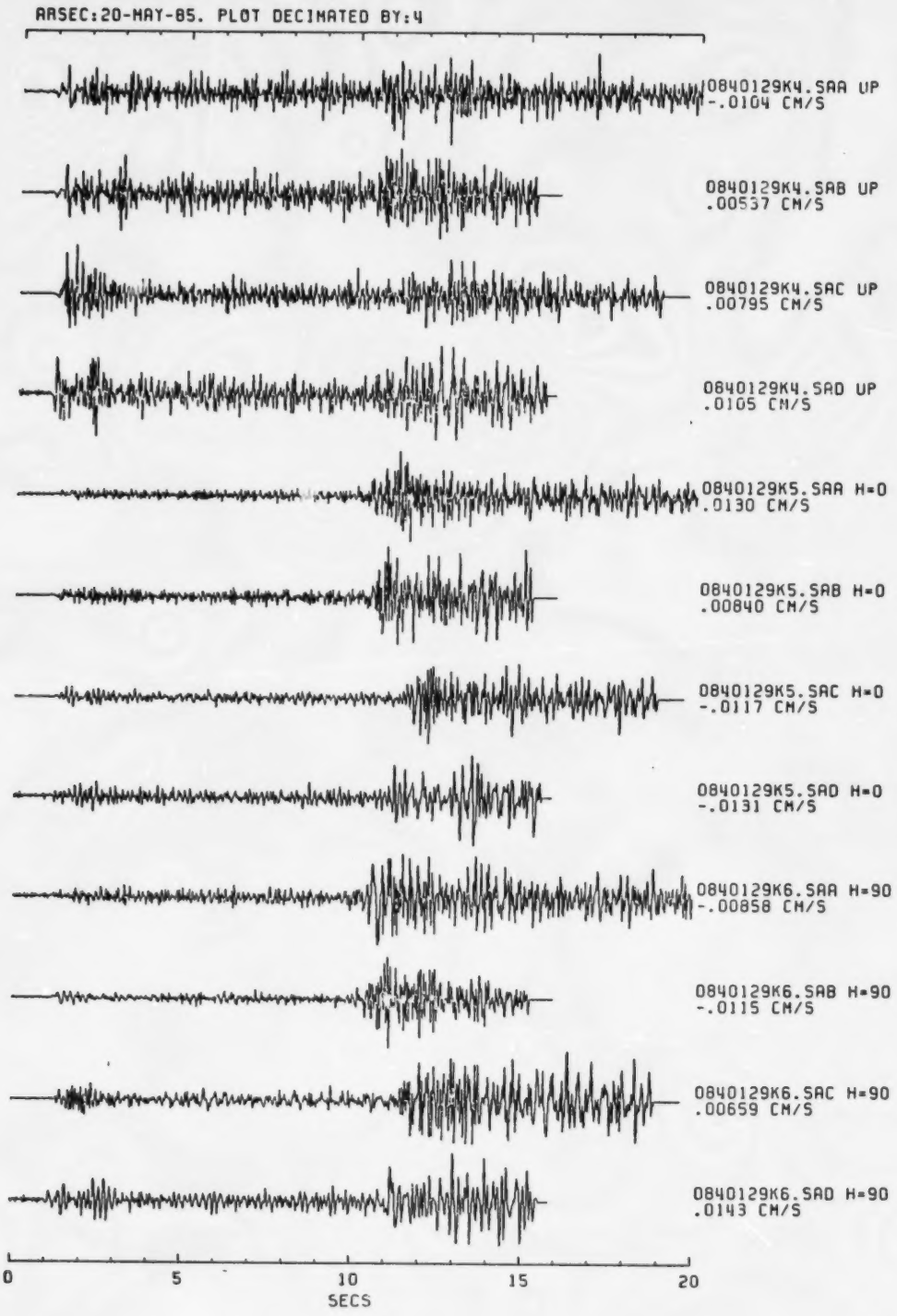

Figure 3.--Scaled amplitude plots for event 0840129. Hypocentral P-wave arrivals are aligned at 1 second. If the recorder triggered on S, the trace is arbitrarily shifted. Peak velocity is annotated.

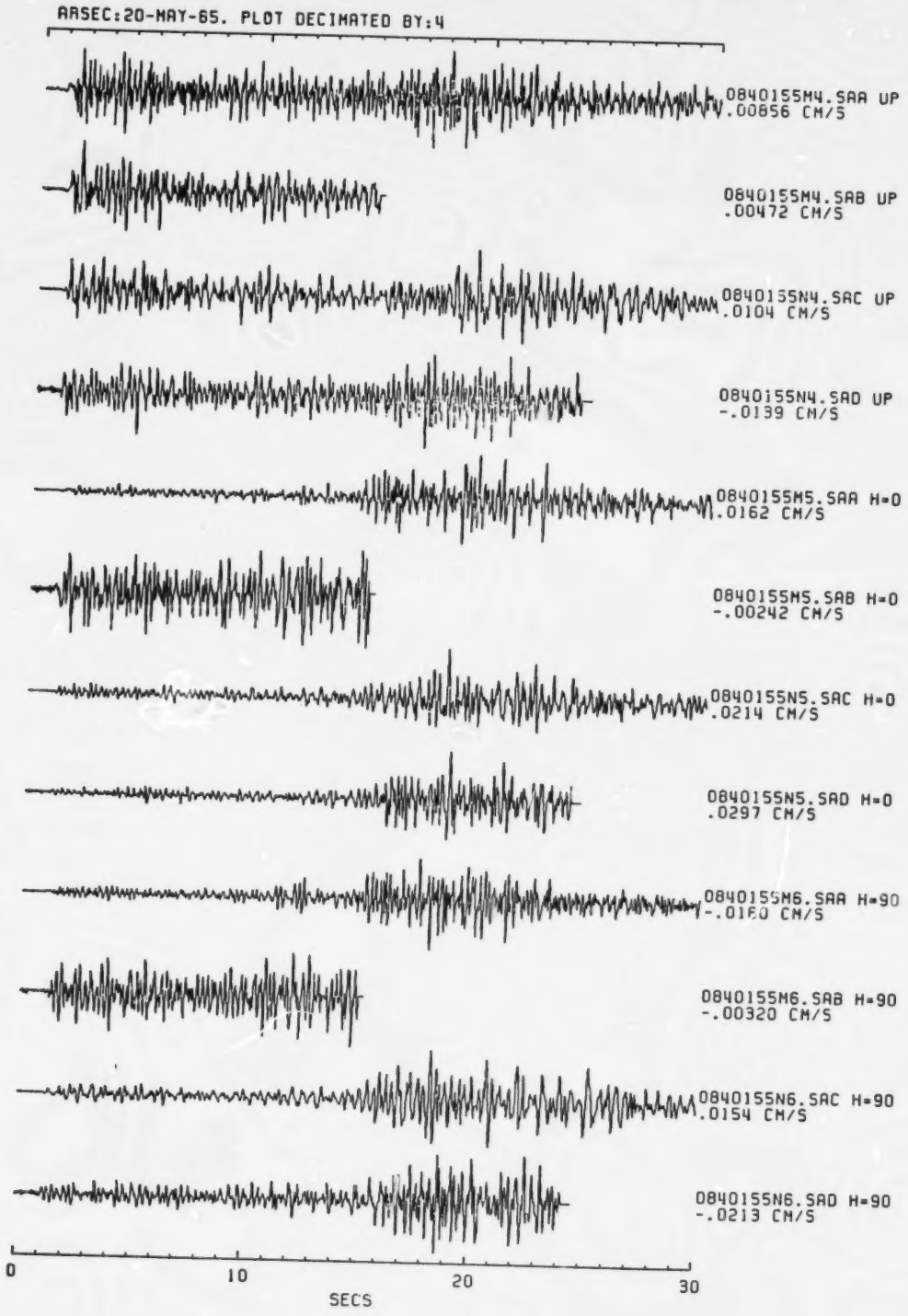

Figure 4.--Scaled amplitude plots for event 0840155. Hypocentral P-wave arrivals are aligned at 1 second. If the recorder triggered on S, the trace is arbitrarily shifted. Peak velocity is annotated.

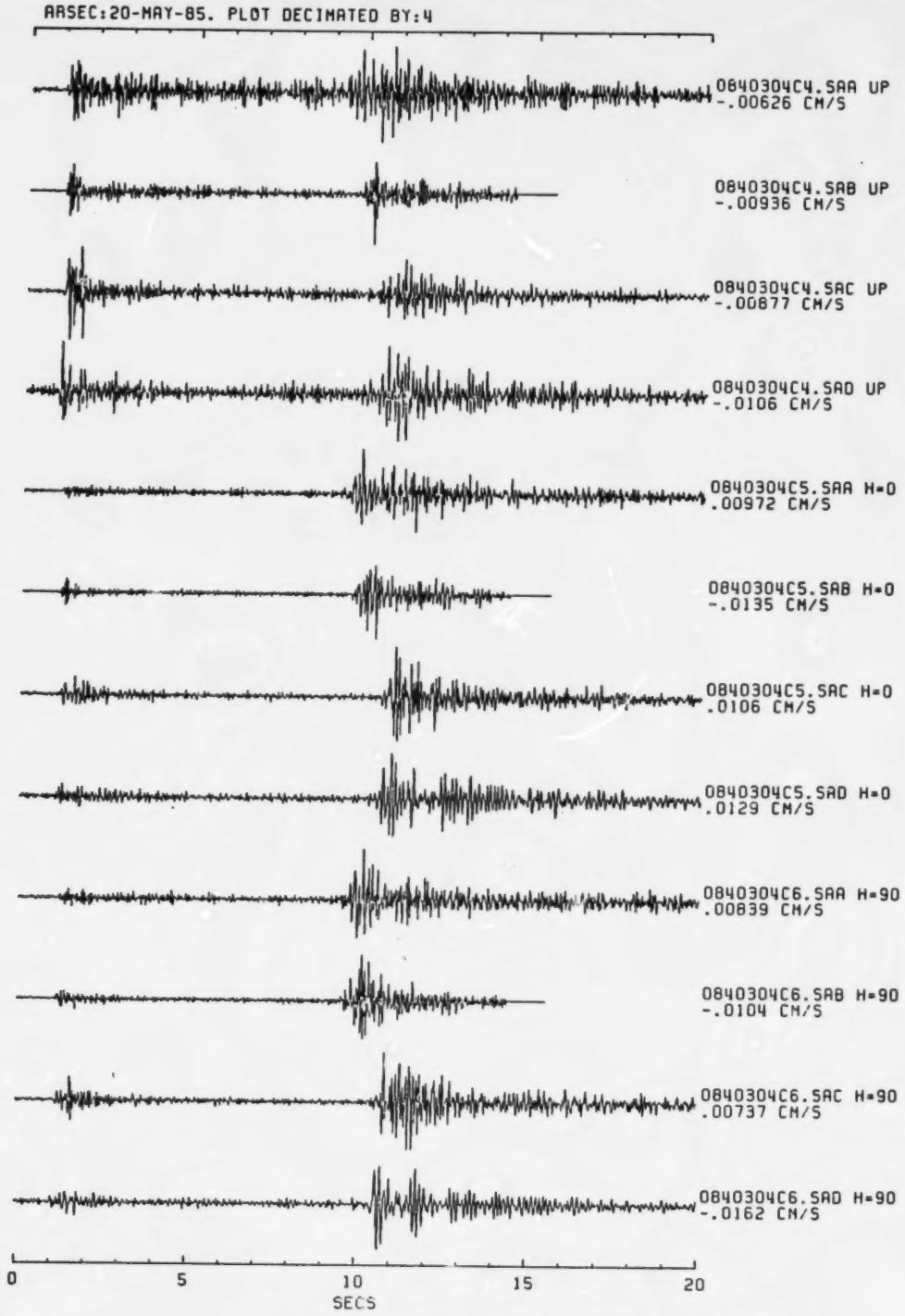

Figure 5.--Scaled amplitude plots for event 0840304. Hypocentral P-wave arrivals are aligned at 1 second. If the recorder triggered on S, the trace is arbitrarily shifted. Peak velocity is annotated.

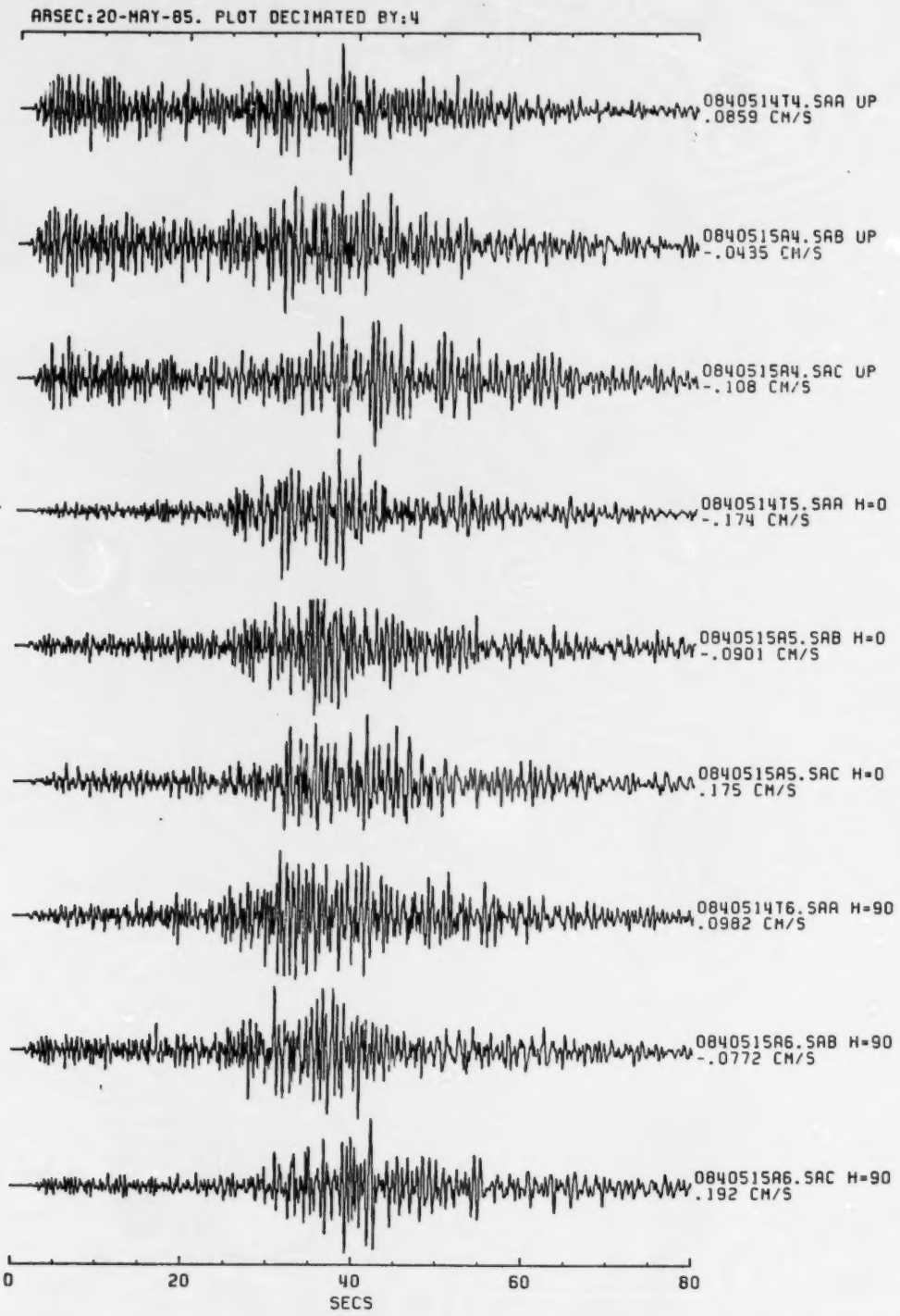

Figure 6.--Scaled amplitude plots for event 0840514. Hypocentral P-wave arrivals are aligned at 1 second. If the recorder triggered on S, the trace is arbitrarily shifted. Peak velocity is annotated.

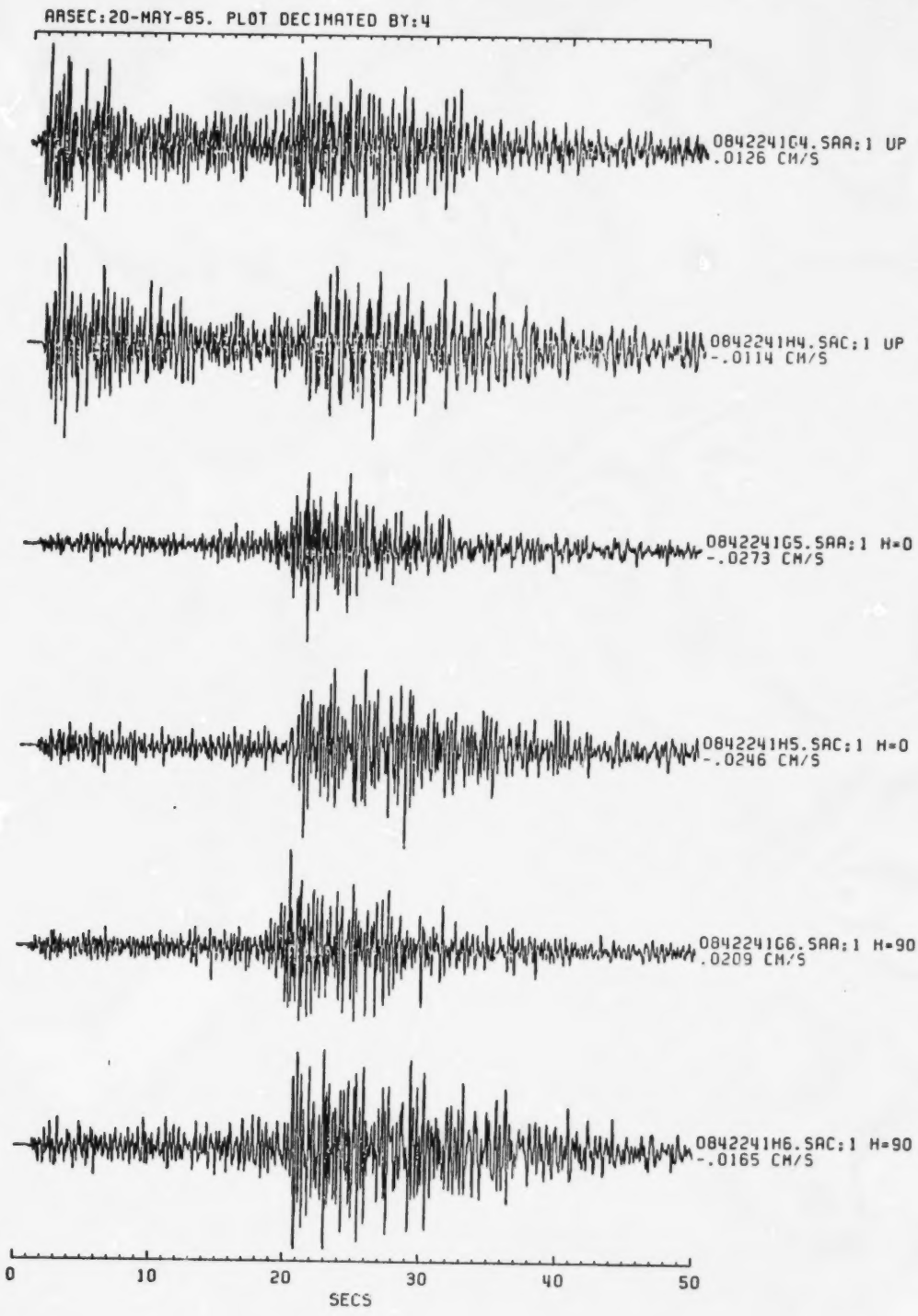

Figure 7.--Scaled amplitude plots for event 0842241. Hypocentral P-wave arrivals are aligned at 1 second. If the recorder triggered on S, the trace is arbitrarily shifted. Peak velocity is annotated.

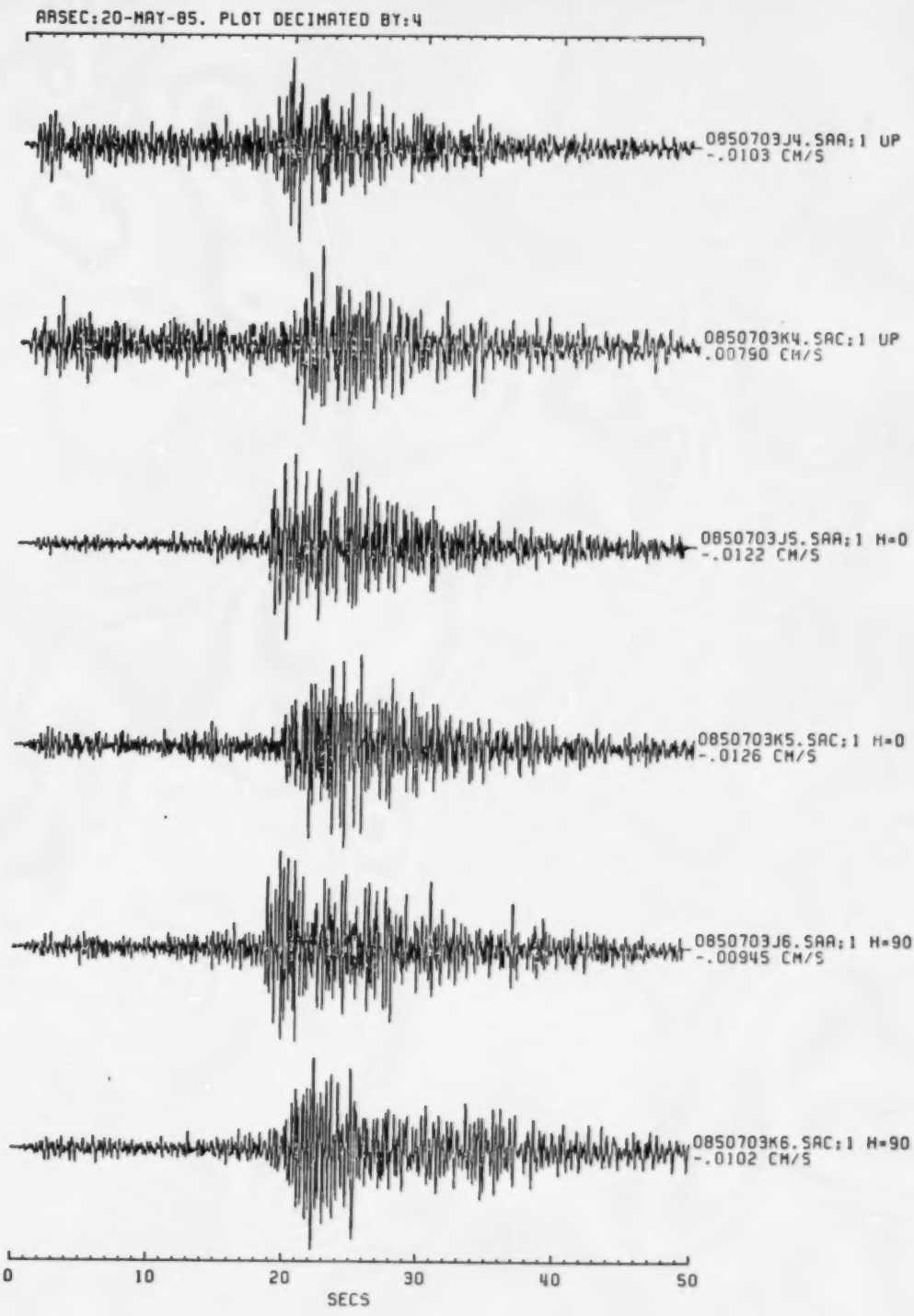

Figure 8.--Scaled amplitude plots for event 0850703. Hypocentral P-wave arrivals are aligned at 1 second. If the recorder triggered on S, the trace is arbitrarily shifted. Peak velocity is annotated.

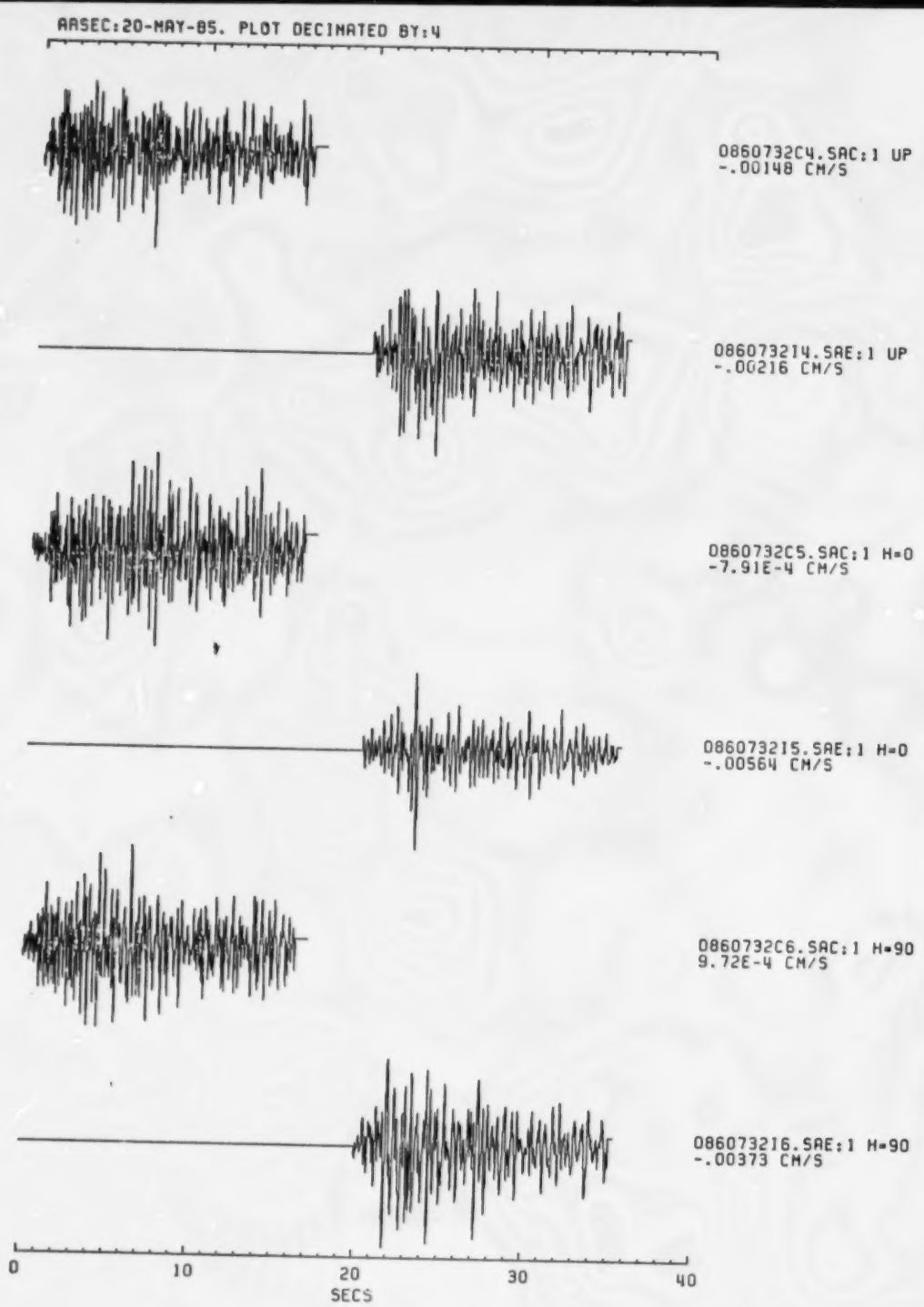

Figure 9.--Scaled amplitude plots for event 0860732. Hypocentral P-wave arrivals are aligned at 1 second. If the recorder triggered on S, the trace is arbitrarily shifted. Peak velocity is annotated.

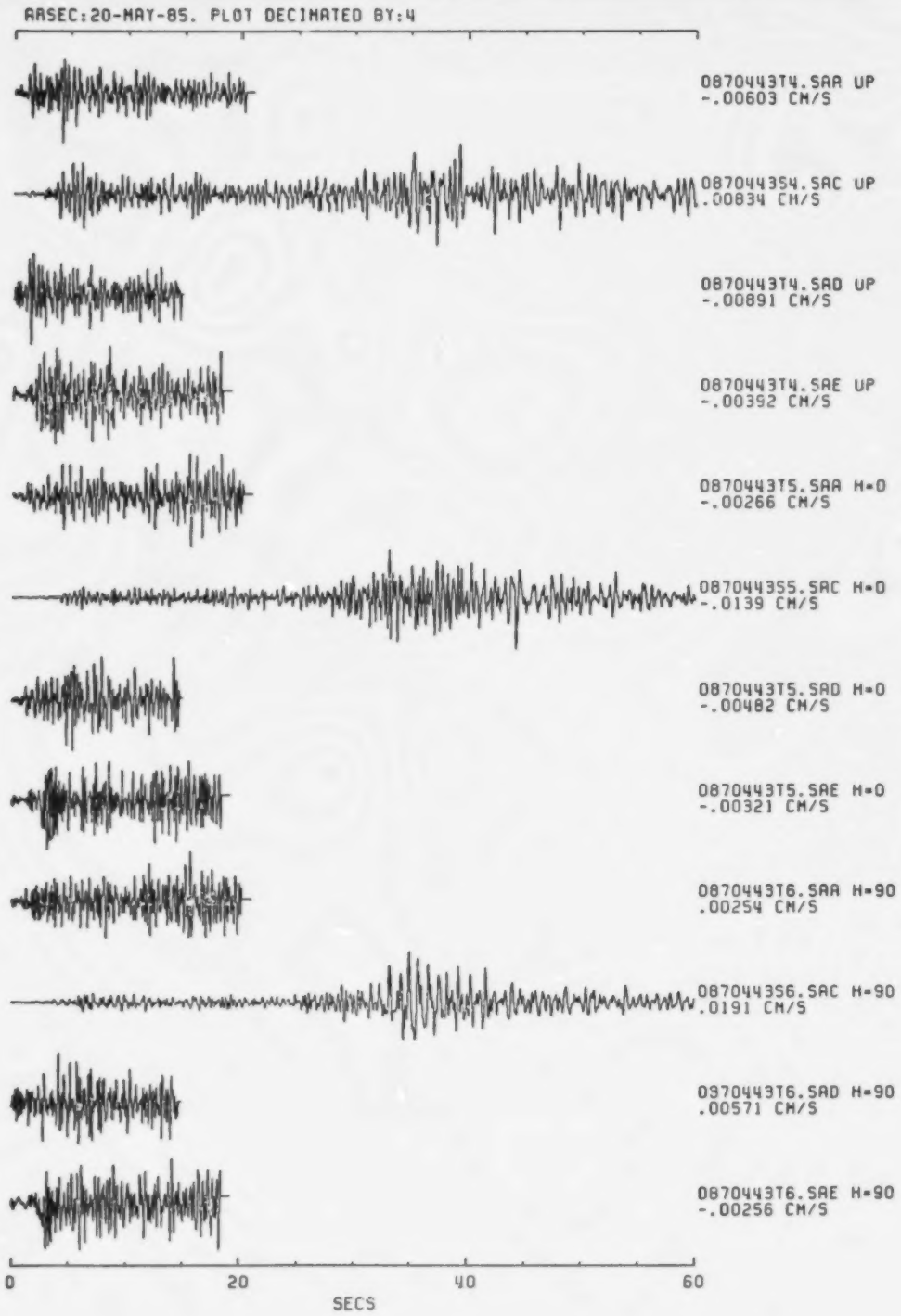

Figure 10.--Scaled amplitude plots for event 0870443. Hypocentral P-wave arrivals are aligned at 1 second. If the recorder triggered on S, the trace is arbitrarily shifted. Peak velocity is annotated.

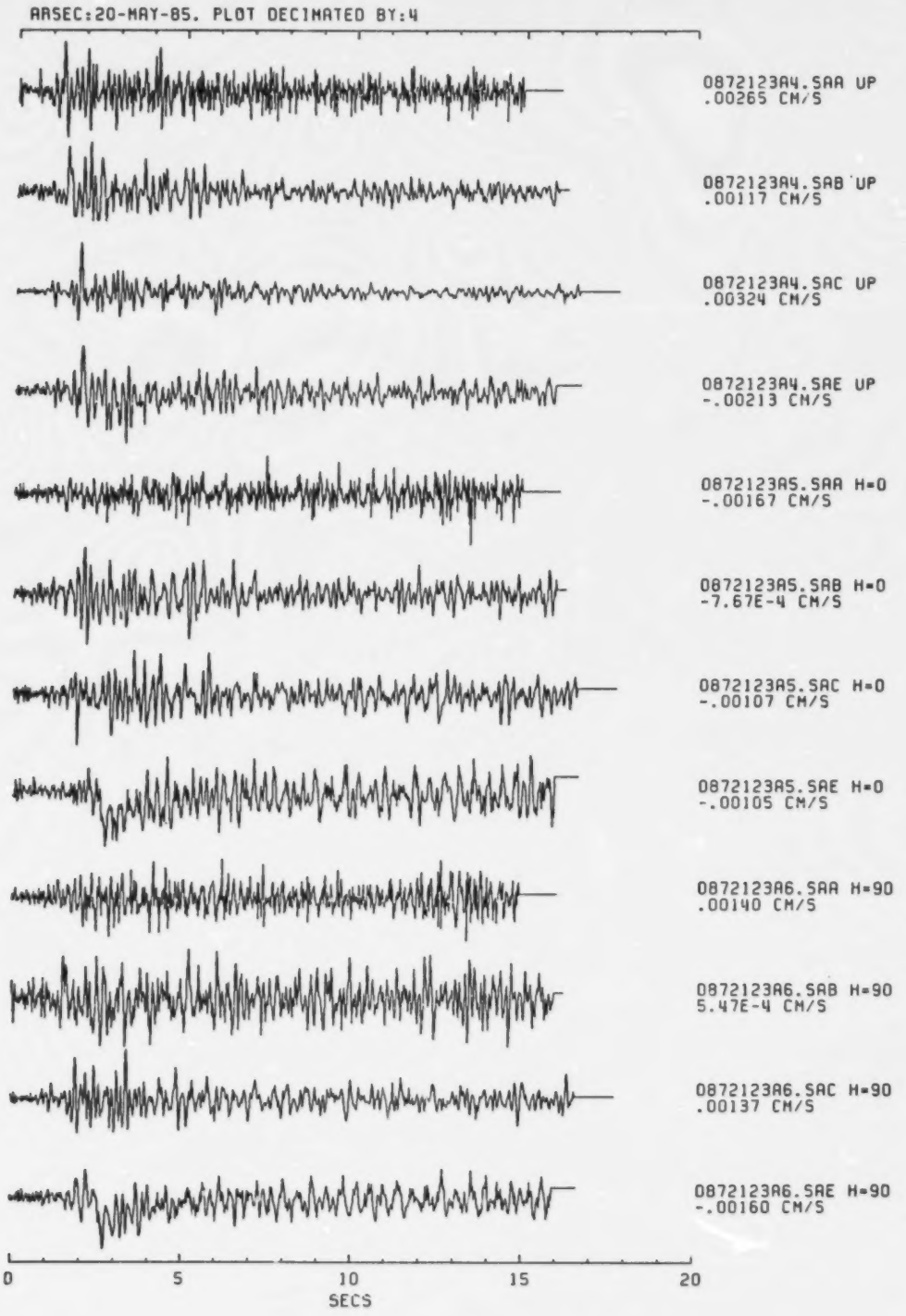

Figure 11.--Scaled amplitude plots for event 0872123. Hypocentral P-wave arrivals are aligned at 1 second. If the recorder triggered on S, the trace is arbitrarily shifted. Peak velocity is annotated.

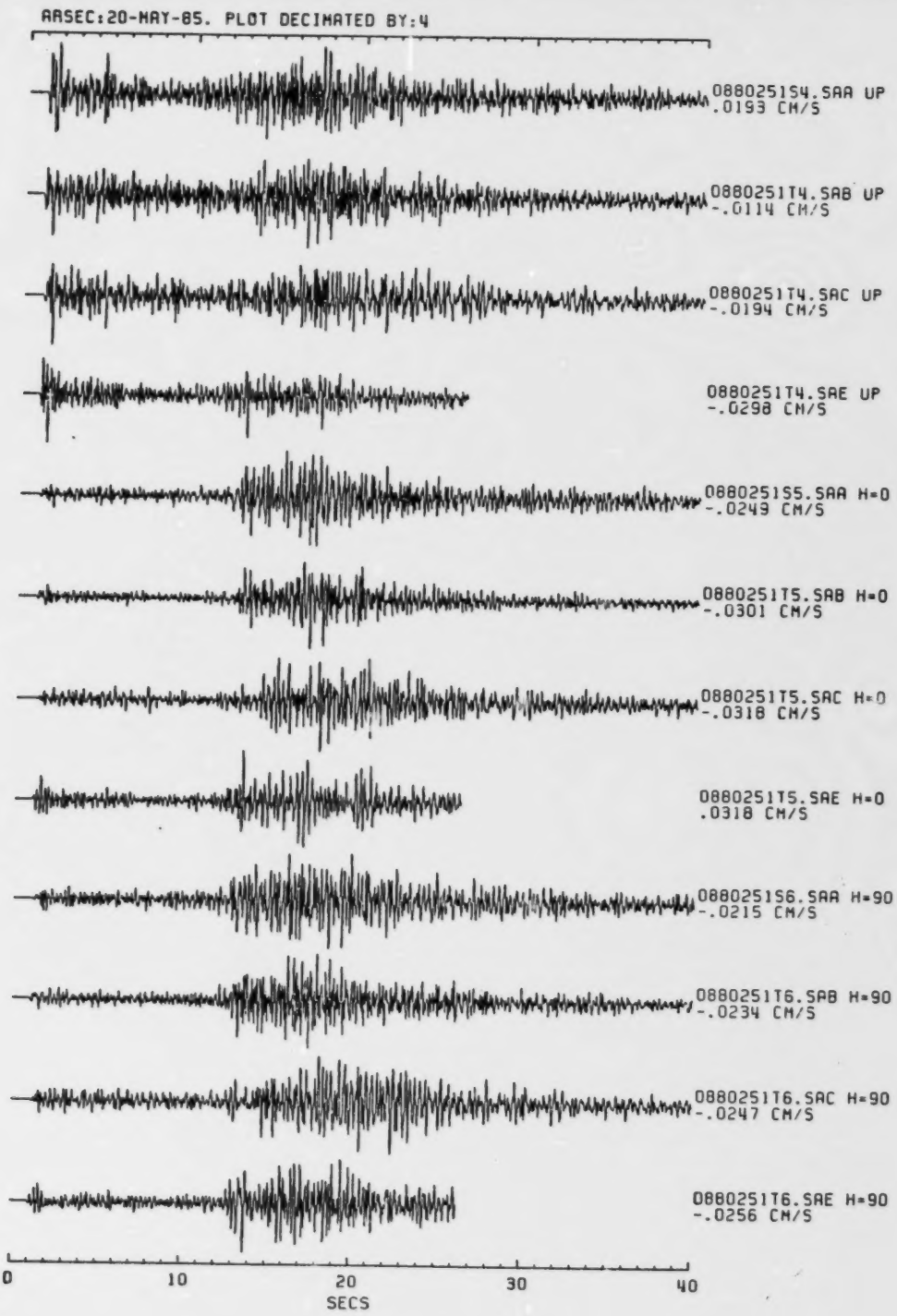

Figure 12.--Scaled amplitude plots for event 0880251. Hypocentral P-wave arrivals are aligned at 1 second. If the recorder triggered on S, the trace is arbitrarily shifted. Peak velocity is annotated.

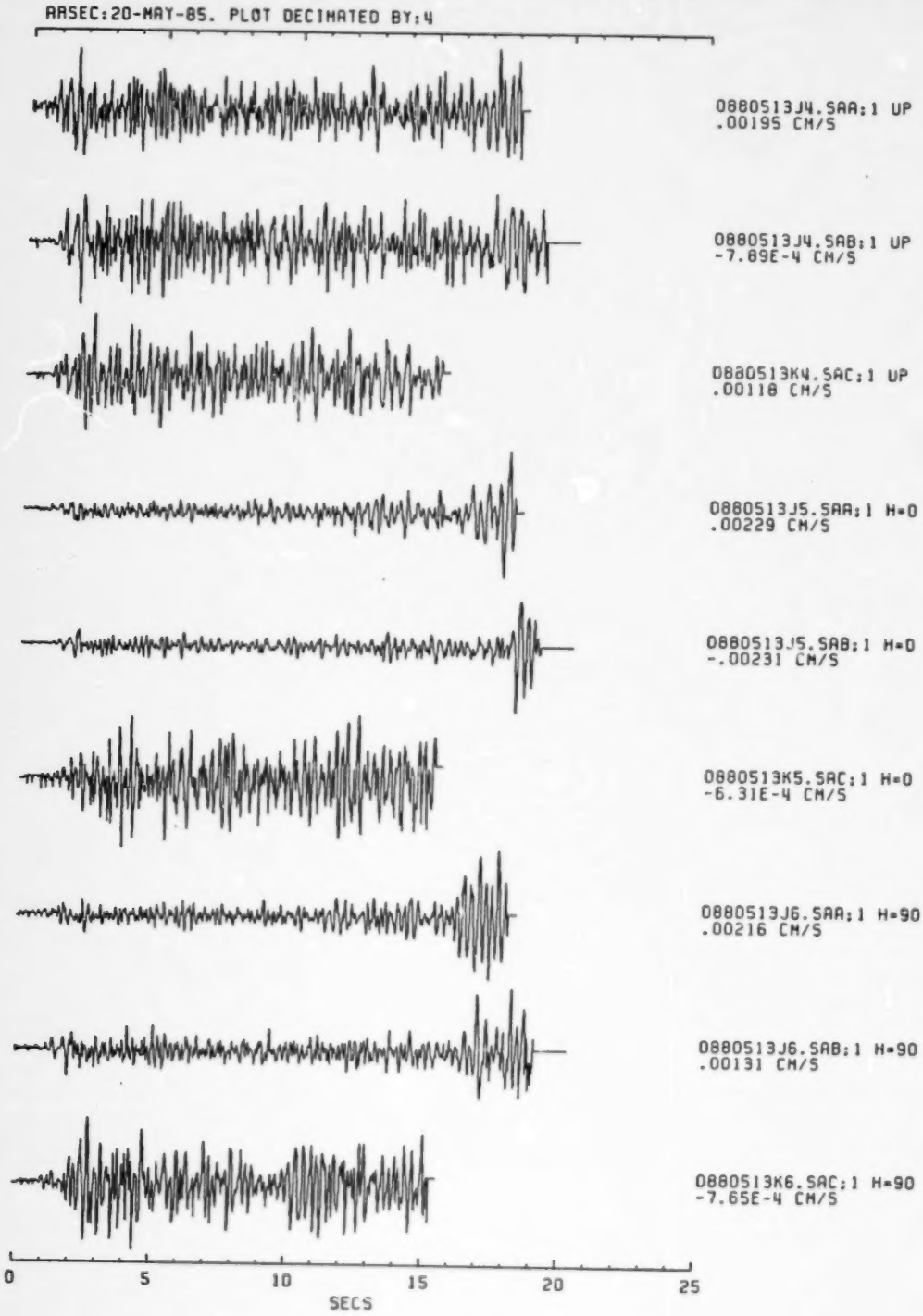

Figure 13.--Scaled amplitude plots for event 0880513. Hypocentral P-wave arrivals are aligned at 1 second. If the recorder triggered on S, the trace is arbitrarily shifted. Peak velocity is annotated.

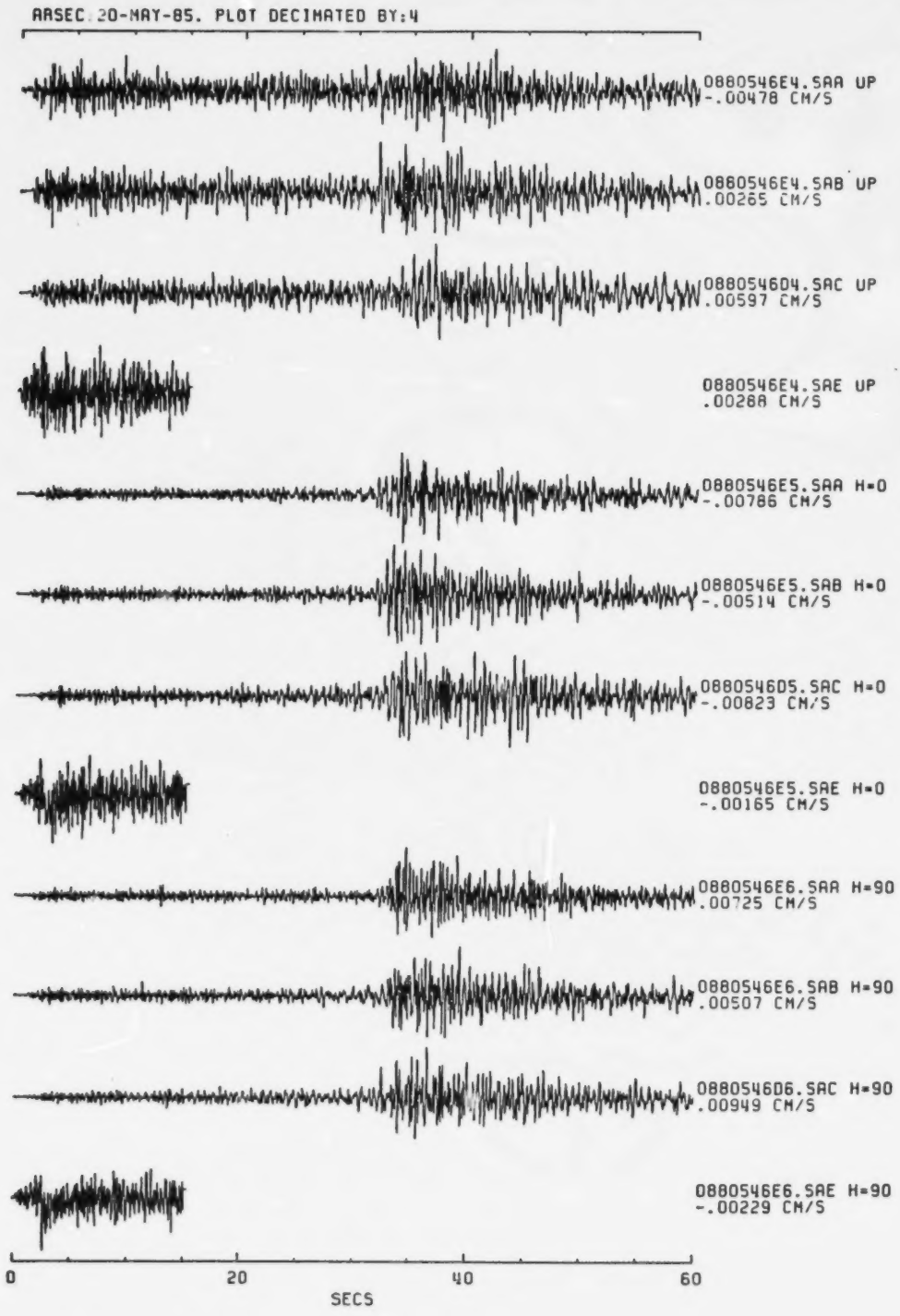

Figure 14.--Scaled amplitude plots for event 0880546. Hypocentral P-wave arrivals are aligned at 1 second. If the recorder triggered on S, the trace is arbitrarily shifted. Peak velocity is annotated.

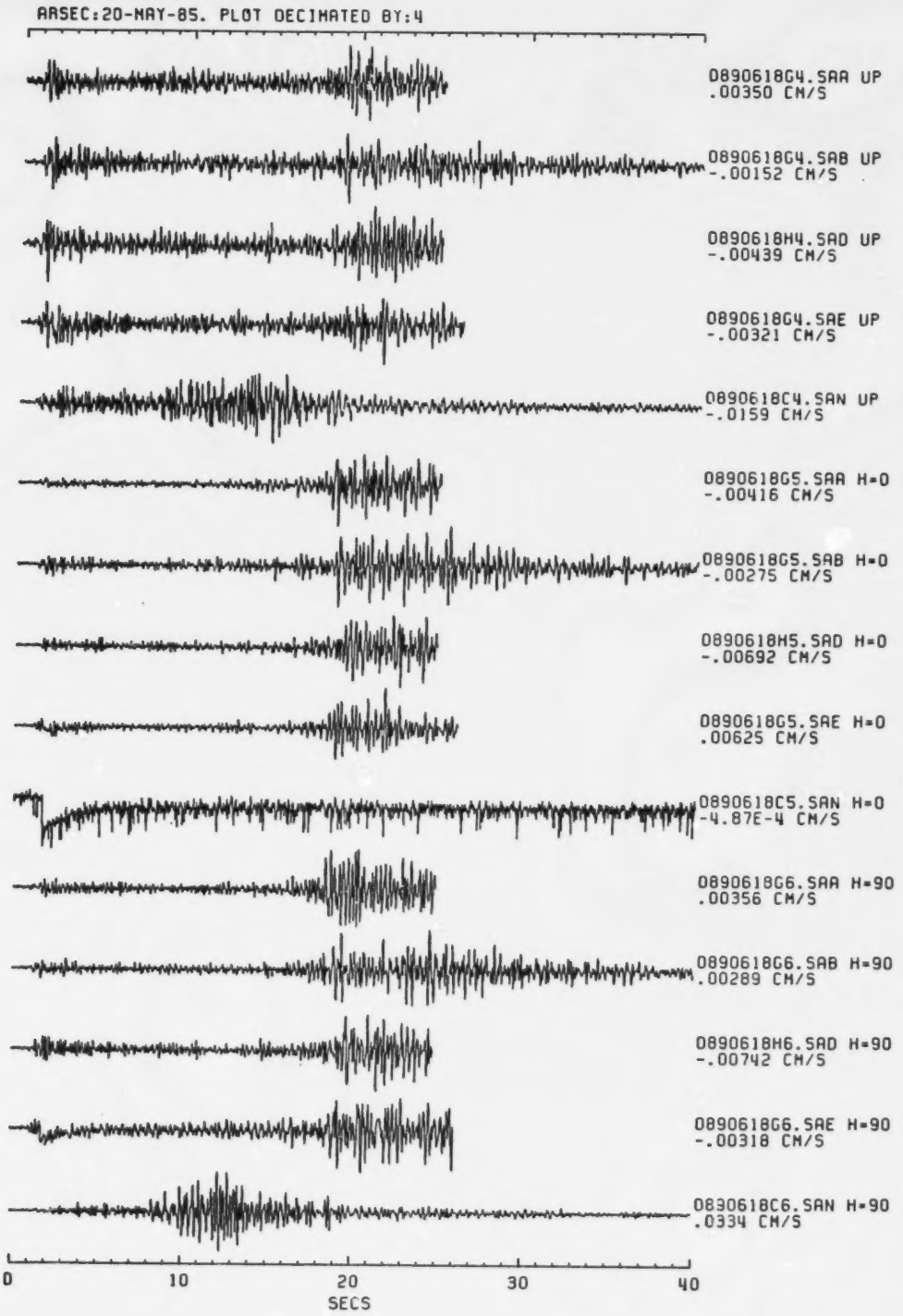

Figure 15.--Scaled amplitude plots for event 0890618. Hypocentral P-wave arrivals are aligned at 1 second. If the recorder triggered on S, the trace is arbitrarily shifted. Peak velocity is annotated.

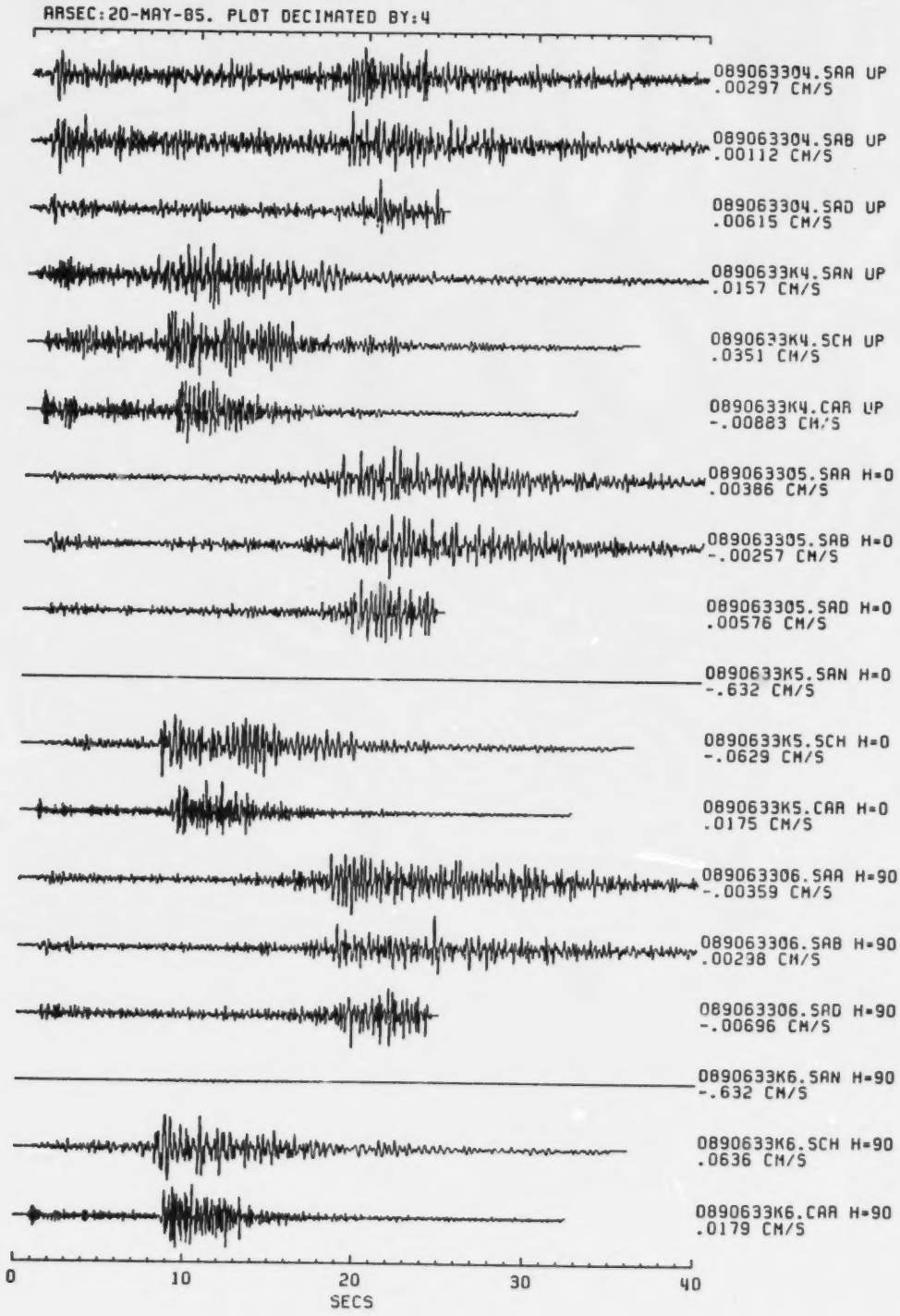

Figure 16.--Scaled amplitude plots for event 0890633. Hypocentral P-wave arrivals are aligned at 1 second. If the recorder triggered on S, the trace is arbitrarily shifted. Peak velocity is annotated.

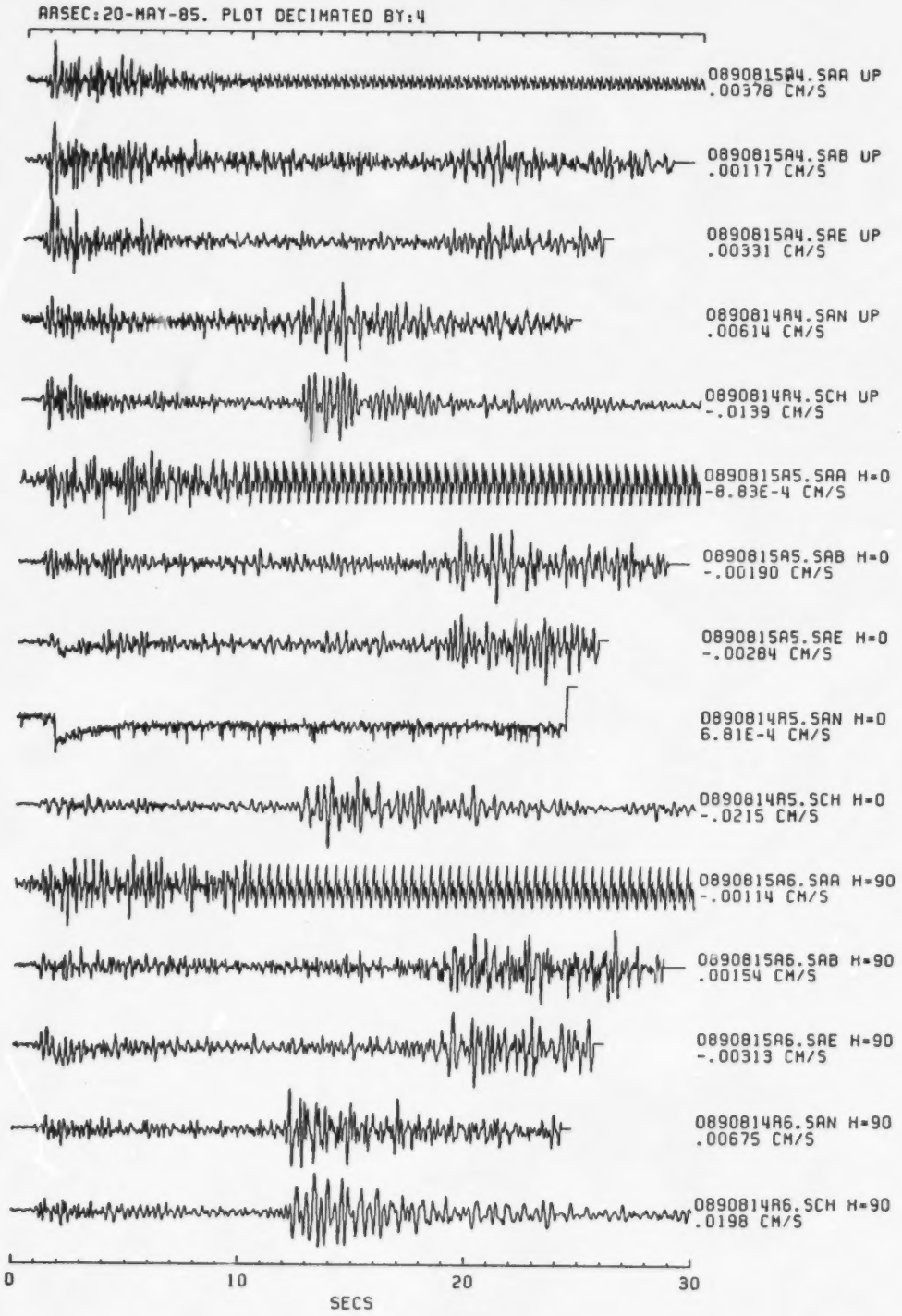

Figure 17.--Scaled amplitude plots for event 0890815. Hypocentral P-wave arrivals are aligned at 1 second. If the recorder triggered on S, the trace is arbitrarily shifted. Peak velocity is annotated.

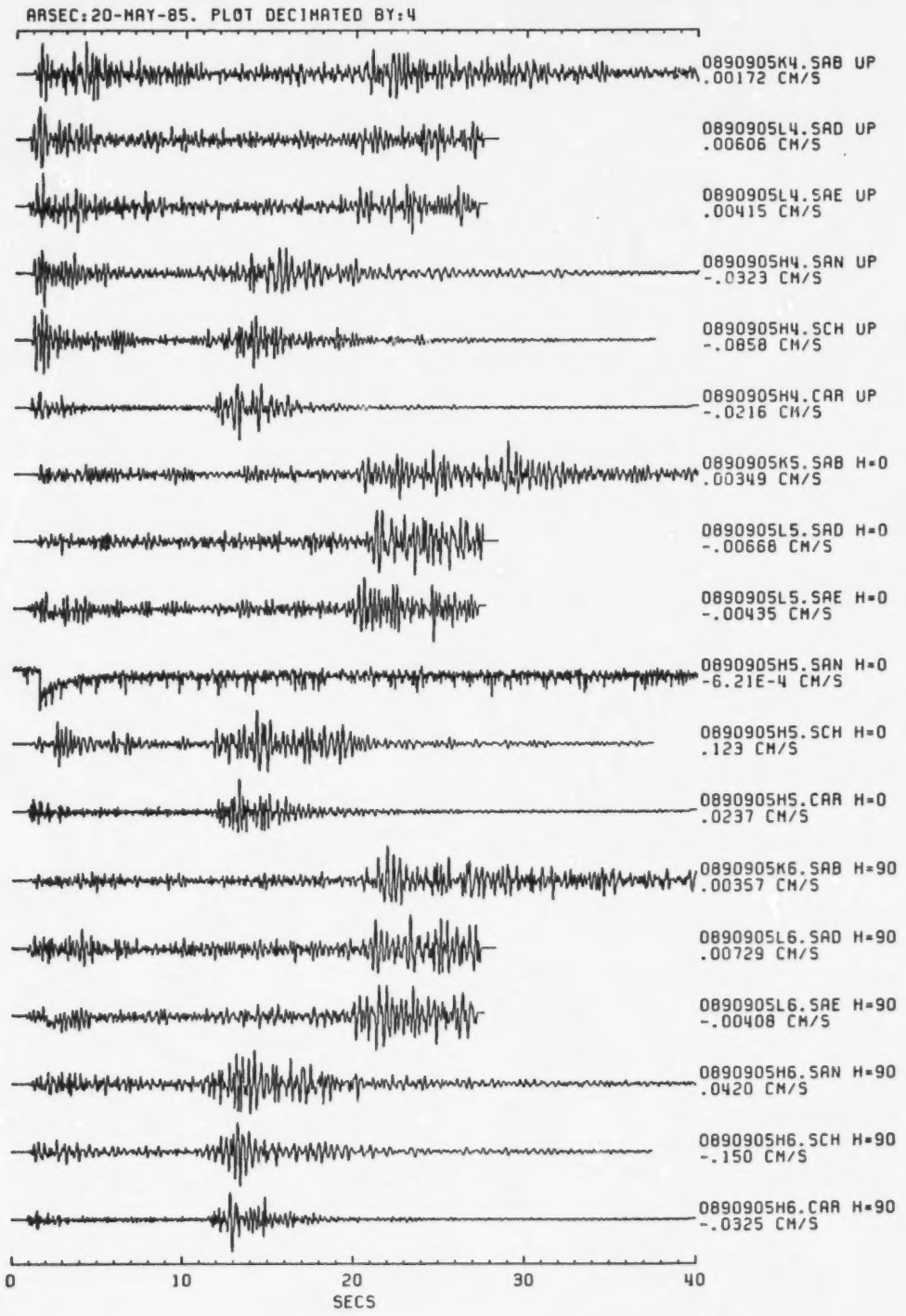

Figure 18.--Scaled amplitude plots for event 0890905. Hypocentral P-wave arrivals are aligned at 1 second. If the recorder triggered on S, the trace is arbitrarily shifted. Peak velocity is annotated.

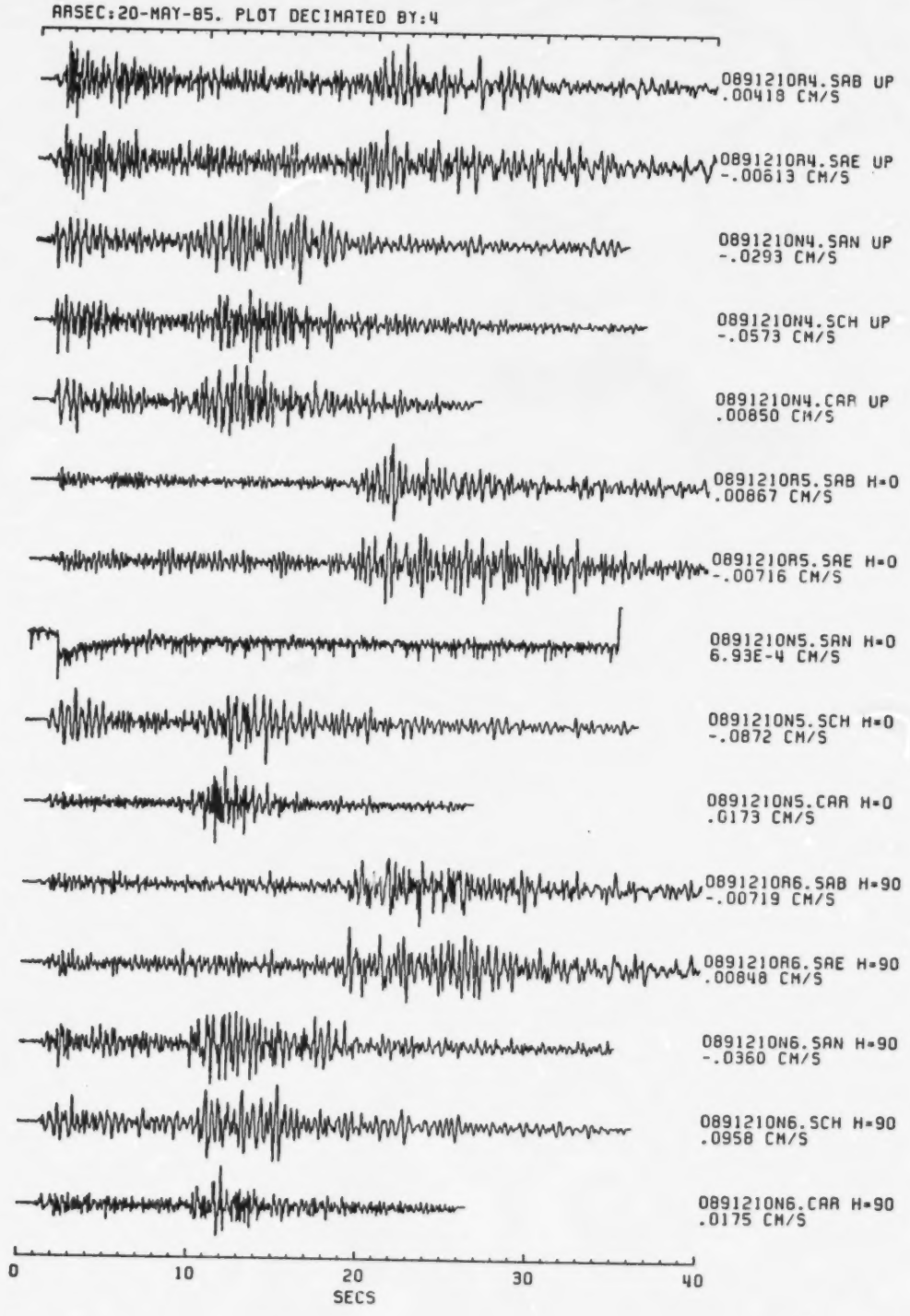

Figure 19.--Scaled amplitude plots for event 0891210. Hypocentral P-wave arrivals are aligned at 1 second. If the recorder triggered on S, the trace is arbitrarily shifted. Peak velocity is annotated.

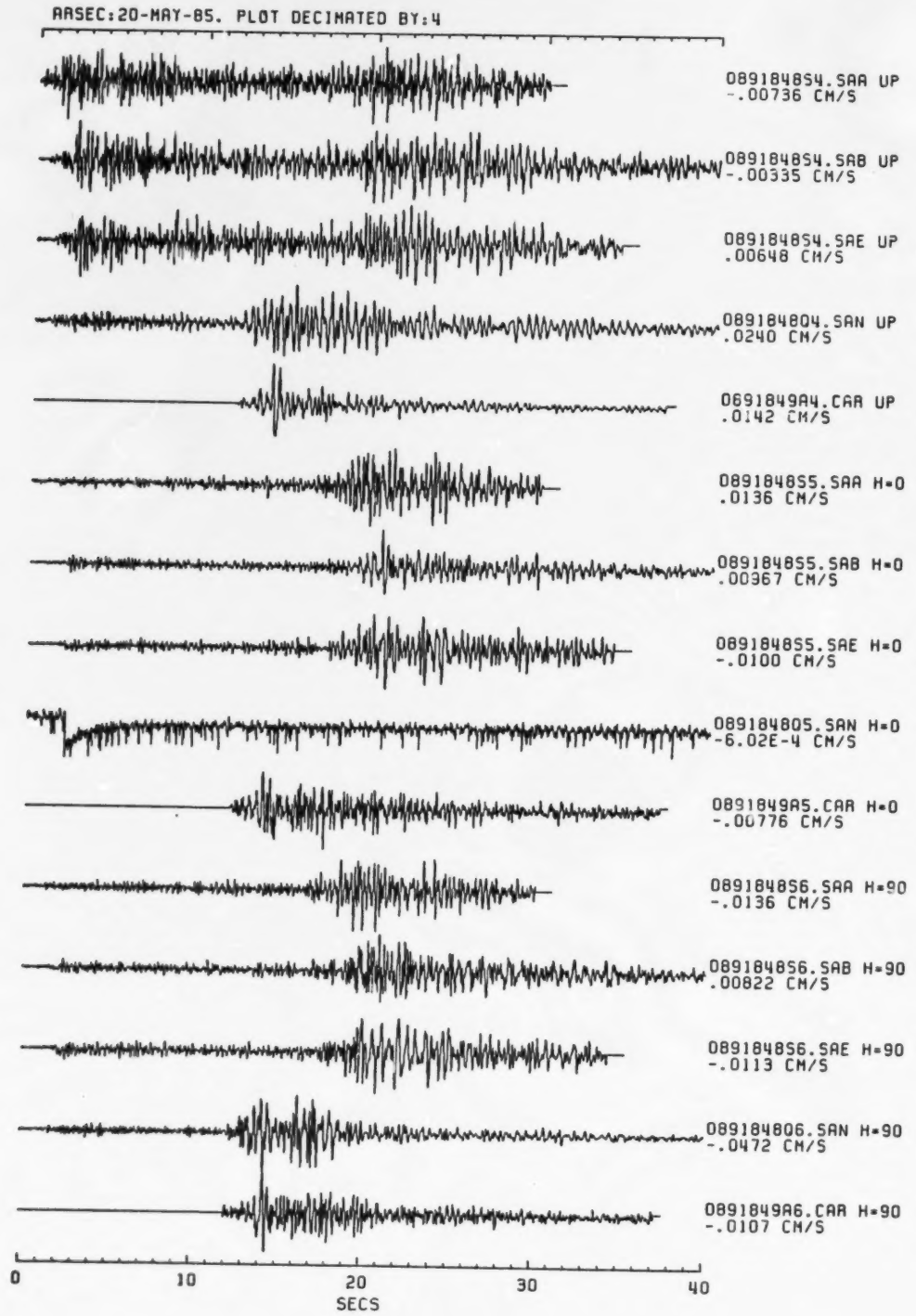

Figure 20.--Scaled amplitude plots for event 0891848. Hypocentral P-wave arrivals are aligned at 1 second. If the recorder triggered on S, the trace is arbitrarily shifted. Peak velocity is annotated.

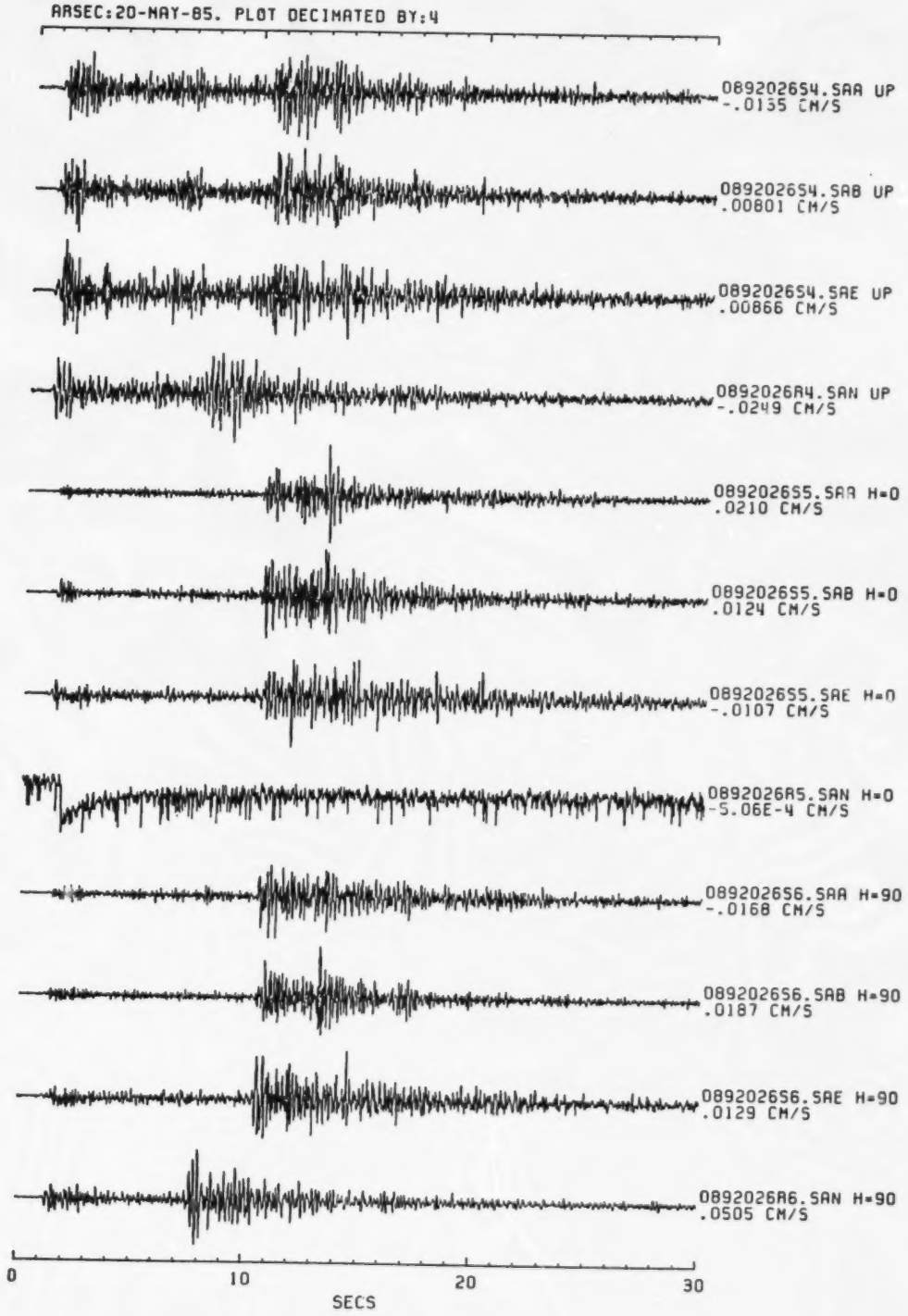

Figure 21.--Scaled amplitude plots for event 0892026. Hypocentral P-wave arrivals are aligned at 1 second. If the recorder triggered on S, the trace is arbitrarily shifted. Peak velocity is annotated.

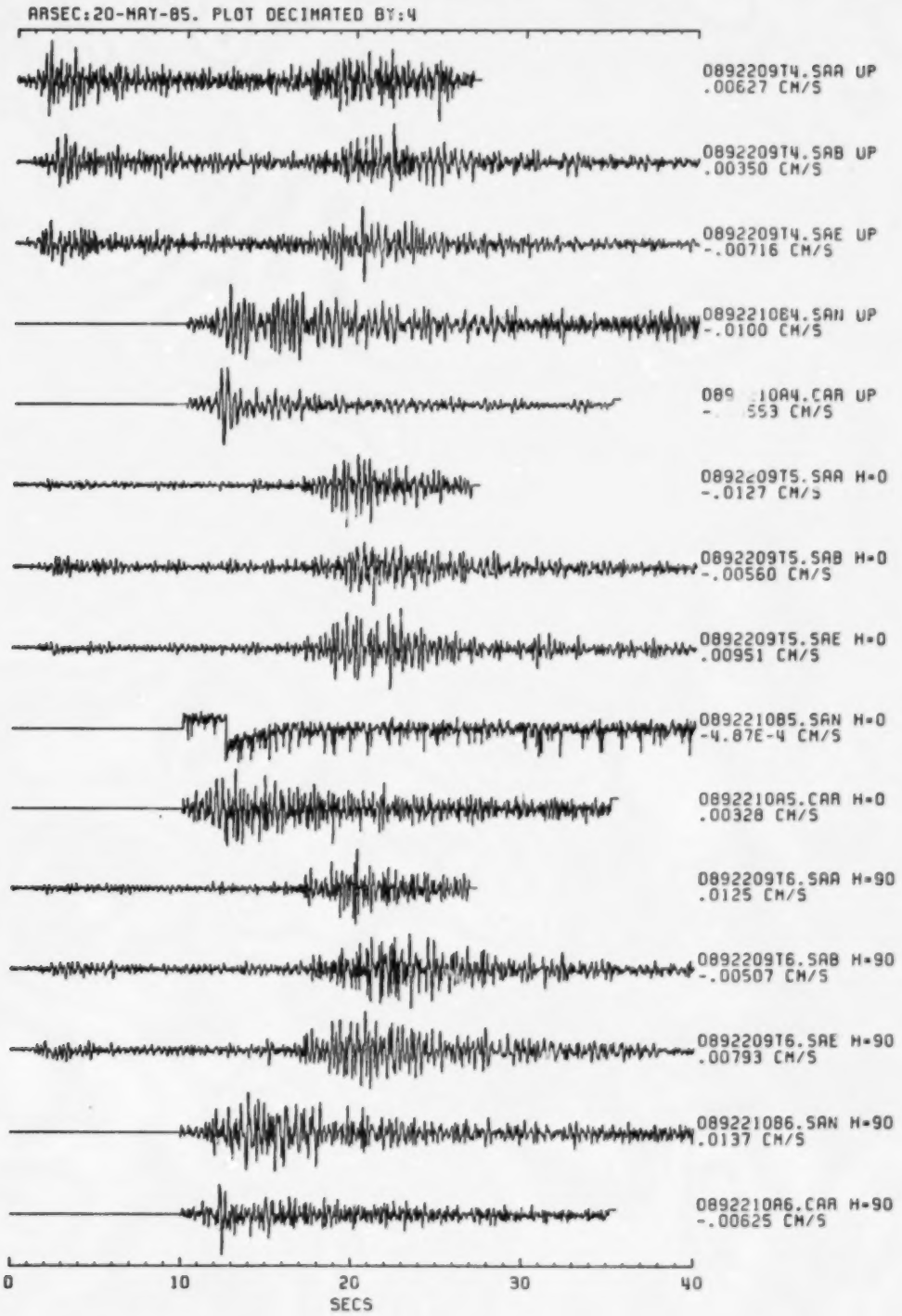

Figure 22.--Scaled amplitude plots for event 0892209. Hypocentral P-wave arrivals are aligned at 1 second. If the recorder triggered on S, the trace is arbitrarily shifted. Peak velocity is annotated.

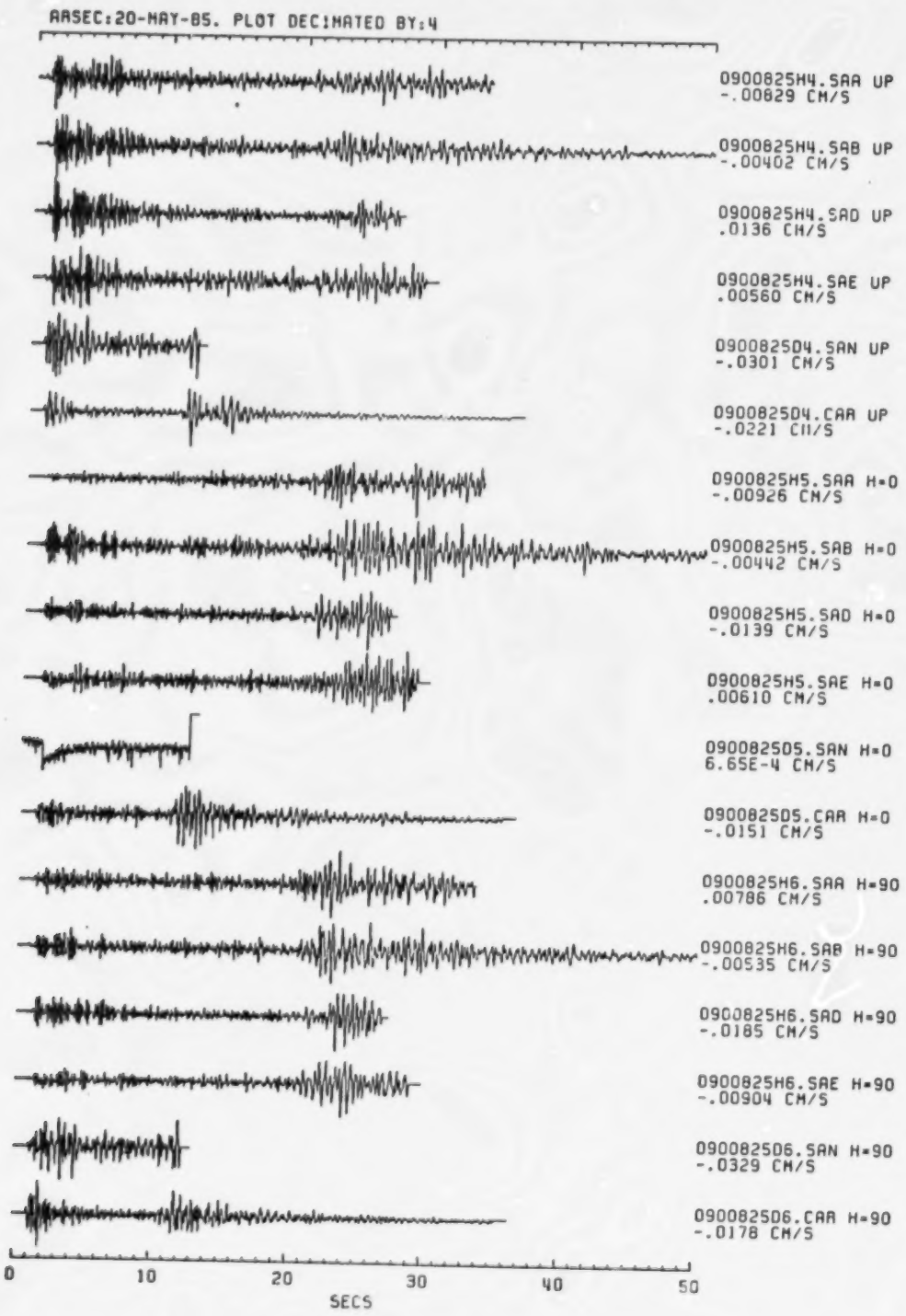

Figure 23.--Scaled amplitude plots for event 0900825. Hypocentral P-wave arrivals are aligned at 1 second. If the recorder triggered on S, the trace is arbitrarily shifted. Peak velocity is annotated.

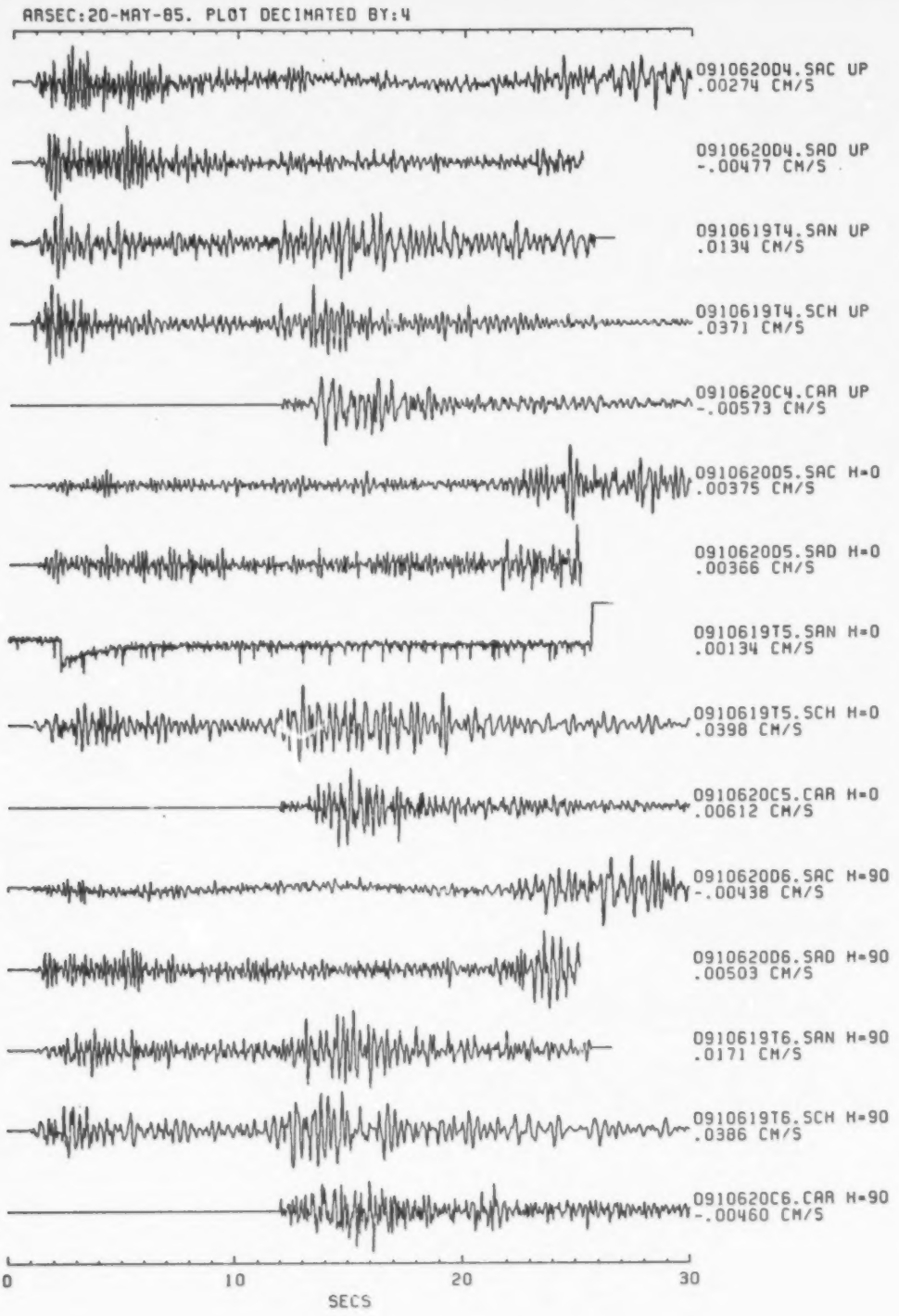

Figure 24.--Scaled amplitude plots for event 0910620. Hypocentral P-wave arrivals are aligned at 1 second. If the recorder triggered on S, the trace is arbitrarily shifted. Peak velocity is annotated.

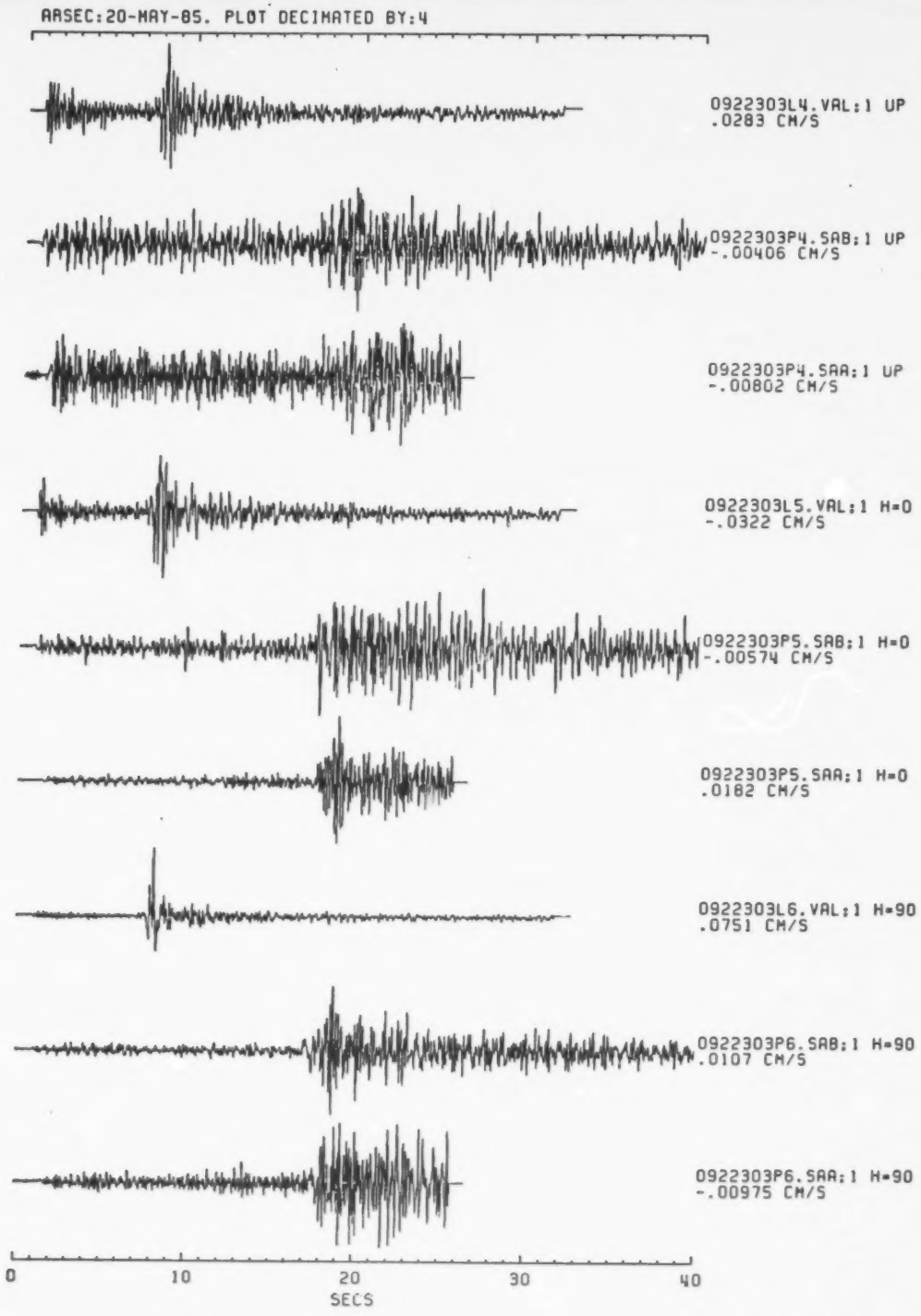

Figure 25.--Scaled amplitude plots for event 0922303. Hypocentral P-wave arrivals are aligned at 1 second. If the recorder triggered on S, the trace is arbitrarily shifted. Peak velocity is annotated.

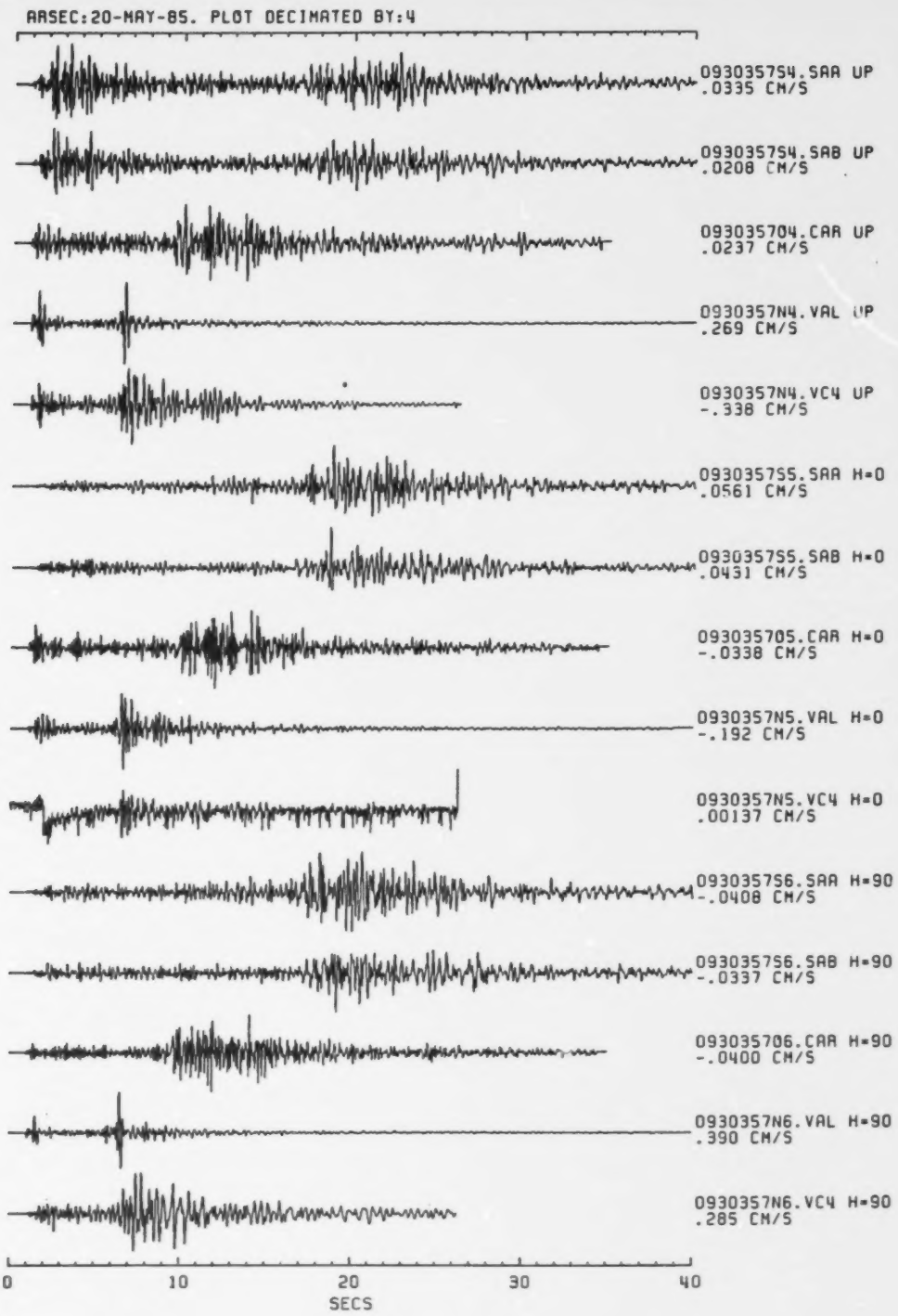

Figure 26.--Scaled amplitude plots for event 0930357. Hypocentral P-wave arrivals are aligned at 1 second. If the recorder triggered on S, the trace is arbitrarily shifted. Peak velocity is annotated.

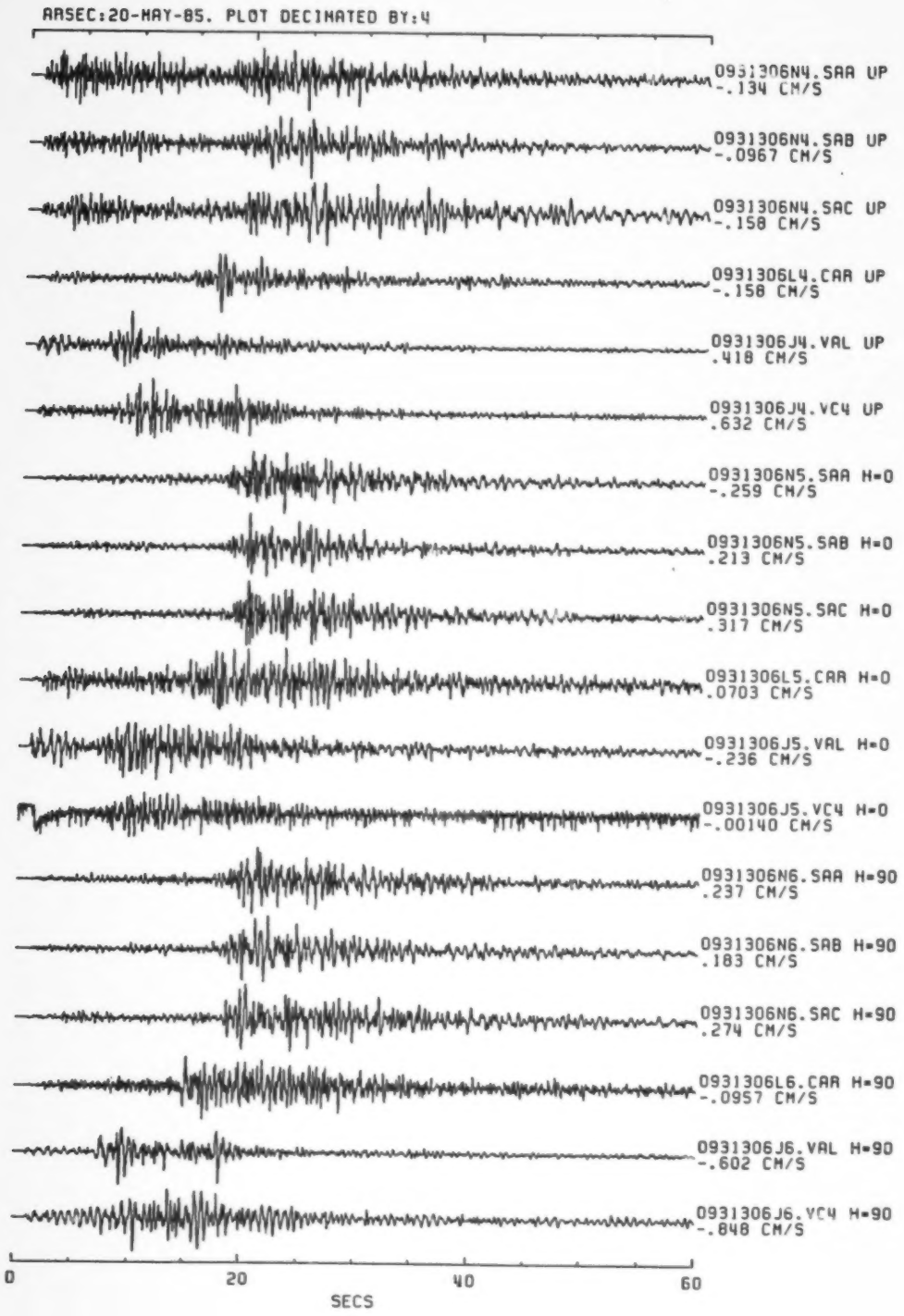

Figure 27.--Scaled amplitude plots for event 0931306. Hypocentral P-wave arrivals are aligned at 1 second. If the recorder triggered on S, the trace is arbitrarily shifted. Peak velocity is annotated.

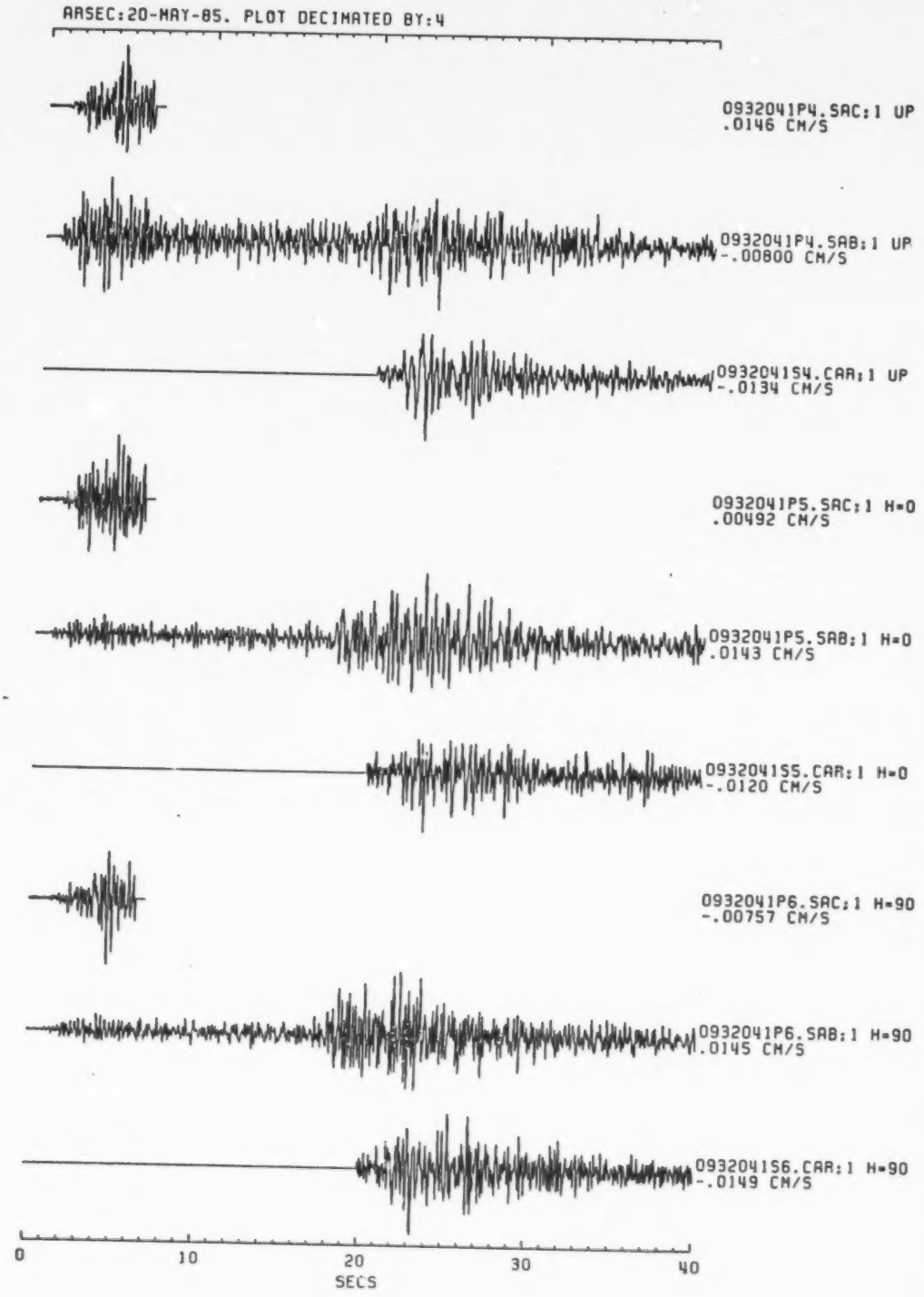

Figure 28.--Scaled amplitude plots for event 0932041. Hypocentral P-wave arrivals are aligned at 1 second. If the recorder triggered on S, the trace is arbitrarily shifted. Peak velocity is annotated.

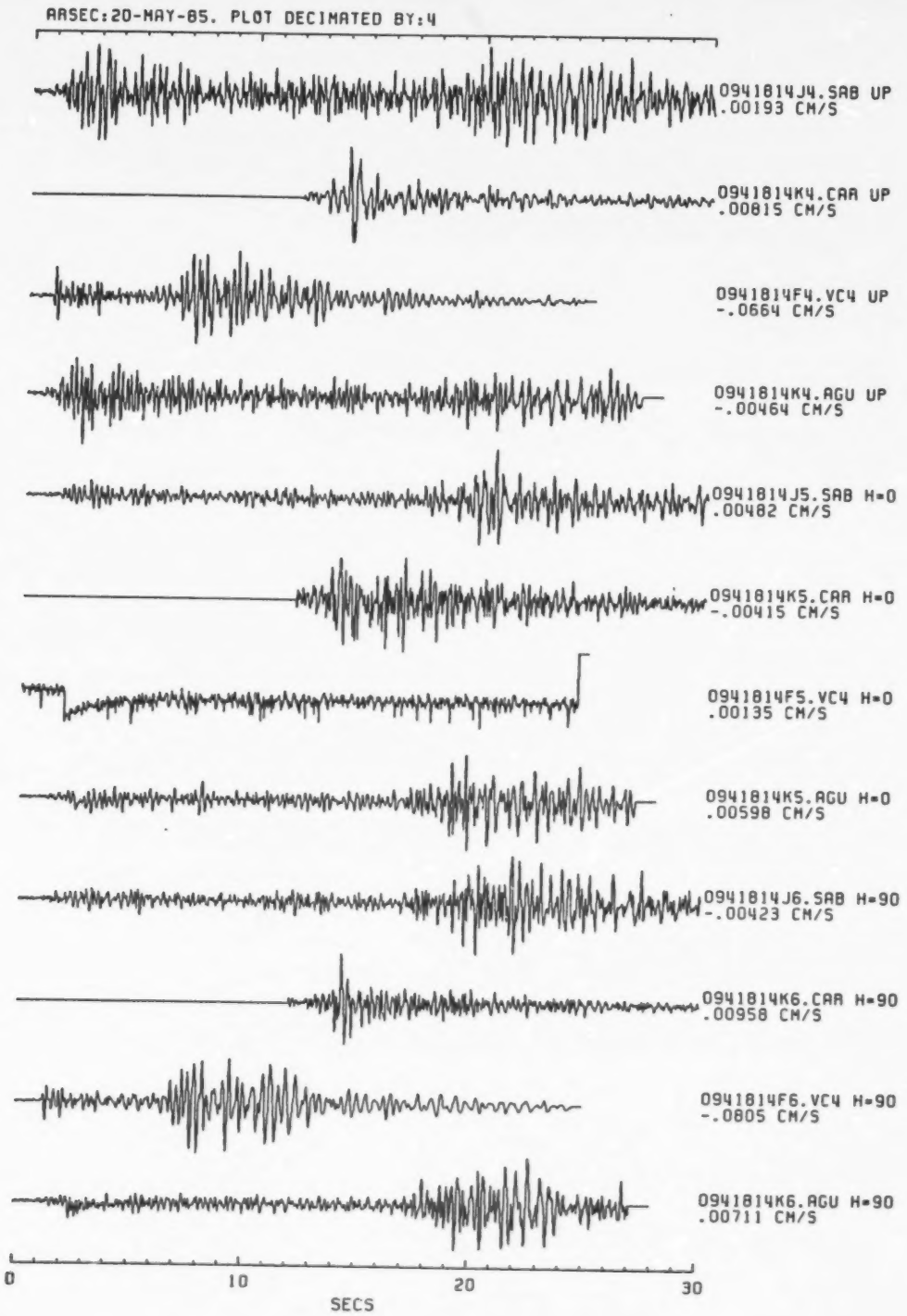

Figure 29.--Scaled amplitude plots for event 0941814. Hypocentral P-wave arrivals are aligned at 1 second. If the recorder triggered on S, the trace is arbitrarily shifted. Peak velocity is annotated.

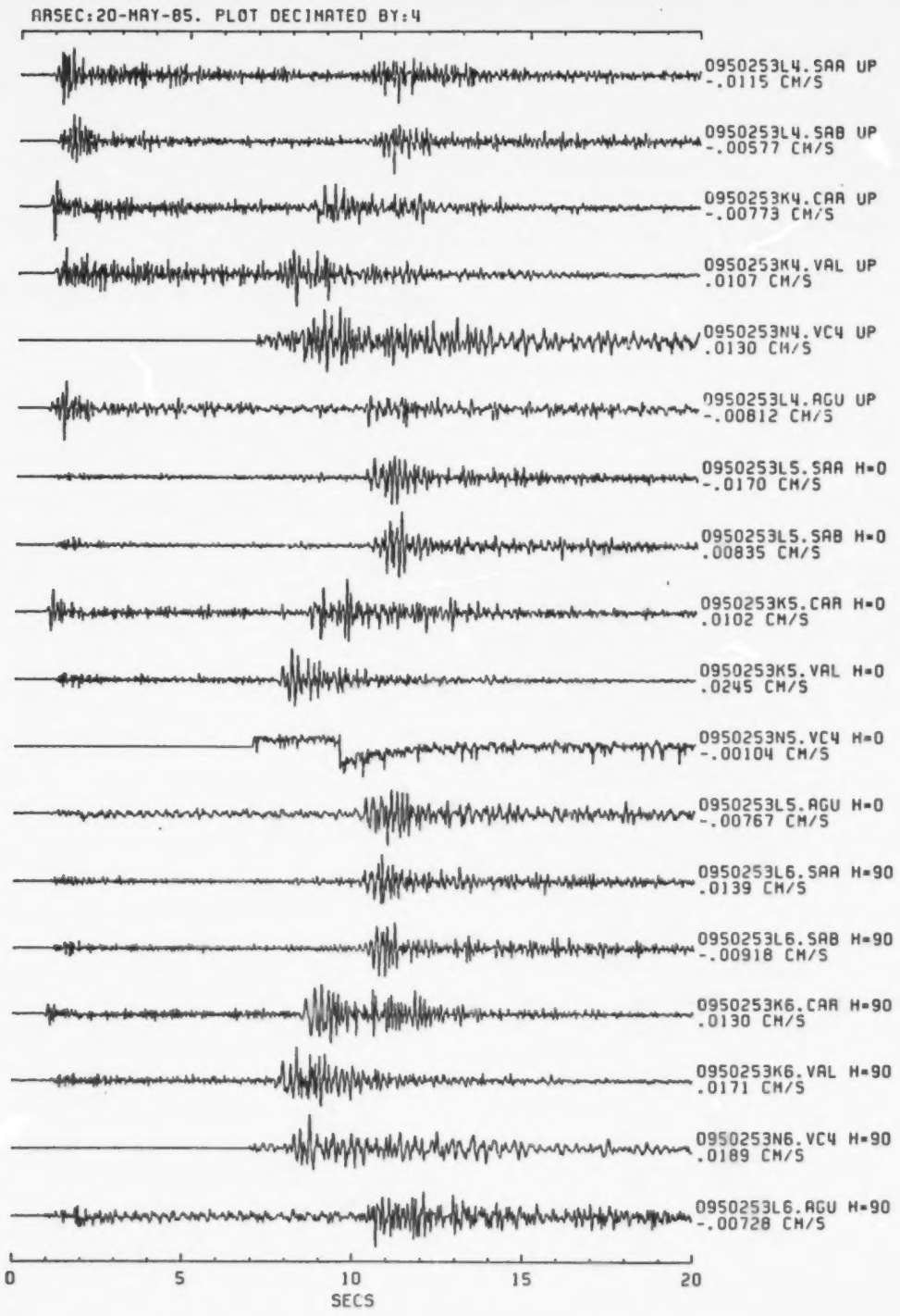

Figure 30.--Scaled amplitude plots for event 0950253. Hypocentral P-wave arrivals are aligned at 1 second. If the recorder triggered on S, the trace is arbitrarily shifted. Peak velocity is annotated.

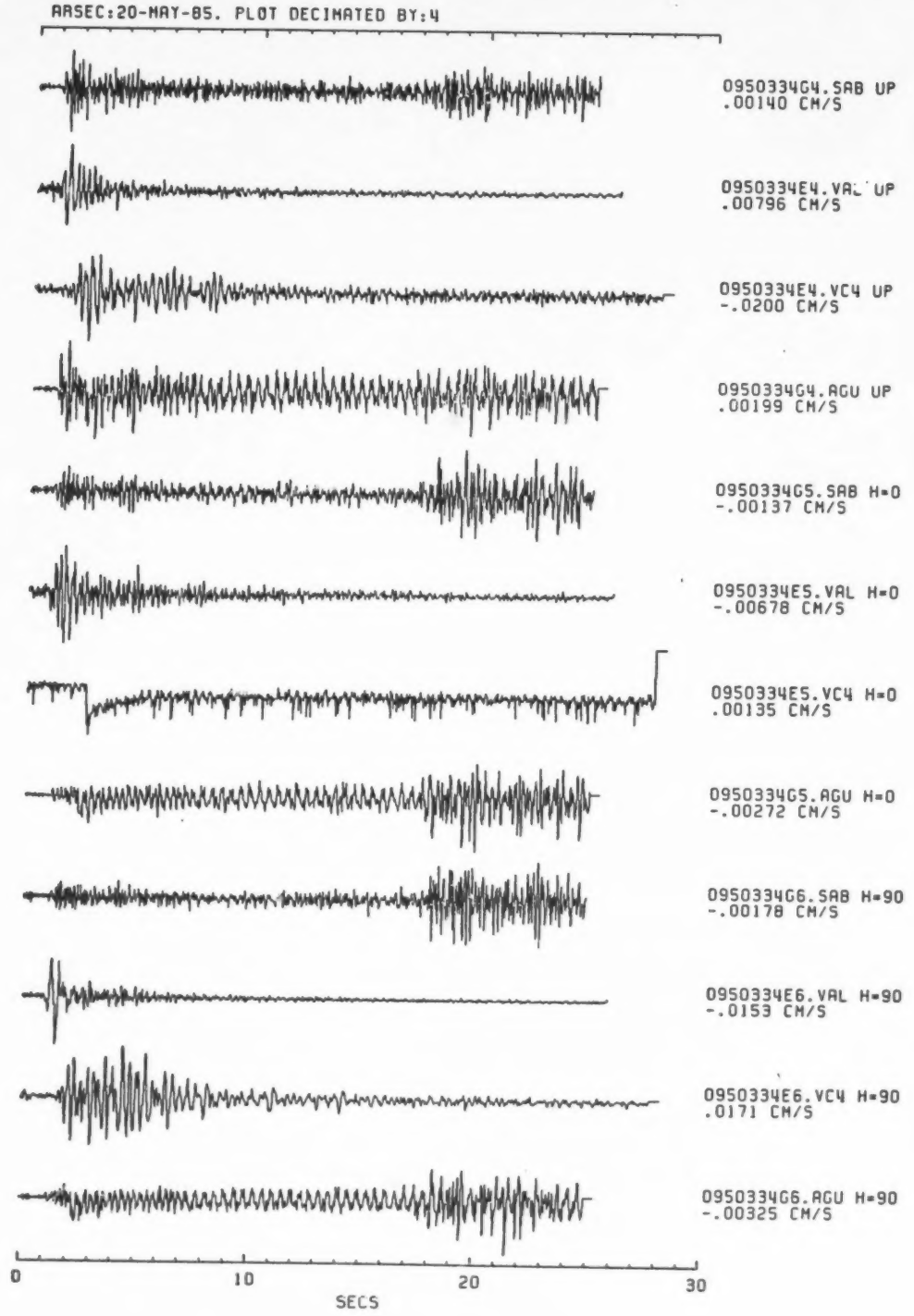

Figure 31.--Scaled amplitude plots for event 0950334. Hypocentral P-wave arrivals are aligned at 1 second. If the recorder triggered on S, the trace is arbitrarily shifted. Peak velocity is annotated.

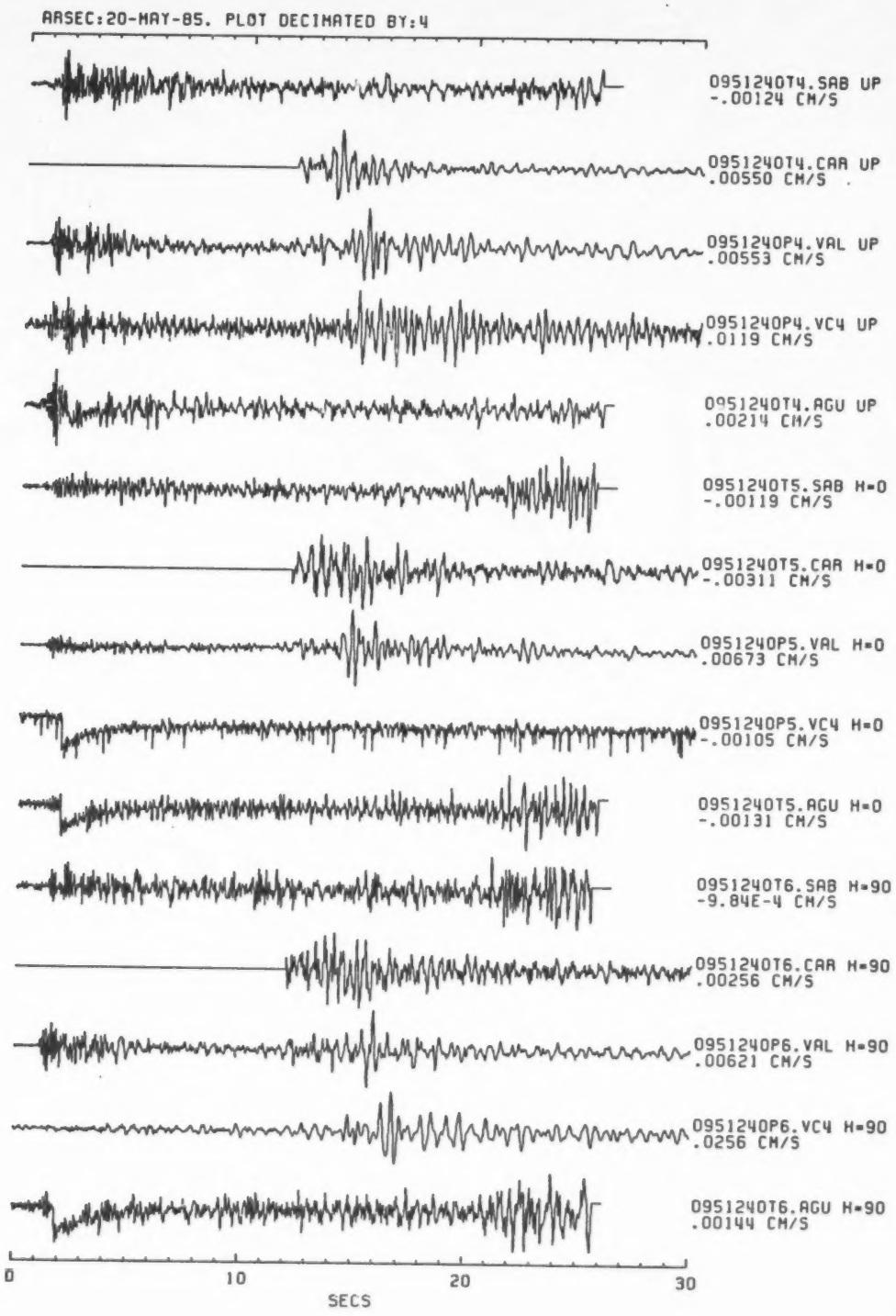

Figure 32.--Scaled amplitude plots for event 0951240. Hypocentral P-wave arrivals are aligned at 1 second. If the recorder triggered on S, the trace is arbitrarily shifted. Peak velocity is annotated.

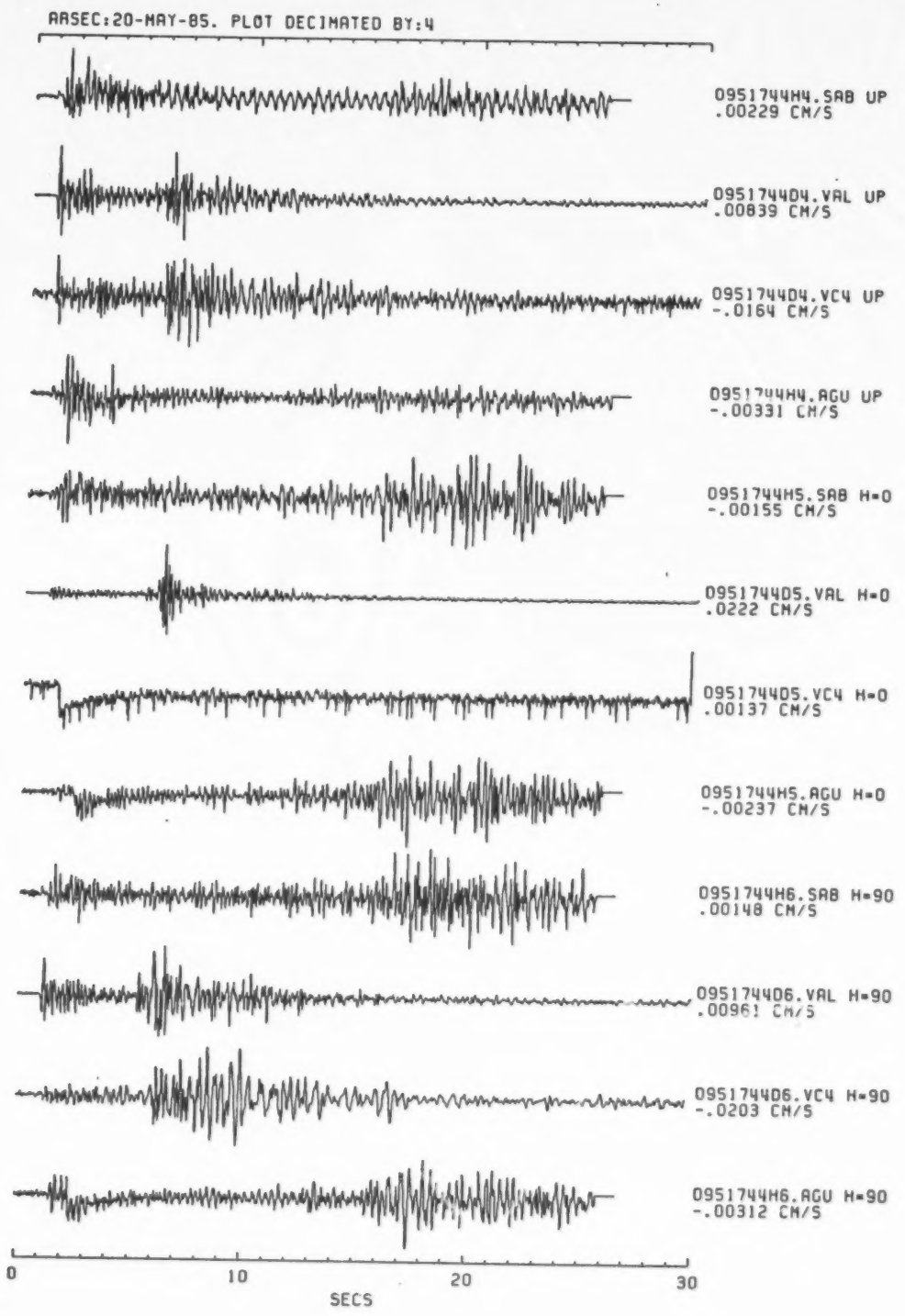

Figure 33.--Scaled amplitude plots for event 0951744. Hypocentral P-wave arrivals are aligned at 1 second. If the recorder triggered on S, the trace is arbitrarily shifted. Peak velocity is annotated.

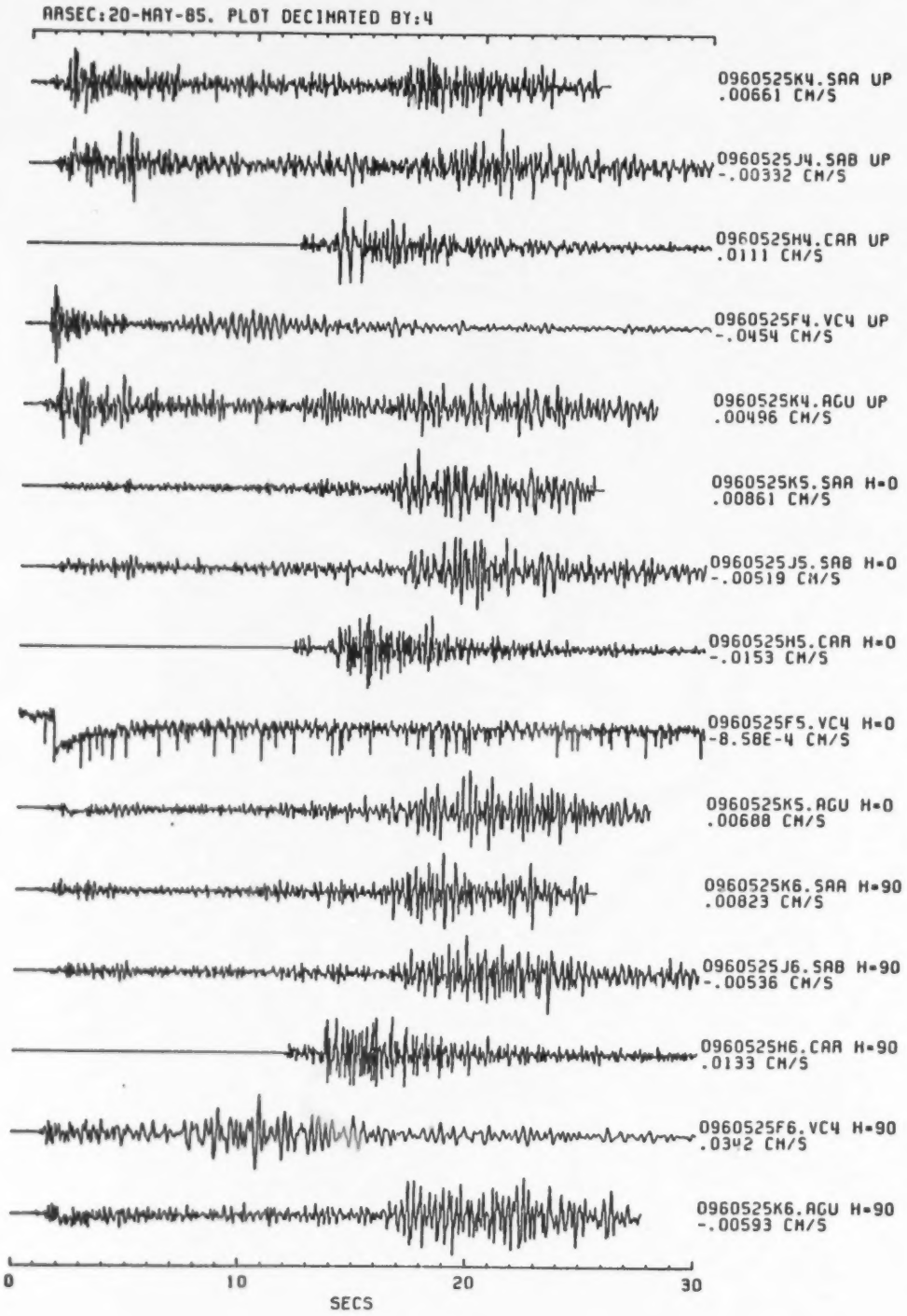

Figure 34.--Scaled amplitude plots for event 0960525. Hypocentral P-wave arrivals are aligned at 1 second. If the recorder triggered on S, the trace is arbitrarily shifted. Peak velocity is annotated.

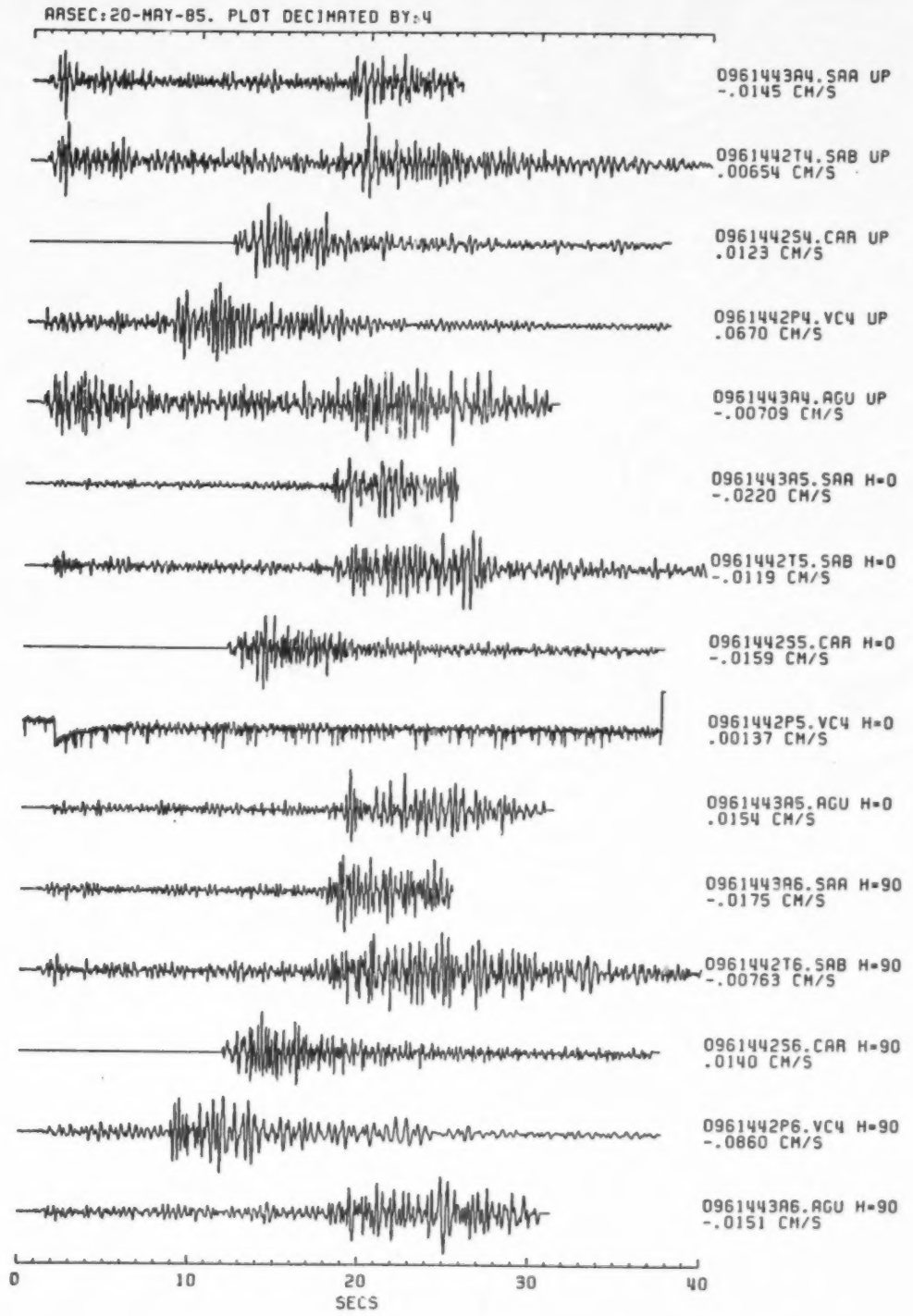

Figure 35.--Scaled amplitude plots for event 0961443. Hypocentral P-wave arrivals are aligned at 1 second. If the recorder triggered on S, the trace is arbitrarily shifted. Peak velocity is annotated.

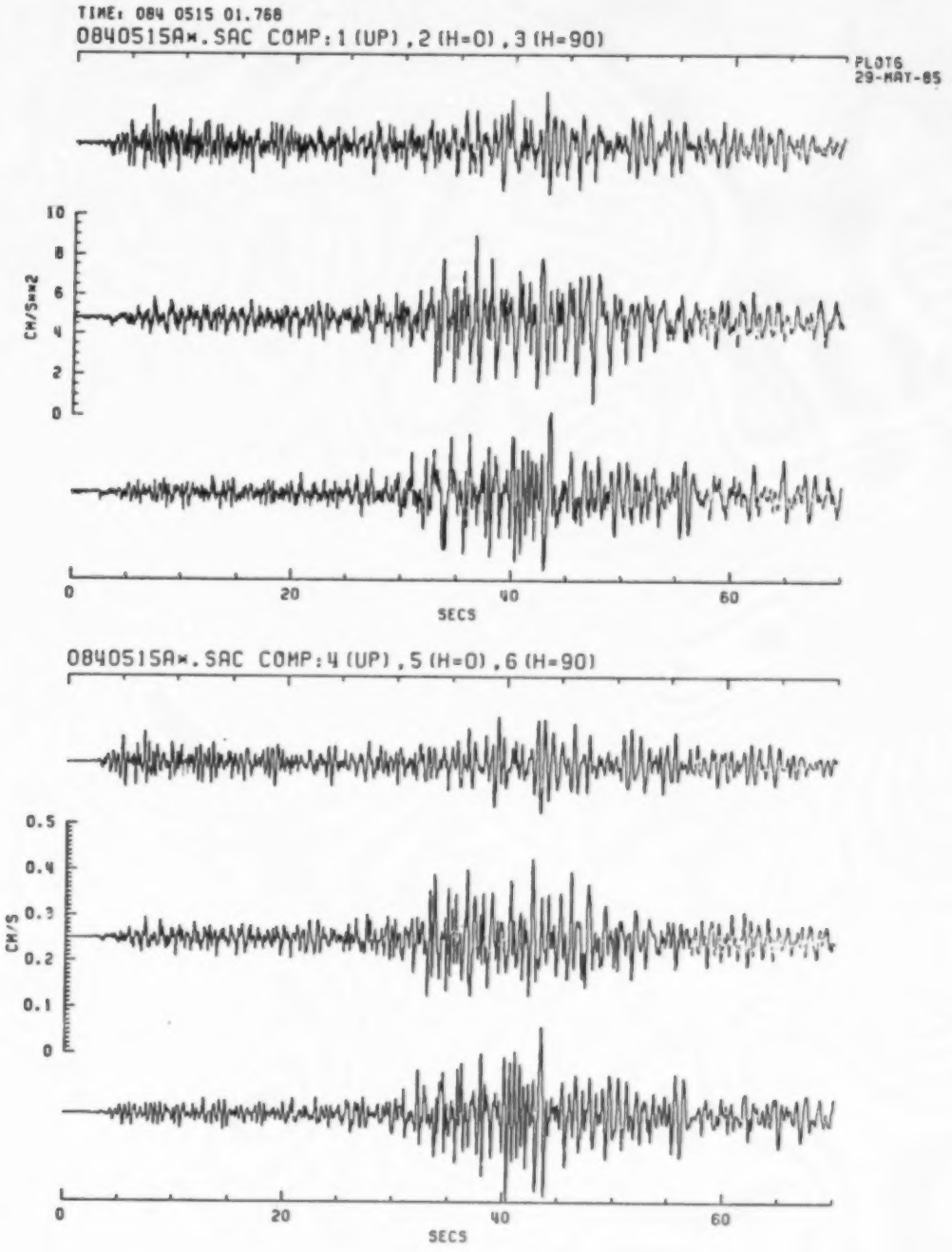

Figure 36.--Recorded acceleration and velocity for event 0840515 at SAC.

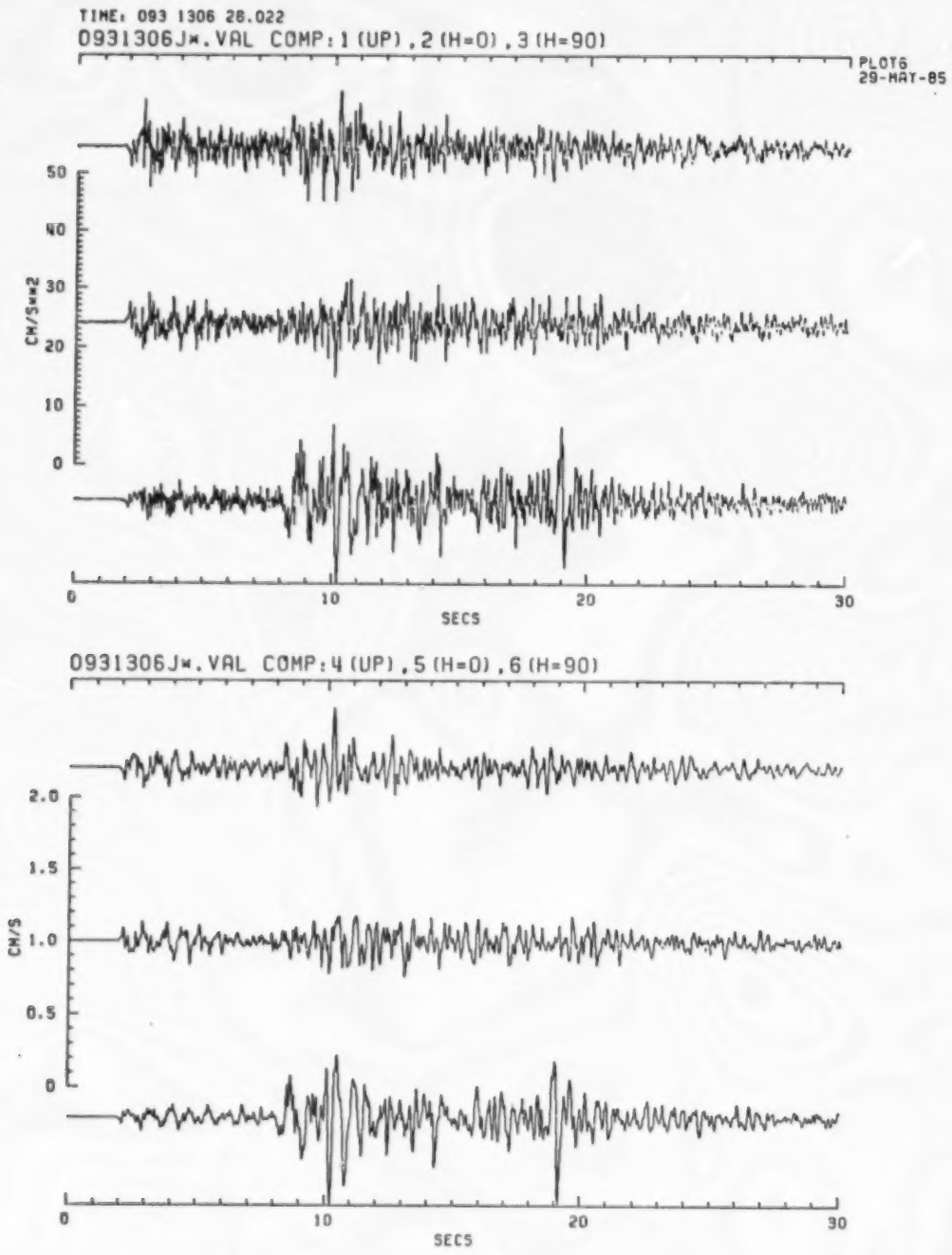

Figure 37.--Recorded acceleration and velocity for event 0930316 at VAL.

SITE SPECTRA AND SPECTRAL RATIOS

by

B. Askew, U.S. Geological Survey, Denver, CO 80225;
C. Mueller, A. Converse, and J. Watson, U.S. Geological Survey, Menlo Park, CA 94025; S. T. Algermissen, U.S. Geological Survey, Denver, CO 80225; R. Borcherdt, U.S. Geological Survey, Menlo Park, CA 94025; and
A. Tarr, U.S. Geological Survey, Denver, CO 80225

Site spectra and spectral ratios were computed from the aftershock data of the May 3, 1985, Chile earthquake, using the winnowed velocity data stored on the VAX 11/750 in the Branch of Engineering Seismology and Geology. The spectral analysis techniques used here are described in Rogers and others (1980).

The programs used to compute spectra and spectral ratios were written originally by Roger Borcherdt and were later modified by Al Rogers and Mark Meremonte. Additional programming was done by April Converse and Bonny Askew for this project. These programs process the signal by (1) filling an array appropriately sized for a Fast Fourier Transform with data points over a selected window, (2) removing any DC component from the signal, (3) applying a leakage correction to taper the signal, and (4) padding the array as necessary with zeroes. The spectrum is smoothed using a triangular window of a specified length and the power spectral density of the signal is then computed. The same processing is also applied to a section of input data taken before the arrival of an event in order to define the spectrum of the noise in the system. The signal-to-noise ratio is then computed, and, where this falls below a given discriminant, the signal spectrum is set to a value equal to the minimum value of the spectrum (determined where the signal-to-noise ratio is greater than the discriminant). The seismogram, after processing, and the spectrum, with noise removed, are plotted. For a given event, spectral ratios are computed between each station in the input data set and a specified reference station. Spectral ratios are set to a value close to zero at points where the signal-to-noise ratio is less than the discriminant for either of the two stations in the ratio. These spectral ratios are also plotted.

In order to process the data from the Chile aftershocks, a subset of the winnowed data was selected consisting of events recorded at three or more stations. Three reference stations were selected: SAB, CAR, and VAL. Each reference station and the stations associated with it is called a group. These groups are listed in table 1. As an example, a given event might have one group of data referenced to SAB, another group referenced to CAR, but none referenced to VAL. If, for a given event, data were recorded at a reference station but no other stations in the reference group, these data were taken out of the input set. Data recorded for a given event at stations in a reference group for which no data were recorded at the appropriate reference station were taken out of the input set. Other data were deleted because the signal was not of sufficient quality or had not triggered properly. Spectra and spectral ratios were computed from the remaining data set and these spectra and ratios are shown in table 2.

TABLE 1.—Reference Groups

Reference station	SAB	CAR	VAL
	SAA	SAN	VC4
	SAC	SCH	END
	SAD		
	SAE		
	AGU		

A signal-to-noise discriminant value of 3 was used for all the data. Thus spectra and spectral ratios were computed only where the signal was at least three times as great as the noise. For all data, the first 1.5 sec was used as the noise sample. The length of the signal was determined for each reference group of each event after examining the playbacks for those records. All signal samples were chosen to begin at 1.5 sec after the instrument triggered. The length of the smoothing window was chosen to be 7 points (with 200 points per sec) for events where the signal was up to 60 sec long, and 15 points for signals greater than or equal to 60 sec long.

A sample of the spectra and spectral ratio plots are included in figures 1 through 40. Included with each plot of the signal spectrum is the processed time series signal from which the spectrum was computed. The signal spectrum is plotted with noise removed. The technique for removing noise as previously described accounts for the abrupt dropoff to a constant low level in portions of some spectra. Plots of spectral ratios are also included. The horizontal 0-degree component for the stations SAN and VC4 are not included because these components did not record properly.

REFERENCES

Rogers, A. M., Covington, P. A., Park, R. B., Borcherdt, R. D., and Perkins, D. M., 1980, Nuclear event time histories and computed site transfer functions for locations in the Los Angeles region: U.S. Geological Survey, Open-File Report 80-1173, 37 p.

TABLE 2.—Spectral Ratio Sets

Event Day Hour	Ref. Station	Stations used to compute ratios		
083-2346	SAB:	SAA	SAC	SAD
084-0129	SAB:	SAA	SAC	SAD
084-0304	SAB:	SAA	SAC	SAD
088-0251	SAB:	SAA	SAC	SAE
088-0546	SAB:	SAA	SAC	
089-0618	SAB:	SAA	SAD	SAE
089-0633	SAB:	SAA	SAD	
	CAR:	SCH		
089-0814	SAB:	SAA	SAE	
089-0905	SAB:	SAD	SAE	
	CAR:	SAN	SCH	
089-1210	SAB:	SAE		
	CAR:	SAN	SCH	
089-1848	SAB:	SAA	SAE	
	CAR:	SAN		
089-2026	SAB:	SAA	SAE	
089-2209	SAB:	SAA	SAE	
	CAR:	SAN		
090-0825	SAB:	SAA	SAD	SAE
	CAR:	SAN		
091-0619	CAR:	SAN	SCH	
093-0357	SAB:	SAA		
	VAL:	VC4		
093-1306	SAB:	SAA	SAC	
	VAL:	VC4		
095-0253	SAB:	SAA		
	VAL:	VC4	AGU	
095-0334	VAL:	VC4	AGU	
095-1240	VAL:	VC4	AGU	
095-1744	VAL:	VC4	AGU	
096-0525	SAB:	SAA		
096-1442	SAB:	SAA		

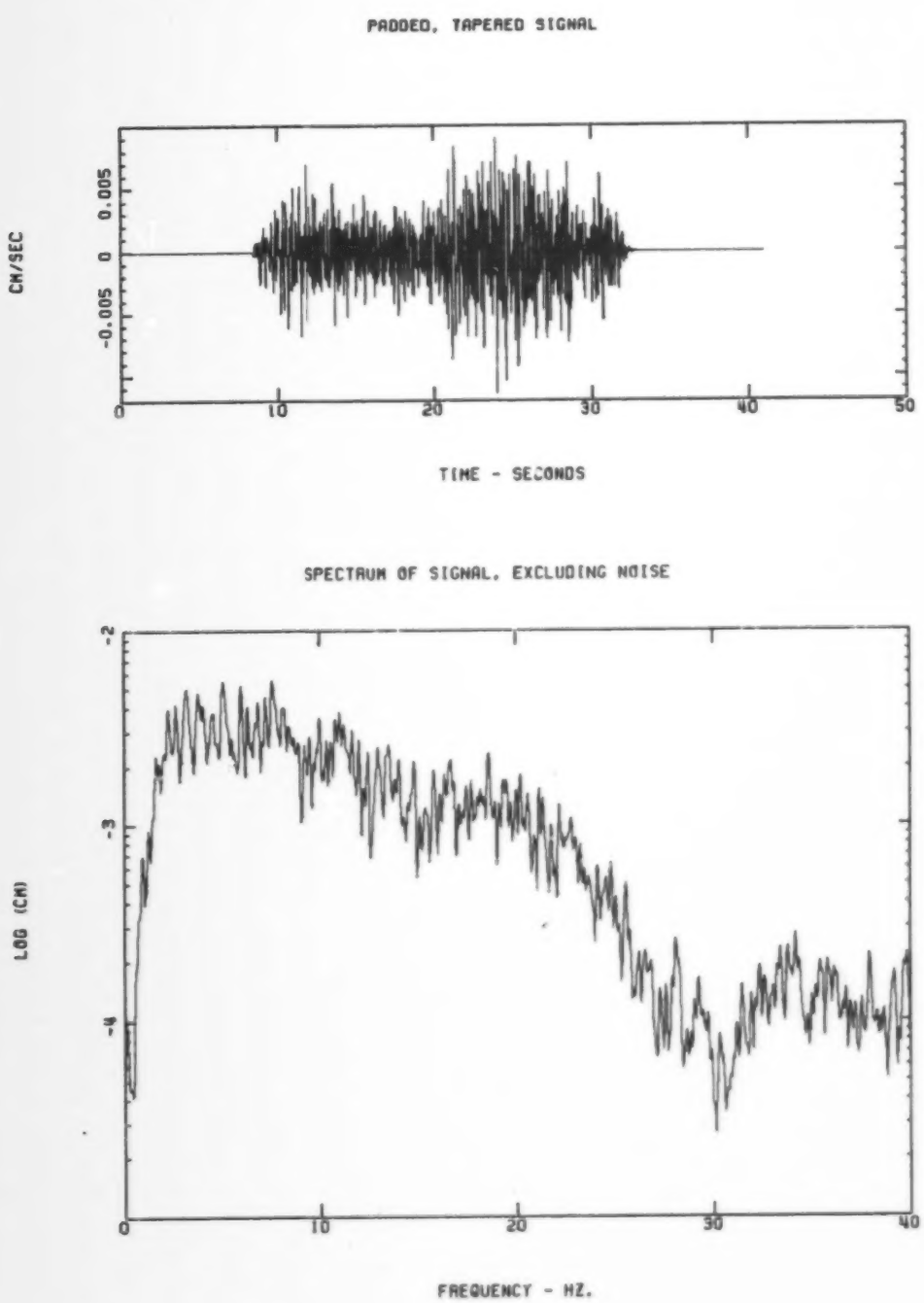

Figure 1.--Time series and spectrum of event on March 29 at 02:51:57 for the vertical component at station SAB.

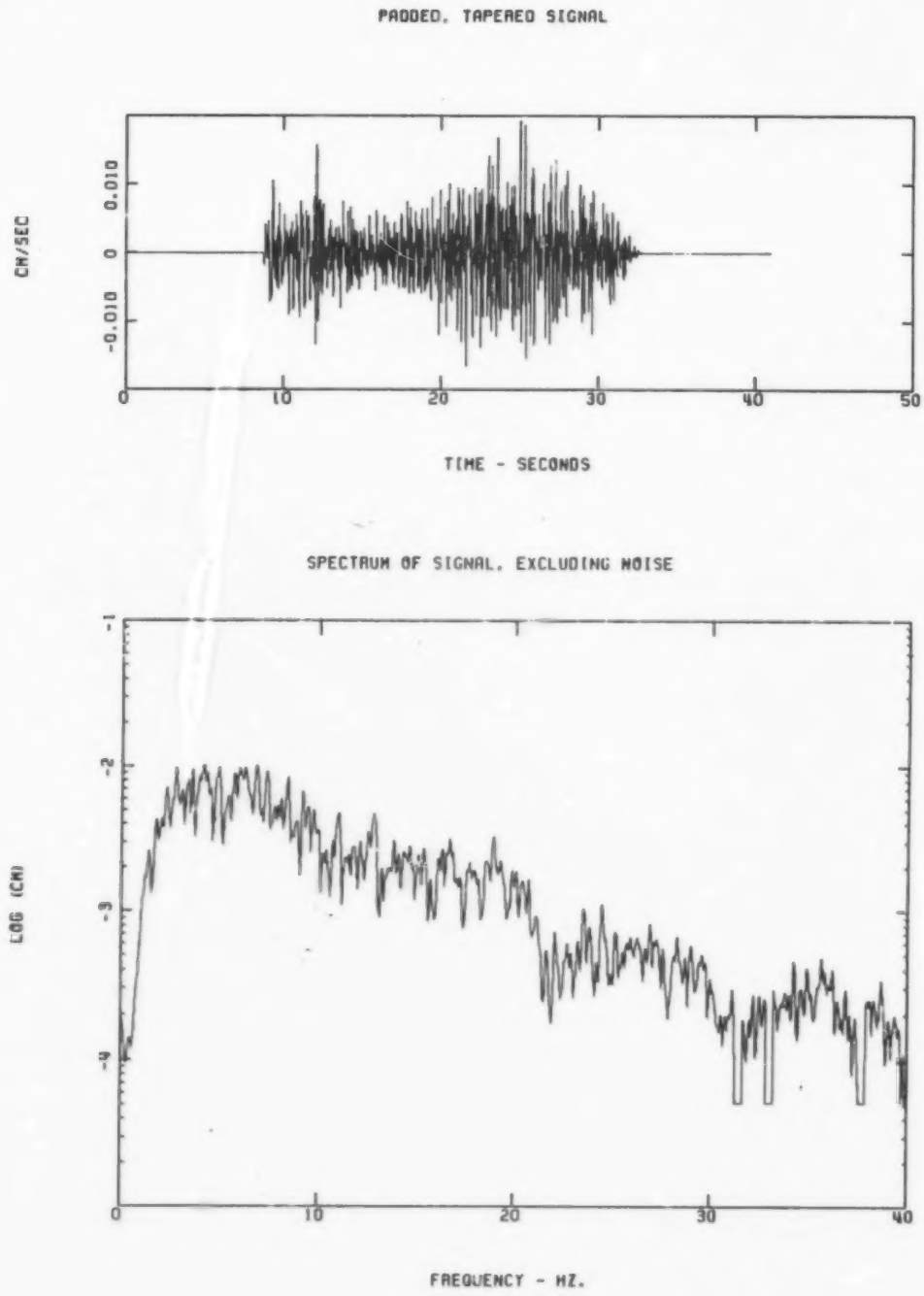

Figure 2.--Time series and spectrum of event on March 29 at 02:51:57 for the vertical component at station SAA.

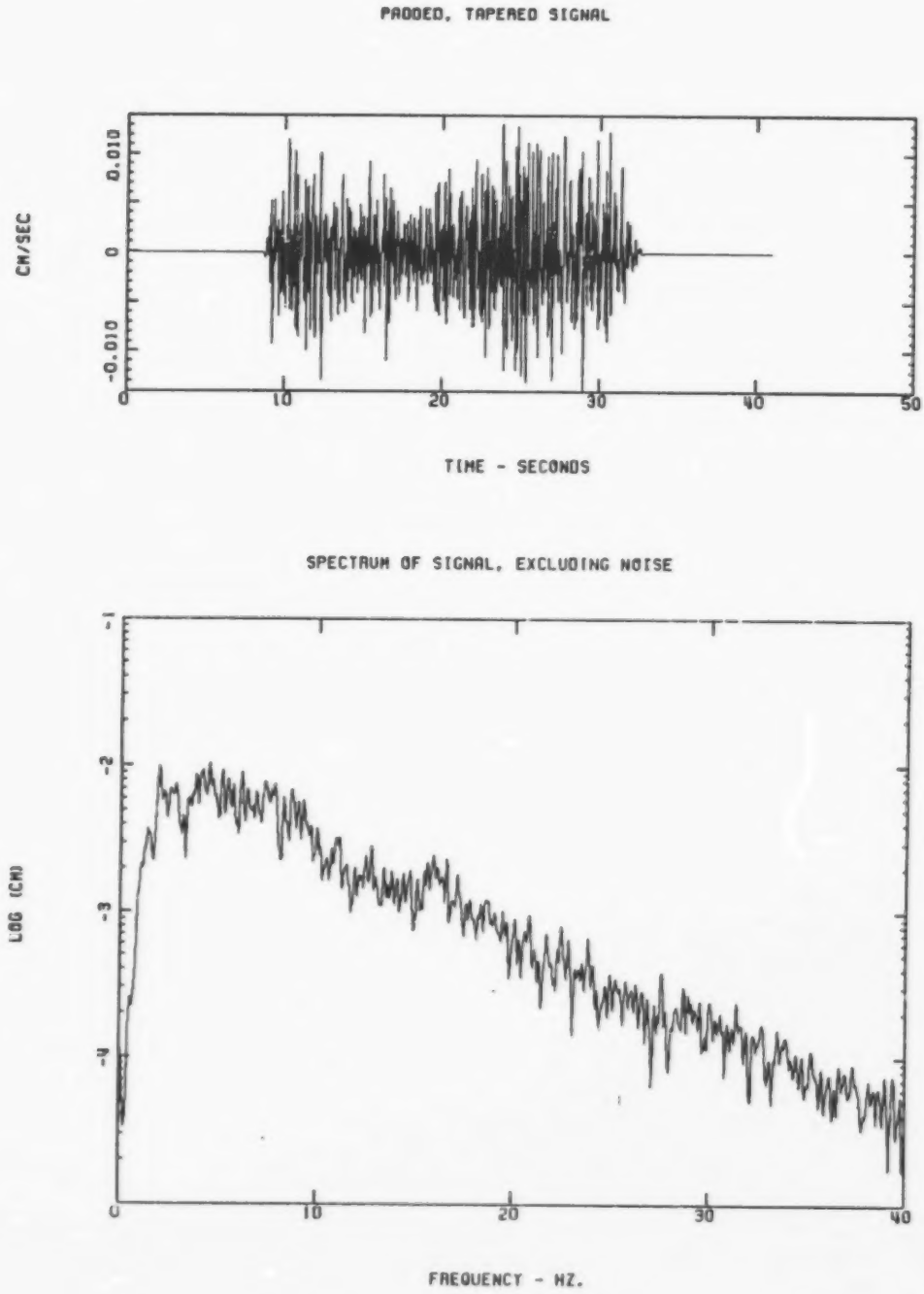

Figure 3.--Time series and spectrum of event on March 29 at 02:51:57 for the vertical component at station SAC.

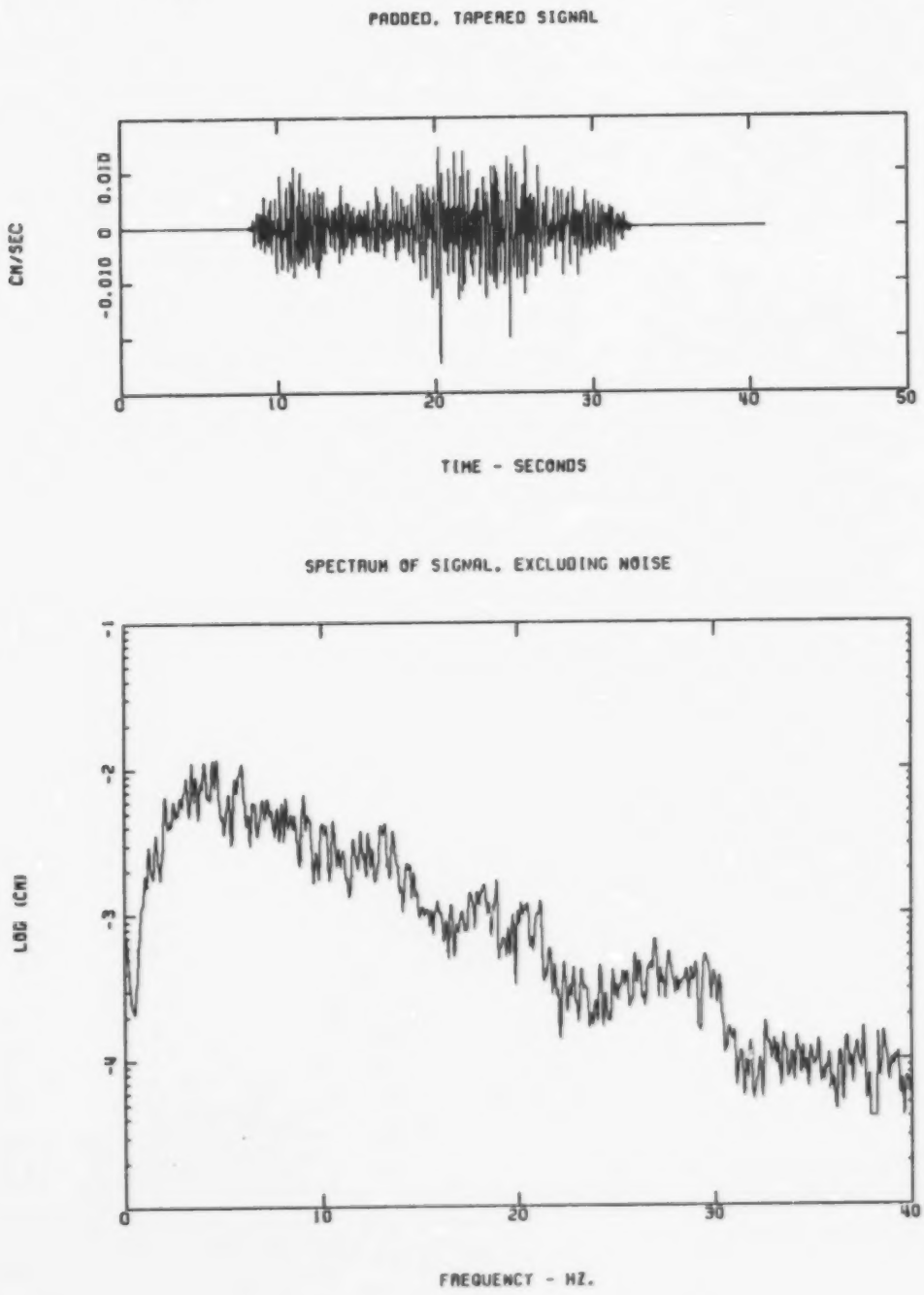

Figure 4.--Time series and spectrum of event on March 29 at 02:51:57 for the vertical component at station SAE.

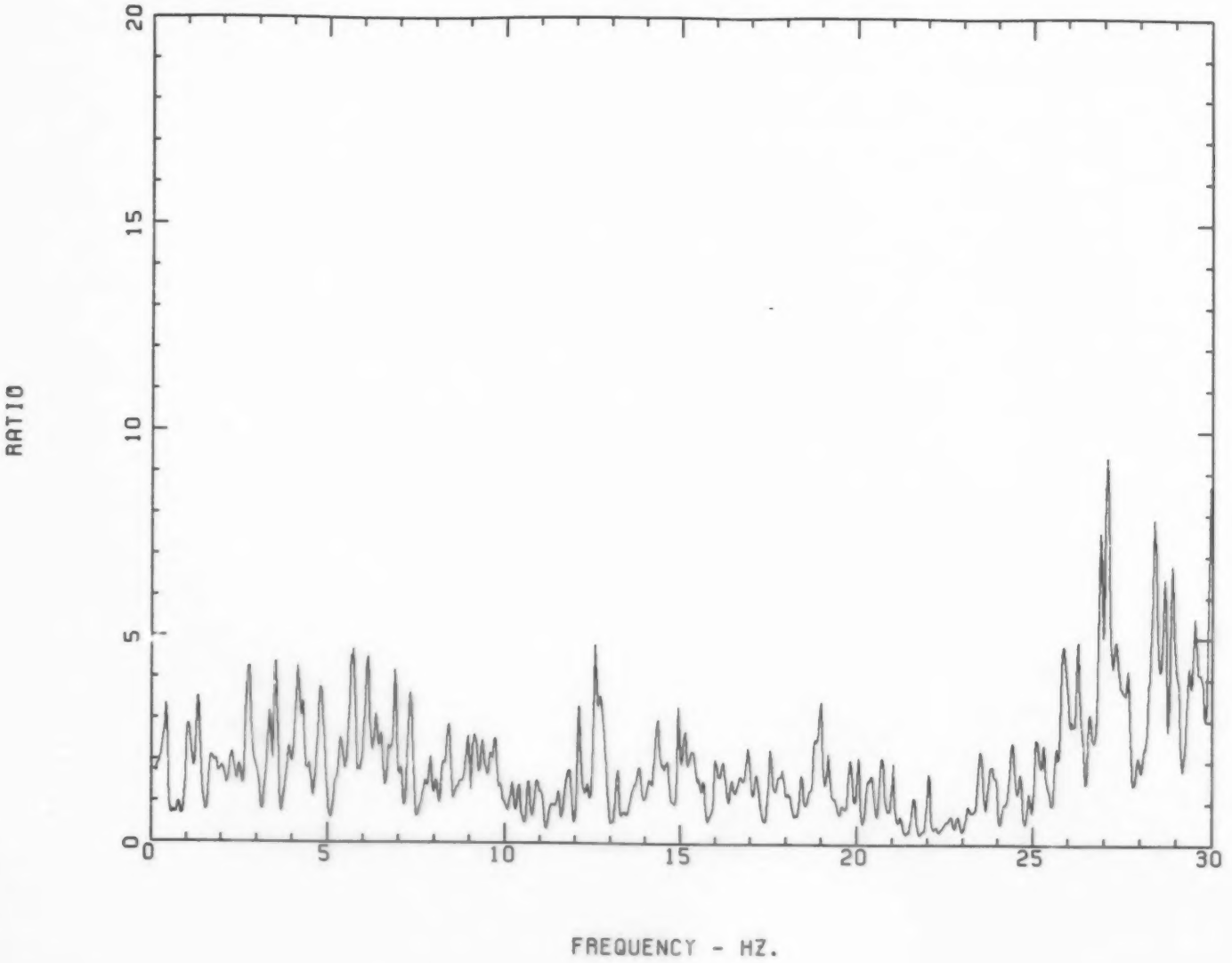

Figure 5.--Ratio of signal spectra of stations SAA/SAB for event on March 29 at 02:51:57 for the vertical component.

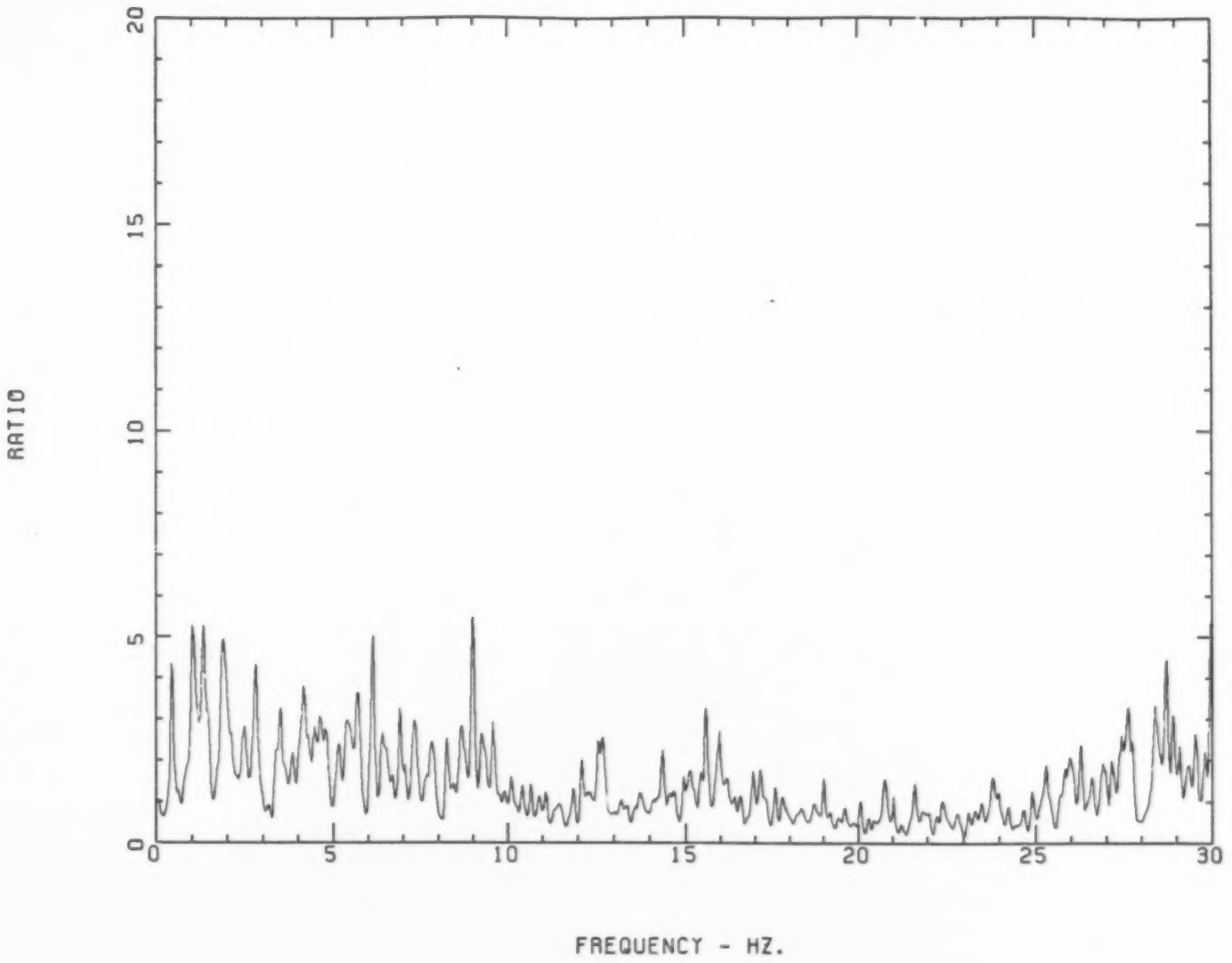

Figure 6.--Ratio of signal spectra of stations SAC/SAB for event on March 29 at 02:51:57 for the vertical component.

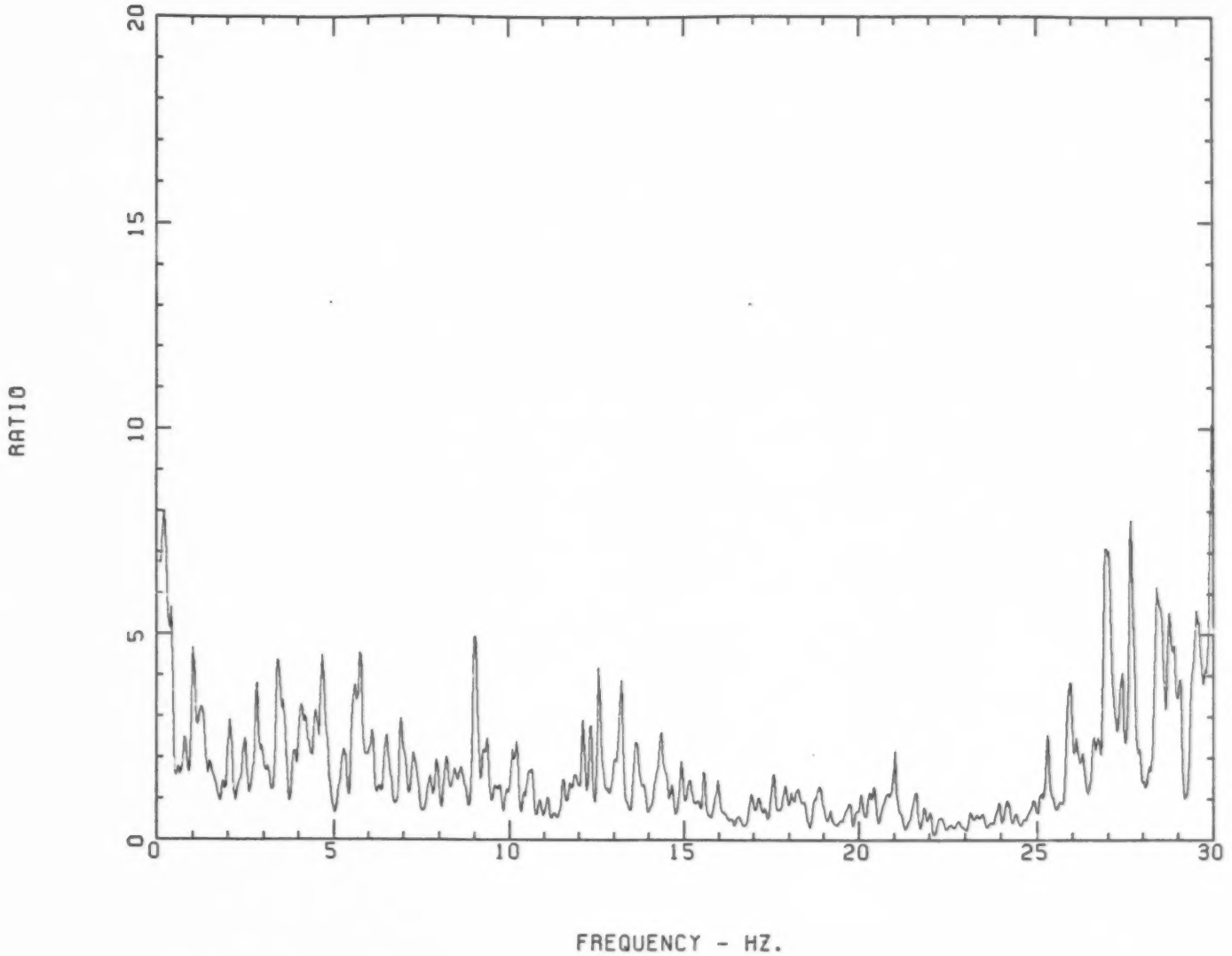

Figure 7.--Ratio of signal spectra of stations SAE/SAB for event on March 29 at 02:51:57 for the vertical component.

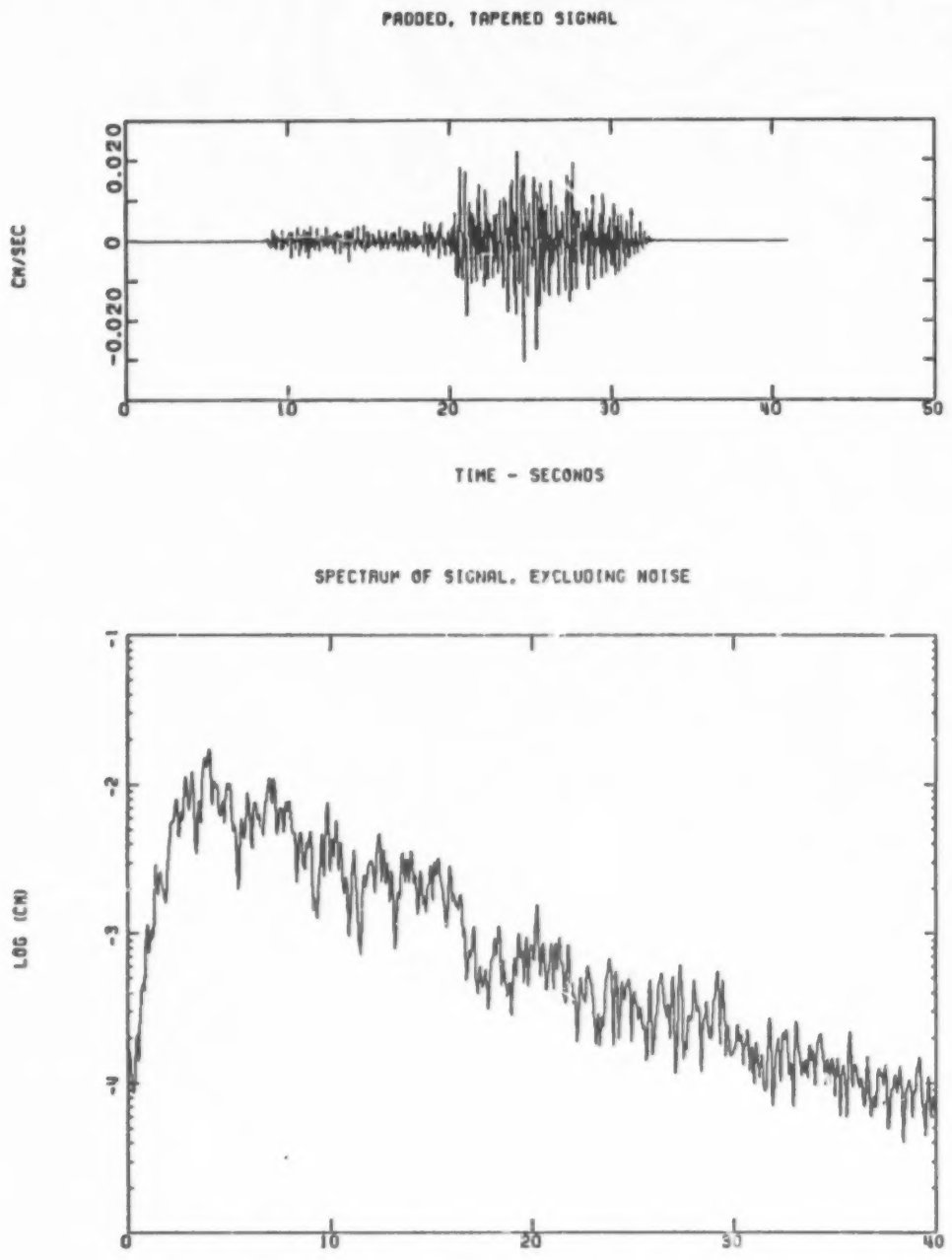

Figure 8.--Time series and spectrum of event on March 29 at 02:51:57 for the horizontal 0-degree component at station SAB.

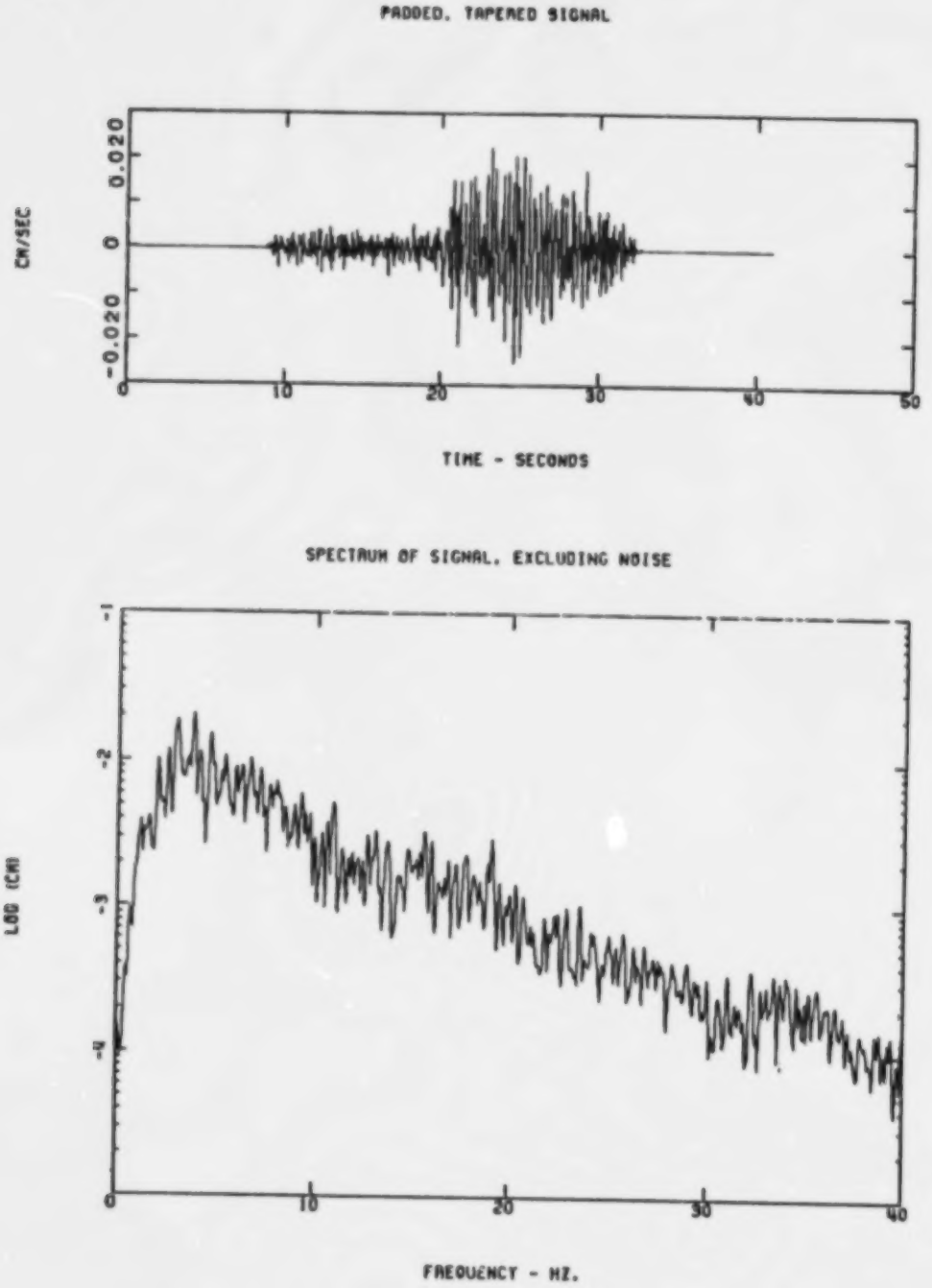

Figure 9.--Time series and spectrum of event on March 29 at 02:51:57 for the horizontal 0-degree component at station SAA.

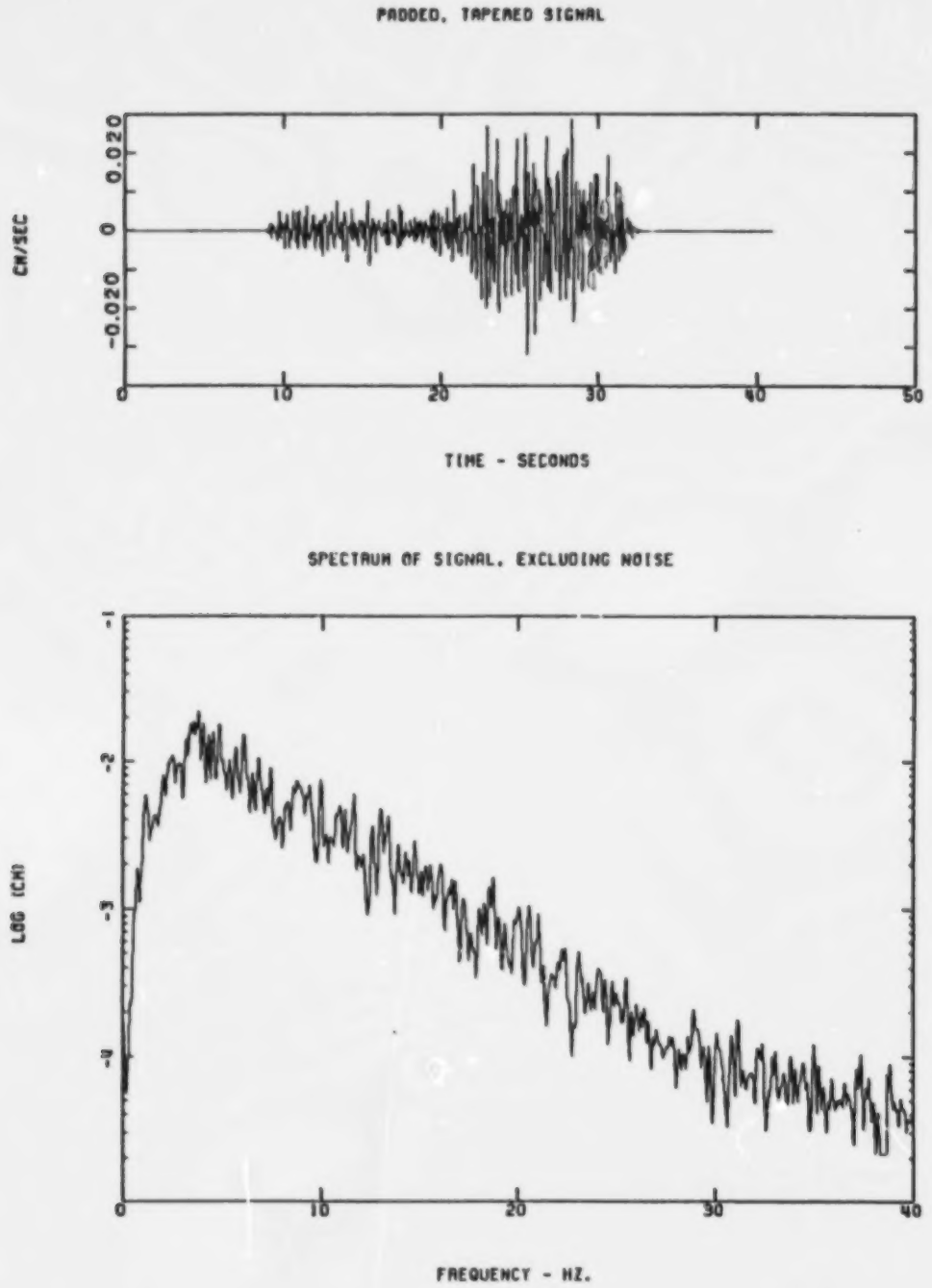

Figure 10.--Time series and spectrum of event on March 29 at 02:51:57 for the horizontal 0-degree component at station SAC.

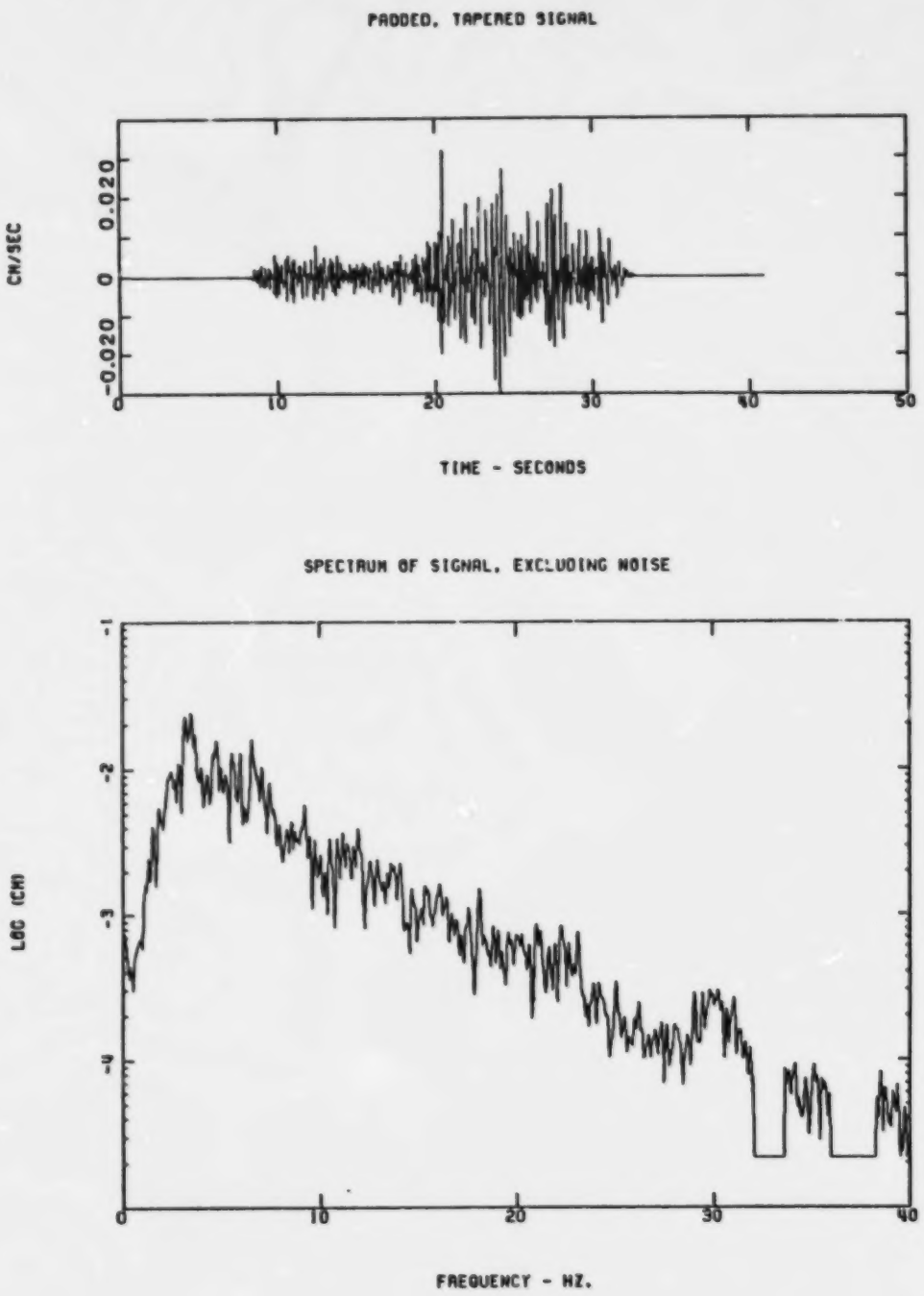

Figure 11.--Time series and spectrum of event on March 29 at 02:51:57 for the horizontal 0-degree component at station SAE.

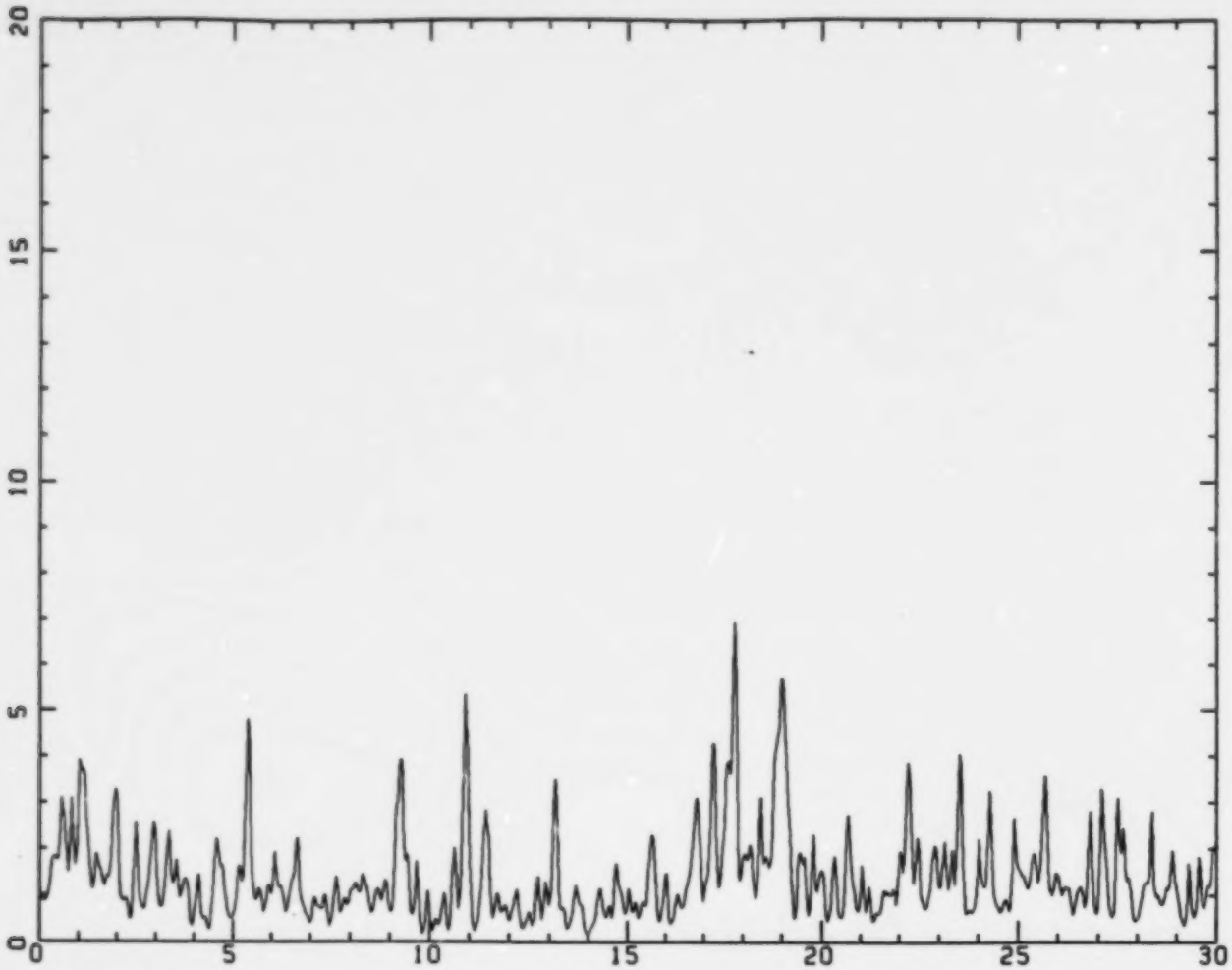

Figure 12.--Ratio of signal spectra of stations SAA/SAB for event on March 29 at 02:51:57 for the horizontal 0-degree component.

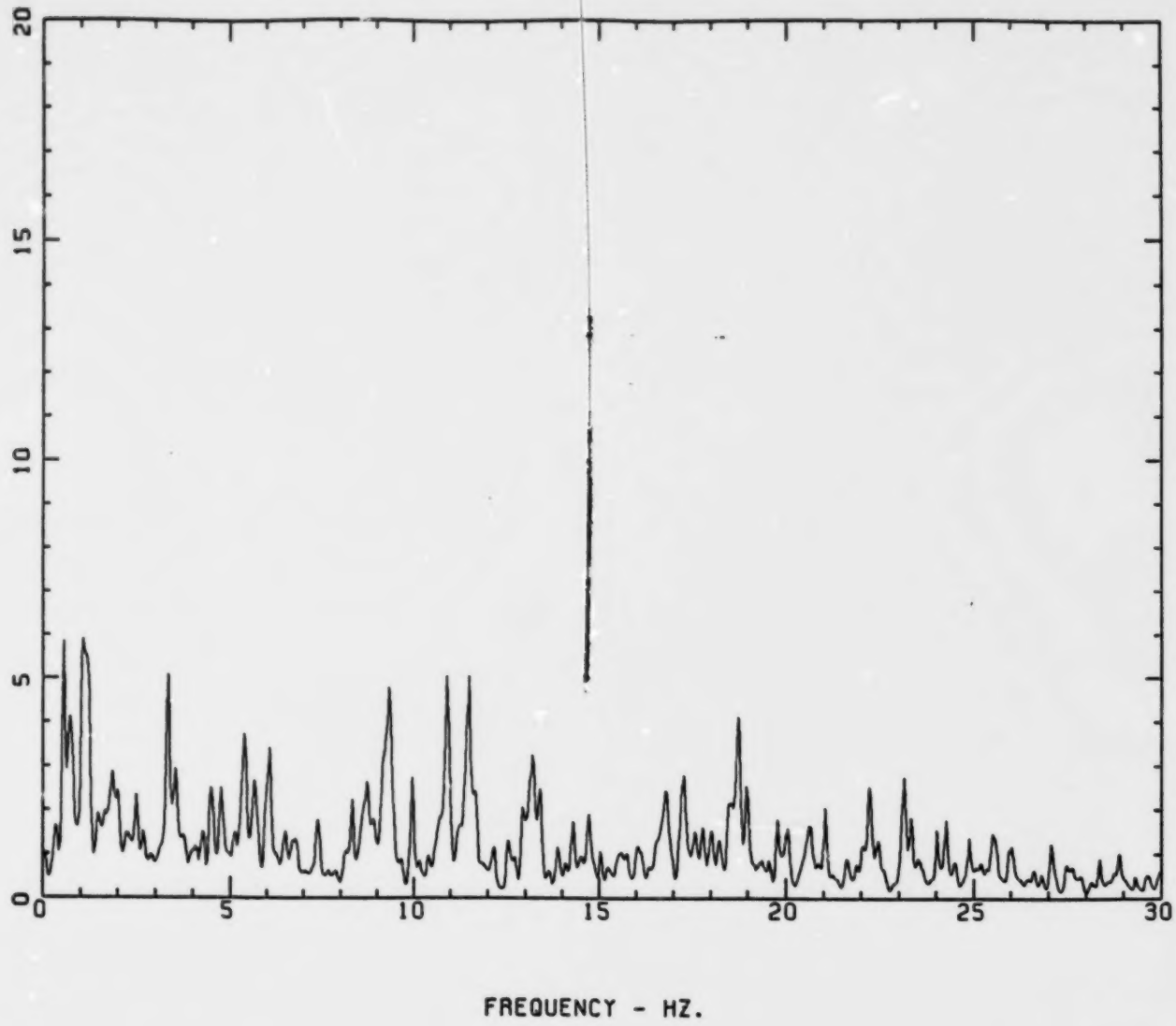

Figure 13.—Ratio of signal spectra of stations SAC/SAB for event on March 29 at 02:51:57 for the horizontal 0-degree component.

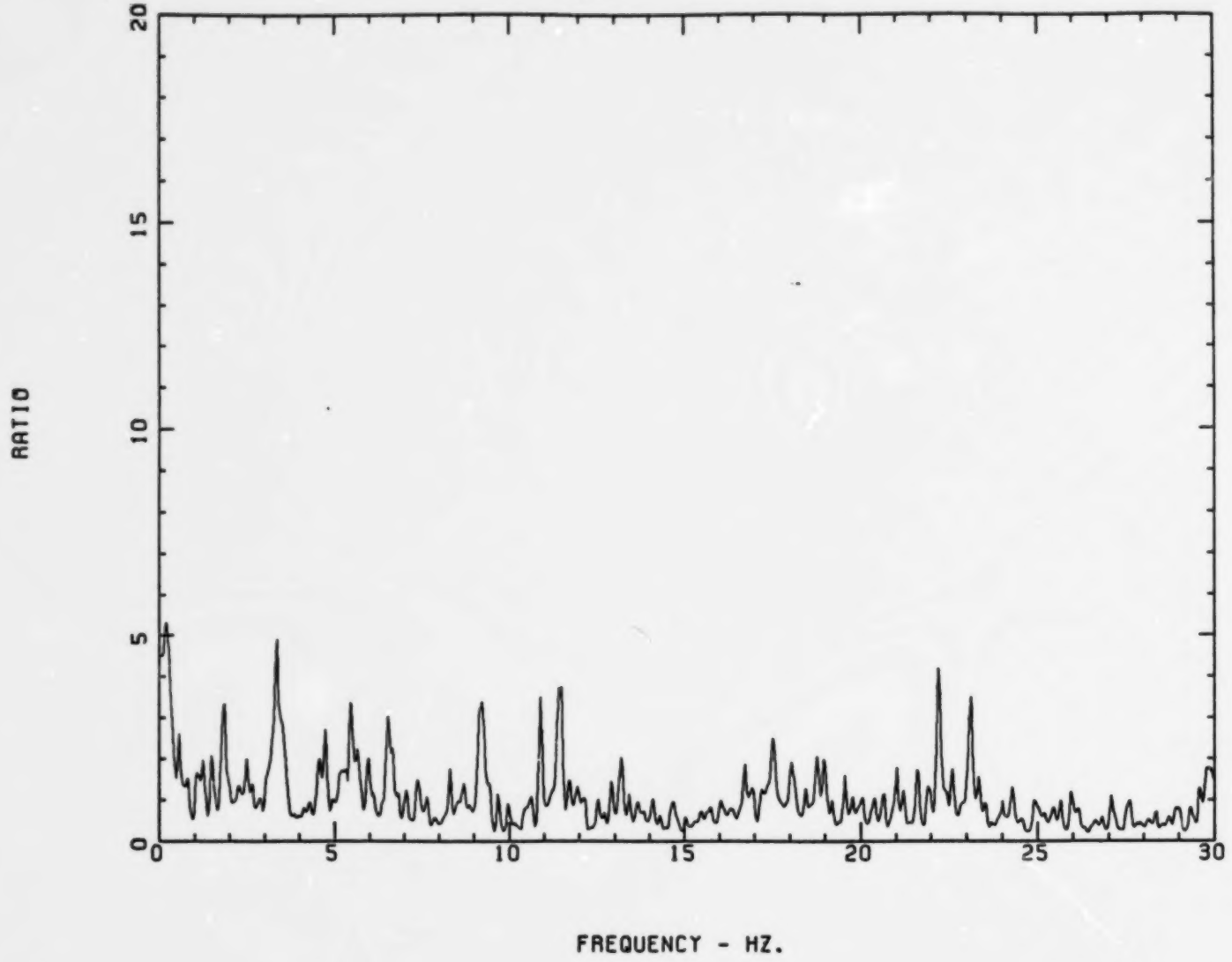

Figure 14.--Ratio of signal spectra of stations SAE/SAB for event on March 29 at 02:51:57 for the horizontal 0-degree component.

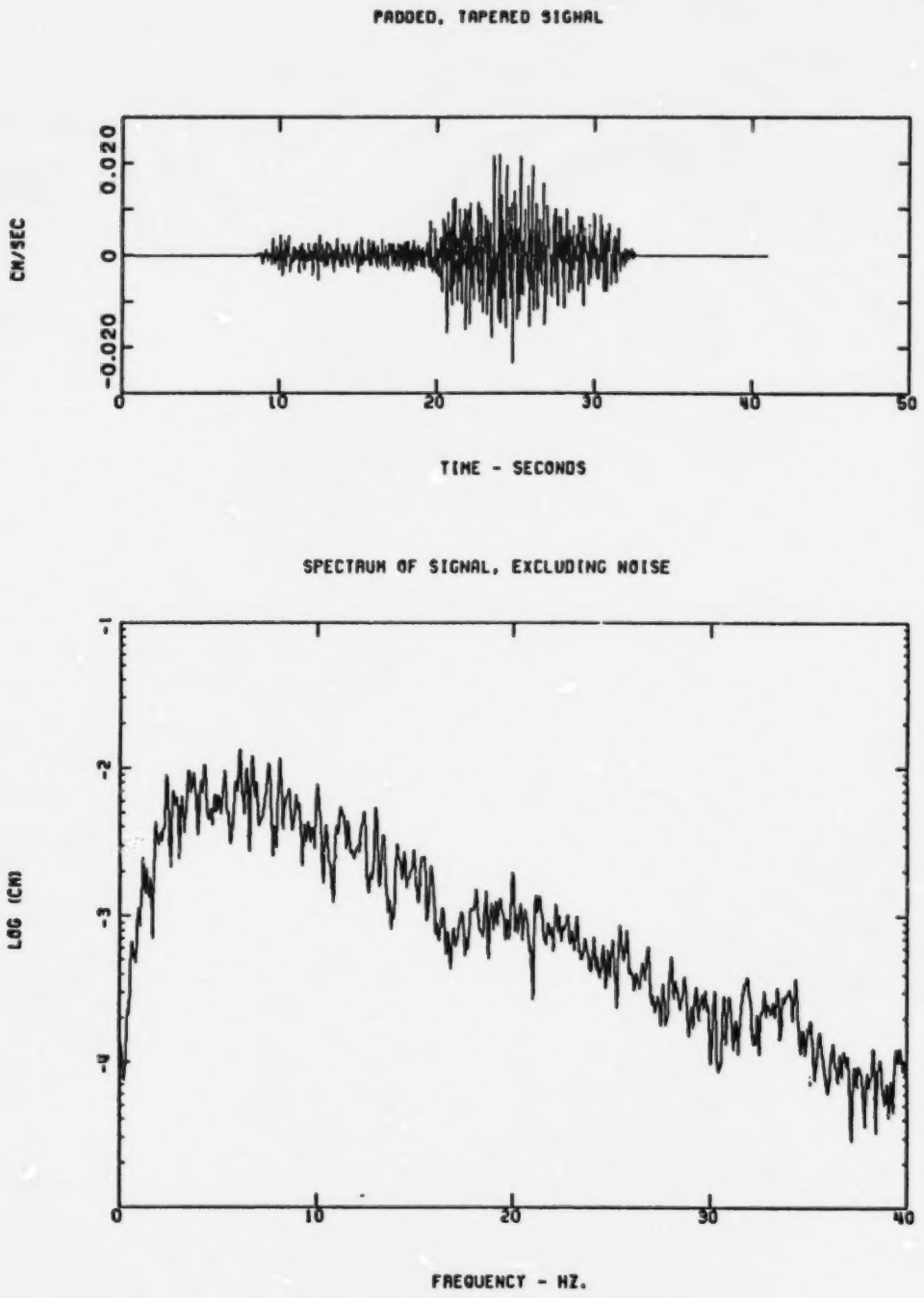

Figure 15.--Time series and spectrum of event on March 29 at 02:51:57 for the horizontal 90-degree component at station SAB.

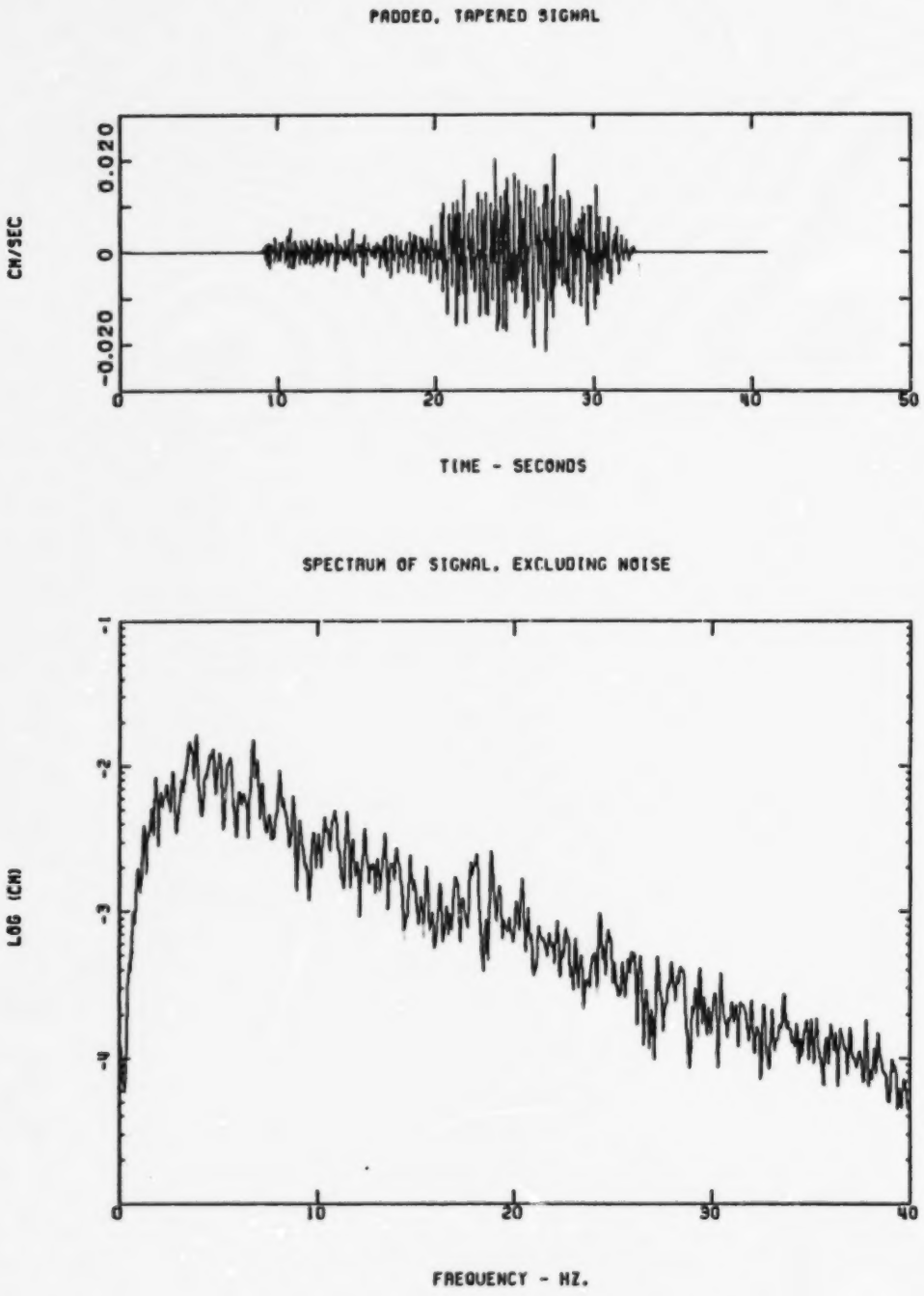

Figure 16.--Time series and spectrum of event on March 29 at 02:51:57 for the horizontal 90-degree component at station SAA.

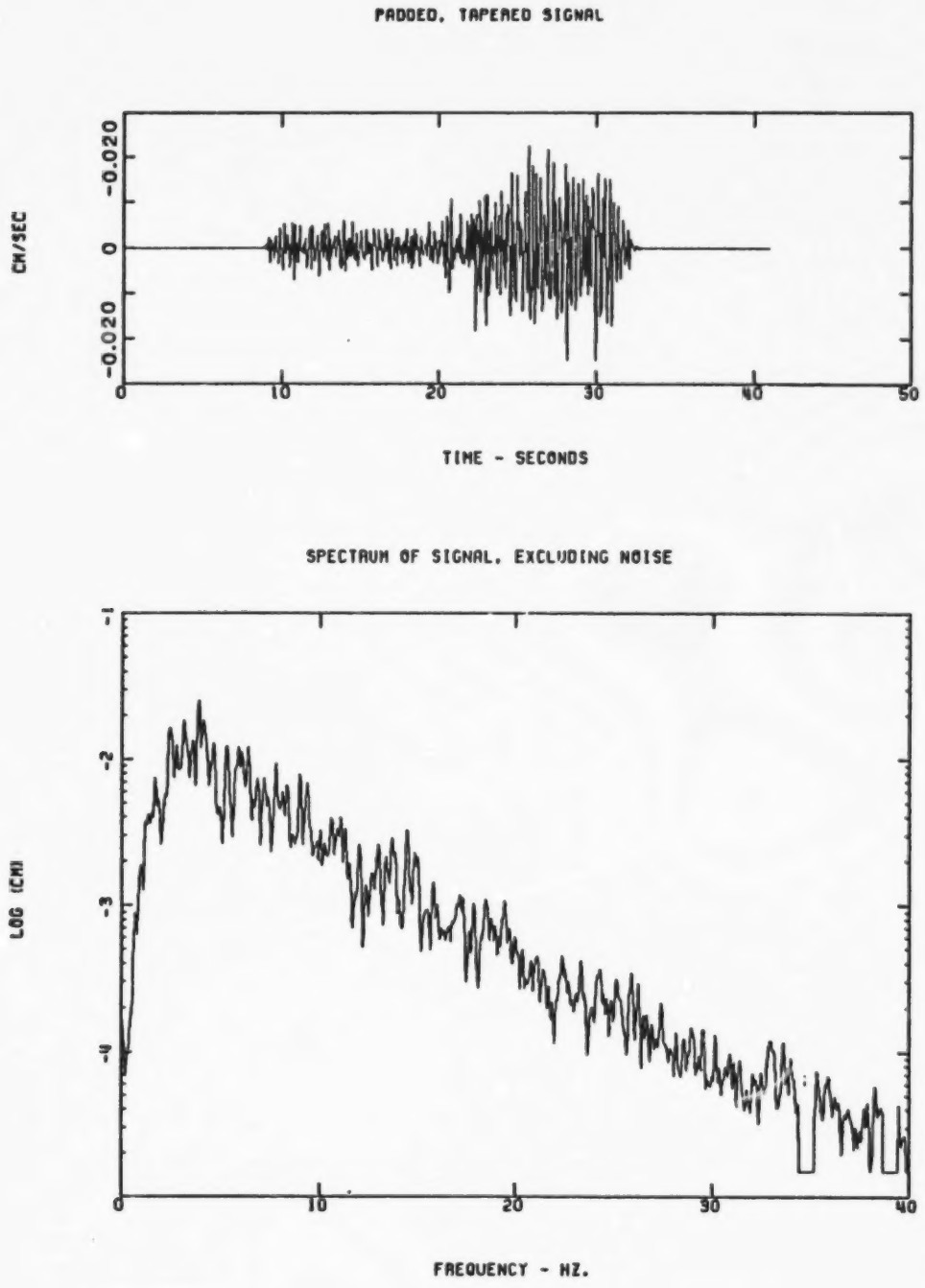

Figure 17.--Time series and spectrum of event on March 29 at 02:51:57 for the horizontal 90-degree component at station SAC.

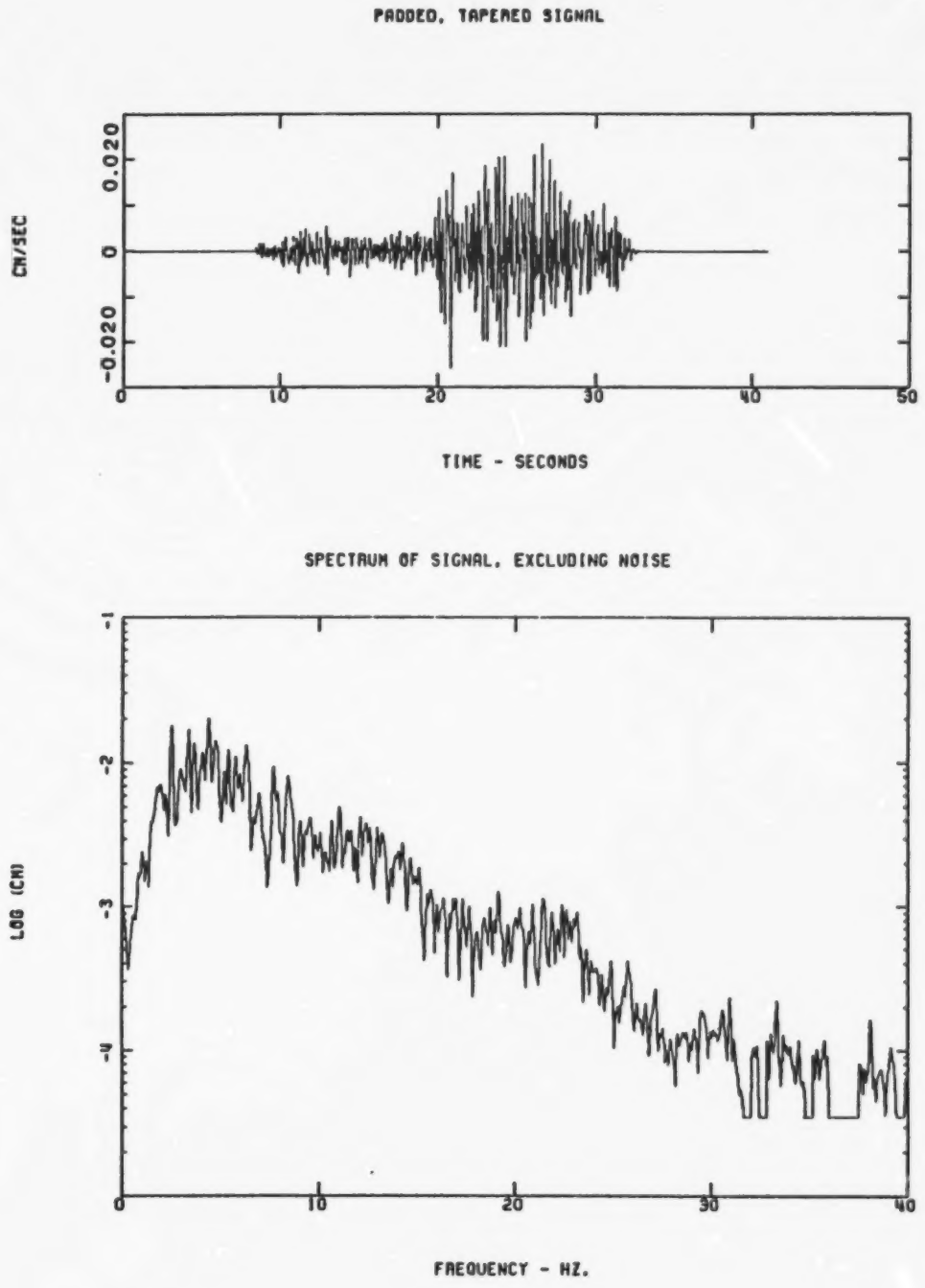

Figure 18.--Time series and spectrum of event on March 29 at 02:51:57 for the horizontal 90-degree component at station SAE.

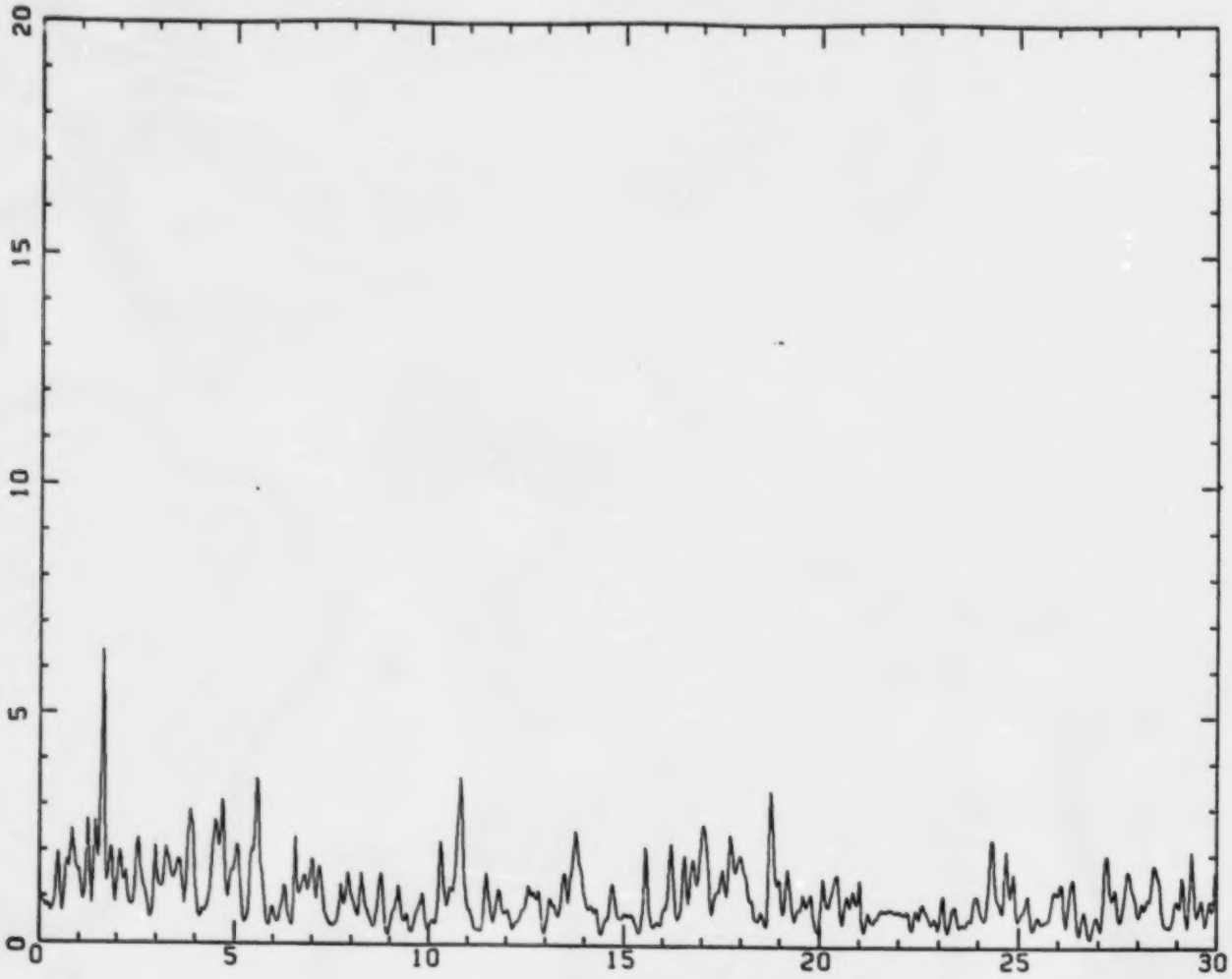

Figure 19.--Ratio of signal spectra of stations SAA/SAB for event on March 29 at 02:51:57 for the horizontal 90-degree component.

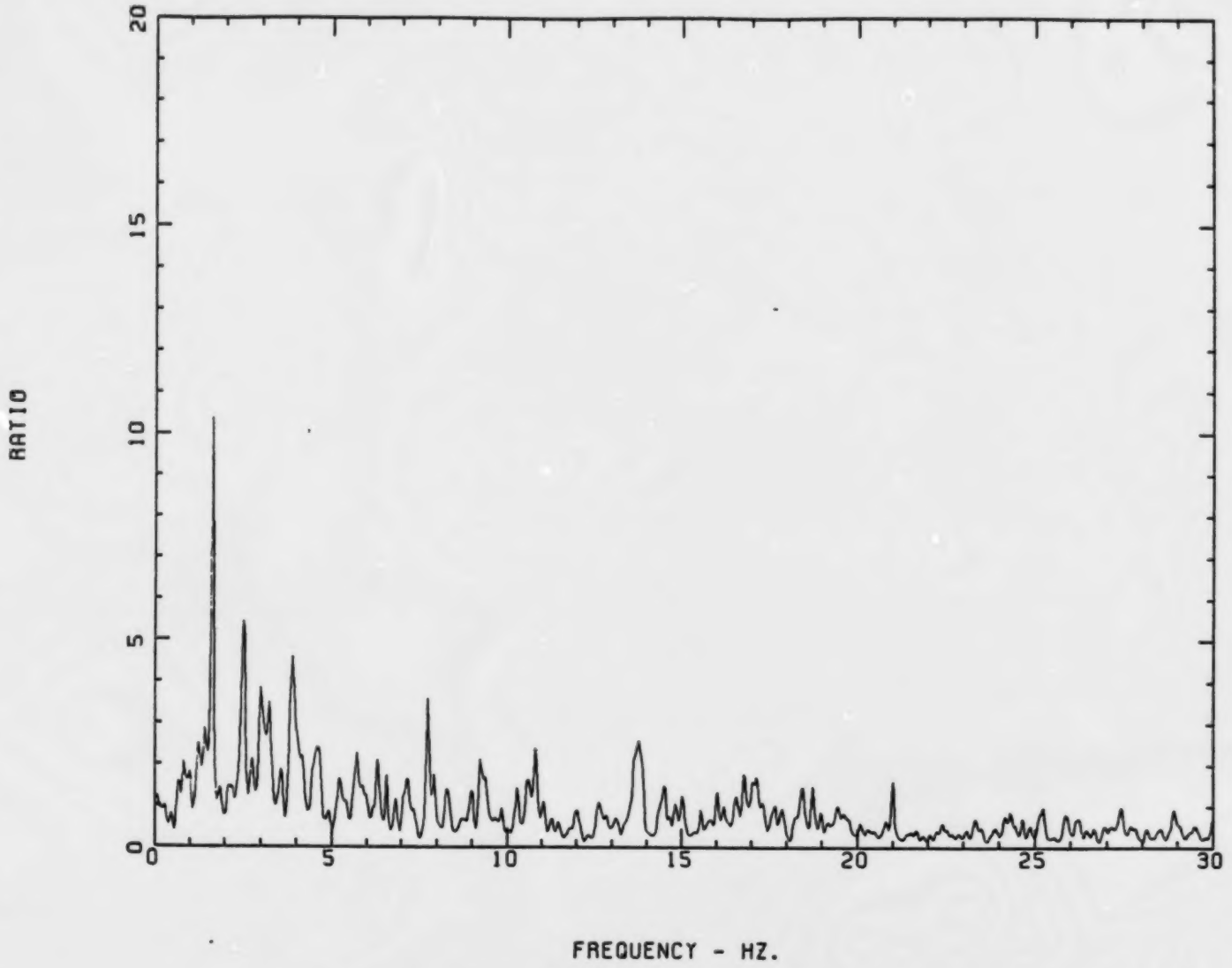

Figure 20.--Ratio of signal spectra of stations SAC/SAB for event on March 29 at 02:51:57 for the horizontal 90-degree component.

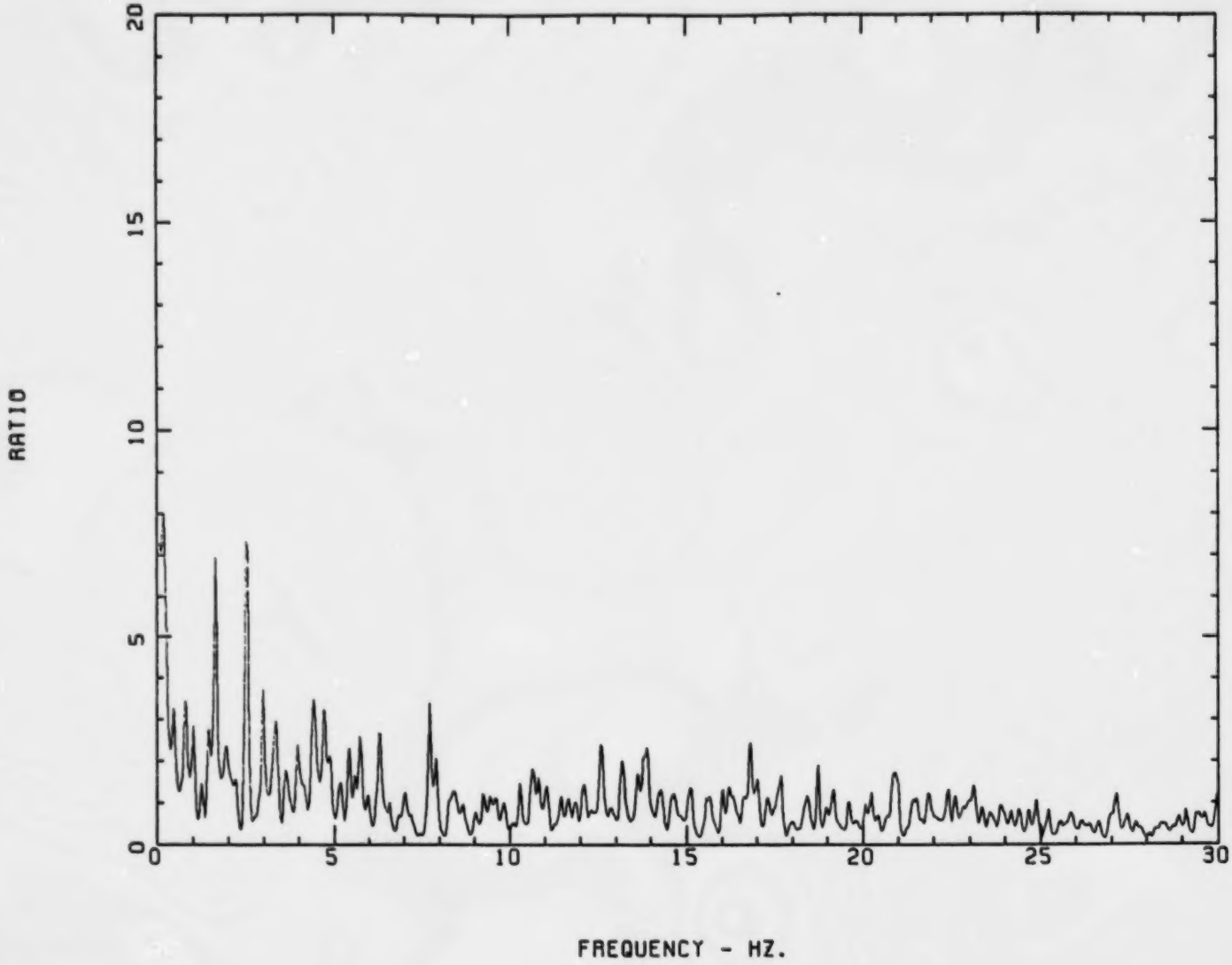

Figure 21.—Ratio of signal spectra of stations SAE/SAB for event on March 29 at 02:51:57 for the horizontal 90-degree component.

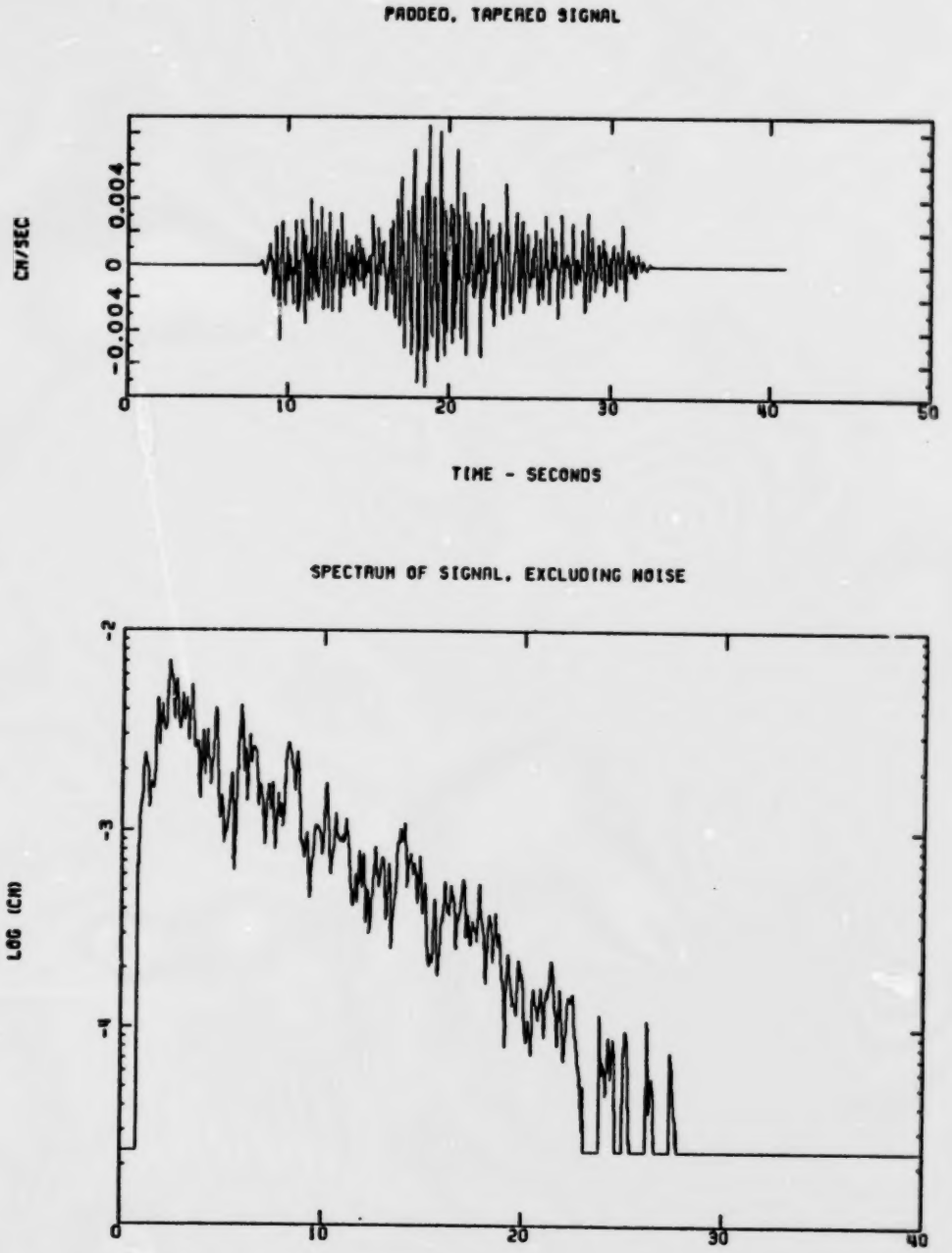

Figure 22.--Time series and spectrum for event on March 30 at 12:10:39 for the vertical component at station CAR.

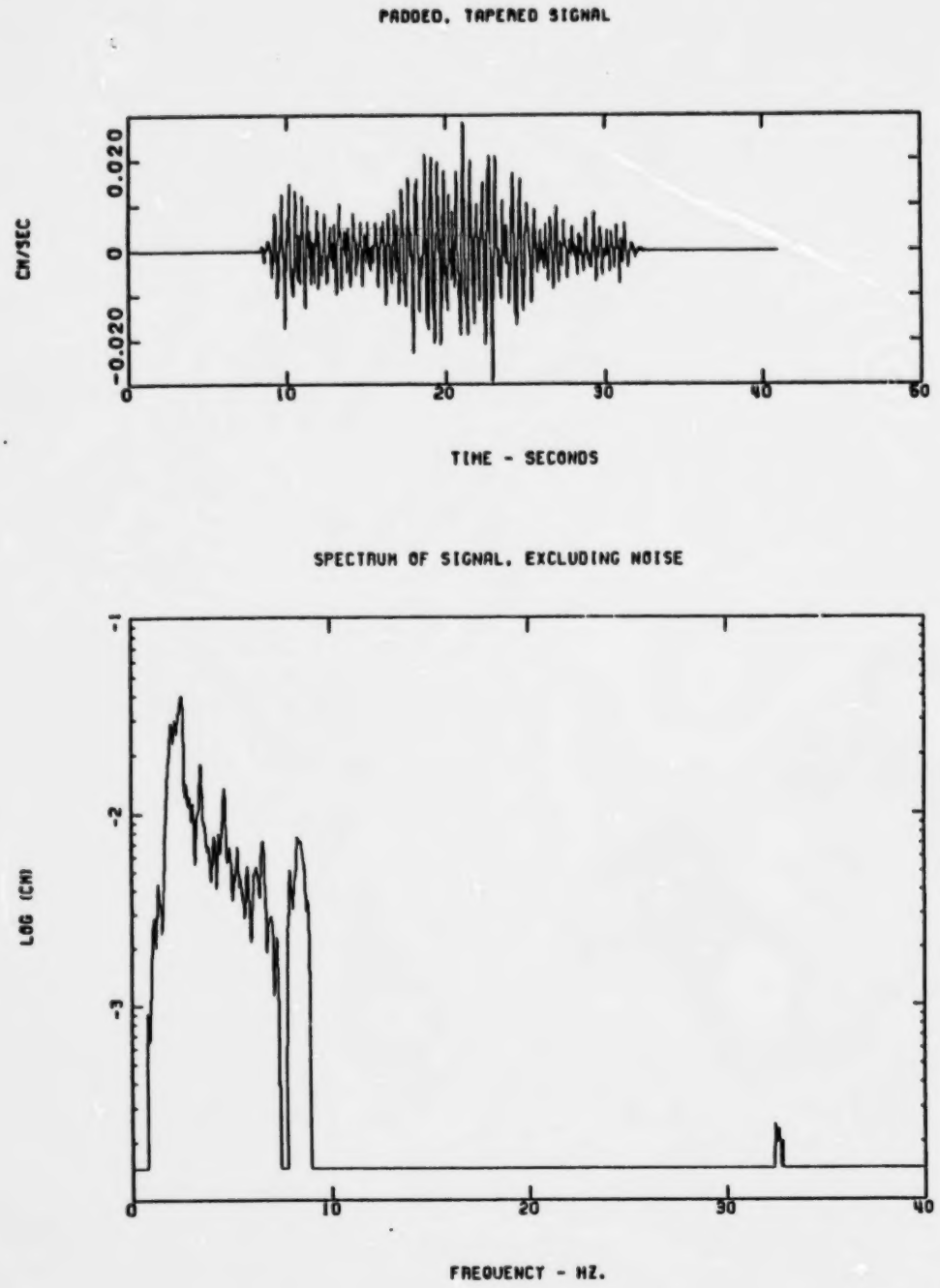

Figure 23.--Time series and spectrum for event on March 30 at 12:10:39 for the vertical component at station SAN.

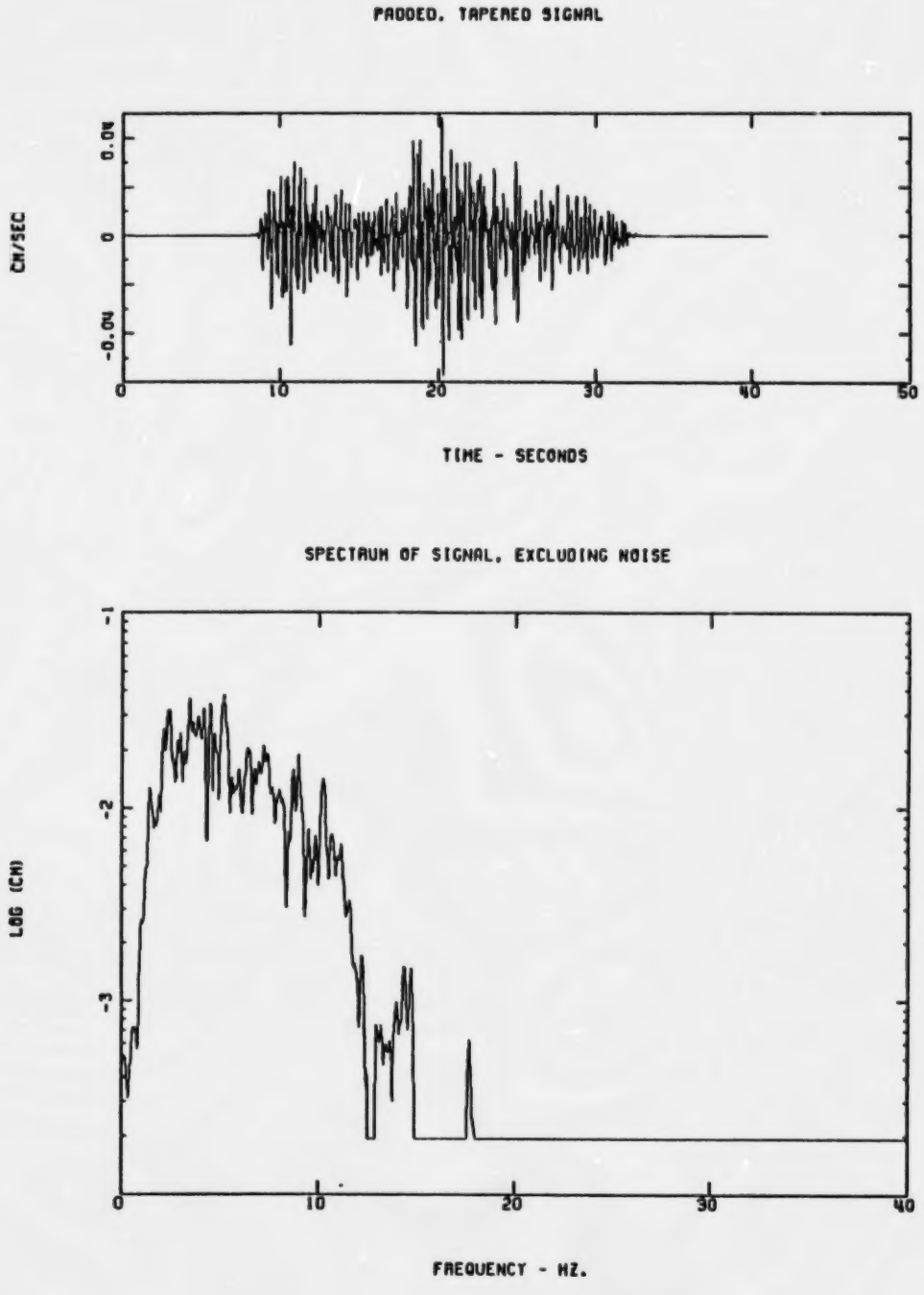

Figure 24.--Time series and spectrum for event on March 30 at 12:10:39 for the vertical component at station SCH.

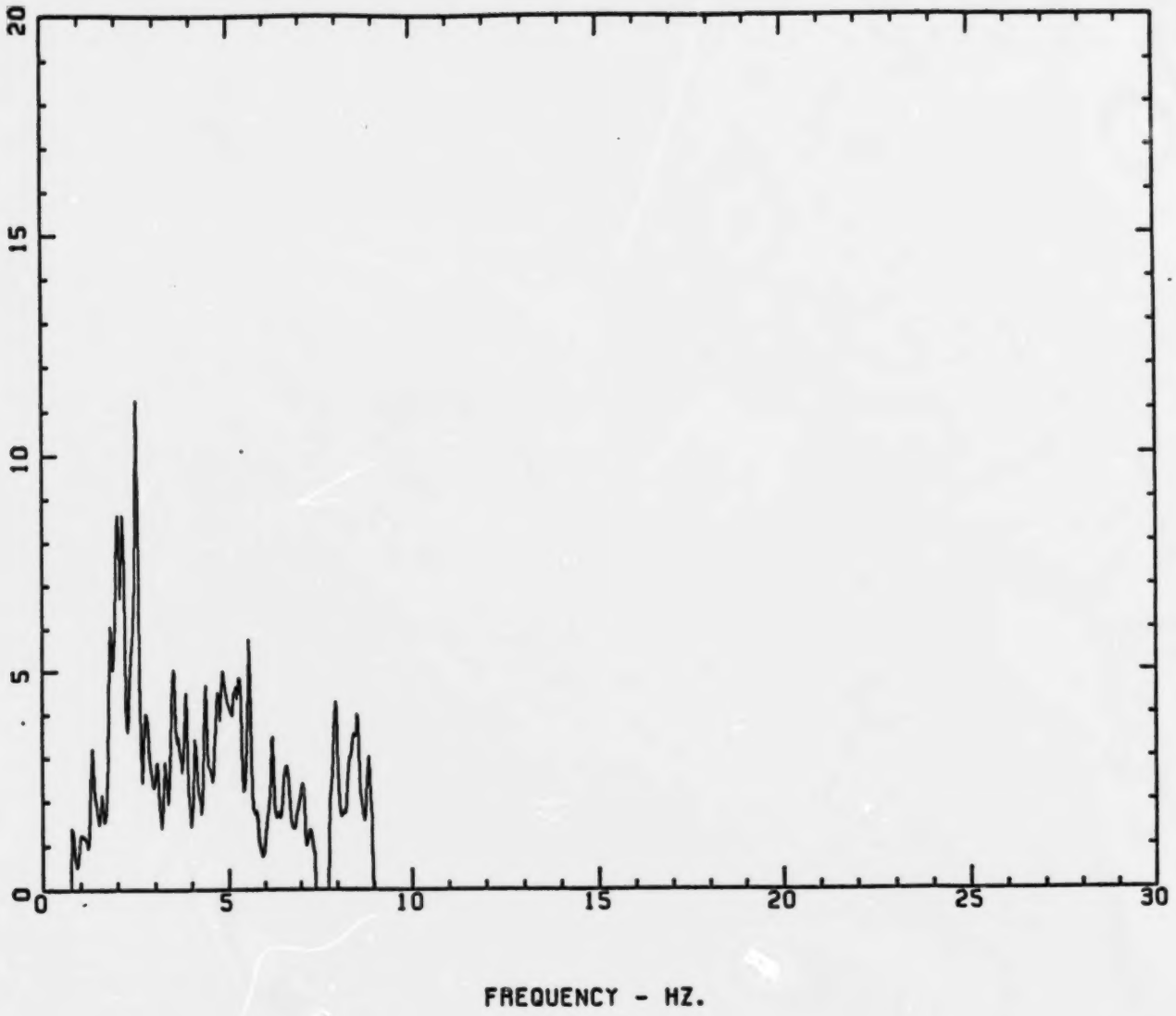

Figure 25.—Ratio of signal spectra of stations SAN/CAR for event on March 30 at 12:10:39 for the vertical component.

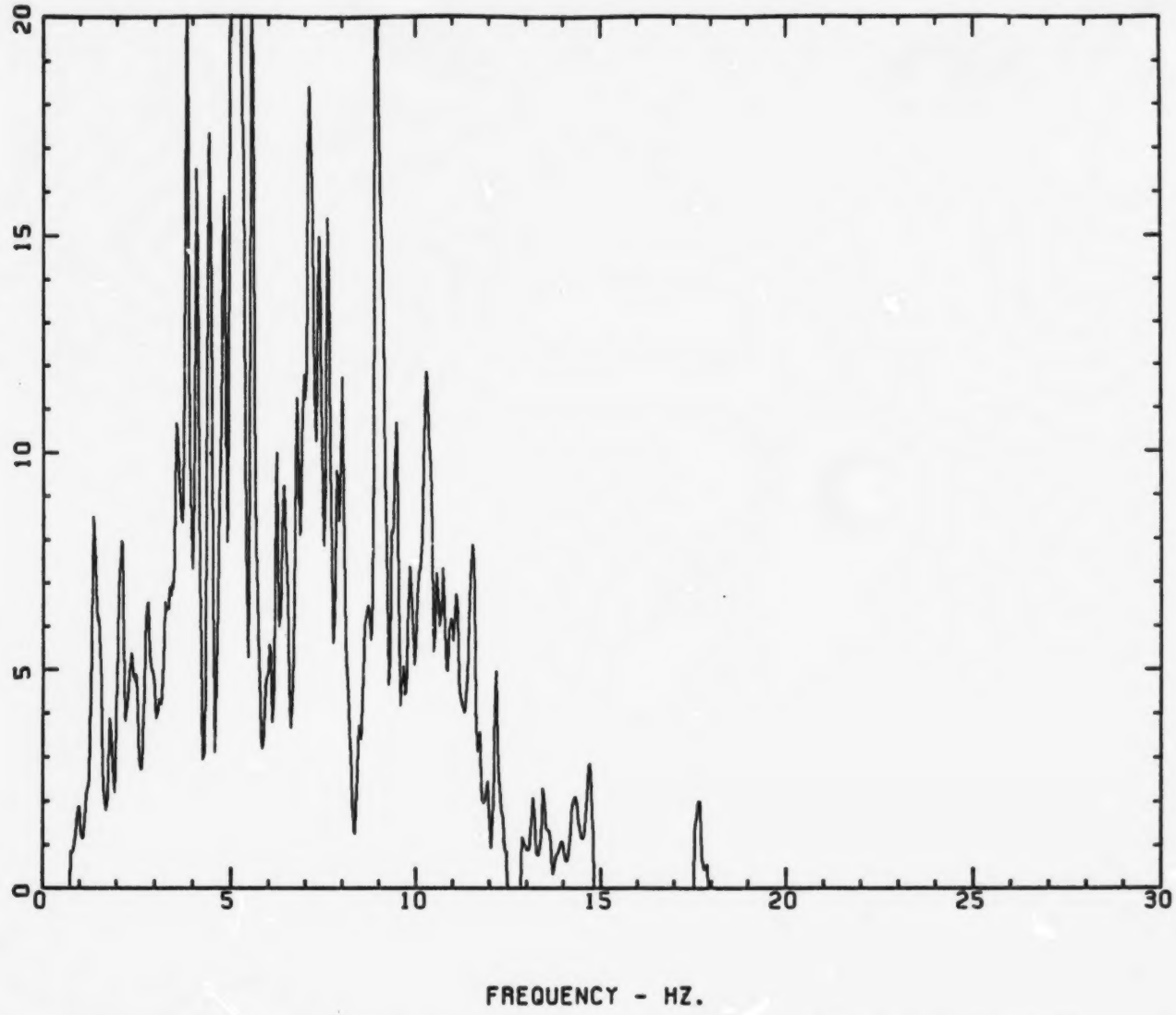

Figure 26.—Ratio of signal spectra of stations SCH/CAR for event on March 30 at 12:10:39 for the vertical component.

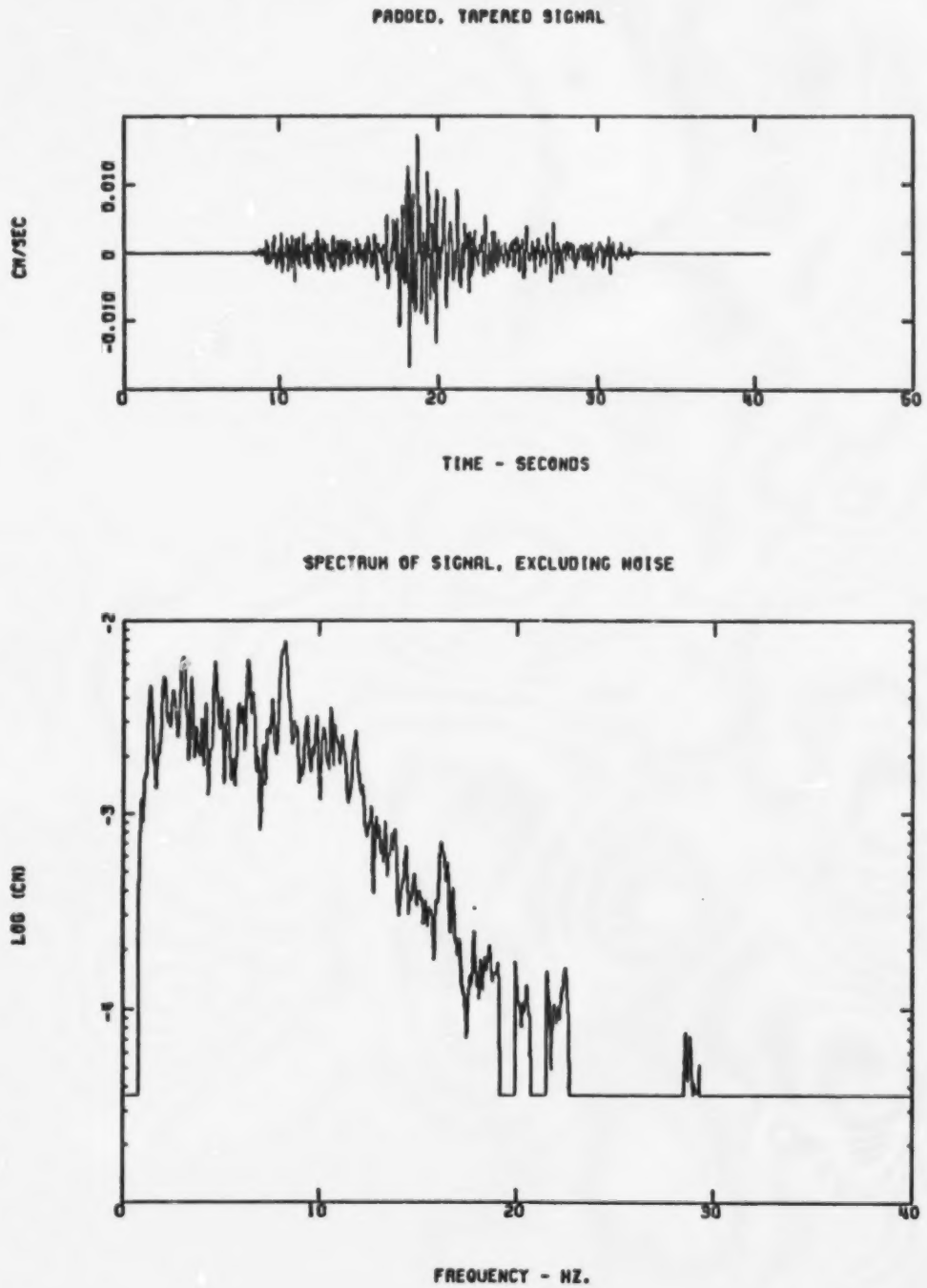

Figure 27.--Time series and spectrum for event on March 30 at 12:10:39 for the horizontal 0-degree component at station CAR.

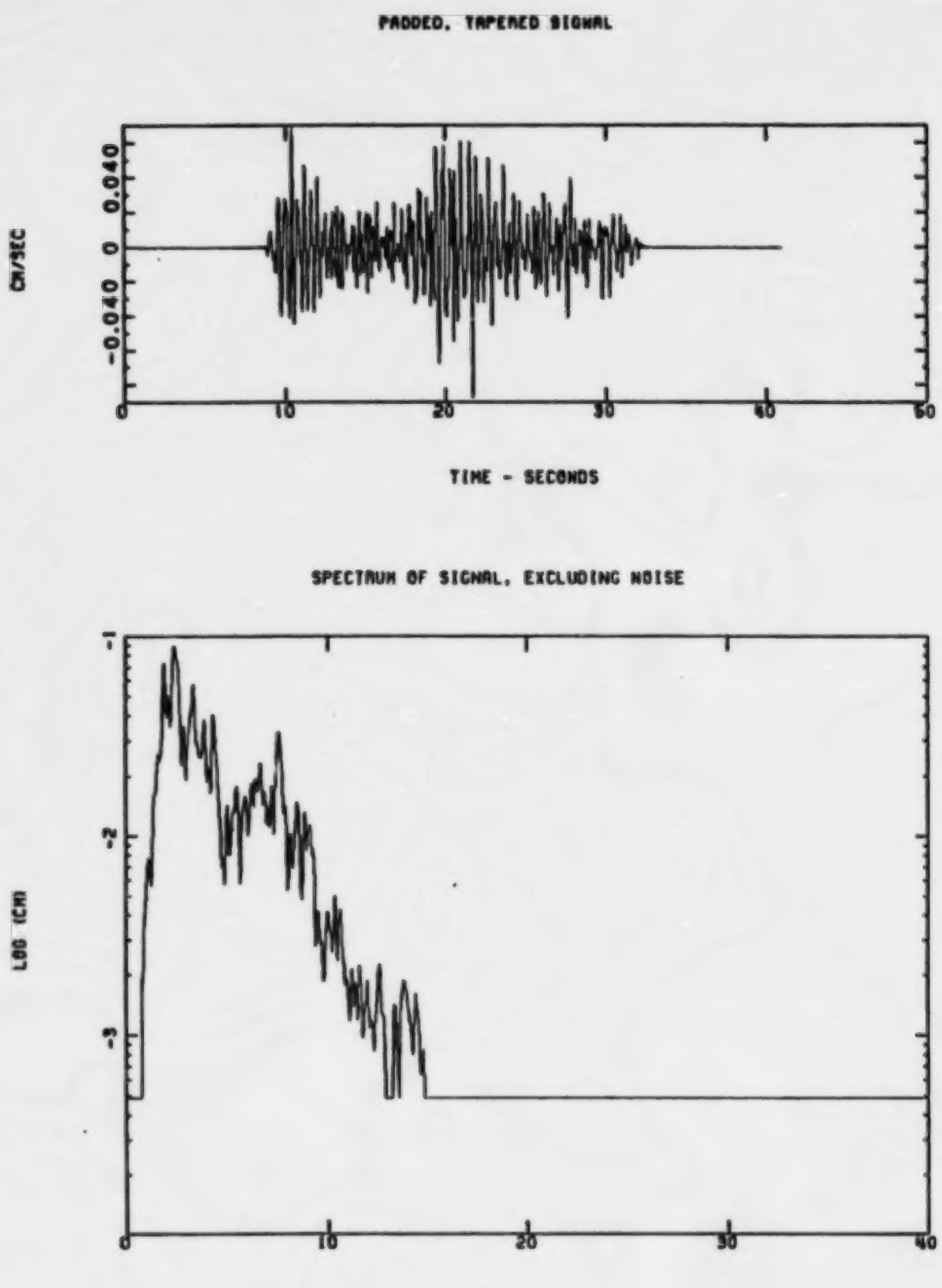

Figure 28.--Time series and spectrum for event on March 30 at 12:10:39 for the horizontal 0-degree component at station SCH.

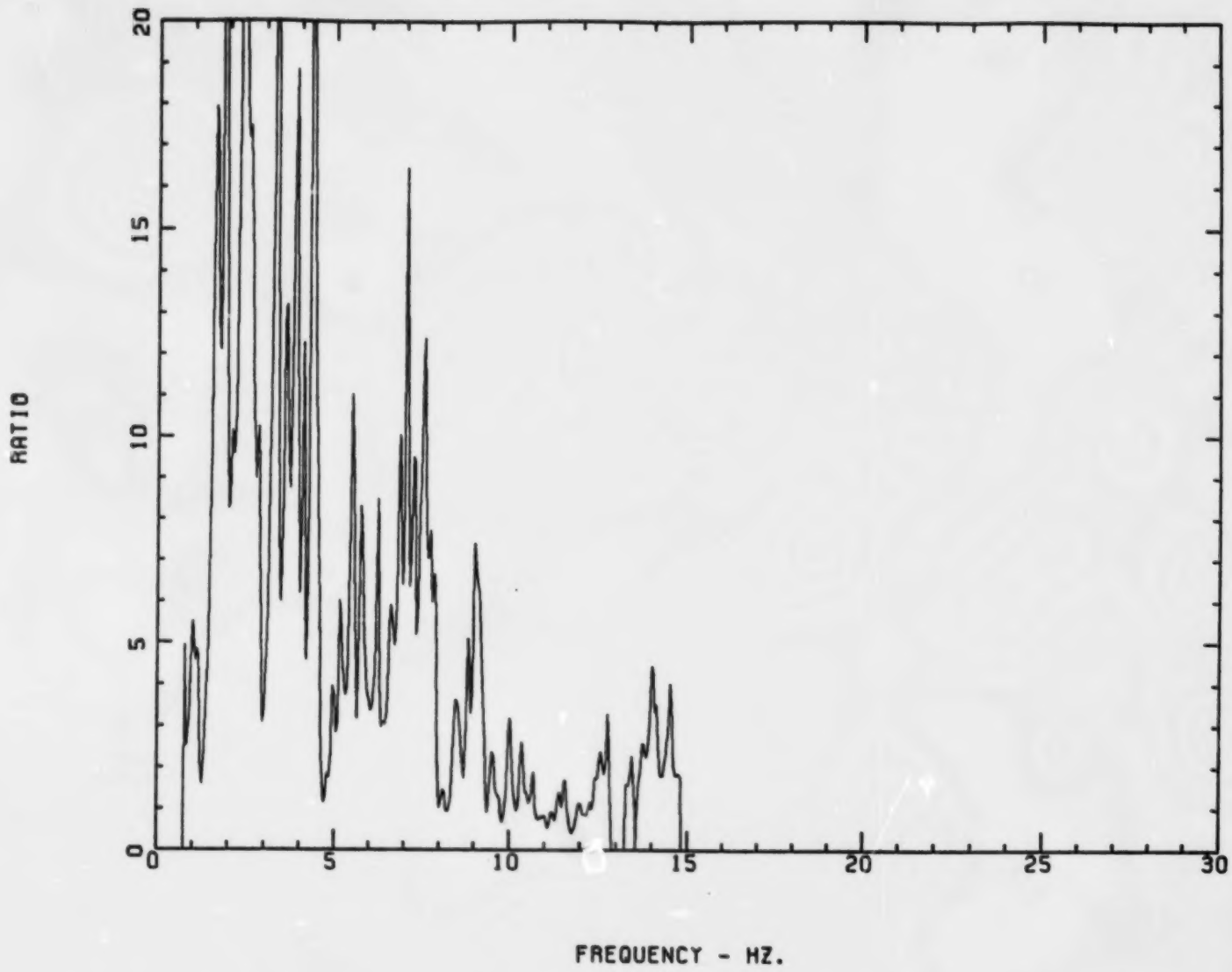

Figure 29.—Ratio of signal spectra of stations SCH/CAR for event on March 30 at 12:10:39 for the horizontal 0-degree component.

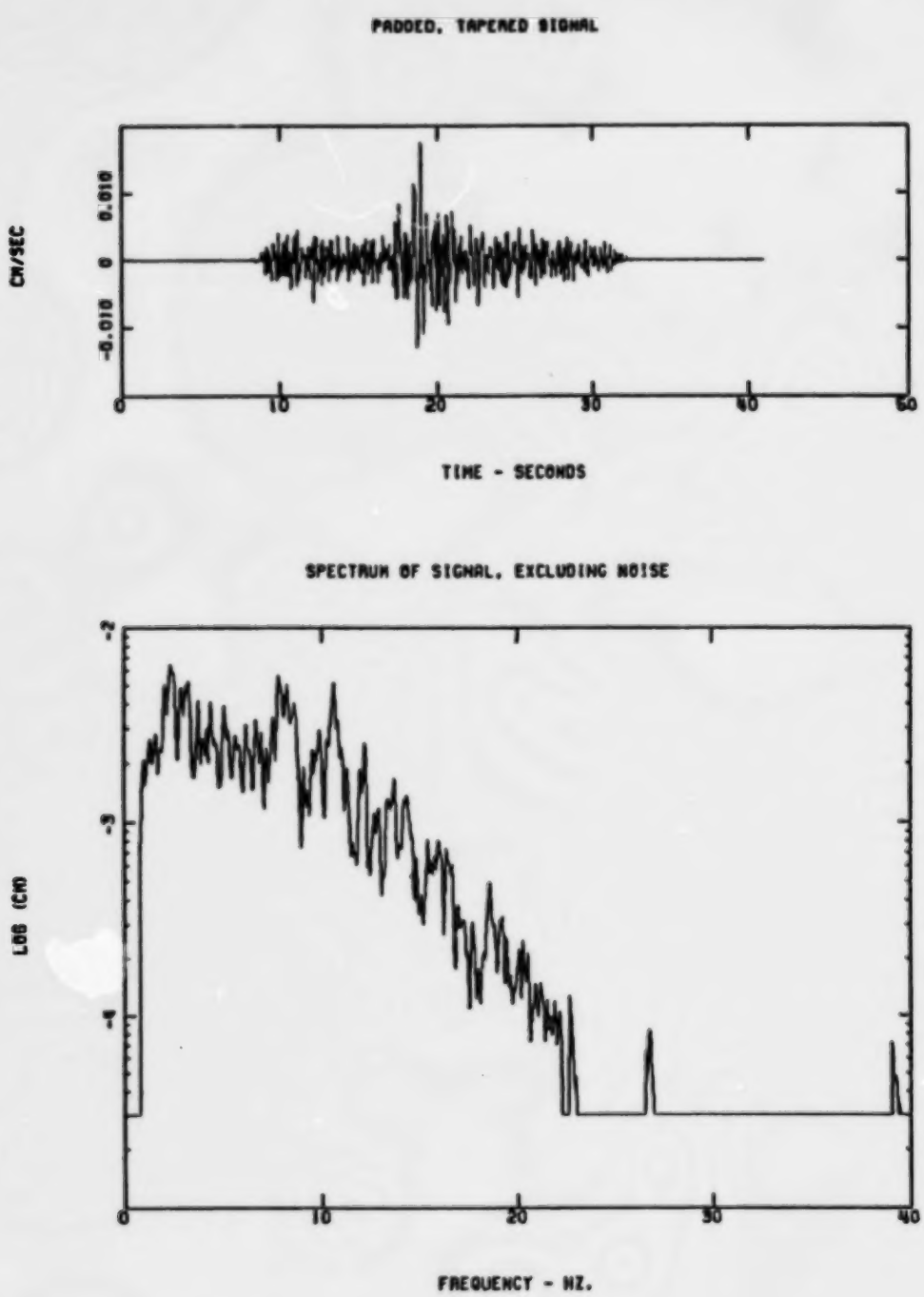

Figure 30.--Time series and spectrum for event on March 30 at 12:10:39 for the horizontal 90-degree component at station CAR.

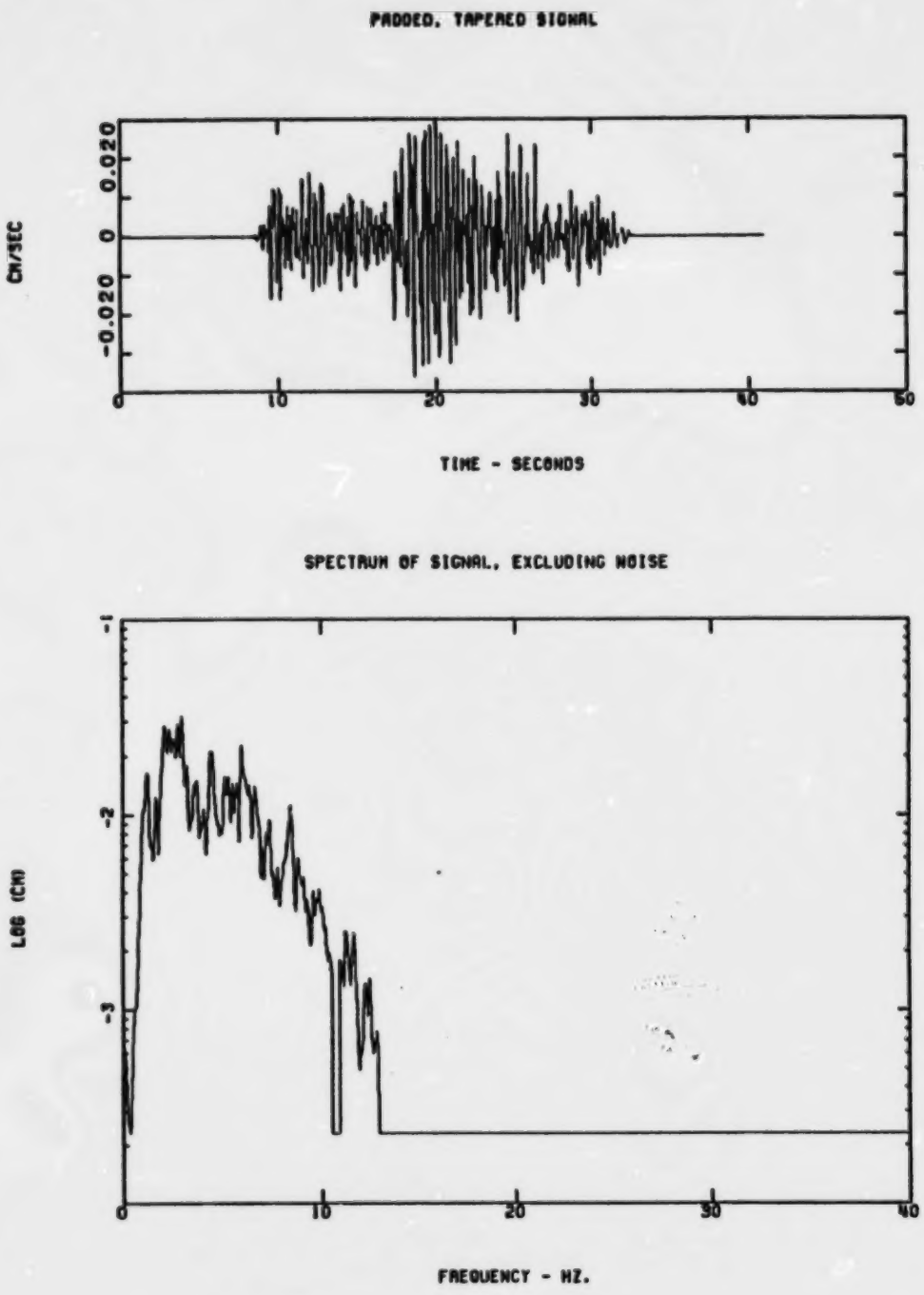

Figure 31.—Time series and spectrum for event on March 30 at 12:10:39 for the horizontal 90-degree component at station SAN.

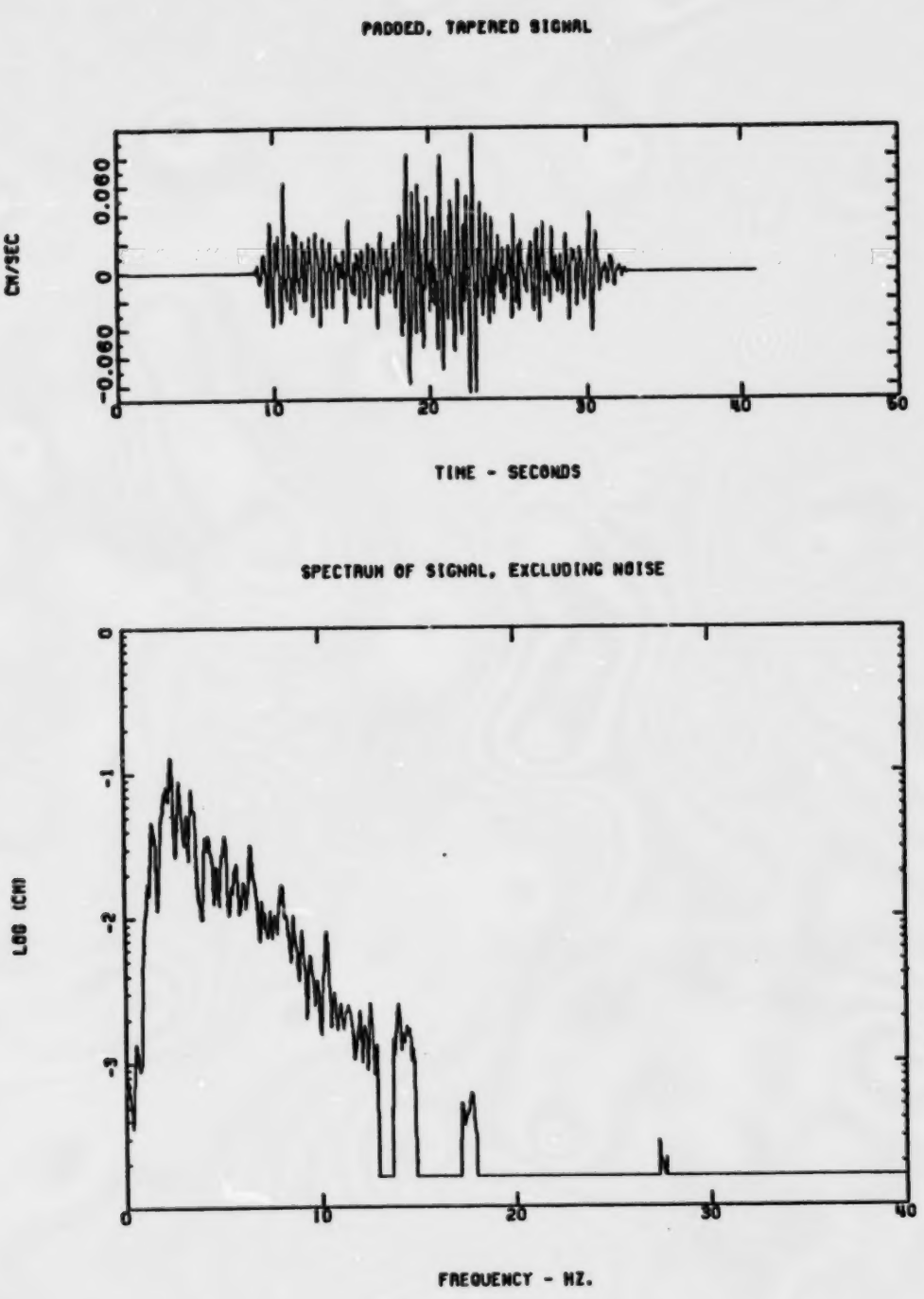

Figure 32.—Time series and spectrum for event on March 30 at 12:10:39 for the horizontal 90-degree component at station SCH.

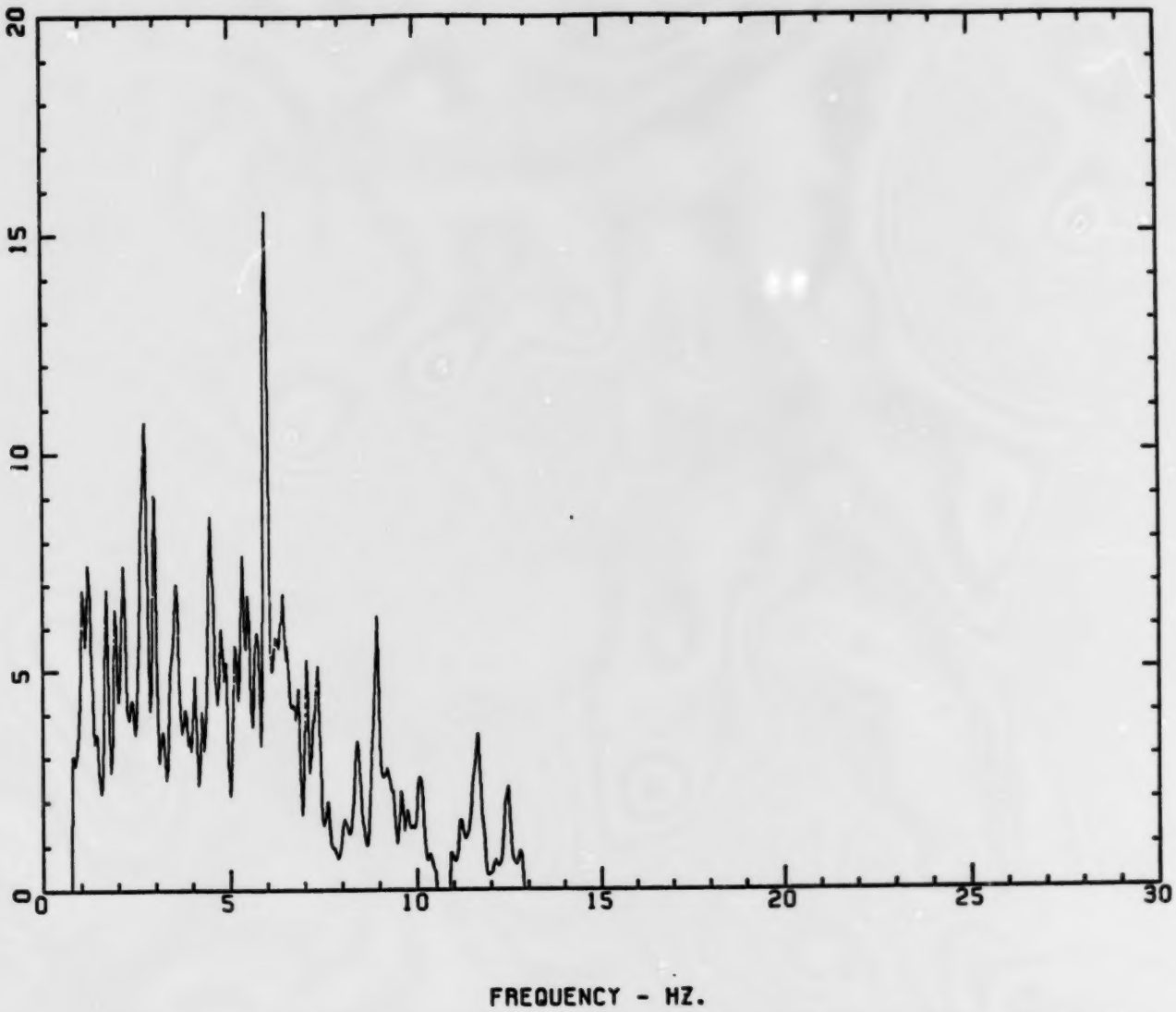

Figure 33.—Ratio of signal spectra of stations SAN/CAR for event on March 30 at 12:19:39 for the horizontal 90-degree component.

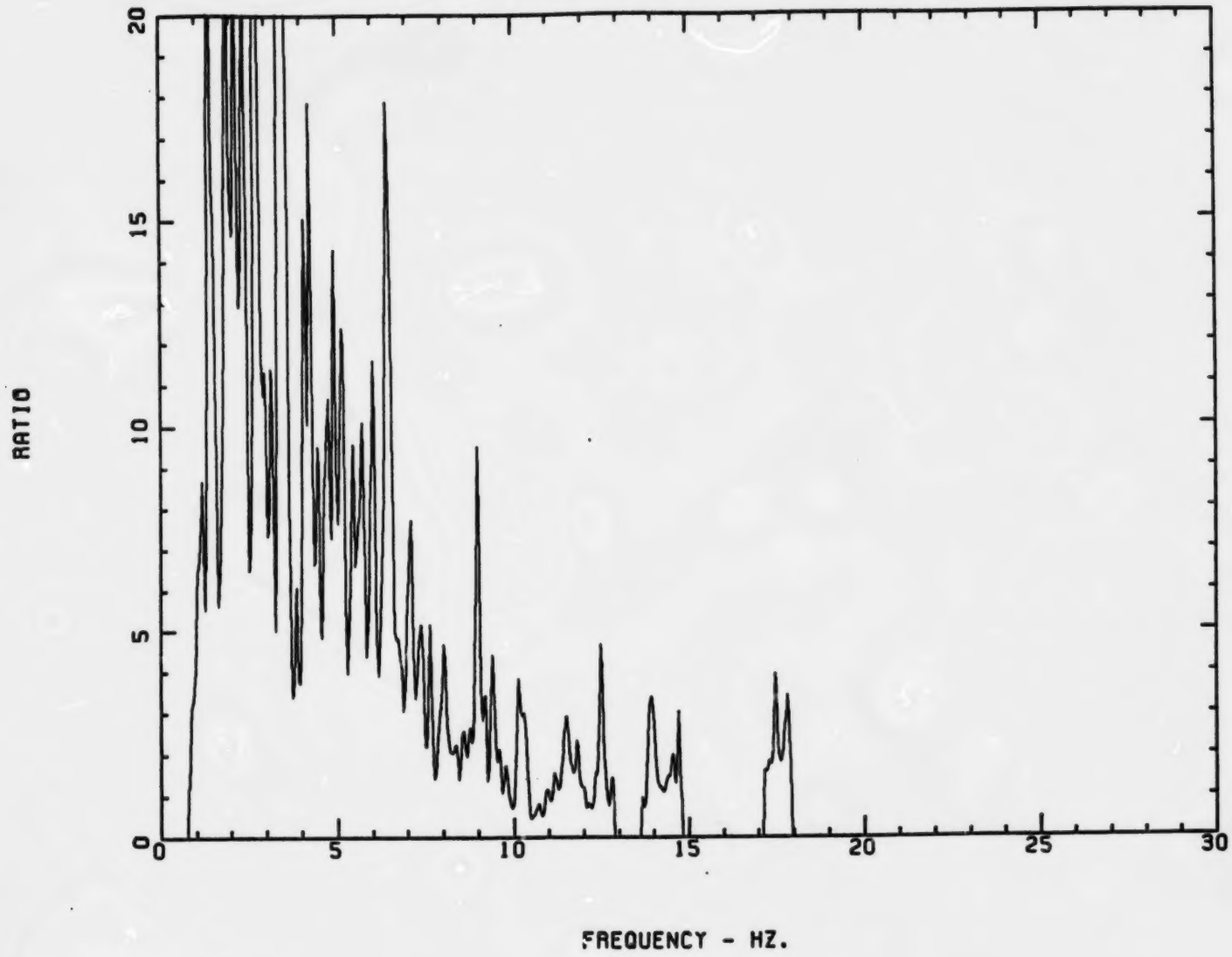

Figure 34.—Ratio of signal spectra of stations SCH/CAR for event on March 30 at 12:10:39 for the horizontal 90-degree component.

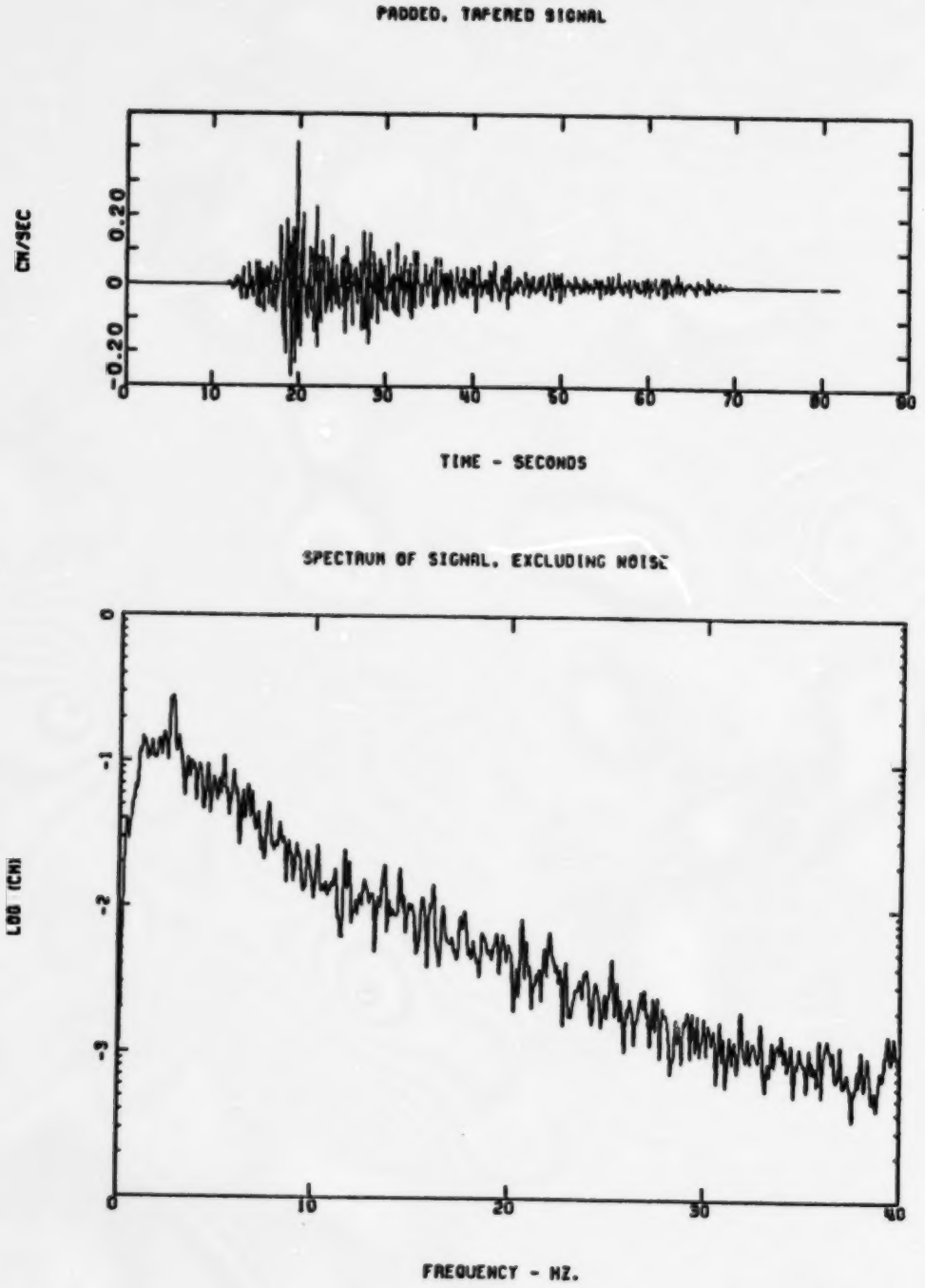

Figure 35.—Time series and spectrum for event on April 5 at 13:06:27 for the vertical component at station VAL.

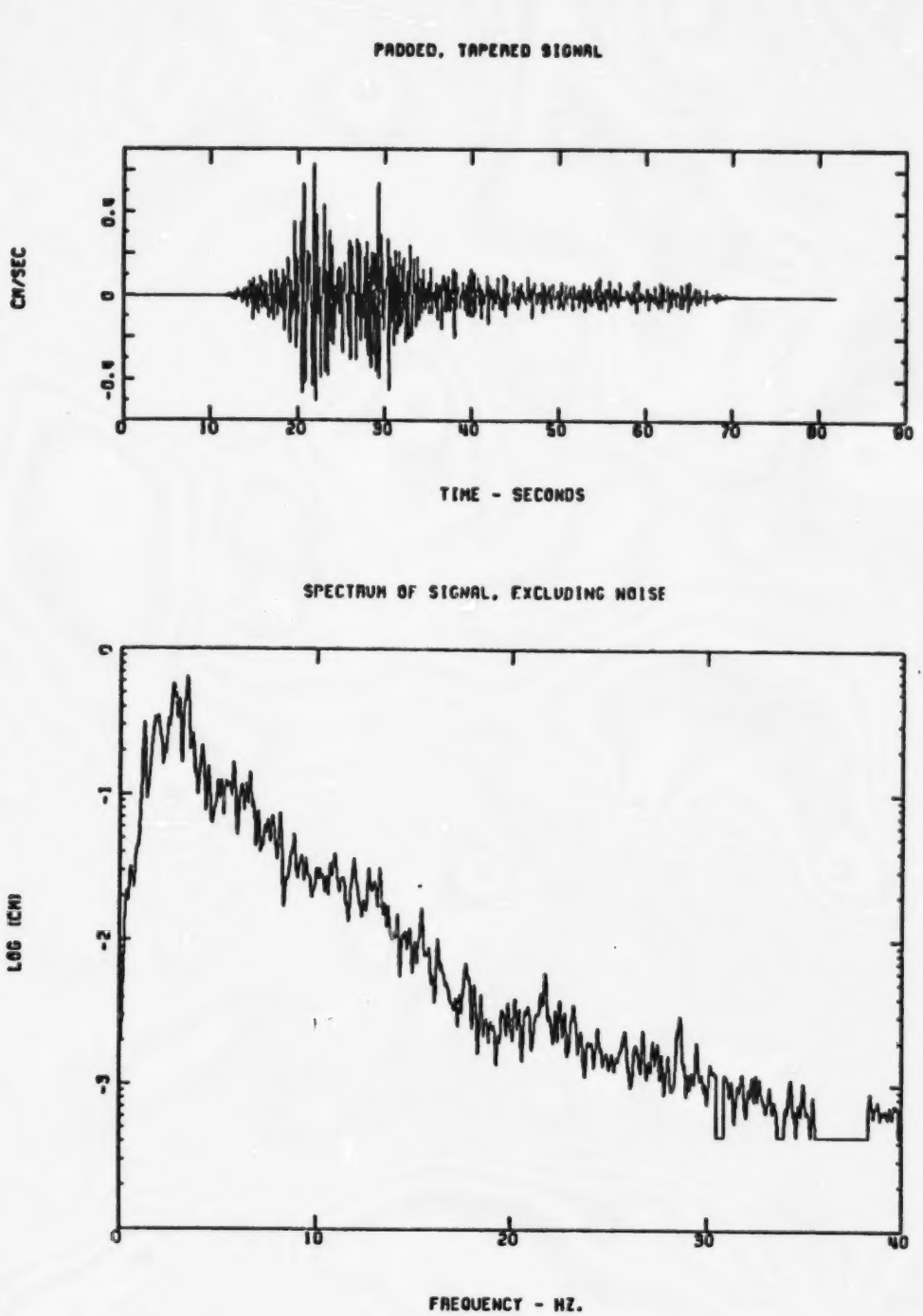

Figure 36.--Time series and spectrum for event on April 5 at 13:06:27 for the vertical component at station VC4.

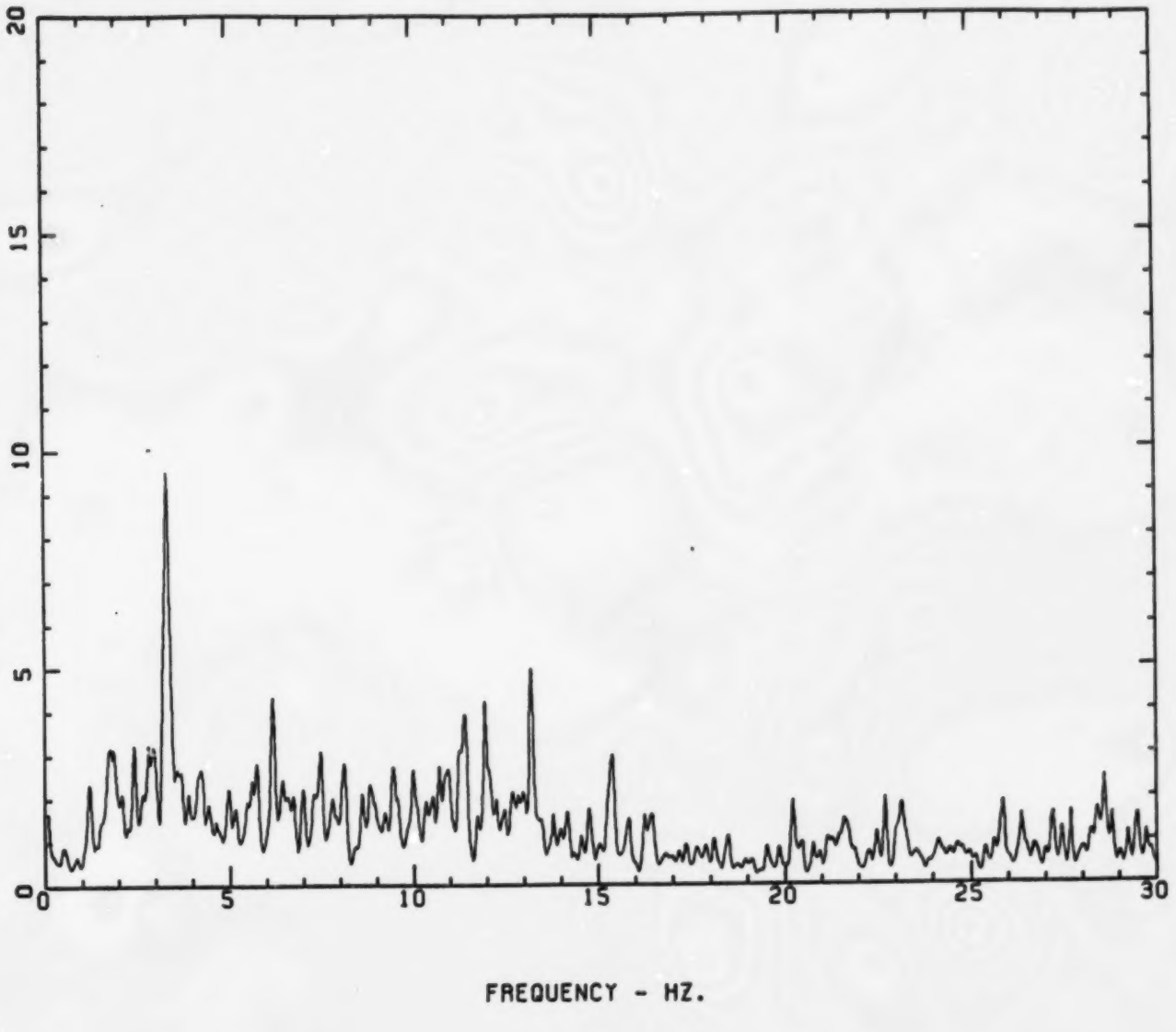

Figure 37.—Ratio of signal spectra of stations VC4/VAL for event on April 5 at 13:06:27 for the vertical component.

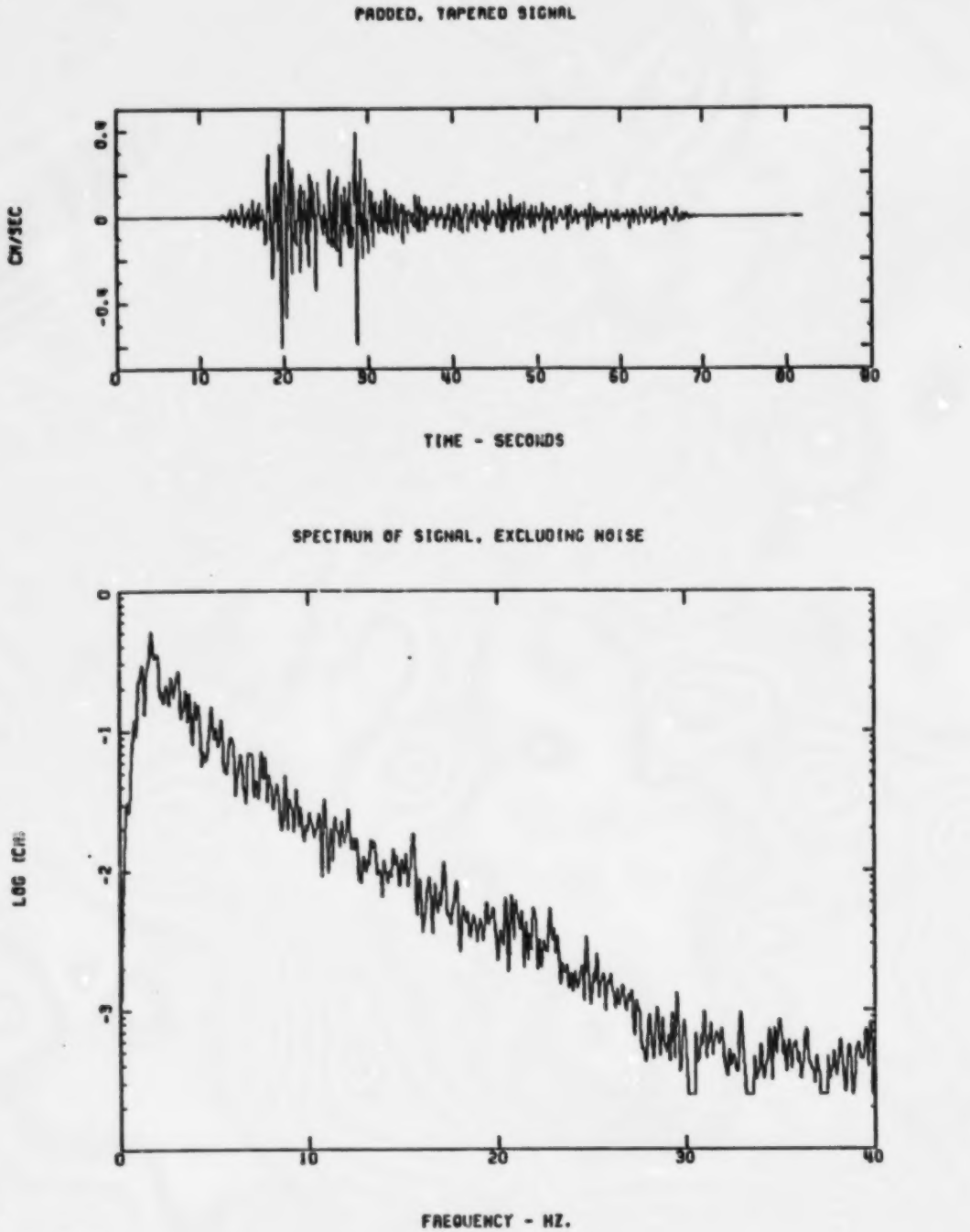

Figure 38.--Time series and spectrum for event on April 5 at 13:06:27 for the horizontal 90-degree component at station VAL

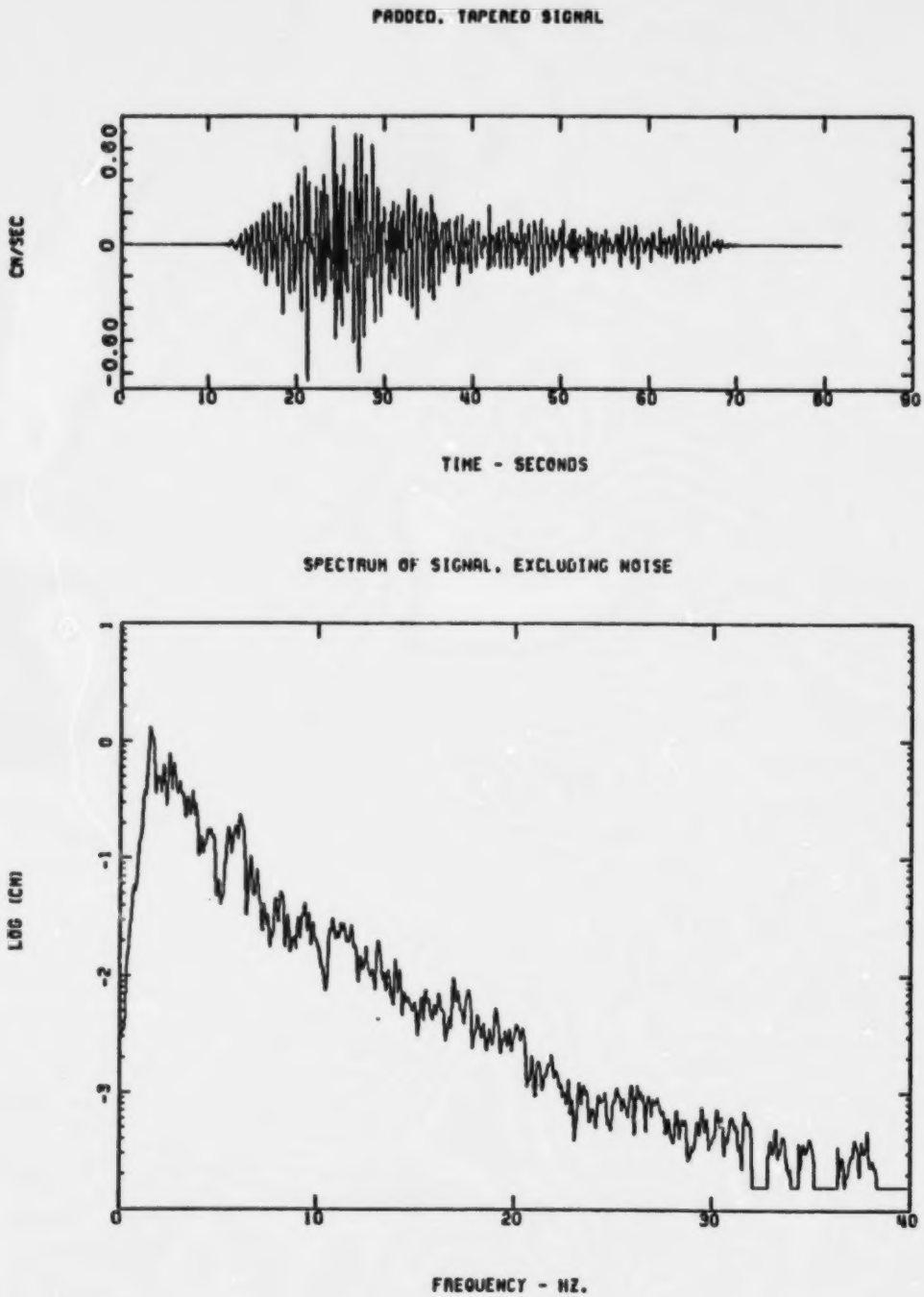

Figure 39.--Time series and spectrum for event on April 5 at 13:06:27 for the horizontal 90-degree component at station VC4.

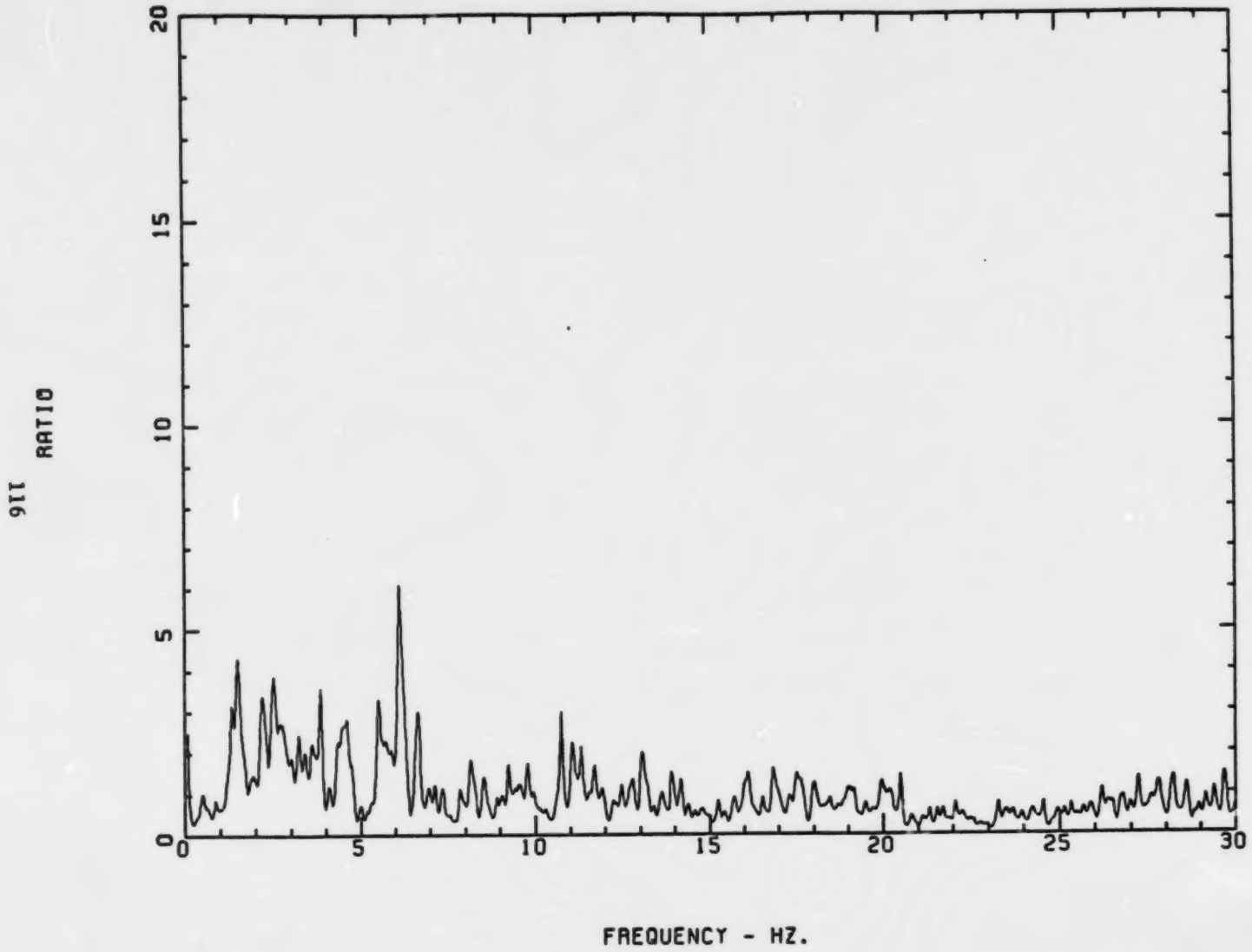

Figure 40.—Ratio of signal spectra of stations VC4/VAL for event on April 5 at 13:06:27 for the horizontal 90-degree component.

PRELIMINARY ANALYSIS OF GROUND RESPONSE AND OBSERVED INTENSITY

S. T. Algermissen, U.S. Geological Survey, Denver, CO 80225;
E. Kausel, University of Chile, Santiago, Chile;
C. Mueller and R. Borcherdt, U.S. Geological Survey,
Menlo Park, CA 94025; P. C. Thenhaus and B. Askew,
U.S. Geological Survey, Denver, CO 80225

This report is a preliminary analysis of site response based on a selection of data recorded at the sites previously discussed. The earthquakes used together with the stations at which ground motion was recorded are shown in table 1. The epicentral locations of the shocks are shown in figure 1. The stations in Santiago - SAA, SAC, SAD and SAE were referenced to station SAB, a rock site, and the spectral ratios SAA/SAB and SAC/SAB, SAD/SAB and SAE/SAB were formed. The stations near San Antonio on the coast--SAN and SCH were referenced to CAR, a rock site, and the spectral ratios SAN/CAR and SCH/CAR formed. In Valparaiso, the rock site is VAL and the spectral ratio VC4/VAL was formed. Data from stations END and AGU are not considered in this report since spectral ratios using data from these stations have not yet been analyzed. Furthermore, only the relationship of site response to Modified Mercalli intensity observed after the main shock are analyzed in this report.

The spectral ratios were averaged using a geometric mean over three period ranges: 0.1 to 0.2 sec, 0.2-0.5 sec and 0.5-1.0 sec for both the vertical component and the horizontal component of ground velocity. The horizontal component was obtained by averaging the spectral ratios obtained from the two orthogonal horizontal ground motion components recorded. A careful evaluation of the degree of damage (or lack of damage) was undertaken at each recording site and a Modified Mercalli intensity (MMI) was assigned to each site. The difference in intensity between each station location and the intensity at each rock (reference) station site was noted. Figures 2 through 7 show comparisons of shaking response (relative to crystalline rock) with differences in Modified Mercalli intensity observed at various stations and at a reference station on crystalline rock. The spectral ratios show a strong correlation with increased observed MMI. For sites with MMI's three degrees higher than the reference crystalline rock site vertical component velocity, spectral ratios are as large as 8:1; for horizontal component velocity spectral ratios, the ratios are as large as 12:1. Preliminary analysis of the spectral data indicates that recording small- to moderate-size earthquakes at a variety of sites and analysis of the variation in level of shaking among the sites may serve as a valuable tool in estimating shaking levels and damage that might occur in large earthquakes.

The levels of ground motion recorded vary greatly from site to site as does the observed MMI. No attempt has been made to correlate site geology with increased intensity of shaking but examination of the descriptions of the materials underlying each site and the corresponding observed intensities (table 1, Site Selection and Field Experiments, Algermissen and others, this report) shows a correlation. We plan to obtain more information on the geology and geotechnical properties of the sites. This aspect of the site response together with additional comparisons between site response and MMI will be the subject of future reports.

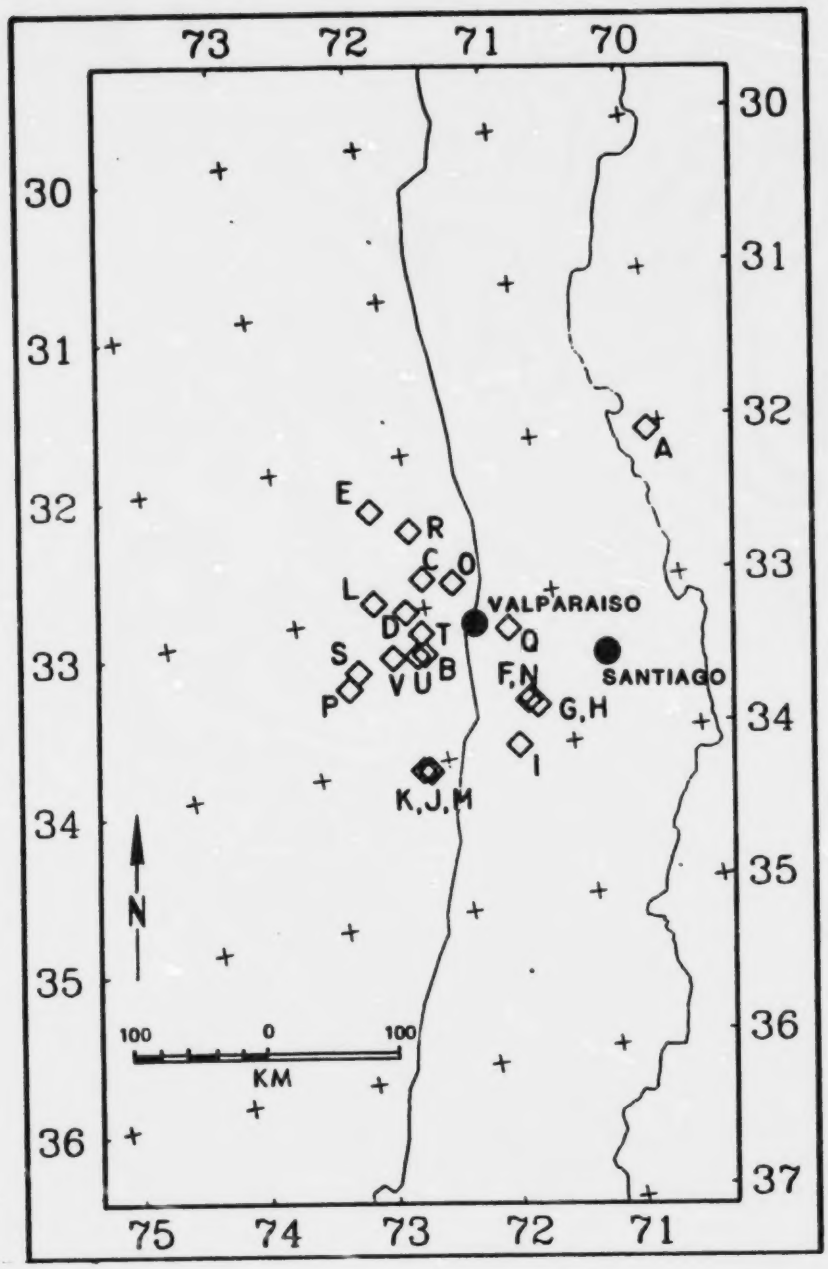

Figure 1.--Locations of aftershocks used in the site response analysis. The letters identify the earthquakes listed in table 1.

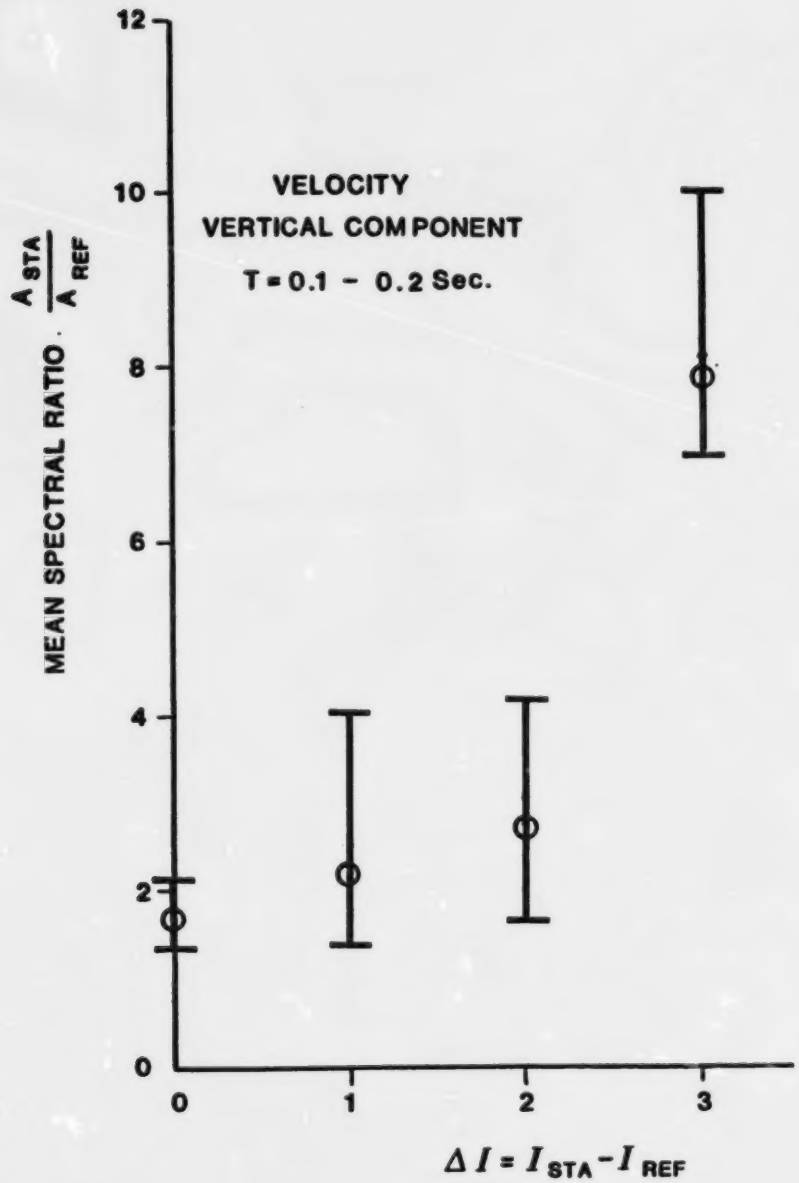

Figure 2.--Comparison of mean spectral ratios of the vertical component of velocity in the 0.1-0.2-second period range with observed differences in Modified Mercalli intensity at various stations (I_{STA}) and the intensity at the reference (rock) station (I_{REF}).

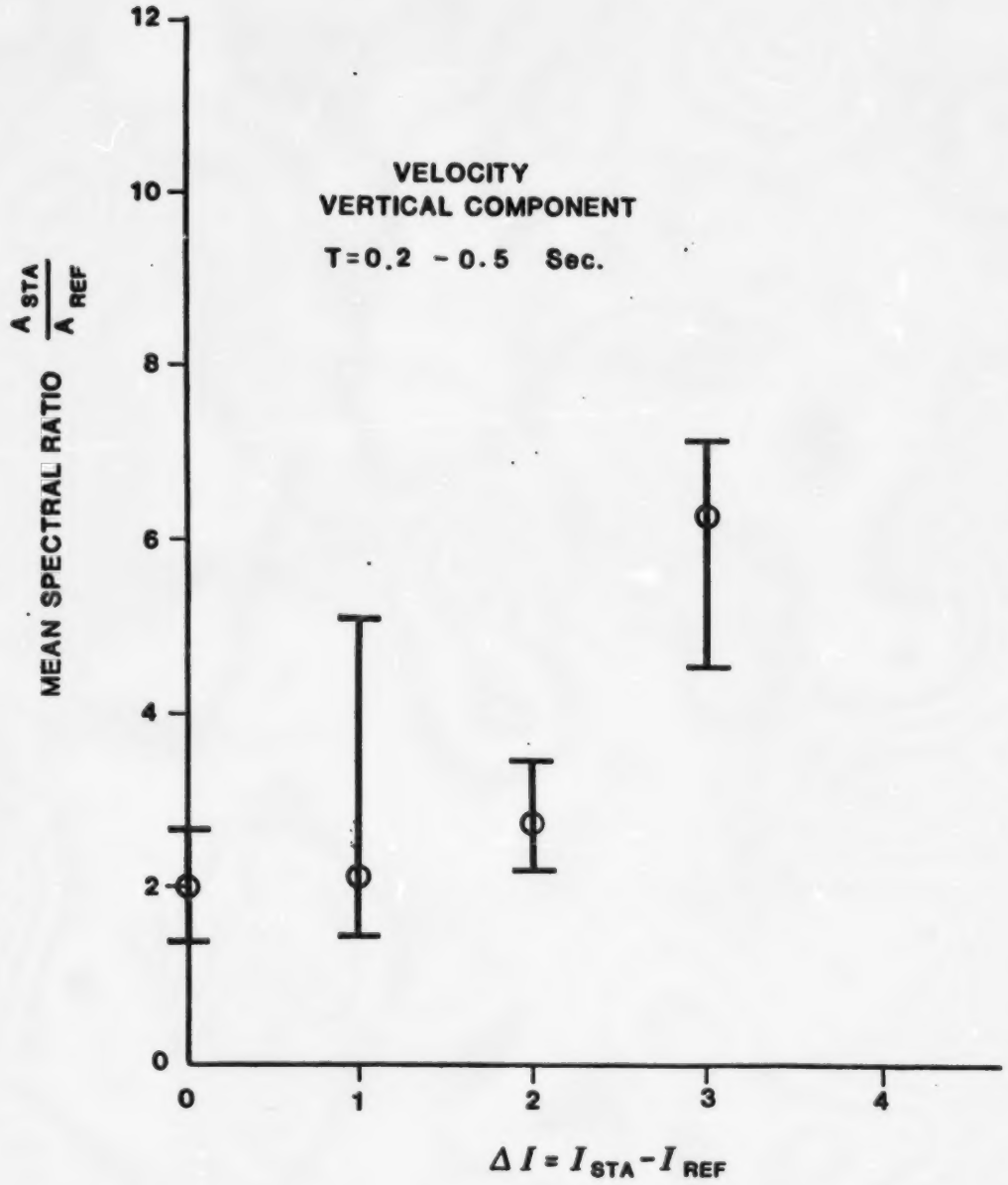

Figure 3.--Comparison of mean spectral ratios of the vertical component of velocity in the 0.2-0.5-second period range with observed differences in Modified Mercalli intensity at various stations (I_{STA}) and the intensity at the reference (rock) station (I_{REF}).

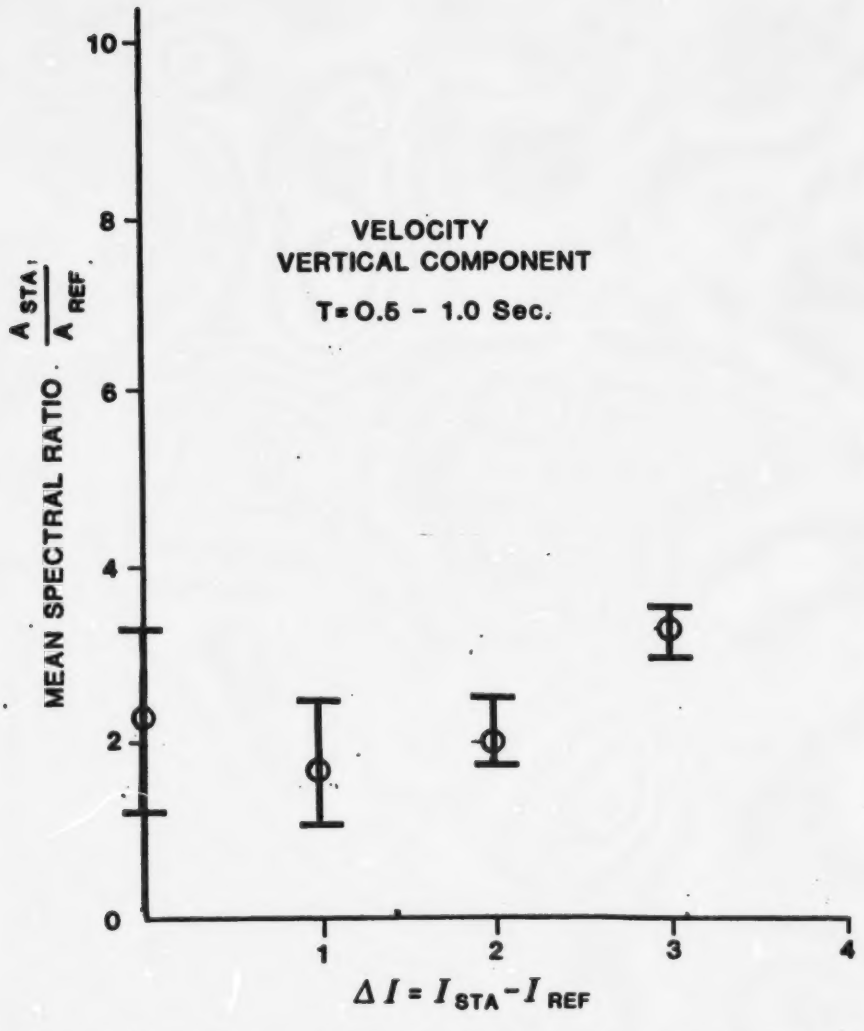

Figure 4.--Comparison of mean spectral ratios of the vertical component of velocity in the 0.5-1.0 second-period range with observed differences in Modified Mercalli intensity at various stations (I_{STA}) and the intensity at the reference (rock) station (I_{REF}).

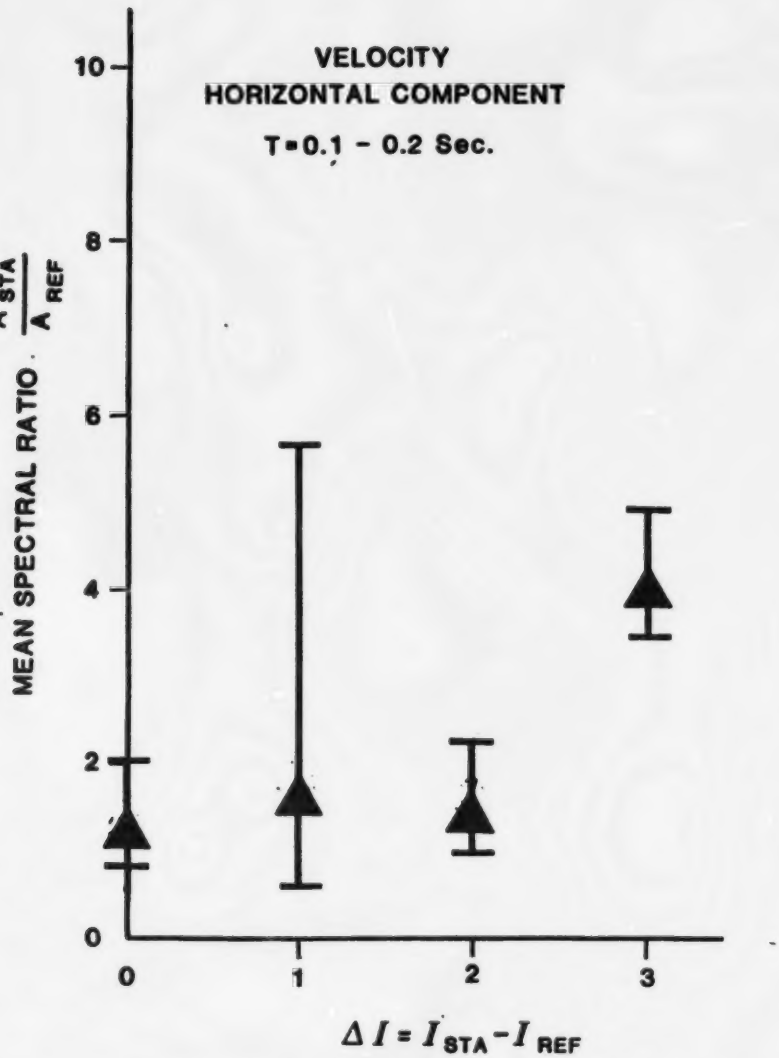

Figure 5.--Comparison of mean spectral ratios of the horizontal component of velocity in the 0.1-0.2-second period range with observed differences in Modified Mercalli intensity at various stations (I_{STA}) and the intensity at the reference (rock) station (I_{REF}).

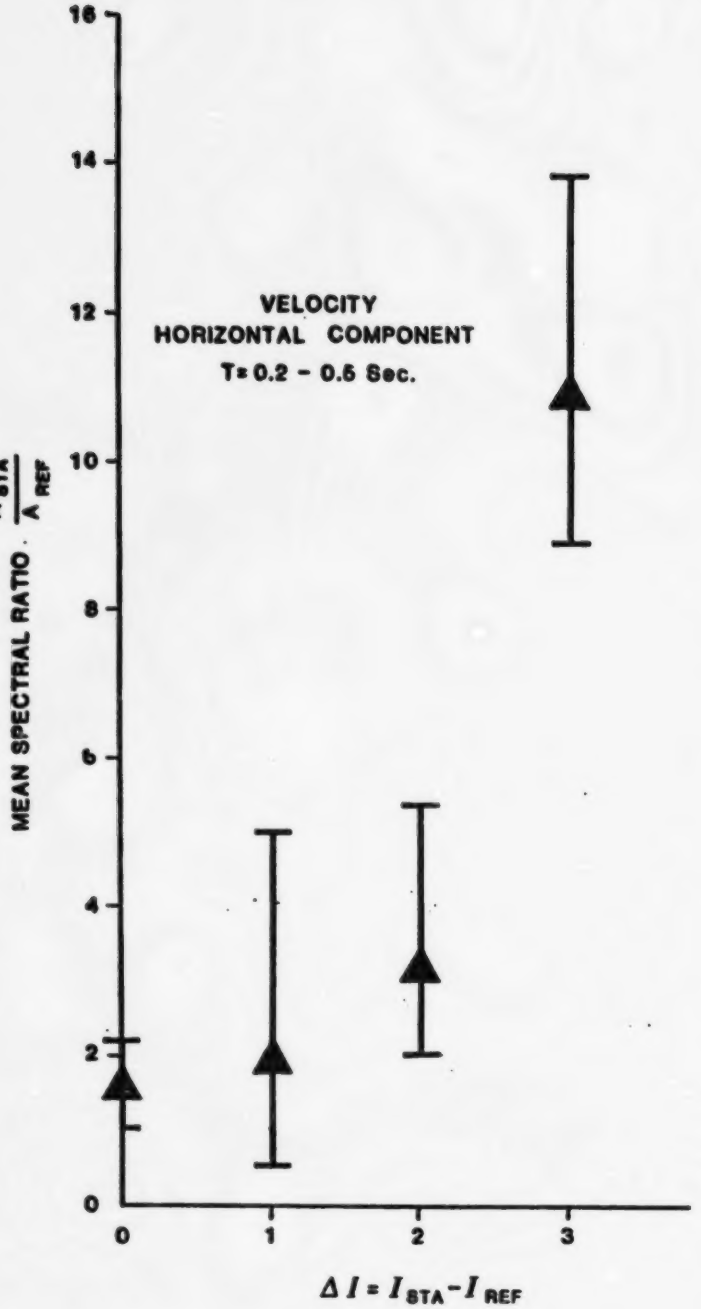

Figure 6.--Comparison of mean spectral ratios of the horizontal component of velocity in the 0.2-0.5-second period range with observed differences in Modified Mercalli intensity at various stations (I_{STA}) and the intensity at the reference (rock) station (I_{REF}).

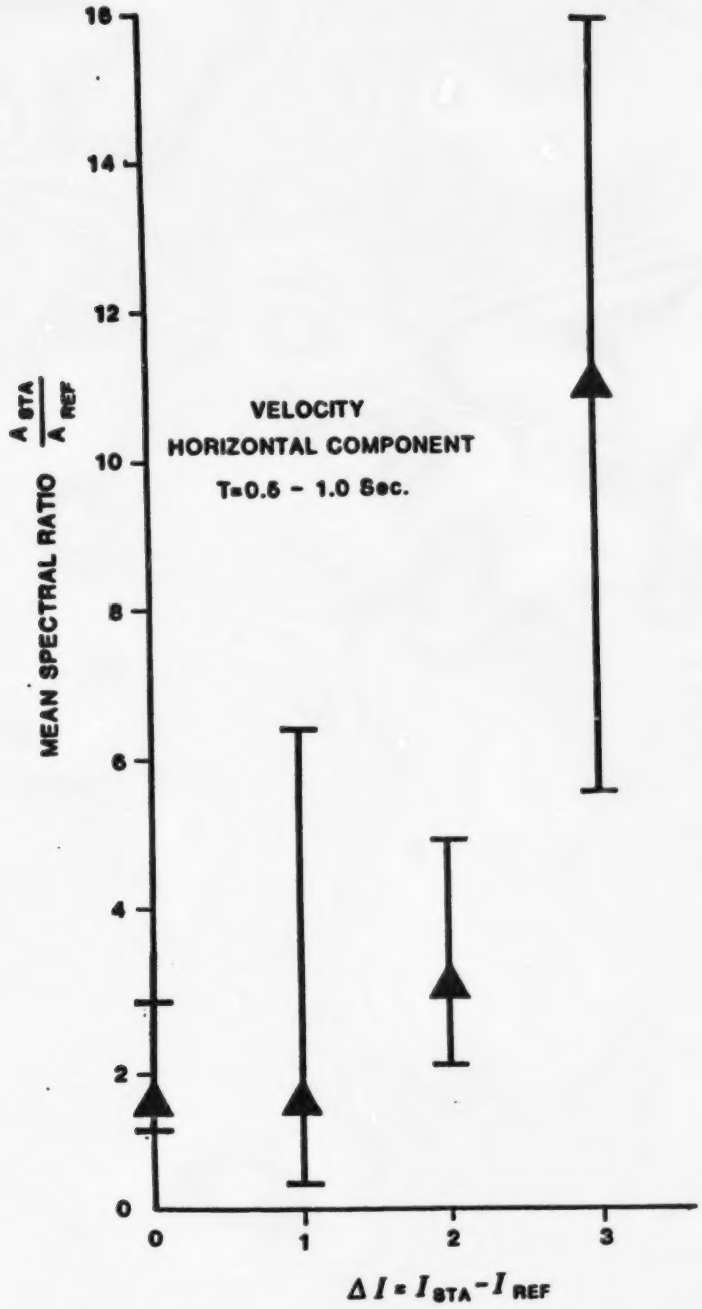

Figure 7.—Comparison of mean spectral ratios of the horizontal component of velocity in the 0.5–1.0-second period range with observed differences in Modified Mercalli intensity at various stations (I_{STA}) and the intensity at the reference (rock) station (I_{REF}).

PRELIMINARY EVALUATION OF PERFORMANCE OF STRUCTURES

by

M. Celebi, U.S. Geological Survey, Menlo Park, CA 94025

in collaboration with

E. Sembera, U.S. Geological Survey, Menlo Park, CA 94025

GENERAL REMARKS

The structures in Central Chile, particularly on the coastal towns of Valparaiso, Viña del Mar, and San Antonio as well as the capital, Santiago, were rigorously tested during the March 3, 1985, main event (M_s=7.8) and the significant aftershocks. Although several engineered structures were damaged, some severely, the overall performance of the majority of engineered structures subjected to the level of shaking generated by the earthquake should be positively rated, particularly when the loss of life was limited to 176 persons, considering the magnitude of this earthquake. Non-engineered structures, particularly old adobe structures, were heavily damaged (especially in San Antonio). Only one engineered building in Santiago partially collapsed. An eight story, reinforced concrete building (Edificio El Faro) in Renecá suburb of Viña del Mar suffered extensive damage (tilting off vertical axis), and as a result was dynamited. Also in Renecá a reinforced concrete structure built on an architectural configuration following the sloping hill was practically broken in two because of the differential settlement due to compaction of the sand underneath. Two modern structures on the coast (Edificio H'Angoroa and Edificio Acapulco) in Viña del Mar were severely damaged. Edificio Acapulco was severely damaged also during the 1971 Chile earthquake. Several hospitals (in San Antonio, Valparaiso, and Melipilla), grain silos, and school buldings, were also severely damaged. Social housing units in various parts of the earthquake stricken area were damaged. Of particular interest is the subdivision of Canal Beagle in Viña del Mar where several structures were damaged and the distribution of damage presents unique indication of terrain amplification.

The distribution of damage, particularly in towns and cities, exhibits a general correlation with the type of soil conditions on which the structures were built. This was particularly true in San Antonio, where due to liquefaction and subsidence, the severity of the damage to structures increased. In Cartagena, only 7 km north of devastated San Antonio, very few adobe structures failed. The structures built on the rocky hills of Cartegena survived. In Valparaiso, the damage was mainly confined in the old river bed part of the town while the structures on more solid ground (hills) performed exceptionally well. In Viña del Mar and Renecá the severity of damage to some of the structures can be attributed to the foundation soil conditions.

Structures other than buildings also experienced damage of varying degrees of severity. These include bridges (Maripo Bridge south of San Antonio), grain silos in Melipilla, an earth dam (at La Marquesa), oil storage tanks (Concom), tailing dams, and some industrial facilities. Two highway tunnels (one 2.8 km long and the other 0.9 km long) between Valparaiso and Santiago were not damaged. No damage was reported on the test reactor near

one of these tunnels. Structures other than buildings will be described elsewhere and therefore will not be treated in this report (Wyllie and Scholl, oral commun., 1985).

PERFORMANCE OF BUILDING STRUCTURES IN DIFFERENT LOCALITIES

Santiago

The only engineered structure in Santiago that collapsed partially is shown in figure 1. This apartment building structure had a soft first story, and the columns in one end failed, thus causing the partial collapse. Identical structures in the same subdivision survived. A typical observation in downtown Santiago is the distress due to hammering or "pounding" of adjacent buildings separated by expansion joints (fig. 2). Other modern engineered structures in Santiago performed without distress.

The majority of the damage in Santiago was inflicted on unreinforced masonry (stone or brick) buildings (e.g., the Library of Universite of Chile and the National Archives Building), a mixture of timber reinforced adobe buildings and the parapets or architectural decoration of older structures.

San Antonio

In reclaimed areas of San Antonio, the columns of the structure in figure 3 settled due to liquefaction. Near this structure at the foot of a hill, a structure with a reinforced concrete first floor and timber reinforced masonry second floor (fig. 4), performed well while the weaker adobe buildings next to it collapsed completely. The docks of the harbor in San Antonio were completely destroyed (fig. 5) with all the cranes turned over because of the complete loss of support due to liquefaction and sandboiling.

Across from the harbor in San Antonio, a new reinforced concrete framed structure still under construction (fig. 6) was severely damaged. This two-block-long structure had short columns (fig. 7) at the top of its very rigid first floor stiffened by infill masonry walls and a tie beam. All of the short columns were severely damaged, the longitudinal reinforcing buckled and the concrete was crushed. It was apparent that sufficient development and embedment length was not provided between the tie-beam and the corner column (fig. 8).

One of the two blocks of the four story Claudio Vicuña Hospital was severely damaged (fig. 9). The damage was concentrated in the second story which effectively was the "soft story" of the structure. The columns were well reinforced; however, the low quality of concrete and thick cover caused extensive spalling (fig. 10). Also, the two story long column (extending between the first and third floors) on the west end of the hospital was severely cracked at the second floor level due to the story force acting at the middle of that column (fig. 11).

The apartment buildings in figure 12 located only two blocks from Claudio Vicuña Hospital suffered no damage.

Valparaiso

In Valparaiso, the harbor dock and related structures were damaged as partially seen in figure 13. The damage to this harbor dock was not as extensive as that in San Antonio.

Figure 1.--Part of this building in Santiago collapsed. The building had soft first story. This building, one of several typical buildings in the same area, is the only one that did not perform well.

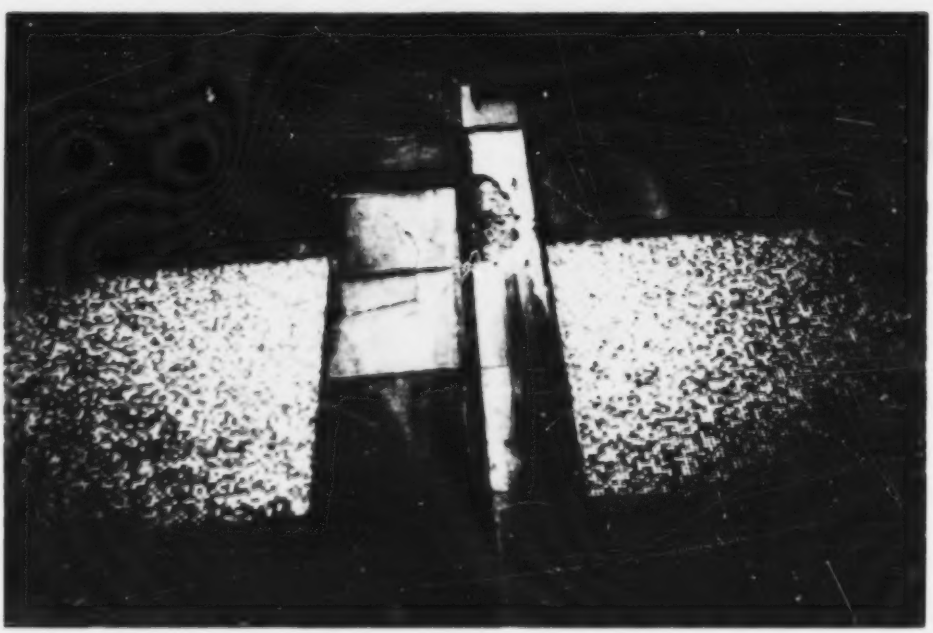

Figure 2.--Typical pounding of buildings in downtown Santiago.

Figure 3.--The columns of the structure in San Antonio settled into the pavement due to liquefaction.

Figure 4.--A unique structure in downtown San Antonio. The first floor is reinforced concrete frame. The added on second floor is masonry reinforced with well braced timber. The building did not suffer any damage. Older adobe buildings adjacent to this building or behind it had completely collapsed.

Figure 5.--The dock of San Antonio Harbor. All cranes either totally or partially tipped over. The unreinforced surface concrete was severely damaged as a result of liquefaction of the pumping of fill-sand underneath.

Figure 6.--A new reinforced concrete framed structure across from the San Antonio Harbor. Note the short columns between the tie beam (in the first floor) and the beam in the second story floor. These short columns were all damaged.

Figure 7.--The short columns of the structure in figure 6.

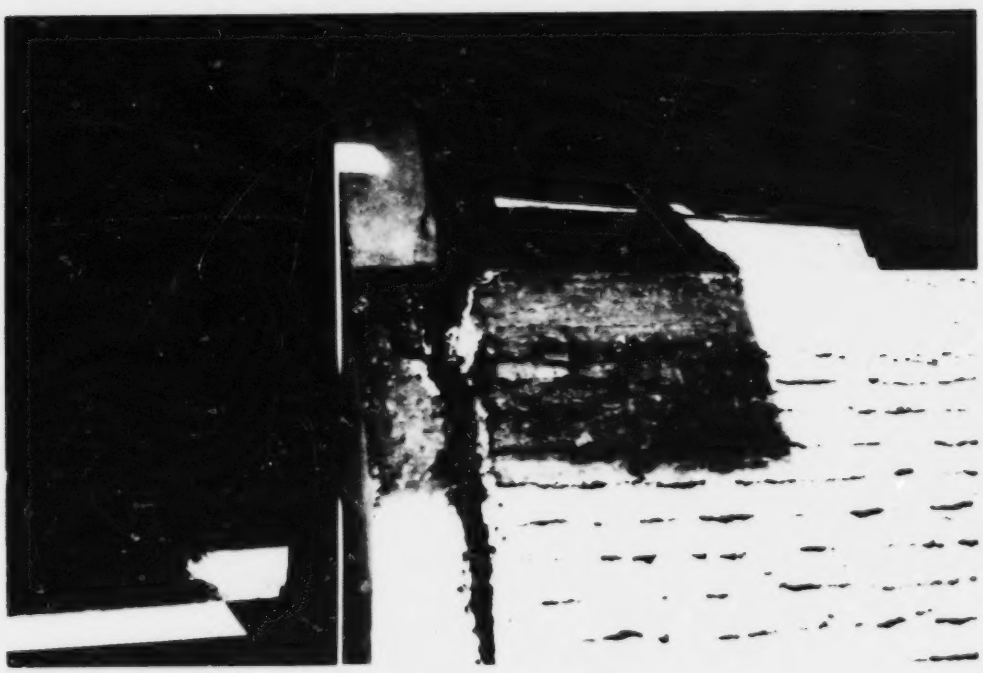

Figure 8.--Sufficient development and embedment length was not provided between the tie beam and the corner columns.

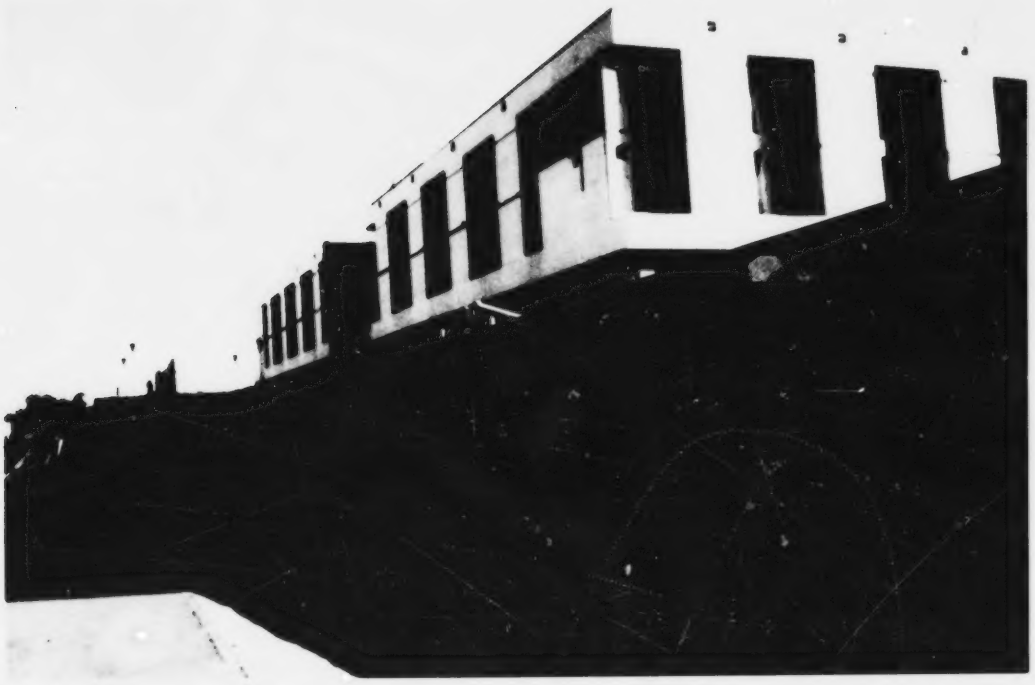

Figure 9.--Claudio Vicuña Hospital in San Antonio. The second story is the "soft story". The columns, particularly in one of the two blocks were damaged.

Figure 10.--Extensive spalling at the exterior and cracking in the confined concrete core of the column. The concrete quality appeared poor.

Figure 11.--Two story long column at the west end of the hospital severely cracked in the middle.

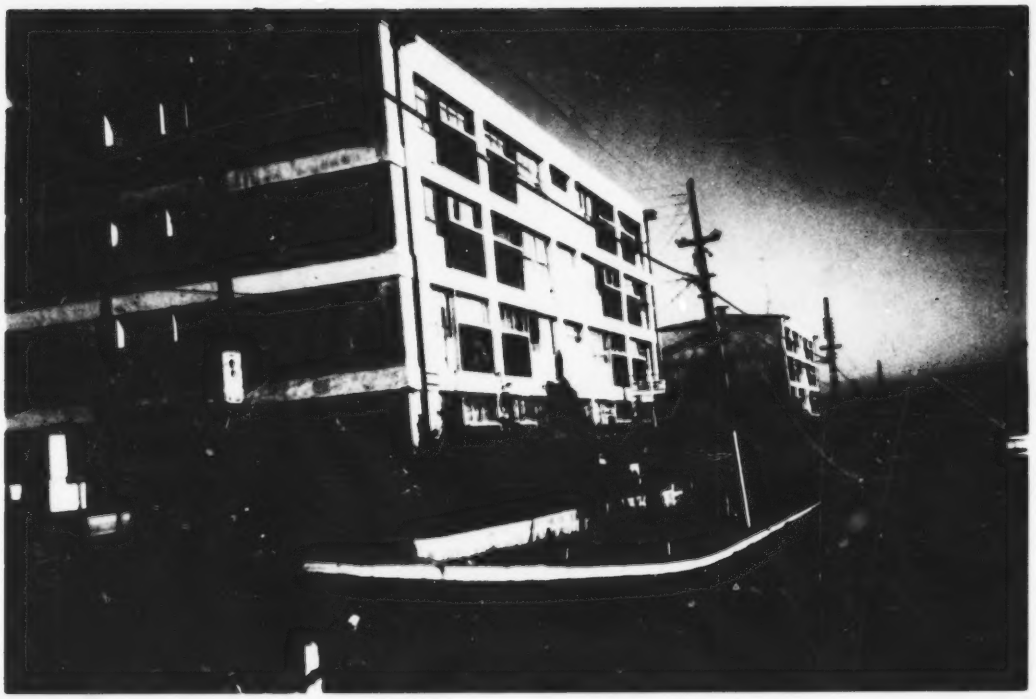

Figure 12.--These apartment buildings near Claudio Vicuña Hospital were not damaged.

Figure 13.--Harbor dock in Valparaiso. The surface of the dock was deformed and cracked in several locations.

Figure 14.--Sermana Hospital in Valparaiso. Outside appearance does not reveal any distress; however, most of the divider panels inside the hospital were damaged or turned over. The concrete shear walls on the side were severely damaged, exhibiting typical diagonal cracks.

In downtown Valparaiso, Sermana Hospital seen in figure 14, was severely damaged. Typical diagonal shear cracks developed in the shear walls as seen in figure 15.

Near this hospital, other structures, particularly modern symmetrical structures with center shear wall core and columns in the exterior perimeter (fig. 16) performed well. This type of construction has been applied also in Viña del Mar and Santiago. No damage has been reported on these types of structures in those towns either.

Another hospital in Valparaiso (C. Van Buren Hospital) also suffered some damage, but none structurally. The hospital had two reinforced concrete framed blocks (8 and 6 stories) separated by a steel framed glass "corridor" structure providing access to, and between, both blocks (fig. 17a). The operating room of the hospital and contents were damaged. The prefabricated wall panels, acting as infill walls, were separated from the frame, thus creating the possibility of falling partially or entirely on patients. The anchorage details of these prefabricated wall panels were not available. The steel structure used as a corridor between the two blocks was bolted to the concrete. The bolts were sheared off during the earthquake (fig. 17b).

Viña del Mar

This coastal town 3 km north of Valparaiso was sustained damage to several modern structures and extensive damage to a low cost housing subdivision (Canal Beagle). A more extensive description of Canal Beagle is presented under the social housing section.

On the coastal end (west) of Viña del Mar and its suburb Reneca, several low rise buildings (5-15 stories) with unique architectural configurations suffered damage. Of these structures, (three are particularly significant) Edificio Acapulco and Edificio H'Angoroa, both on the beach and next to one another, were severely damaged. Locations of these buildings as well as others in the immediate vicinity are qualitatively shown in figure 18. Edificio Acapulco (fig. 19) had very serious cracking on the exterior shear walls (fig. 20). The floor slabs of the building were completely "hinged" and the structure, in essence, behaved as shown in figure 21. Edificio H'Angoroa (fig. 22), on the other hand, had fifteen stories of walls and slabs cracked continuously throughout each its floors. The cracks and extensive damages were concentrated particularly in the right wing as qualitatively shown in figure 23.

The third structure, Edificio El Faro, on top of the sand dunes of Reneca was a shear wall structure constructed on a continuous wall footing foundation. The foundation was not embedded effectively. The footing thickness was consistently 0.50 meters and the footing wall thickness varied between 0.20-0.30 m (only in one location the wall of the footing was 0.85 m thick, while generally the footing wall height is 2.5 m). The footings extended throughout the whole plan of the structure, leaving very small uncovered areas; therefore, for all practical purposes, the footing acted as a mat of 0.50 m thickness and with openings. The highly unsymmetrical layout of the shear walls is exhibited in figure 24. The total floor area accommodating three units of apartments per floor was 140 m^2. The total weight of the structure was estimated to be 800-900 kips. At the entrance floor level there was approximately 11.5 m^2 of shear wall in each direction. In the upper floors the shear wall area was approximately 5.50 m^2 in each direction. If

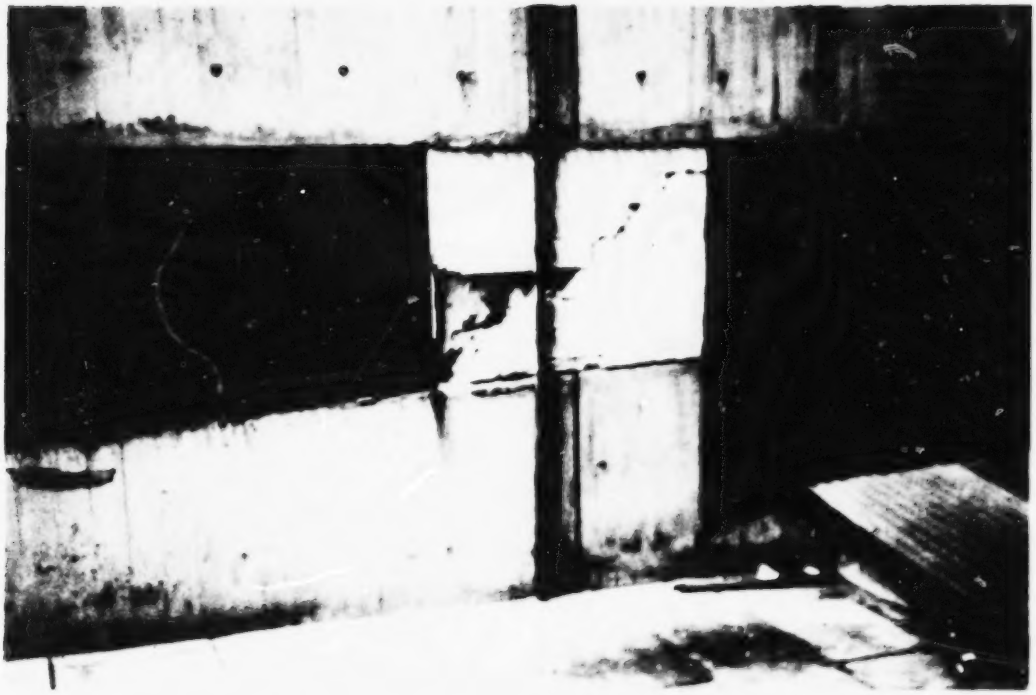

Figure 15.--Typical diagonal shear cracks developed in a short shear wall of the Sermana Hospital.

Figure 16.--A modern symmetrical reinforced concrete structure near the Sermana Hospital. The building had a reinforced concrete core shear wall and columns around the perimeter. No damage was reported in this structure or other similar structures in Viña del Mar and Santiago.

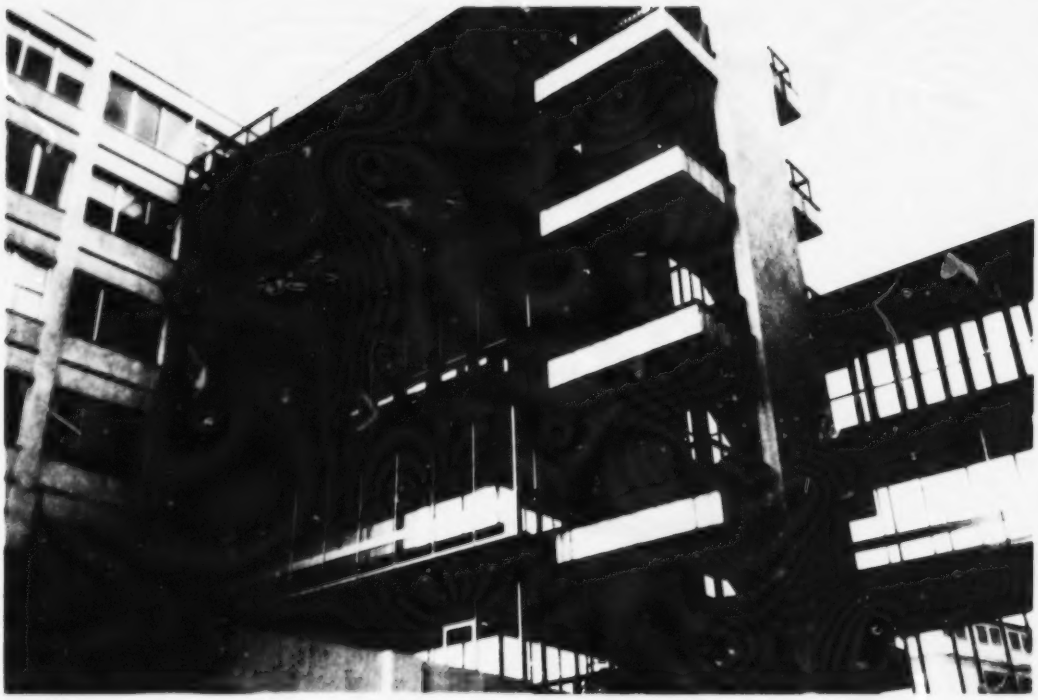

Figure 17a.--C. Van Buren Hospital in Valparaiso. There was no structural damage. However, the prefabricated infill panels separated from the frame elements in several locations. The operating room was damaged. The two blocks of this hospital is connected by a steel framed glass corridor.

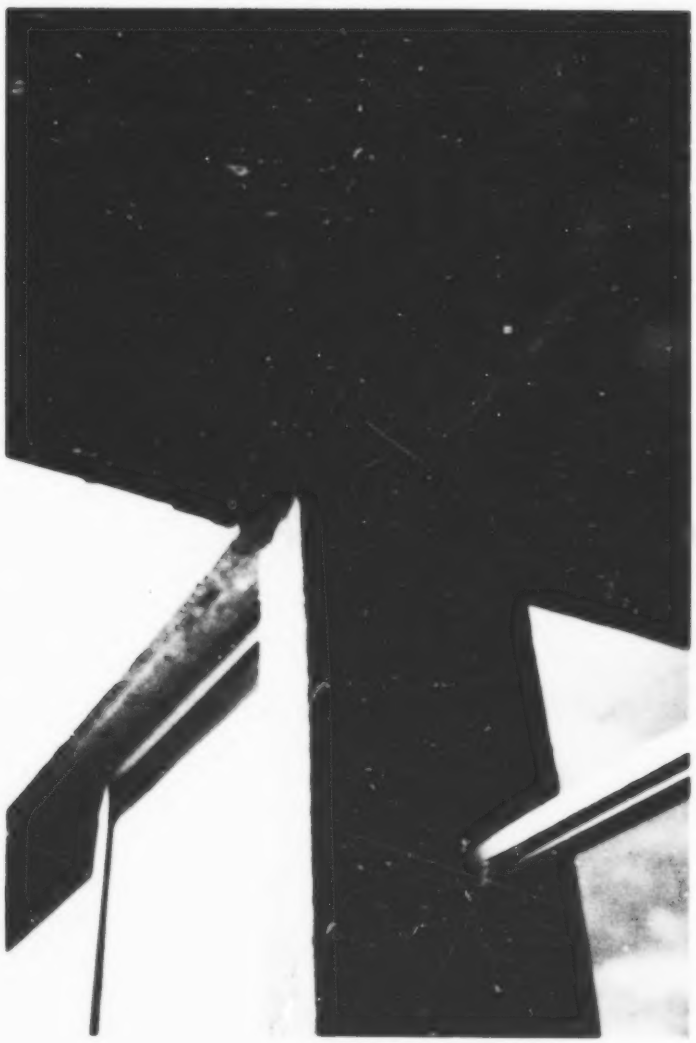

Figure 17b.--The bolts of the glass corridor structure attaching it to the concrete walls sheared off.

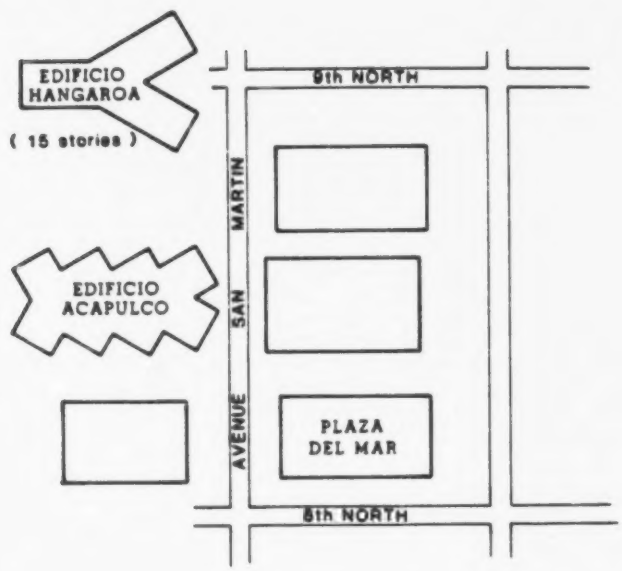

Figure 18.--Locations of low-rise damaged and undamaged buildings on the coast of Viña del Mar. See text for discussion.

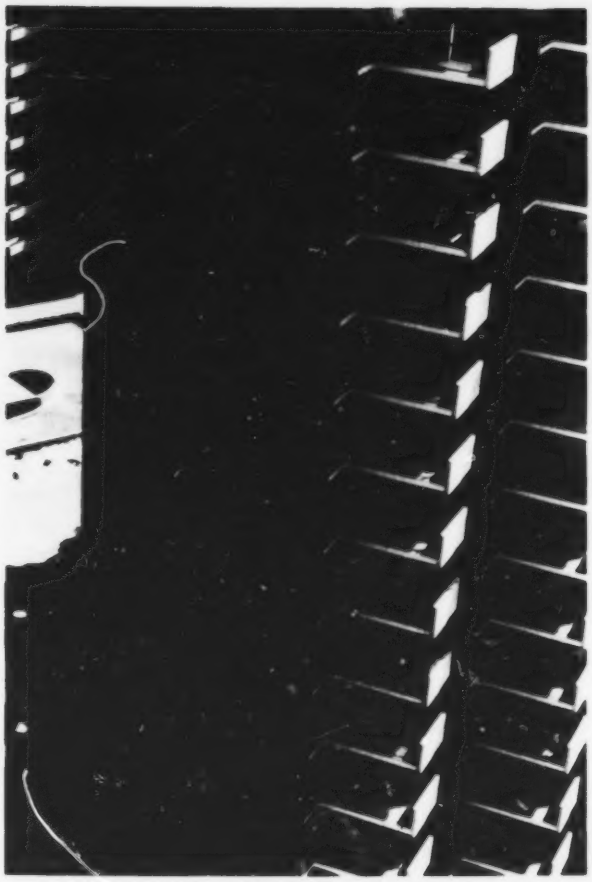

Figure 19.--Edifico Acapulco on San Martin Avenue - a modern structure on the beach of Viña del Mar. The shear walls were severely damaged and floor diaphragms cracked. This building was damaged also during the 1971 Chile earthquake.

Figure 20.--Damage to shear wall - Edificio Acapulco.

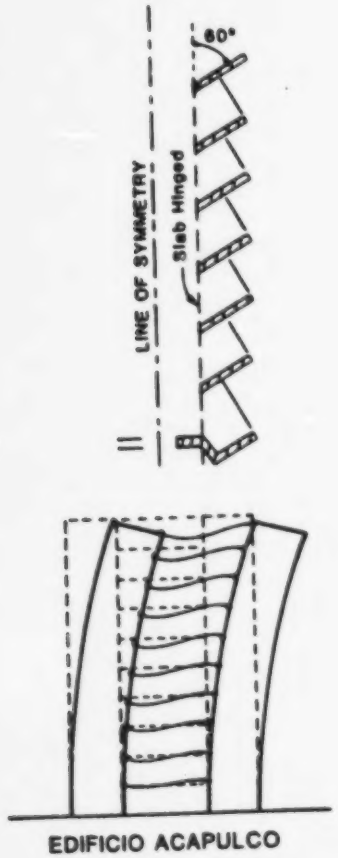

Figure 21.--Qualitative behavior of Edifico Acapulco.

A

B

C

Figure 22.--Edificio H'Angoroa - 15 stories next to Edificio Acapulco. All fifteen floors had cracks in the diaphragms and the shear walls.

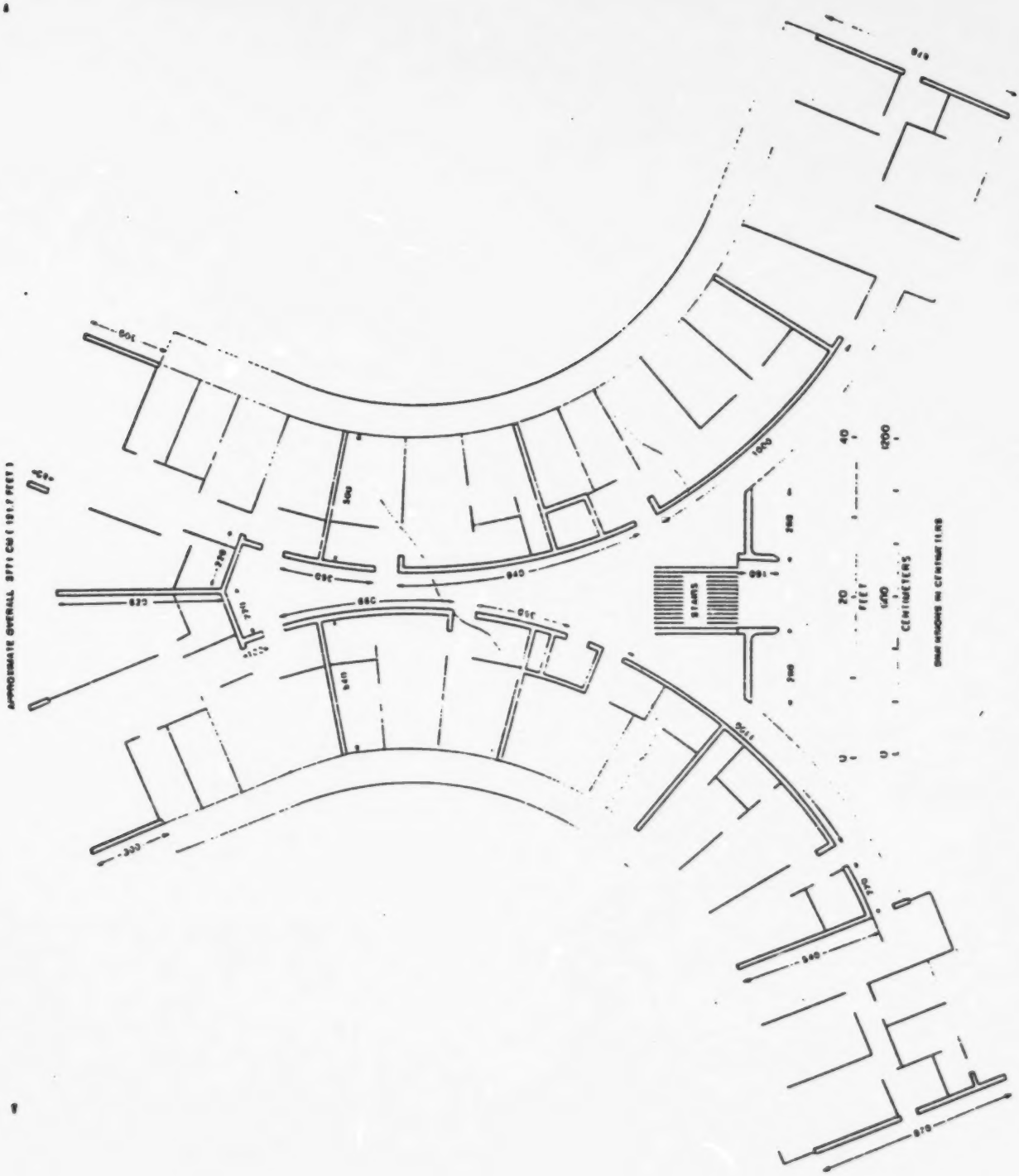

Figure 23.--Qualitative propagation of cracks in Edificio H'Angoroa.

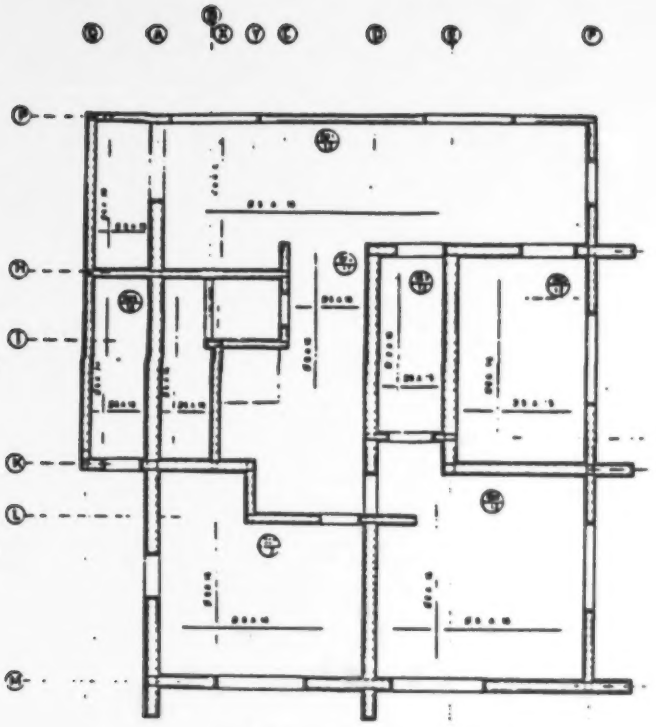

PLAN VIEW OF FIRST FLOOR SHEAR WALLS

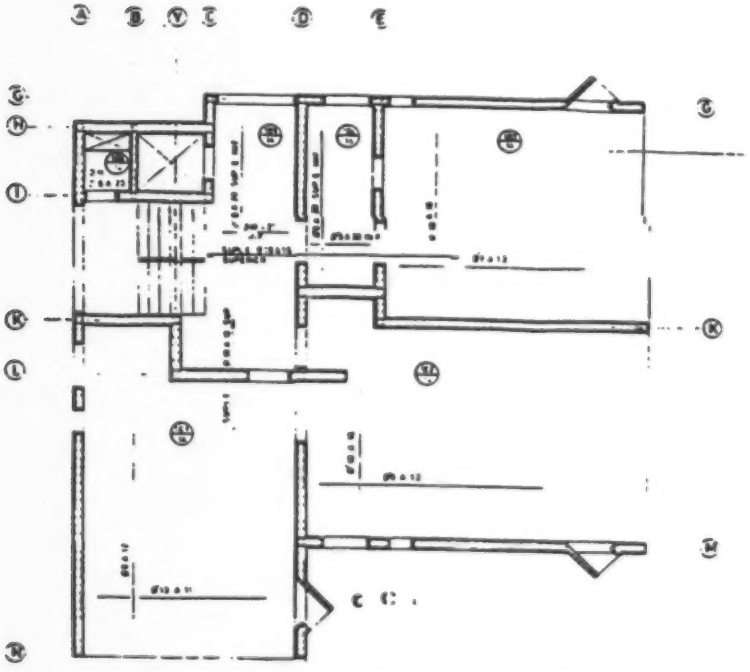

PLAN VIEW OF UPPER FLOOR SHEAR WALLS

Figure 24.—Plan view of the shear walls of Edificio El Faro - on the hilltop of sand dunes of Reneca.

only direct shear forces are considered, the available shear walls appear to be sufficient even when minimum concrete shear resistance is considered. However, preliminary evaluations point out that the structure may have been subjected to rocking and uplift, particularly since its foundation had little or no effective embedment. Also, it may have been subjected to torsional effects. Considering the fundamental period of the structure incorporating soil structure interaction as compared with that of sand, it is totally conceivable that the structure was also in resonance. During the earthquake, the walls in the first floor of such a structure were completely crushed and the structure tilted off its vertical axis by 12-15° (fig. 25). As a consequence, the structure was dynamited to level it off on the ground. Further detailed analysis into the failure aspects of ths structure is being performed by the author.

In close proximity to Edificio El Faro (approximately 150 yards), and on the steep hilltop, a new reinforced concrete structure still under construction was not damaged (fig. 26). Also, another new reinforced concrete framed structure still under construction on rock right on the coast and down from the sand dune hill where Edificio El Faro once stood, was not damaged at all (fig. 27).

Two other structures of interest are Edificio Tahiti and Edificio del Mar. Edificio Tahiti, next to Edificio Acapulco, had minor damage while Edificio del Mar (a new 23 story condominium structure) had a curved offset in its lower floors exterior shear wall which cracked (fig. 28) due to incorrect placement of reinforcing bars that followed that specific outline of the shear wall of the building. Inside this structure, numerous prefabricated brick panels were damaged extensively, as seen in figure 29, and furniture was moved around during the main event.

Only two blocks away from the structures in figure 18, the 23 story symmetrical structure (fig. 30) with central core shear wall performed well without distress.

PERFORMANCE OF SOCIAL HOUSING STRUCTURES CANAL BEAGLE SUBDIVISION IN VIÑA DEL MAR

The subdivision of Canal Beagle east of Viña del Mar sustained damage of various degrees of severity. The subdivision consists of one and two story buildings (Type A), four story buildings (Type B), and five story buildings (Type C). General layout of the whole Canal Beagle subdivision depicting the location of different types of buildings is presented in figure 1. The Canal Beagle structures were constructed approximately 10 years ago.

The general topography of the subdivision can be best described to consist of three steep sloped ridges (marked on fig. 31) emerging from a less steep hilltop on which Type A structures have been constructed. Most Type B and all of Type C structures are on the steep sloped ridges.

The geological formation of the ridges separated by canyons is decomposed granite (locally known as Maicillo). Visually, the top soil appears to be dense granular silty and clayey sand.

The buildings in Canal Beagle are essentially of typical design. In figures 32 and 33, the general architectural configuration and typical plan of a four story structure are shown. The particular vertical configuration of

Figure 25.--Tilted view of Edificio El Faro before it was dynamited. The first story shear wall had been completely crushed.

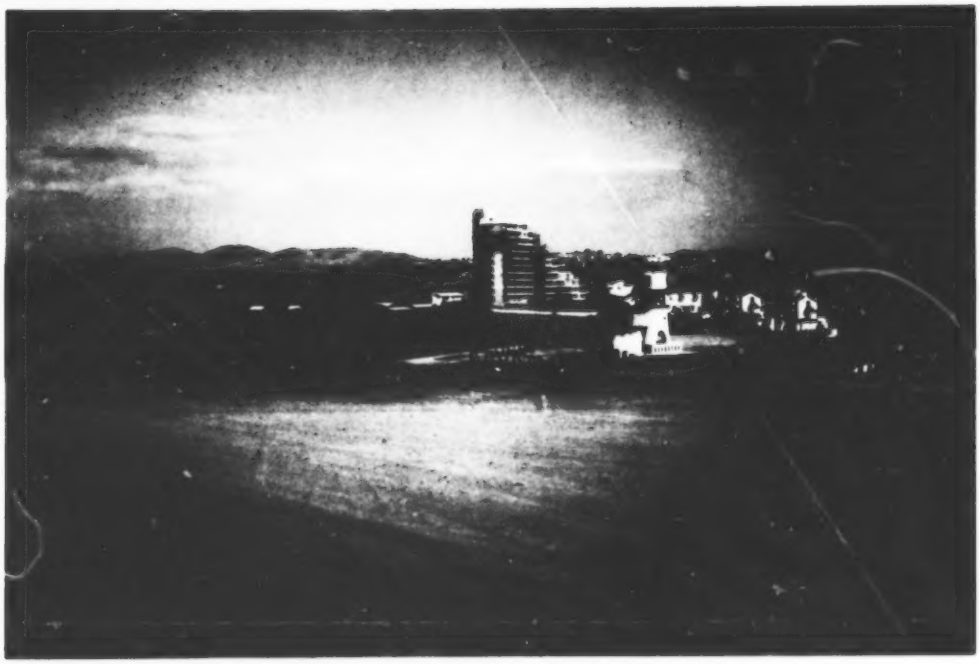

Figure 26.--On the same hill as Edificio El Faro, this new structure under construction suffered no damage.

Figure 27.--Down from the hilltop where Edificio El Faro was located, this new structure under construction on the rocky part of the beach suffered no damage. Note, to the right, modern condominium structures built on the slope.

Figure 28.--Edificio Del Mar: minor structural damage in the exterior curved shear wall.

Figure 29.--Prefabricated brick panels of Edificio Del Mar cracked extensively, particularly in the top floors.

Figure 30.--Another symmetrical structure with central concrete shear wall core on Avenue San Martin performed well.

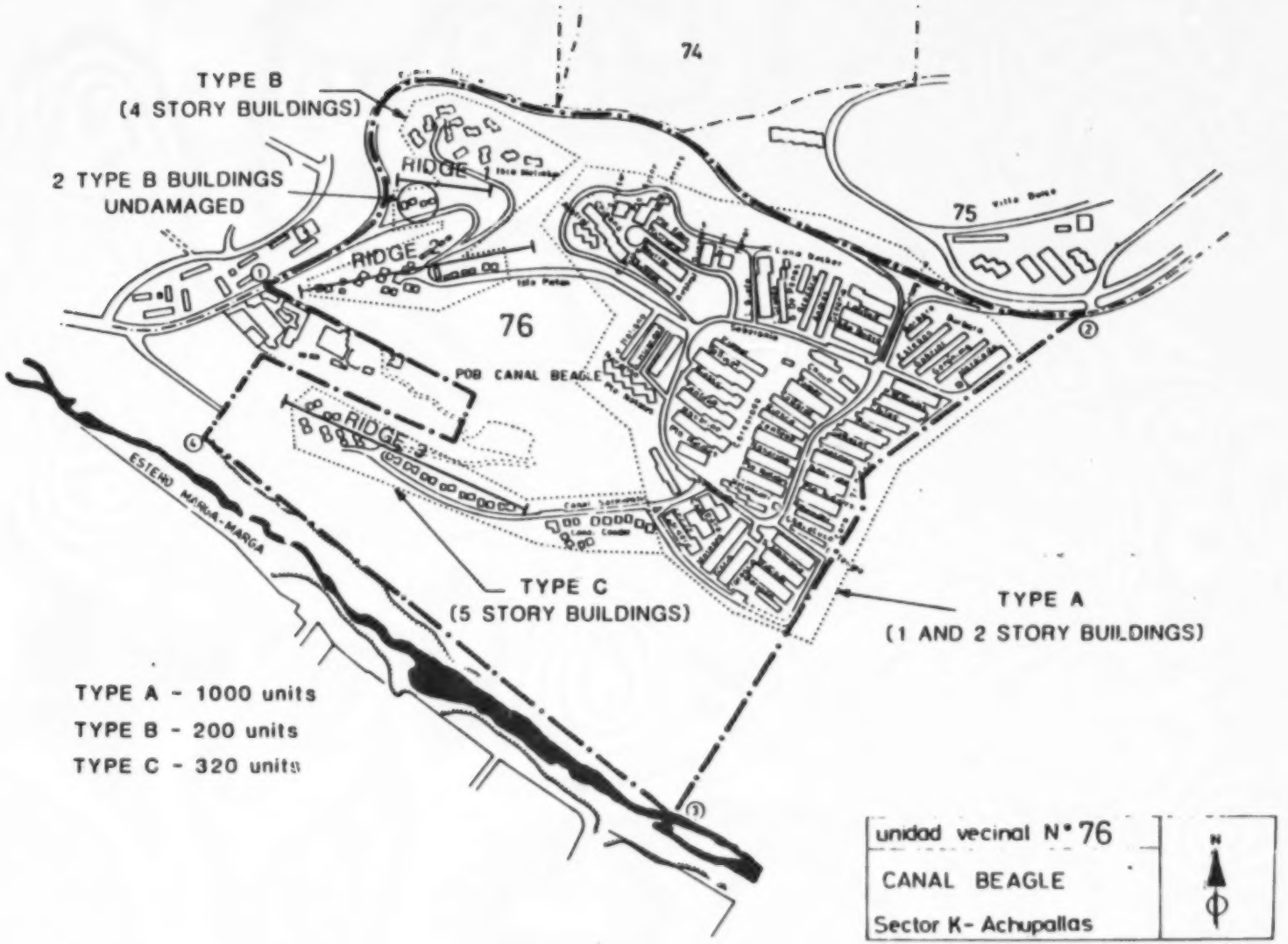

Figure 31.--General layout of Canal Beagle Subdivision. Note locations of Type A, B, and C structures. Also, qualitatively, major axis of the three ridges are given.

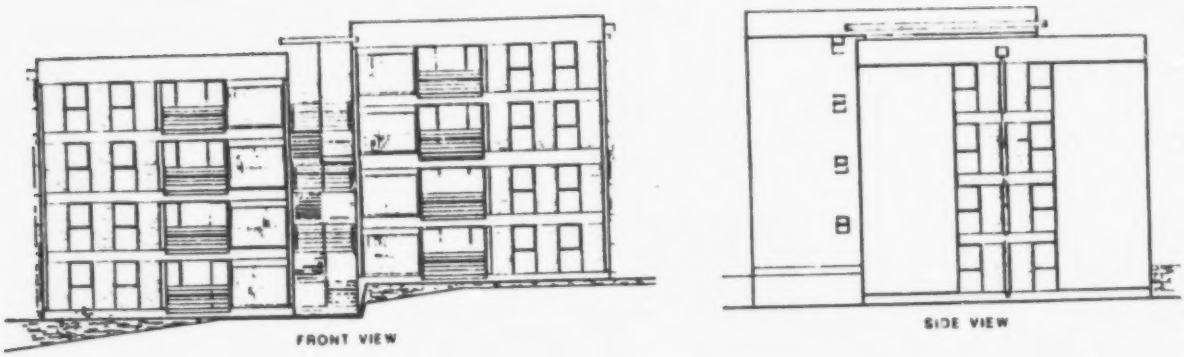

Figure 32.--Front and side architectural views of Canal Beagle Type B structures. Each building has 2 blocks. The vertical configuration has been particularly chosen to accommodate the sloping terrain.

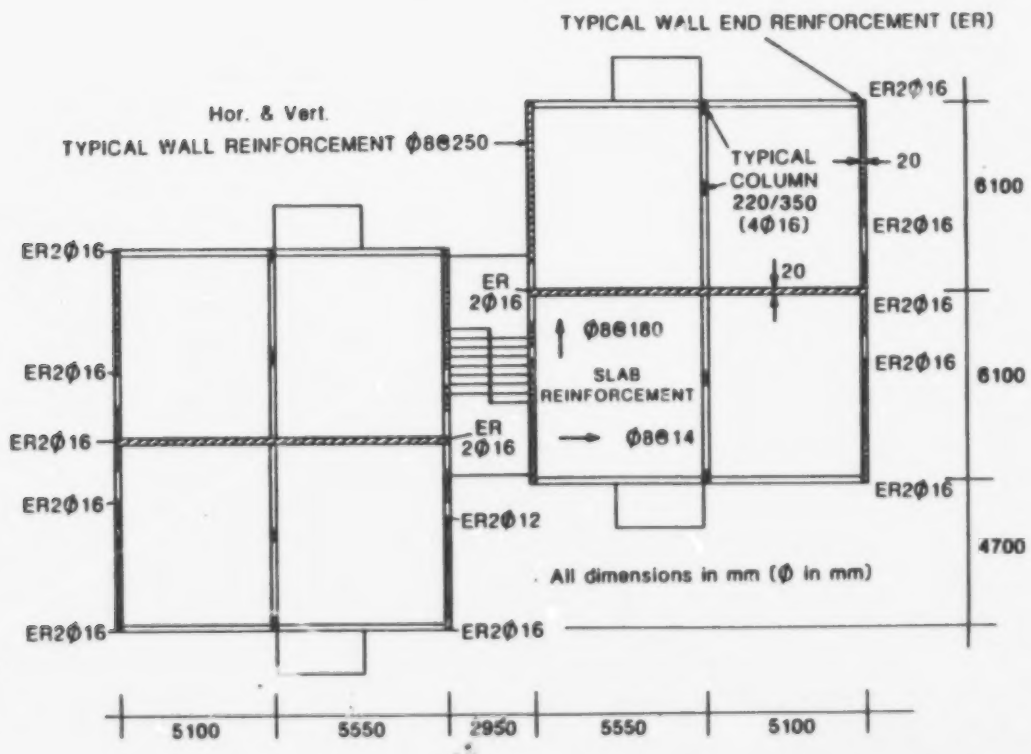

Figure 33.--Typical plan of Canal Beagle units. In this case Type C plan is provided.

these structures has been chosen to accommodate the sloping terrain. Where necessary, stone masonry retaining walls of varying heights have been constructed to provide stability to the slopes.

As seen in figure 33, the construction of the Canal Beagle subdivision is realized with reinforced concrete shear walls as well as brick masonry infill walls. In the design of these structures, the Chilean Code for Earthquake Resistant Design of 1972 has been followed (International Association of Earthquake Engineers, 1972). Accordingly, the base shear coefficient taken was 0.1.

GENERAL DESCRIPTION OF PERFORMANCE OF STRUCTURES AT CANAL BEAGLE

The performance of Canal Beagle structures is scientifically dilemnatic in the sense that although the structures are all typical and in general each type was constructed by the same contractor, signifying that construction quality was probably uniform for each type, the following pattern of severity of damage was observed:

TABLE 1.--Canal Beagle Statistics

Type & design	No. of bldgs.	No. of units	No. of buildings severely damaged	Remarks
A Single- and two-story buildings.		1,000	2	Built on easier slope at the top of the hill where three ridges merge.
B Four-story buildings.	25	200	23	Built on three separate locations: a) At foot of one of the ridges with easier slope (two buildings - no damage); b) On steep slopes (Isle Picton) all damaged; c) On easier slope at top (Isle Melinka) minor damage.
C Five-story buildings	16	320	16	Built on a ridge with steep slopes, all severely damaged.

Fig 1. Two Type B structures (fig. 34) at entrance to the Canal Beagle Subdivision were not damaged at all. These two structures were constructed on relatively flat land at the foot of one of the ridges.

2. Similar Type B structures (fig. 35) on top of a steep ridge next to the entrance to the subdivision were severely damaged. This particular part of Canal Beagle is called Isle Picton.
3. Isle Melinka consisting of Type B structures is founded on less steep slopes at the top of the ridge. This part of the subdivision was less severely damaged.
4. All of Type C structures were constructed on another ridge. Panoramic view of these structures is provided in figure 36. Type C structures were all severely damaged. The degree of severity in general was more extensive near the steep slopes.
5. Type A structures founded on relatively easier slopes of the hill from which the described ridges emerge performed well except for two. The two damaged Type A structures (one seen in fig. 37) are on a street which is next to a steep canyon. The street had cracked extensively (fig. 38) and the canyon next to the street is seen in figure 39. Pertinent information on these structures as well as the general distribution of damage is summarized in Table 1.

TOPOGRAPHICAL EFFECTS

The above "tour" of the subdivision is intended to pinpoint the fact that the more severe damage distribution is mainly on the steep sloped ridges or next to a canyon. This particular aspect clearly indicates that there may have been substantial terrain amplification at this particular site. Past work related to the effect of topography on the incoming seismic waves by Boore (1962; 1972) clearly proved that these waves are amplified under distinct conditions. Recently Bard and Tucker (1985) showed by theory and experiment that the ridge site effect on amplification of seismic waves is a reality. Bard and Tucker (1985) indicate that the various theoretical models do not necessarily duplicate the results obtained through measurements performed on specific sites; therefore, they strongly recommend experimental means over theoretical models in evaluation of ridge site effects.

The possibility of amplification due to topography has been preliminarily investigated by the writer. One set of velocity transducers (with two horizontal and one vertical component) were placed at nearby free field grounds of each of two Type B structures on sloping terrain. One of these structures was damaged only slightly (designated as Site 1), and the other was heavily damaged (designated as Site 2). Figure 40 illustrates a portion of the velocity response obtained with General Earthquake Observation System (GEOS) detailed description of which is provided elsewhere (Borcherdt and others, 1985). As exhibited in figure 40, there is substantial amplification of velocity response in each of the components at Site 2 as compared with Site 1. However, this evidence is very preliminary, and further detailed measurements need to be obtained at the Canal Beagle Subdivision.

OTHER CAUSES OF DAMAGE

The severity of damage in different locations of Canal Beagle could not be attributed only to terrain amplification. Other possible causes of the damage are: i) incipient slope failure, ii) design errors, and iii) construction/quality control.

Figure 34.--These two Type B structures at entrance to the Canal Beagle subdivision were not damaged at all. These two structures were constructed on relatively flat land at the foot of one of the ridges.

Figure 35.--These Type B structures (Isle Picton of Canal Beagle Subdivision) on top of one of the ridges next to entrance to the subdivision were severely damaged.

Figure 36.--Panoramic view of Type C structures on another ridge of Canal Beagle Subdivision. All of the type C structures were severely damaged.

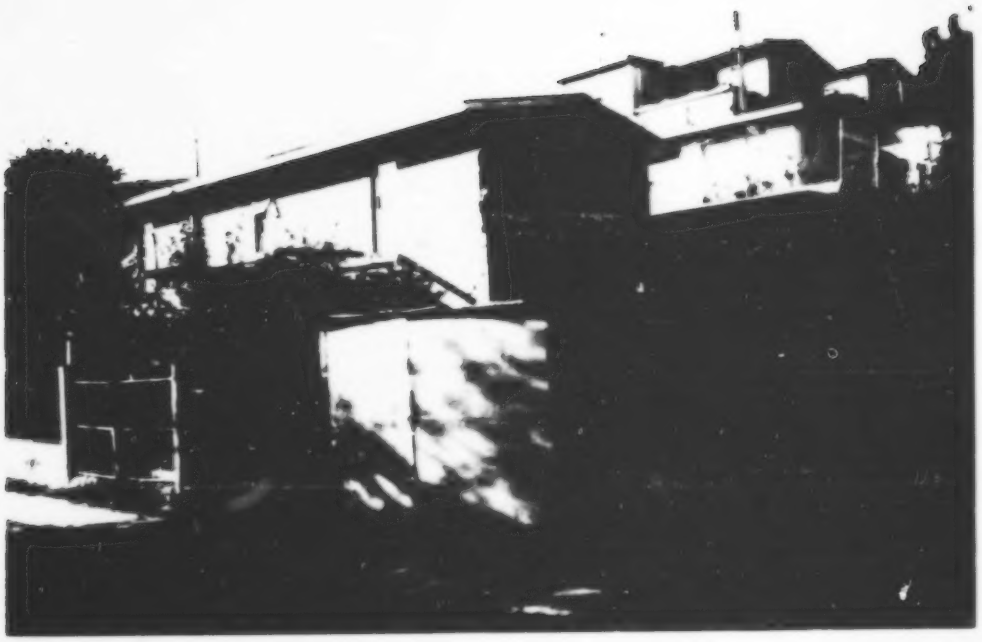

Figure 37.--One of the two Type A structures damaged. These structures are on a street next to a steep canyon.

Figure 38.--The two damaged Type A structures are on this street which cracked extensively.

Figure 39.--Canyon next to the street with the two damaged Type A structures.

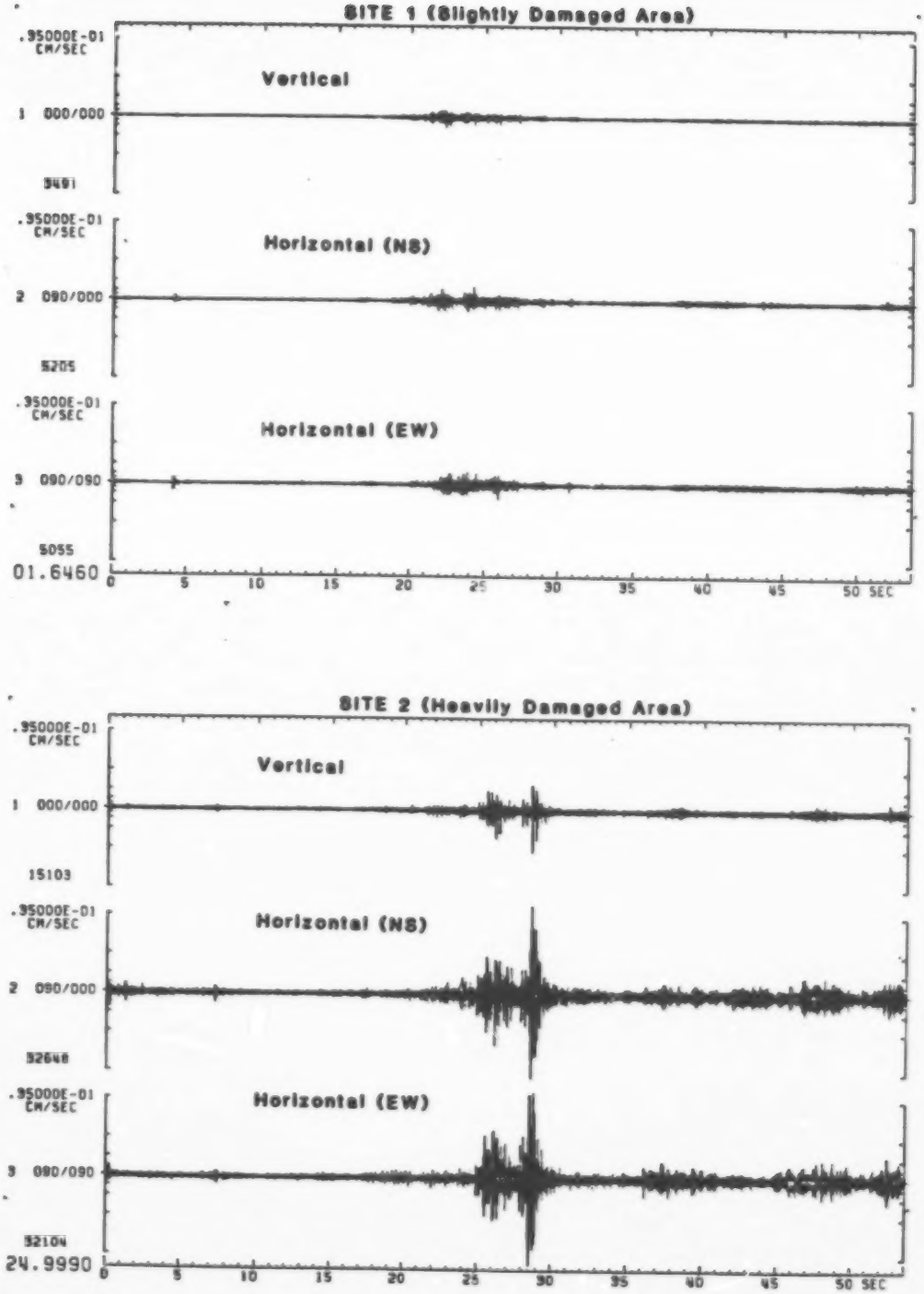

Figure 40.—Comparison of three components of velocity responses of noise at two sites at Canal Beagle (Site 1 was slightly damaged, whereas Site 2 was heavily damaged). Although this is a very limited and preliminary result, it indicates qualitatively that there is amplification at Canal Beagle topography.

There was evidence of incipient slope failure (and/or ground cracking) at the Canal Beagle development. Figures 41 to 42 illustrate specific locations where such distress has been observed. Figures 43 and 44 exhibit cracking in retaining walls at two different locations.

Sample illustrations of design or construction problems associated with the damage are provided in figures 45 through 49. Clearly these figures exhibit: a) insufficient shear reinforcement, b) low quality of concrete (with large river bed gravels), c) inadequate embedment lengths, d) discontinuous reinforcement of walls perpendicular to each other (or perpendicular walls not tied to one another).

SUMMARY OF EVALUATION AT CANAL BEAGLE

The damage sustained by these structures can be attributed to the following reasons:

- In accordance with the Chilean Code of Practice of 1972, the structures were designed for 0.1g. The shaking in Viña del Mar produced accelerations much higher than code specified minimum.
- There is distinctive evidence of the possibility of amplification of motions due to: a) terrain and/or, b) sliding of slope(s). Slope failures were observable in several locations. Surface cracking could be traced continuously between and underneath two neighboring Type C structures.
- There is a possibility that the structures were not all on good cut foundation material. On the steeper slopes, there may be some structures, part of which lie on fill material derived from the cut to level off the property. The cracks in the ground around the perimeter of some of these buildings and the cracks in the retaining walls point to this possibility.
- There are design and construction flaws also. The concrete quality appeared to be poor. Furthermore, the concrete spalled out, the gravel sizes were too large and the reinforcing steel details were not proper and/or sufficient. Construction joints were not implemented properly. In several locations, it was observed that the concrete surface on the foundation mat and walls was smoothed before pouring the new concrete walls.
- Use of infill brick walls created coupled shear wall effect in the four and five story buildings. In some Type C structures, the owners built up with brick masonry half height of the window openings on the sides of the buildings (fig. 49). These walls were not in original design and were not reinforced. In other locations, infilled walls created "short" columns.

MELIPILLA SOCIAL HOUSING BUILDINGS

In the east end of Melipilla, there are ten three-story reinforced concrete framed buildings with unreinforced masonry infill walls. Each building has 12 units of apartments. These homes, built on flat ground, are 6 yrs old. Particularly, the first floors of all ten buildings were severely damaged, while the remaining floors had varying degrees of severity of damage.

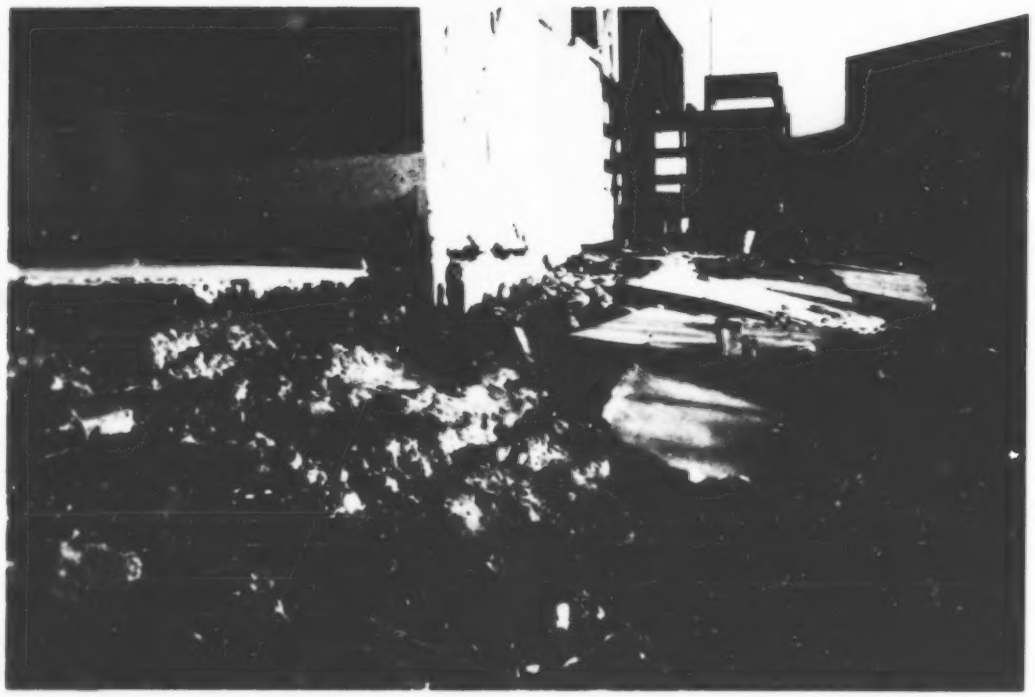

Figure 61.--Incipient slope failure caused the darwaes around and to the building of this Type B structure which was at the top of a steep slope of one of the ridges.

Figure 5.--Ground cracking started under the foundation of one of the type C buildings. This crack could be followed down the slope through a retaining wall and around the perimeter of another type C structure.

Figure 43.--A short retaining wall (cracked) in the vicinity of a Type B building (Isle Picton).

Figure 44.--A taller retaining wall cracked in the vicinity of two Type C buildings. These cracks extend from underneath the building above the retaining wall and follow down to the surrounding of the building below the retaining wall.

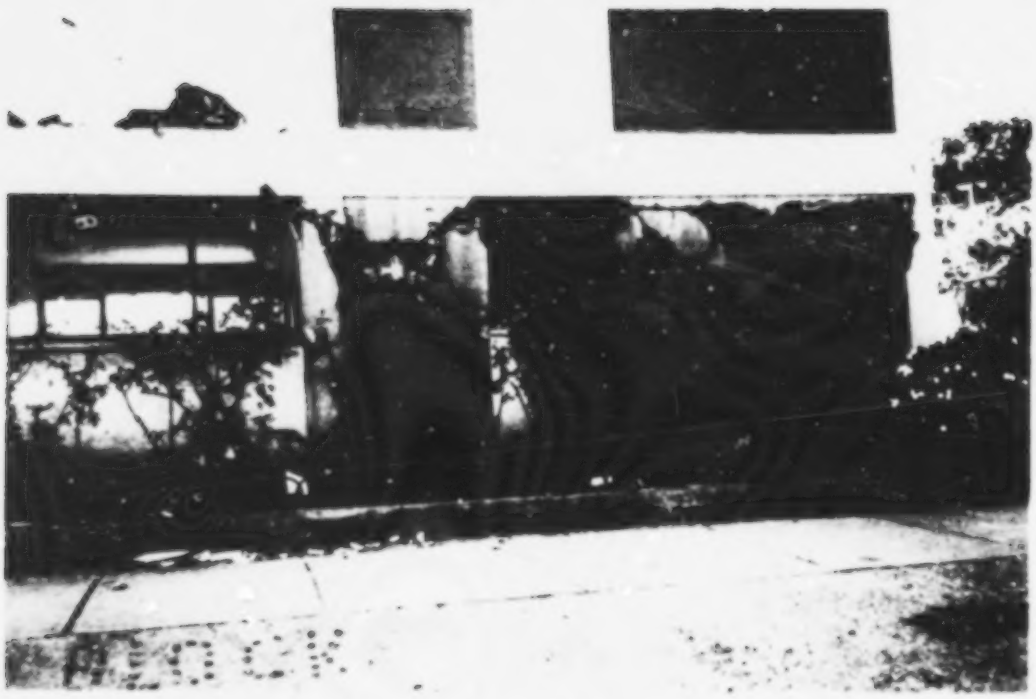

Figure 45.--Severely damaged Type 3 building. Note the damage to "short" column and brick infill wall.

Figure 46.--Insufficient reinforcement in walls not tied to one another caused this damage. Concrete quality was poor and there was no bond between concrete surfaces.

Figure 47.--Damage to shear wall (typical flexural crack).

Figure 48.--Typical damages (diagonal shear cracks) in the brick infill walls.

Figure 49.--Typical diagonal shear cracks in the infill walls that behaved as coupling beams (Type C buildings). These infill walls in window openings are not by design, but were installed by the owners of the apartment units.

In figure 50, a general view of these buildings is provided. Figures 51a through 51d depict the type of damage that was repetitious in these structures. Typically, distress occurred at beam to column connections at the corners of the buildings as well as diagonal cracks in the infill brick walls. The ground floor mat appeared not to have suffered any distress. The damaged sustained by these structures can generally be attributed to insufficient lateral resistance of the ground floor and specifically may be attributed to: 1) design deficiencies such as large openings, insufficient shear reinforcement for columns and the embedment length of rebars, and 2) construction deficiencies such as poor quality of concrete (large gravels, low strength concrete), poor quality mortar, and possibly low quality bricks used in the masonry.

An interesting aspect of this particular site was that across the street in the next block were numerous single story (social housing) buildings (fig. 52), none of which were damaged. These homes were constructed well and each had an effective tie-beam on the load bearing masonry walls, which were strengthened by four reinforced concrete columns that were not in the corners of the buildings.

PERFORMANCE OF PRE-CAST SOCIAL HOUSING STRUCTURES IN VIÑA DEL MAR & VALPARAISO

In the northeast of Viña del Mar, in the subdivision of Estero Viejo, 20 four-story precast structures have been erected from standardized prefabricated panels to provide social housing. It was reported by the civil engineer working for the contractor of these buildings that in the various suburbs of Viña del Mar and Valparaiso, approximately 150 of these structures have been constructed to defray the shortage of low-cost housing. Each four-story building consisting of two blocks separated by an expansion joint has a total of 32 units of apartments. Only two of these structures suffered partial and minor damage during the March 3, 1985, earthquake.

A general view of these structures is provided in figure 53. General vertical layout of the front and middle line of panels and plan layout of the panels is provided in figure 24. These panels (each 3.20 m wide and 2.7 m high) were welded together and grouted at connections. Also shown in this figure is the plan view of one block (half of total) of each structure (54c). Figure 55 shows one of each of the typical external and internal panels with openings and their reinforcements.

The damage in the two structures in Estero Viejo consisted of diagonal cracks in the internal panels only on the first and second floors. Typical cracks in these panels are shown in figure 56. It can be generally stated that these precast structures performed well during the earthquake and the two structures that received damage can be repaired without much difficulty.

CONCLUSIONS AND RECOMMENDATIONS

The following general conclusions can be drawn from the study of structures:

1. The March 3, 1985, Chile earthquake (M_s=7.8) caused substantial damage to engineered and non-engineered structures in different localities. This extent of damage to engineered structures and in turn the number

Figure 50.--Three story reinforced concrete framed apartment buildings in Melipilla. The brick masonry infill walls with large openings, particularly in the first floor of these buildings were all damaged. Most of the beam-to-column connections at the corners of the second story floor level of these buildings were damaged.

a

Figure 51.--Typical damages sustained by the infill walls and concrete frame elements as well as corner beam to column connections (a,b,c,d).

51b

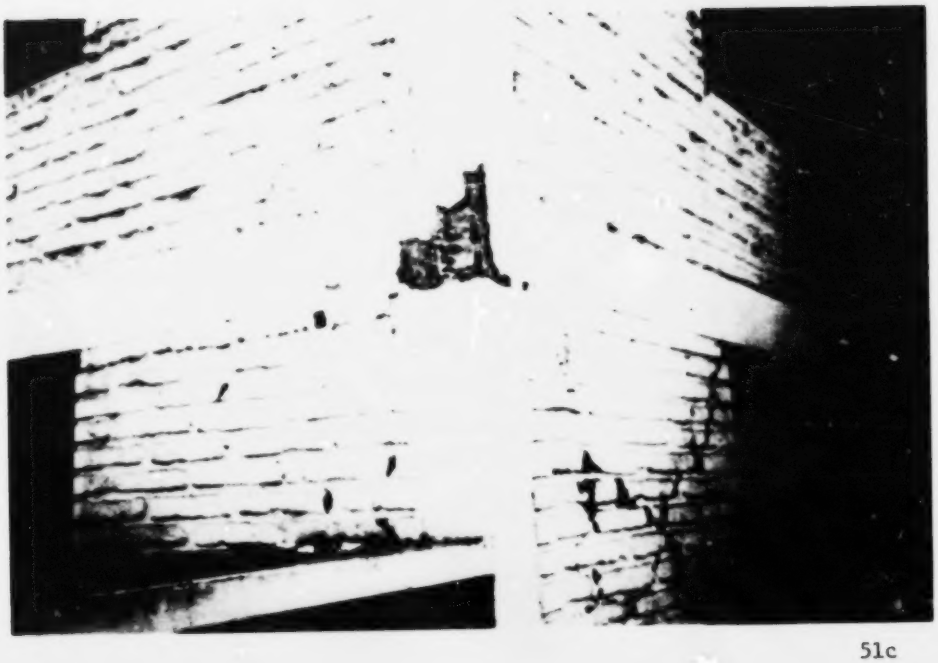

51c

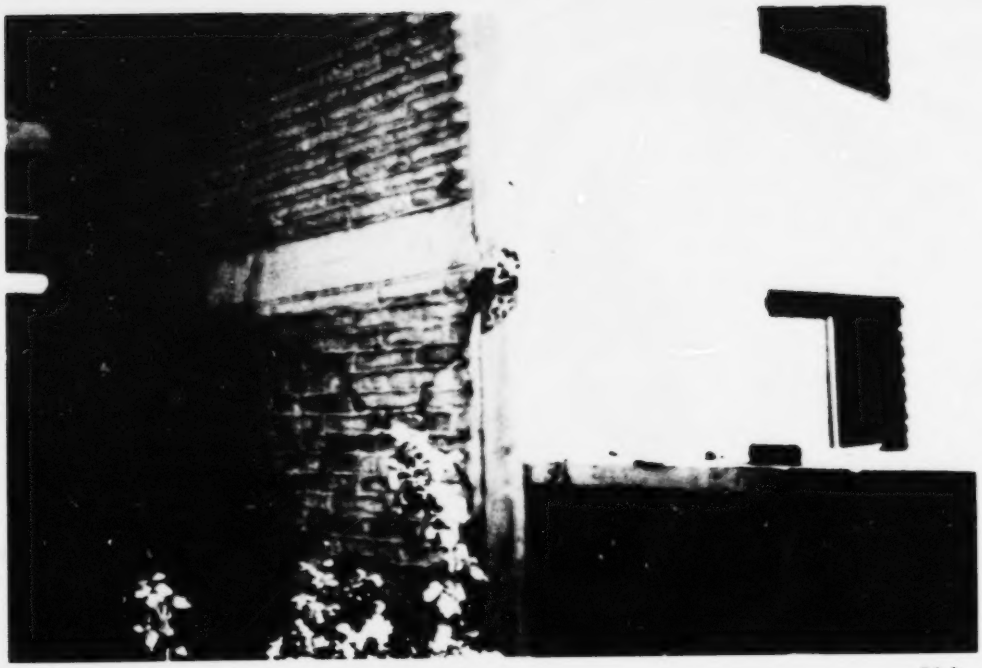

51d

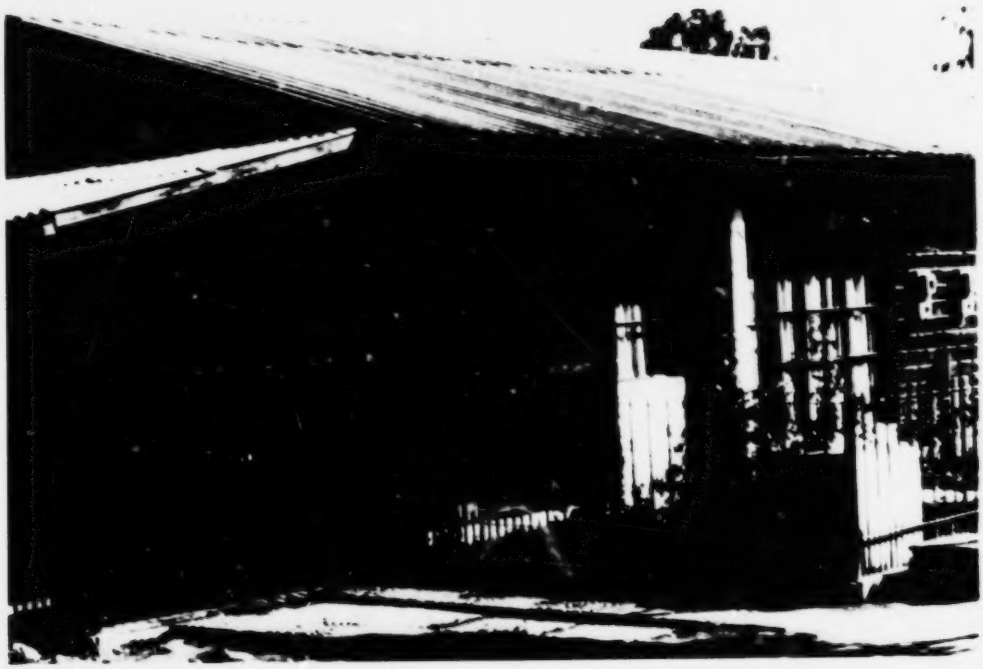

Figure 52.--Single story social housing structures in Melipilla. These structures were not damaged. They are in the next block from the three story reinforced framed structures that were damaged.

Figure 53.--General view of precast structures built with prefabricated panels. Approximately 150 of these structures were built in Viña del Mar and Valparaiso. Only two suffered minor damage.

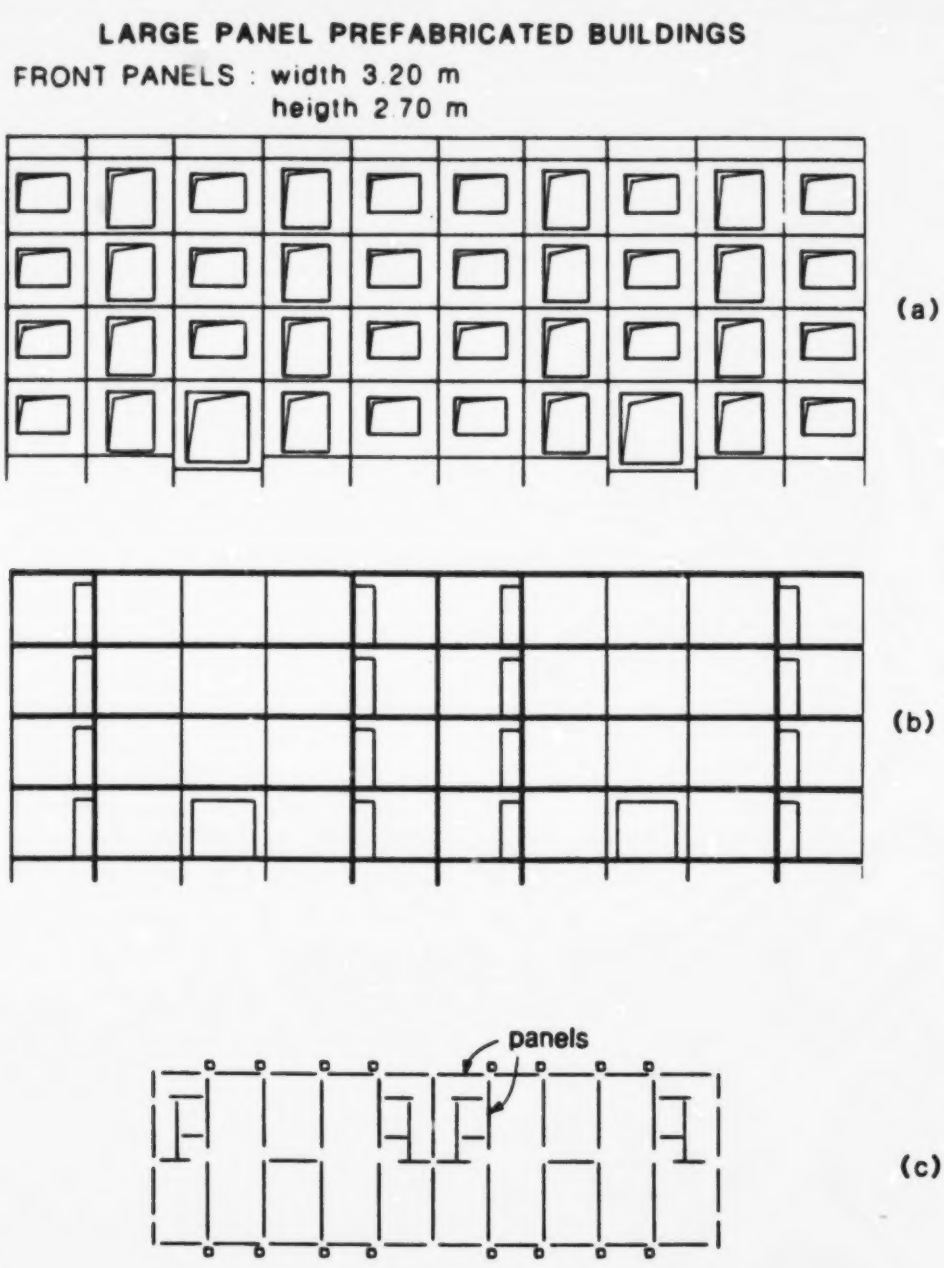

Figure 54.—General front panel view (a), interior panel view (b), and plan layout of panels (c) of the precast structures.

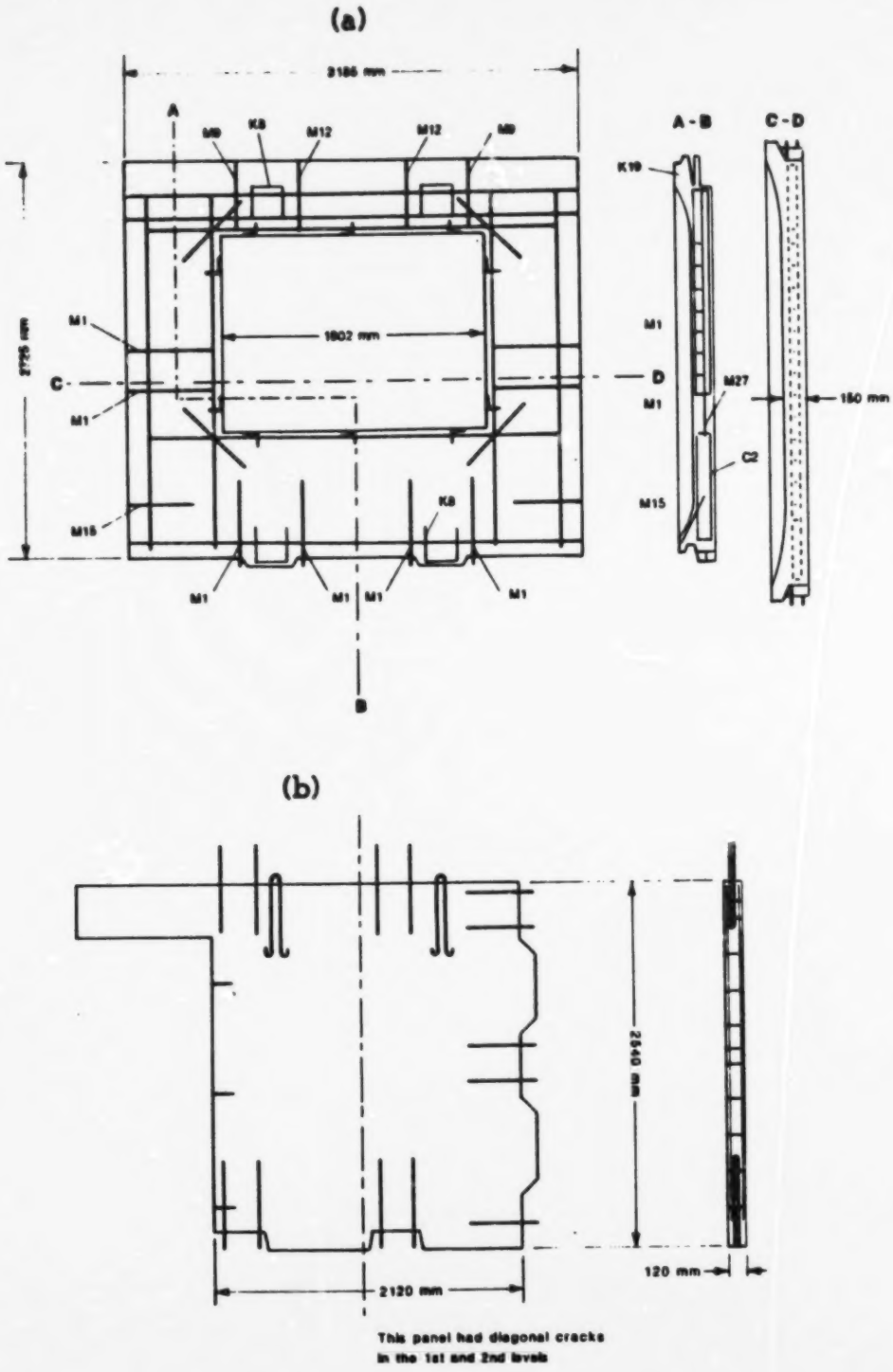

Figure 55.--Typical external and internal panel with openings.

Figure 56.--Typical diagonal crack in one of the panels in the precast structures.

of lives lost (176) during the earthquake are not excessive corresponding to an earthquake of this magnitude with epicenter close to (50-150 km) centers with sizeable population.

2. Engineered structures, although several suffered severe damages, in general performed well. There are lessons to be learned from the performance of the engineered structures. For example, the low-rise reinforced concrete symmetrical structures with central shear wall core and columns around the perimeter performed well (in Valparaiso, Viña del Mar and Santiago). A lesson relearned during this important earthquake as well as others is the effect of foundation and the influence of underlying soil conditions to the behavior and performance of structures.
3. Special construction types (e.g., prefabricated panel buildings) performed well during the earthquake.
4. Adobe and unreinforced masonry type non-engineered structures that were not constructed properly or that were not braced well resulted in the collapse or severe damage of these structures.
5. Once again, the seismic detailing of connections (beam-to-column connections) is an important factor in the performance of structures during an earthquake.
6. Effect of partial infill walls, infill walls or panels, to the behavior has been demonstrated. The stiffness characteristics and therefore the dynamic performance of structures has been altered while providing infills to framed systems. In other cases, infill walls have greatly decreased the seismic performance by shortening the effective length of columns.

The following preliminary recommendations are made as a result of the preliminary evaluation of the performance of structures:

1. The repair process of the structures which will continue should be carefully followed. Since seismic events recur frequently in the region, rather than quick patching up, careful application of the well proven repair methods should be followed.
2. Further work on the possible terrain amplification at Canal Beagle in Viña del Mar should be performed. This effort will facilitate understanding the phenomena better as well as providing insight for future zoning of such sites.
3. Amplification studies in two perpendicular lines in Viña del Mar should be performed to understand the effect of the different alluvial deposits as compared to rock sites.
4. One or more specific structures in Viña del Mar (preferably at alluvial type soil conditions) should be instrumented to provide sufficient data into its behavior during future events.

REFERENCES

International Association of Earthquake Engineers, 1972, Regulations for earthquake resistant design of buildings in Chile, in Earthquake Resistant Design Regulations - A World List: Tokyo, Japan, International Association of Earthquake Engineers.

Boore, D. M., 1972, A note on the effect of simple topography on seismic SH waves: Seismological Society of America Bulletin, v. 62, no. 1, p. 275-284.

Boore, D. M., 1962, The effect of simple topography on seismic waves: Implications for the accelerations recorded at Pacoima Dam, San Fernando Valley, Calif.: Seismological Society of America Bulletin, v. 63, no. 5, p. 1603-1609.

Bard, P. Y., and Tucker, B. E., 1985, Underground and ridge site effects: A comparison of observation and theory: (in press, advance copy courtesy of B. Tucker).

Borcherdt, R. D., Fletcher, J., Jensen, E., Maxwell, G., Van Schaack, J., Warrick, R., Cranswick, E., Johnston, M., and McClearn, R., 1985, A general earthquake observation system (GEOS): Seismological Society of America Bulletin (in press).

ACKNOWLEDGMENTS

The research described in this report was funded by the Office of Foreign Disaster Assistance, Agency for International Development (OFDA/AID) and by the U.S. Geological Survey. In addition, the cooperation and field work collaboration by fellow scientists and engineers in Chile deserves special acknowledgment. Indeed, without their help the investigations could not have been carried out successfully. E. Kausel, R. Saragoni, H. Fuenzalida, M. Pardo, O. Gonzalez-Ferran, F. Eisenberg and J. Monge of the University of Chile, Santiago, and P. Bonelli of the University Frederico Santa Maria in Valparaiso, as well as others, greatly facilitated arrangements in Chile and provided much scientific and technical information. Furthermore, guidance and assistance of Sra. Eugenia de la Rivera, Mayor of Viña del Mar is acknowledged.